Electrochemical reduction of CO2 to fuels by molecular polypyridyl catalysts of 3d transition metals

Noemie Elgrishi

Université Pierre et Marie Curie

École Doctorale de Chimie Moléculaire de Paris Centre (ED 406)

Laboratoire de Chimie des Processus Biologiques (UMR 8229)

Réduction électrochimique du CO_2 en carburants catalysée par des complexes polypyridines moléculaires de métaux abondants

Electrochemical reduction of CO_2 to fuels by molecular polypyridyl catalysts of 3d transition metals

Par Noémie Elgrishi

Thèse de doctorat de Chimie

Dirigée par Marc Fontecave

Thèse soutenue le 4 mai 2015 au Collège de France devant un jury composé de :

Jean-Michel SAVÉANT	Directeur de Recherche Émérite CNRS, Paris	PRÉSIDENT DU JURY
Hubert GIRAULT	Professeur à l'EPFL, Lausanne	RAPPORTEUR
Yves LE MEST	Directeur de Recherche CNRS, Brest	RAPPORTEUR
Anna PROUST	Professeur à l'UPMC, Paris	EXAMINATRICE
Eric LAFONTAINE	Docteur HDR DGA, Bagneux	EXAMINATEUR
Marc FONTECAVE	Professeur au Collège de France, Paris	DIRECTEUR DE THÈSE

Acknowledgments

First and foremost I would like to thank Marc Fontecave for agreeing to take me on as a PhD student back in 2010, before I left for the Nocera lab.

I suppose the story of my PhD started in spring of 2010, when I decided to come back from my M1 internship in Cambridge in the Nitschke group to go to Paris for a day to attend a Conference that looked like fun: “Frontiers of Chemistry: From Molecules to Systems”. It was on a Friday, only 75€, and I had to be back in France that weekend anyway. So why not go to a conference where 4 Nobel laureates were going to talk, in the middle of Paris? I was bound to get a clearer idea of what to do next for my Master 2 and eventually my PhD. The symposium was great, and two amazing things happened at lunch break: Clément Sanchez came to talk to me and Damien Baigl, after asking me which talk I liked best, introduced me to Marc Fontecave, who wanted to set up a chemistry lab in the middle of Paris to work on artificial photosynthesis and energy storage.

Fast forward to December 2010: I now knew that I wanted to work in the field of renewable energies, on energy storage and small molecule activation. I contacted Marc again to know if he would still be interested by a PhD student for the lab he wanted to create. I was going to MIT for my Master 2 internship working for Dan Nocera, but I could be back in France in fall 2011 to start a PhD. Marc said that he really wanted an “American style lab”, with not many permanents, heavily relying on PhD students and Post-Docs so they can learn more, learn to be independent, and through taking on more responsibilities learn to be better chemists and exist and maintain a successful lab environment. This sounded perfect to me, so a deal was made: if Marc found money to fund my PhD, starting fall 2011, then I would come work in the soon-to-be-created lab here in Collège de France.

I left to go to MIT and loved every minute of my time in the Nocera lab: the way labs are structured, very similar to the labs in the University of Cambridge, the way labs operate, the people…everything. And of course I met Matt. Then came July and I still had not heard back from Marc about a definitive funding source for my PhD. But that was fine, because I really liked it at MIT, and Dan had agreed to take me on as a student anyway “if the French thing doesn’t work out”. Mid July hit and I got the call: the Direction Générale de l’Armement has agreed to fund your PhD! Back to France it is!

The beginnings of the PhD are rough: reverse culture shock is real. The way responsibilities are distributed, what people expect, how people work, hours, scientific culture, … not much reminded me of the American style Lab I was sold on. But it was ok and things got better. First, the Sanchez lab was lending us space, and everyone was extremely welcoming and supportive. Second, although

everything came with more *red tape* than I thought possible, instruments eventually got purchased, delivered and were painstakingly and slowly set up. The potentiostat was delivered and set up by the end of March 2012; the GCs were functional by September 2012 for H_2 measurements and February 2013 for CO measurements; the ionic exchange chromatography was delivered in January 2013. Only to name the ones that have been used the most in this document.

Expertise is also slow to create from thin air, and I thank Vincent Artero, along with Jennifer Fize, for taking the time to give me a kick-starting course in practical electrochemistry over the course of a week in November 2012. And of course in May 2013 Matt started in the lab as a Post-Doc and scientific exchanges were facilitated. Another turning point was fall of 2013, when I had the opportunity to attend electrochemistry classes at Paris 7 given by Jean-Michel Savéant and Marc Robert. I thank them immensely for providing the much needed expertise and confidence to move on with my electrochemistry project.

In September 2013, things started to fall into place: product detection methods were operational to my satisfaction, data collection could begin and the PCCP paper was written and submitted. The paper was published in March 2014, and in early April we moved the entire lab out of our small room in the LCMCP labs and into the big brand new lab space in building E. Obviously moving and setting up a lab again takes time, although practice makes perfect and I can now confidently say that moving a lab is part of my skill set. February 2014 was also the start of my time in Chimie ParisTech working with Sophie Griveau and Fethi Bedioui on grafted electrodes. As often happens (or so I'm told), the last semester of a PhD is when everything starts working, and indeed by the time the lab was properly set up again and I was getting results here in Collège de France and in Chimie ParisTech, the end of my PhD was near. Luckily Marc was able to secure funding for 6 extra months to allow me to have enough time to finish experiments, write and submit papers and submit my thesis, and I thank him for that.

I thank Marc Fontecave for agreeing to take me on as a student in his lab, as well as Clément Sanchez for lending lab space and the great welcome that I had in the lab.

I thank the Direction Générale de l'Armement for the 3-year PhD fellowship, as well as the generous donators of the Fondation de l'Orangerie for the 6 months of salary to finish my PhD.

I thank the UFR de Chimie of UPMC for letting me teach classes and lab classes to bachelor students in catalysis and inorganic chemistry.

I thank the DGA for pushing me to register to the Sorbonne Université Doctoriales® in April 2015, where I learned an incredible amount of new things, and met wonderful people.

I thank L. Klein from the Physical Chemistry of Surfaces group of Chimie ParisTech for performing preliminary AFM analyses of grafted electrodes, as well as F. Prima and P. Vermaut from IRCP – Metallurgie Structurale – Chimie ParisTech for assistance in electrode manufacturing.

I thank SciFidner and all the wonderful FLIC alumni I met through the Future leaders in Chemistry Program which was a breath of fresh air.

I thank the ChADoC association, and its members, for their willingness to drive interesting projects such as the Fête de la Science and the Journée Pluridisciplinaire de PSL.

I thank all the members of the jury to have agreed to take time to read, review and asses my thesis and take time to be on the jury the day of the defense.

I thank especially Anna Proust as head of the doctoral school of Molecular Chemistry for her support, for letting me write my thesis in English and for allowing me to prolong my PhD by 6 months to allow me to finish my work and make sure the project was in a state to be able to be picked up by another chemist.

I have a special thank you for Fethi Bedioui, for agreeing to be on my “comité de suivi de thèse”, and through these presentations to have assessed the situation and agree to set up a collaboration so I could come and work in the lab to benefit from the expertise in electrode functionalization. Working in a different lab, with a different lab culture, and interacting with chemists working on completely different thematics and with different expertise I could learn from was a very valuable experience. A big thank you to Sophie Griveau, for all the day-to-day interactions, help and ideas. I thank the entire lab as a whole, and the team « Synthèse, Electrochimie, Imagerie et Systèmes Analytiques pour le Diagnostic » in particular.

A thank you to Benjamin Le Ouay for coffee breaks the first year and scientific conversations throughout my PhD, as well as Sam, Johanna, Anaël, Laila and all the other young chemists from the Sanchez lab I was privileged to meet.

A major thank you to Johanna Toupin for her upbeat and positive attitude, as well as the book projects we worked on for Belin. These projects came at a perfect time, and discovering the world of book publishing from the inside was enlightening.

It would be tedious to mention everyone in Marc’s lab, but I’d like to give a special thank you to Alex, Tanya, Xia, Giorgio, Charles and the other young chemists and biologists who have joined the group over the years, each addition was beneficial to broaden the scientific culture of the lab and promote a better working environment. I would also like to thank Caroline and Djemel for helpful and insightful discussions, as well as the rest of the Laboratoire de Chimie des Processus Biologiques, including Marie-Pia without whom administrative paperwork would be oh-so-much worse.

Finally, I would like to thank my family who supported me from La Rochelle throughout the entire duration of my life as a student, and say that I would not have been able to accomplish this without the constant help and support from Matthew Chambers. And of course a special mention to Ivy for moral support!

Noémie Elgrishi

Table of Contents

Chapter I – Introduction: from natural photosynthesis to CO_2 reduction catalysed by metal-polypyridyl complexes

Chapter II – Materials and methods

Chapter III – Evaluation of CO_2 reduction by first row transition metal complexes of the ubiquitous terpyridyl ligand

Chapter IV – CO_2 reduction selectivity over H^+ reduction by **Co-tpy**

Chapter V – Electrode functionalisation with a terpyridyl ligand: preparation, metallation and catalysis

Chapter VI – Epilogue

Chapter I

–

Introduction: from natural photosynthesis to CO_2 reduction catalysed by metal-polypyridyl complexes

Parts of section 2 and 3 are based on the work reported in:
N. Elgrishi, V. Artero and M. Fontecave, *L'Actualité Chimique*, 2013, **371–372**, 95.

1. A brief look at the global energy landscape

1.1. Global Energy outlook

The procurement of a reliable secure carbon-neutral energy supply is the biggest challenge facing our societies for the 21st century. The world population is predicted to reach up to 13 billion in 2100 (compared to 7 billion today).[1] At the same time, the standard of living continues to rise in the developing world such that the global energy consumption is estimated to keep increasing, by 41 % from 2012 to 2035[2] and up to 56% by 2040.[3]

The current global energy landscape mainly relies on the burning of fossil fuels, in the form of coal (30.1%), oil (32.9%) and natural gas (23.7%), which since recently includes shale gas. These sources of energy combined represent 86.7% of the current global energy demand.[4] The rest is supplied through nuclear energy (4.4%) and hydroelectricity (6.7%), with other renewable energy sources accounting for only 2.2% of the global energy output.

With additional concerns about a potential peak in oil production around 2030[5] and the volatile nature of oil prices, a global initiative is underway towards greater energy efficiency and an increase in the energy output from renewable energies. The eventual and inevitable depletion of carbon-containing natural resources (coal, oil, gas…) will make it necessary to find new sources of carbon to exploit as chemical feedstock and as new sources of energy. Vigilance is needed however, as the temptation of resorting to shale gas as a new cost effective and reliable source of fossil fuel looms. Burning fossil fuels, regardless of the source of the fossil fuel, still produces large quantities of carbon dioxide (CO_2) that are for the most part released in the atmosphere.

1.2. CO_2 and climate change

Since more CO_2 is emitted than ecosystems can absorb, anthropomorphic CO_2 emissions contributed to rising CO_2 levels in the atmosphere since the industrial revolution. Theories on climate change explain global warming in part through the increase of CO_2 concentration in the atmosphere as a greenhouse gas (Figure I-1). With exponentially increasing atmospheric CO_2 levels (399.96 ppm in 2015[6] compared to 279.5 ppm in 1789[7]), an energy revolution is needed to face this challenging situation.[8]

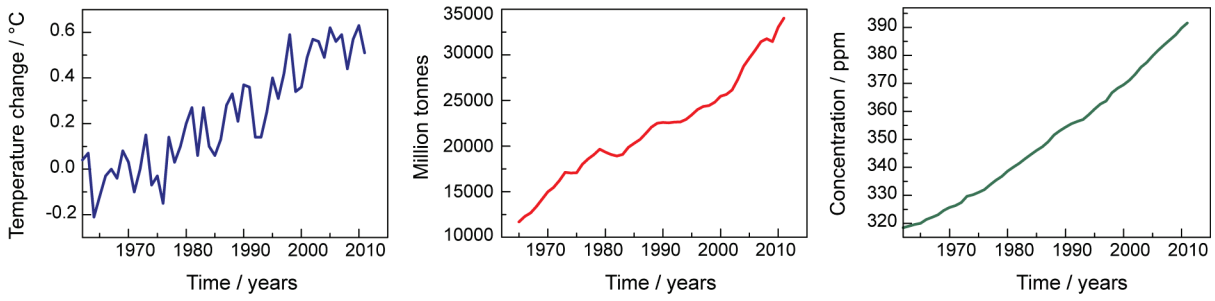

Figure I-1 Evolution of global temperature (blue, left), CO_2 emissions (red, centre) and atmospheric CO_2 levels (green, right) from the 1960s to the early 2010s.

1.3. The solar fuel solution

One solution to finding new carbon sources is to recycle CO_2 into fuels. This solution offers the benefit of keeping the advantages offered by carbon-containing chemical fuels in terms of graviometric and volumetric energy density.[9] As CO_2 reduction is endergonic, the process of transforming CO_2 back into fuels requires its own carbon-free supply of energy to drive the reaction. Renewable energy sources are attractive options to supply the requisite energy for CO_2 reduction; however sunlight is the only renewable energy source with the ability to meet the future global energy demand on its own.[8,10]More solar energy strikes the Earth every hour than is needed by the entire population for a year (4.3 10^{20} J per hour of solar energy compared to 4.1 10^{20} J consumed in 2001).[11] This is not to suggest that solar energy ought to be utilised exclusively as a renewable energy source, although it is highly likely that any future energy system based on renewable energy will rely greatly on solar energy. Many technological solutions already exist to absorb solar energy and transform it into electricity, like the solar panels that have continued to flourish on rooftops of buildings this past decade; however the intermittency of solar energy fosters the need for energy storage.

The chemical fuels that result from CO_2 reduction driven by renewable energy offer an ideal and sustainable solution to energy storage. Fuels achieve high energy densities through the storage of electrons in the small volume of a two-electron bond between light elements (*i.e.*, C—H, and H—H bonds) as opposed to other options such a batteries, capacitors and flywheels.[9] The paradigm shift needed for a solar revolution is to start thinking of chemical fuels as a medium for energy *storage* instead of energy *sources*. The guiding principle is to use the energy of solar photons to drive catalytic cycles composed of endergonic chemical transformations utilizing CO_2 as a reagent. In this way solar energy can be stored in the form of chemical bonds as a “solar fuel”.

1.4. Nature’s solution to the energy storage problem

Photosynthesis is the process nature utilises to store energy, by converting solar energy into chemical bonds. It is useful to remember that atmospheric CO_2 is a fundamental building block of life and that CO_2 is the main source of carbon for all living organisms. Plants assimilate and transform CO_2 into sugar using water and sunlight during photosynthesis. This process is the basis of the existence of all the biomass that we rely on so heavily. Of note, the process of constructing complex sugar molecules does not directly involve energy storage, but rather only energy conversion beginning with the high energetic molecule immediately produced upon light absorption. In non-photosynthetic eukaryotic cells, the energy stored in the molecules of sugars and O_2, produced mainly through photosynthesis by other organisms, are used as a fuel to power the respiration machinery. At its core, respiration is no different than burning fossil fuels to release energy, except nature uses renewable energy and recycled carbon sources.

In this chapter, we will start by briefly describing the natural process of energy storage, to understand the key fundamental steps. Next we will look at other CO_2 activation mechanisms

developed by nature, to better understand the parameters that might provide additional inspiration for the development of artificial CO_2 activation systems. Current artificial photosynthesis strategies and their merits will be briefly discussed, and the strategy chosen by the Laboratoire de Chimie des Processus Biologiques will be presented. Finally, an in-depth review of the field of molecular CO_2 reduction with metal complexes containing polypyridyl ligands will be presented to better understand the state of the art of catalyst development in this field.

2. Natural photosynthesis

2.1. Photochemical energy storage

Energy storage in nature occurs in plants through photosynthesis. A brief description of the natural process will be discussed here to understand the key fundamental steps.

During natural photosynthesis, visible light photons are absorbed by a series of molecular photosensitisers located within photosystem II (PSII). PSII is a protein complex, composed of a dozen different proteins, lipids**,** quinones and metal ions.[12] The absorption of a photon creates an exiton (electron-hole pair) which is stabilised by a very efficient and quick mechanism of charge separation, deigned to prevent recombination of the electron-hole pair by spatially separating the reducing and oxidizing equivalents in different protein structures. When four oxidizing equivalents (the holes) are accumulated on the catalytic site of PSII, the manganese and calcium complex (Mn_4Ca) can then oxidise two water molecules into oxygen (Figure I-2) and protons.

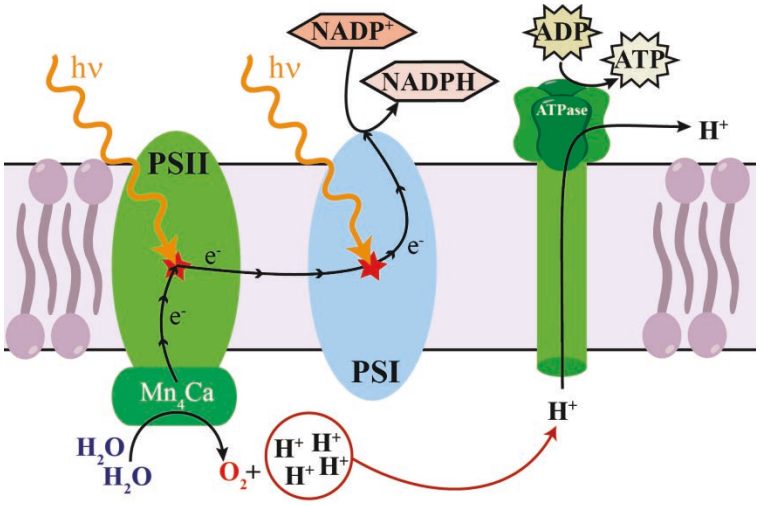

Figure I-2 Simplified representation of natural photosynthesis.‡

The excited electrons are transferred to photosystem I (PSI) through an electron transfer relay composed of quinones. To achieve the necessary reduction potential within PSI to convert the biological cofactor $NADP^+$ to form NADPH, which is the universal cellular reducing agent, each electron is *re-energised* by an additional photon. Upon absorption of a photon within PSI, the resulting hole is ultimately filled by an electron derived from light absorption within PSII. The interconnection of the two light absorption events is commonly referred to as the "Z scheme".[13] Certain photosynthetic organisms are able to use these electrons to reduce protons to hydrogen instead of $NADP^+$ through the intervention of hydrogenase metalloenzymes, effectively splitting water into O_2 and H_2.

The overall result of photosynthesis thus leads to extracting electrons from the water on one side of the membrane and accumulating them as the reducing agent NADPH on the other side of the membrane. The second result is the creation of a proton gradient across the membrane, the energy of

which can be used to power the protein synthesis machinery of ATP. These processes are thermodynamically unfavourable, and are only occurring due to the solar energy absorbed.

2.2. Fixation of CO_2 to produce fuels

Natural photosynthesis continues to proceed through additional steps in which the reducing potential of NADPH and the energy stored in the form of ATP are utilised to convert CO_2 to sugars through the Calvin Cycle; in particular fructose-6-phosphate (Figure I-3).

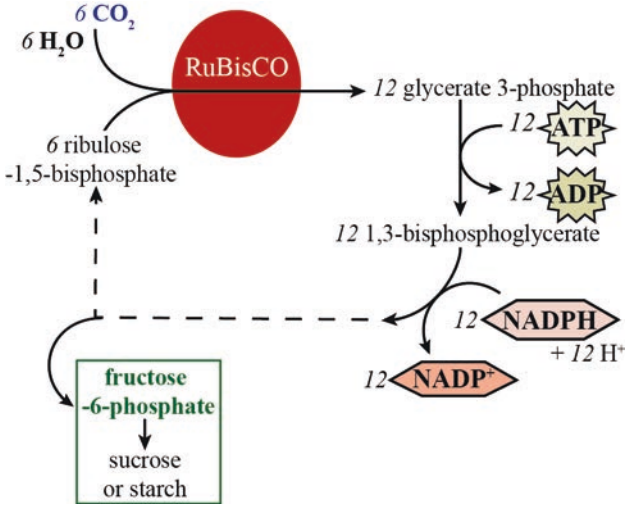

Figure I-3 Schematic representation of the Calvin cycle where CO_2 is fixed by RuBisCO and the following transformations leading to the production of sugars.[§]

In the Calvin cycle, CO_2 reacts first with a molecule of ribulose-1,5-bisphosphate, a 5-carbon sugar, which after subsequent hydrolysis gives rise to two molecules of glycerate 3-phosphate. The enzyme that allows the fixation of CO_2 is called RuBisCO, ribulose-1,5-bisphosphate carboxylase/oxygenase, (Figure I-3) and is the most abundant enzyme on earth. RuBisCo can represent up to 50% of the soluble protein content in photosynthetic organisms. The vast majority of the carbon we depend on (for food, fuel, clothing...) has gone through the active site of RuBisCO at least once. The active site of RuBisCO contains a manganese ion that coordinates and activates a CO_2 molecule before the addition reaction with ribulose-1,5-bisphosphate occurs.

In the next steps of the Calvin cycle, ATP is used to transform glycerate 3-phosphate into 1,3-bisphosphoglycerate which is further reduced using NADPH and protons to eventually lead to sucrose and starch. It ought to be re-emphasised that, within the Calvin cycle, the high energy intermediates ATP and NADPH, formed during the energy storing steps of photosynthesis, are here consumed to regenerate ADP and $NADP^+$. The energy that was stored in these molecules during photosynthesis is transformed by the cell to produce sugars, but no additional energy is stored through the Calvin cycle.

2.3. Enzymatic CO_2 conversion

Beyond directly using CO_2 as a carbon source for biomass, the cell has also developed complex machinery aimed at eliminating the toxic products CO and formate from the cell by converting these potential toxins to CO_2. Given the microscopic reversibility principle, the active sites of these enzymes can prove useful inspiration for the design of CO_2 reduction catalysts to low molecular weight carbon containing products.

The two main classes of enzymes for CO_2 conversion are formate-dehydrogenases and CO-dehydrogenases, in which the cell respectively converts formate and CO into CO_2. Other potential products, such as formaldehyde, are converted to formate before being eliminated as CO_2.

2.3.1. Formate-dehydrogenases

In bacteria, the interconversion between CO_2 and formic acid (eq. I-1), occurs in the active site of formate-dehydrogenases following the overall equation:

$$CO_2 + H^+ + NAD(P)H \leftrightarrow HCO_2H + [NAD(P)]^+ \qquad (I\text{-}1)$$

The active sites of formate-dehydrogenases are arranged around a Mo or W atom, coordinated by dithiolene ligands, commonly referred to as molybdopterin cofactors. The structure of the Mo version is presented in Figure I-4.[14] Besides the two molybdopterins cofactors, the coordination sphere around the Mo atom is completed by a combination of a sulfur ligand (thiol or sulfido) and a coordinated seleno-cysteine. During the catalytic cycle, the Mo centre oscillates between the oxidation states IV and VI, and the sulfur atom is believed to have an active role in the catalytic cycle by assisting CO_2 interaction with the Mo centre by way of a nucleophilic interaction with the carbon atom of CO_2. However, a clear consensus does not exist as to whether or not there is active participation of the Se_{cys} within this process.[15]

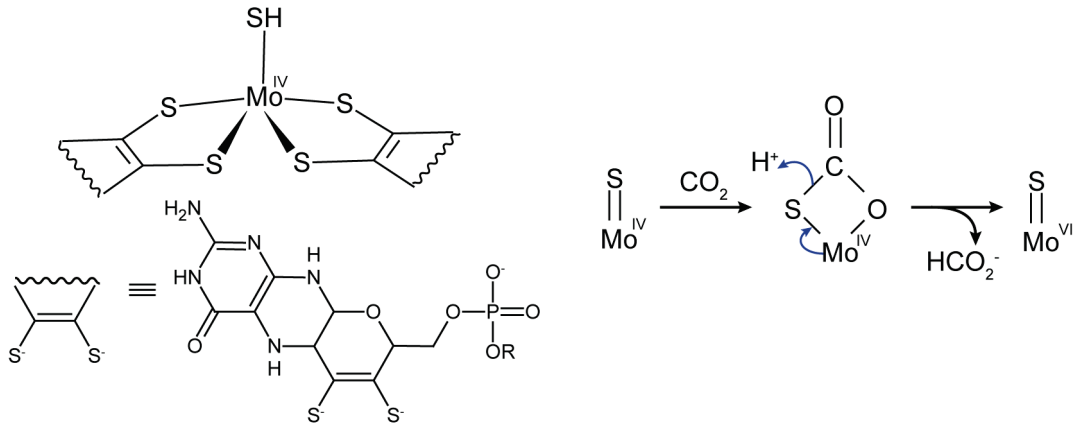

Figure I-4 Active site of molybdenum based formate-dehydrogenases and simplified proposed mechanism.‡

2.3.2. CO-dehydrogenases

CO-dehydrogenases catalyse the interconversion between CO and CO_2 according to the following equation:

$$CO_2 + H^+ + NAD(P)H \leftrightarrow CO + H_2O + [NAD(P)]^+ \quad \text{(I-2)}$$

Two main classes of CO-dehydrogenases have been reported, with active sites containing either $NiFe_4$-sulfur cluster or MoCu active sites. The $NiFe_4$ class is proposed to follow the catalytic cycle depicted in Figure I-5.

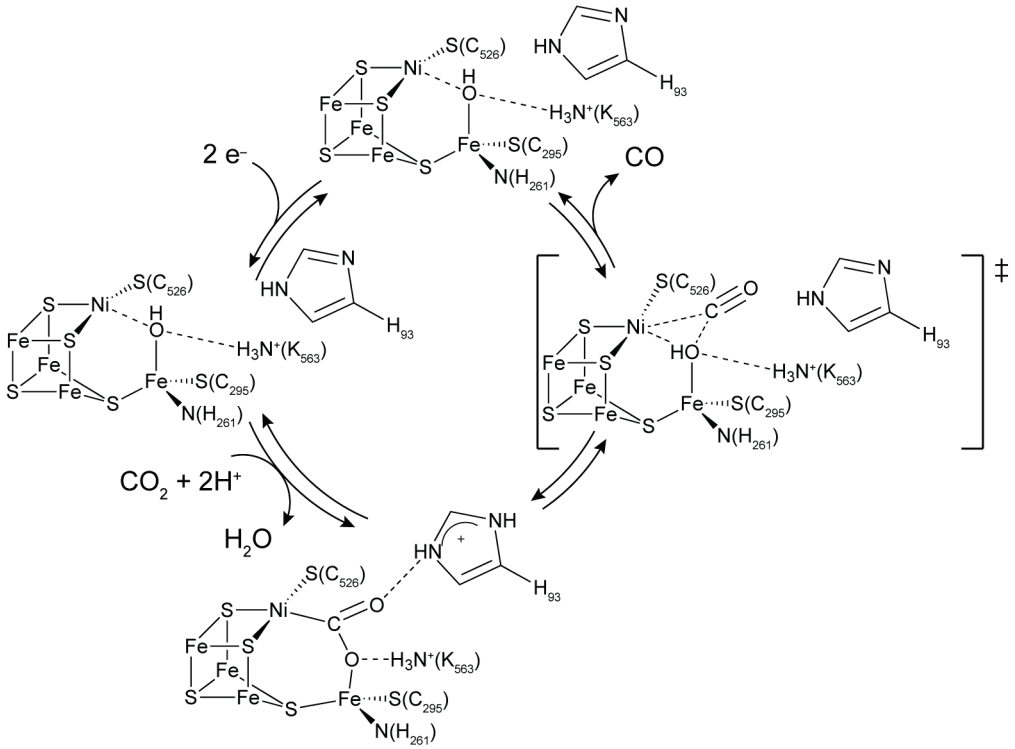

Figure I-5 $NiFe_4$ cluster present in the active site of CO-dehydrogenase and the proposed catalytic cycle for CO oxidation.[16] The same cycle has be proposed for CO_2 reduction.

This mechanism, supported by crystallography and now discussed from the perspective of CO_2 reduction, suggests that only the nickel atom undergoes changes of redox state (Ni^{2+} / Ni^0) and one iron atom acts as a Lewis acid as a CO_2 molecule binds to the reduced active site by bridging the Ni and one Fe atom. The coordination mode for the binding of CO_2 is thought to involve the carbon of CO_2 bound to the Ni and an oxygen atom ligating the Fe. Such a structure promotes the heterolytic cleavage of the C–O bond between the Ni and Fe, which leads to a molecule of CO coordinated to the Ni centre and a hydroxide coordinated to the Fe (Figure I-5).[16]

The second main class of CO-dehydrogenases is based on a molybdenum cation coordinated to a molybdopterin cofactor and bridged to a Cu atom through a sulfide.[17] The general mechanism for this class of CO-dehydrogenases is depicted in Figure I-6.

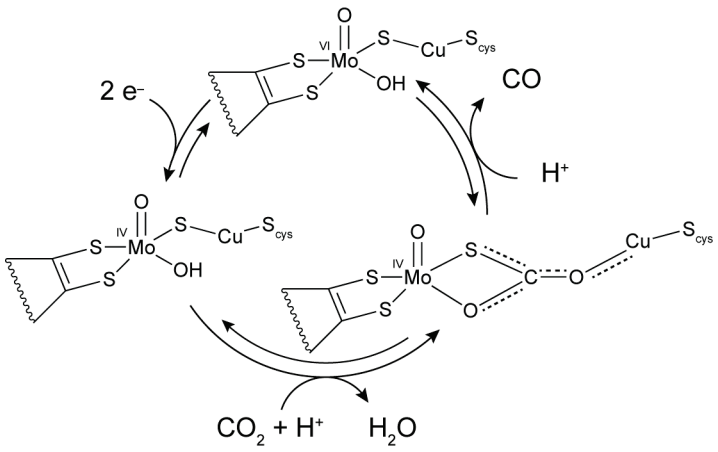

Figure I-6 Active site and proposed mechanism for Mo/Cu CO-dehydrogenases.

The mechanism for the Mo/Cu CO-dehydrogenases is similar to that of the Ni-Fe cluster in that one of the metallic sites facilitates the binding of CO_2 while the other stores redox equivalents (Figure I-6). An additional similarity between the two systems is that the C–O bond that is not cleaved (i.e. remains within the CO molecule produced) is stabilized by a strong Lewis acid-base interaction between the oxygen atom and either a histidine (Ni-Fe) or a copper cation (Mo/Cu). A noteworthy difference between the Ni-Fe mechanism and the Mo/Cu mechanism is that, while the Ni centre of the Ni-Fe cluster acts as both the redox reservoir and a Lewis base, the Mo centre of the Mo/Cu site only stores redox equivalents while the ligated sulfido fulfils the role of Lewis base in the coordination of CO_2. An additional difference is while there is a Lewis acid interaction from a metal bound hydroxide required for the binding of CO, this metal bound hydroxide resides on the redox inert Fe centre within the Ni-Fe cluster but is located on the redox active Mo centre in the Mo/Cu active site. Taken as a whole, these observations strongly suggest the importance of storing multiple redox equivalents within catalytic centres and of Lewis acid-base interactions in activating CO_2. However, these interactions can be designed in many different ways. The Ni-Fe system used a metal as a Lewis base (to interact with the carbon of CO_2) while the Mo/Cu system uses a terminal sulfido to fulfil that role. Furthermore, the Ni-Fe system uses a protonated histidine to hydrogen bond to an oxygen of CO_2, but the Mo/Cu system uses a Cu cation as a Lewis acid to serve the same purpose.

2.4. Conclusions

Natural photosynthesis encompasses several processes which effectively capture solar energy and store it in the form of chemical bonds. During natural photosynthesis the energy storing steps are decoupled from the energy conversion steps. The energy storing step occurs through water splitting whereas the entire Calvin cycle, with CO_2 incorporation, affords energy conversion to more useful forms. Separate from photosynthesis, there exists an alternative set of enzymes that catalyses the interconversion of CO_2 with CO or formate. These enzymes rely on catalytic cycles composed of small finite metallic complexes, with at most two metals being involved in the catalytic sites. Interaction with CO_2 occurs on a reduced metal centre, which stores reducing equivalents. The second metal,

when present, can fulfil the role of templating the interaction between the CO_2 molecule and the redox-active metallic centre.

3. Artificial photosynthesis

3.1. Copying nature

Artificial photosynthesis is the process by which the key steps of photosynthesis – solar energy capture and storage in chemical bonds – are recreated synthetically. The first investigations towards the development of artificial photosynthesis were aimed at directly mimicking the natural system by using components from biology within synthetic structures to effectively produce fuels.

A significant development in achieving an artificial photosynthetic system based on a copy of the natural machinery was developed in the late 90s by Devens Gust, Tom Moore and Ana Moore of Arizona State University (Figure I-7).[18,19] The construct was directly inspired by nature by allowing for photo-induced ATP synthesis, using a triad consisting of a central porphyrin photosensitiser (PS) positioned between an electron donor (D), a carotenoid, and an electron acceptor (A), a quinone. The triad is immobilised within a lipid bilayer that forms a vesicle, in a similar manner to that of a cell membrane. Under illumination of the vesicles, the triad creates an electron-hole pair, which affords a long lived charge separated state by localising the electron on the quinone near the outside of the vesicle while localising the hole on the carotenoid inside the vesicle. The electron is then transferred to a second quinone (Qs) which is mobile and located inside the membrane. The reduced quinone can then abstract a proton from water outside the vesicle forming a transient semiquinone. Upon diffusion towards the interior of the vesicle, the semiquinone can be oxidised by the carotenoid and releases the proton inside the vesicle. These events create a pH gradient between the inside and outside of the vesicle, and thus a membrane potential, in a manner that directly parallels the natural system.

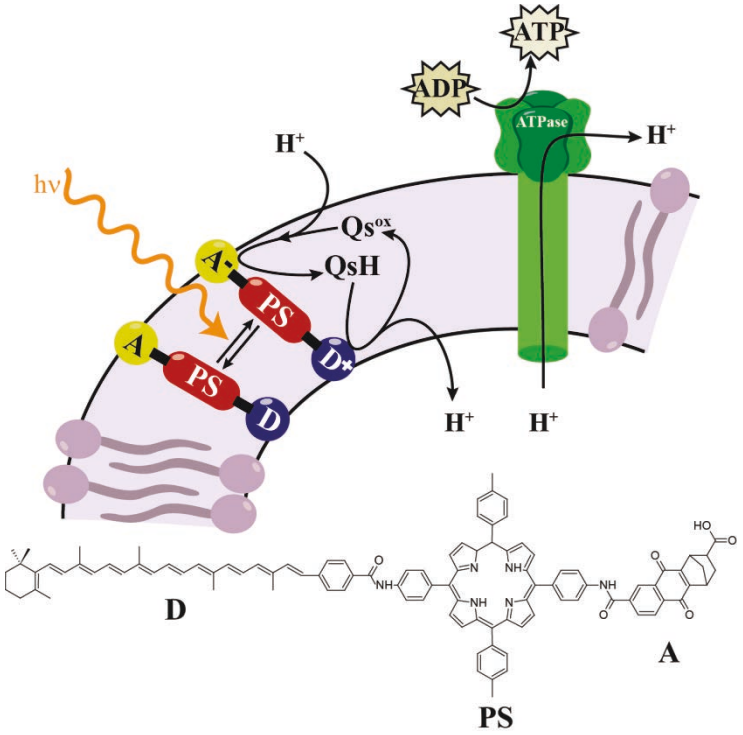

Figure I-7 Artificial photo-induced ATP-synthesis system developed by the Arizona State University team.‡

This pH gradient, just like in the natural system, is then used to power an ATPase inserted into the lipid bilayer and thus effectively synthesises ATP using solar energy. The quantum yield is calculated to be close to 7%, corresponding to the synthesis of one molecule of ATP for 14 photons captured, or about 25 000 molecules of ATP produced by ATPase and per hour. This system is impressive in its simplicity compared to the natural machinery, and its ability to efficiently convert sunlight into energy that is stored as ATP. It cannot however be easily coupled to other systems to make use of this stored energy.

In this first example, the sunlight capturing strategy was a direct mimic of the natural system, but the energy conversion step to create a useful fuel (sugar in natural photosynthesis) was not developed. Recently, several groups have focussed their efforts on the reverse strategy, by focusing on the fuel production step, as opposed to the sunlight capture step. With the development of the solar panel industry, the ability of converting sunlight to electricity, the first step of photosynthesis, is well underway. The second step of photosynthesis – storing this flow of electrons in the form of chemical bonds in a fuel – has thus been the primary focus of research efforts.

In 2007 Armstrong and coll. explored synthetic systems composed of bio-machinery to store energy through CO_2 reduction by immobilising a $NiFe_4$ CO-dehydrogenase from *Carboxydothermus hydrogenoformans* for the purpose of testing the principle of microscopic reversibility. They report CO_2/CO interconverstion catalysed by the enzyme adsorbed on a pyrolytic graphite edge rotating electrode in anaerobic conditions at the equilibrium potential of –0.50 V *vs.* NHE at pH 6.7 at 25°C.[20] In 2008, J. Hirst and coll. proceeded to immobilise a W-based formate-dehydrogenase from the anaerobic bacteria *Syntrophobacter fumaroxidans* onto a graphite electrode.[21] The enzyme was shown to act as an electrocatalyst for the conversion of CO_2 to formate and formate to CO_2, with up to 42 500 catalytic cycles after 1 h at –0.8 V *vs.* NHE at pH 6. The molybdenum-containing formate dehydrogenase enzyme from *E. Coli* was also immobilised and studied by electrochemistry more recently[22]. It was shown to also be a competent, reversible and specific catalyst for the interconversion of CO_2 to formate. The production of formate from CO_2 could be observed electrochemically at reported operative overpotentials as low as 110 mV. These results demonstrate the possibility for the development of bio-electrodes that directly utilise natural bio-machinery. However, the complexity, fragility, and high cost of production of these enzymes represent serious technical hurdles for their use as the base component of artificial photosynthesis systems.

A possibility to overcome these issues would be to not restrict ourselves to the rigorous use of biological components, by focusing on the active sites of the enzymes, and modelling them in the form of molecular complexes of Mo and W dithiolene or Mo-Cu and $NiFe_4$ clusters. Many models have been synthesised, some very close to the actual structures of the active sites of formate and CO-dehydrogenases. However, despite impressively close biological mimics of the primary coordination

sphere of the natural active sites, all the models reported so far have failed to report any noteworthy activity towards CO_2 reduction.[23,24,25,26]

The fully biological systems have limitations in terms of scalability and stability, and direct structural models of the active sites of enzymes do not correlate to functionality of these models. An alternative approach to artificial photosynthesis is to take inspiration from nature and implement the general principles from the biological systems within fully synthetic and optimized materials without restricting ourselves to structural models of biological systems.

3.2. Reflexions on deviations from biomimetic systems

Chemists are not restricted to the narrow chemical toolbox that nature uses, nor do chemists have to design hundreds of compatible catalytic systems simultaneously operating under similar conditions that are required by the cell for its continued existence. Given that chemists are not restricted to the same limited parameters and resources as a cell, inspiration from nature is key, not direct mimetism. As previously presented, some photosynthetic organisms split two equivalents of H_2O to 2 equivalents of H_2 and O_2 (eq. I-3). Alternatively, within most photosynthetic organisms, the "H_2" from water splitting can be considered to exist within the biological reductants NADH and NADPH. As these reductants are essentially hydride sources, taken together with protons they effectively represent H_2. For synthetic systems, water splitting as a target reaction is attractive for many fundamental reasons. Producing O_2 as the anodic product affords an environmentally benign gaseous reagent that can be utilised within energy releasing devices (fuel cells) at atmospheric conditions. Using the resulting electrons to produce H_2 specifically offers several advantages insofar as H_2 can be used either directly in a fuel cell, or in a combustion engine, or used indirectly in the synthesis of liquid fuels. For these reasons, among others, water splitting has been a target reaction for chemists with significant advances being reported in the 1970's using fully synthetic and artificial systems.[27,28,29]

$$2\ H_2O \rightarrow 2\ H_2 + O_2 \qquad \text{(I-3)}$$

The concept of fully artificial systems continues to be developed with several groups reporting versions of *artificial* "*leaves*" capable of directly catalysing the water splitting reaction through light absorption.[30,31,32] Recently, a famous report by Nocera and coll. accomplished the production of an *artificial leaf* using primarily cheap and earth abundant elements.[33] This artificial system, described in Figure I-8, uses triple junction single crystal Si as the light harvesting semiconductor. The p-doped Si (photoanode) is passivated with a layer of a conductive metal oxide (indium tin oxide, ITO) on which a cobalt-phosphate water oxidation catalyst is deposited. The n-doped Si (photocathode) is passivated with steel on which a NiMoZn heterogeneous catalyst is deposited. At the photoanode, the photo-generated holes are sequestered by the cobalt catalyst and are used to catalyse the conversion of water to oxygen and protons. The protons can then freely migrate into the bulk solution, which is in contact with the NiMoZn catalyst on the photocathode. Within the triple junction Si, photo-generated

electrons migrate toward the NiMoZn based film, which catalyses the reduction of H^+ to H_2. Effectively, sunlight energy is directly converted into H_2 and O_2 and neutral pH.

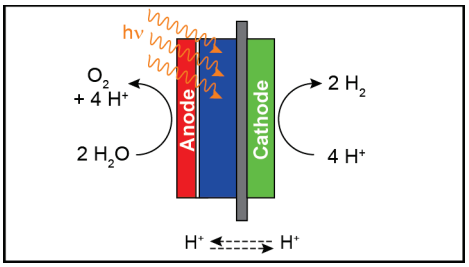

Figure I-8 Schematic representation of the artificial leaf developed by Nocera in 2011. The cathode is a NiMoZn catalyst, and the photo-anode is composed of a triple junction Si wafer (blue) as the photosensitiser, protected by an ITO layer (white) which is coated with a cobalt-phosphate water oxidation catalyst (red).

While seemingly attractive as a solar fuel, H_2 does require significant additional efforts and technological developments to afford efficient storage due to its low volumetric energy density.[9] On the other hand, reduced carbon sources, typically liquid at room temperature, have much more attractive volumetric energy densities and alleviates problems associate with storage and transport. One strategy to achieve this goal is to use the H_2 produced by water splitting to yield carbon containing fuels using CO_2 as a feedstock. Recently Nocera and collaborators achieved this by elaborating on their previous system by incorporating bacteria into their *artificial leaf* device. The incorporated bacteria consume the H_2 produced by the system and fixe CO_2 through the previously described Calvin cycle.[34] This system nicely demonstrates the possibility to integrate systems for CO_2 reduction with water splitting devices to achieve carbon-based fuels.

While the report by Nocera and coll. makes direct use of bacterial machinery to achieve this production of carbon-based fuels, the possibility exists to instead utilise synthetic catalysts that are more amenable to rational system optimisation and tuneability. As a recent example, Meyer and collaborators have achieved a fully synthetic and molecular system capable of storing energy through catalysing direct CO_2 splitting into CO and O_2, as depicted in eq. I-4:

$$2\ CO_2 \rightarrow 2\ CO + O_2 \qquad \text{(I-4)}$$

The strategy implemented by Meyer and coll. uses the ruthenium-based homogeneous complex $[Ru(tpy)(Mebim\text{-}py)(Solv)]^+$ (Solv = solvent) to catalyse CO_2 reduction and H_2O oxidation in separate compartments within the electrochemical cell depicted in Figure I-9. At the anode, the catalyst is in aqueous solution with a phosphate buffer at pH 7.45 and catalyses the electrooxidation of H_2O to O_2 and protons. The protons then cross a Nafion membrane and a frit to reach the cathode, where a solution of $[Ru(tpy)(Mebim\text{-}py)(Solv)]^{2+}$ in MeCN (CH_3CN) catalyses the electroreduction of CO_2 and protons to produce CO and water.[35]

Of note, this system does not operate via light absorption but rather through the application of an external electrical bias and as such only models the energy storage part of photosynthesis.

However, the generation of the required potential bias via a photovoltaic device would afford a fully artificial photosynthetic system.

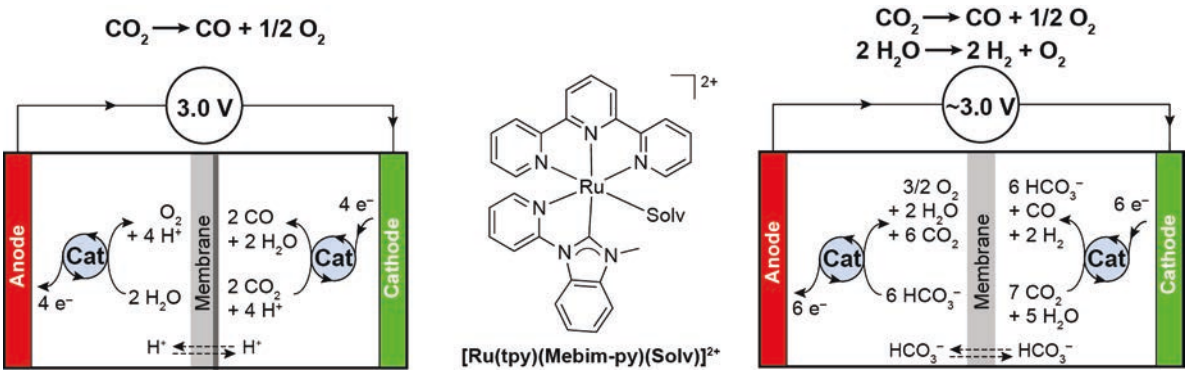

Figure I-9 Electrochemical cells developed by Meyer in reference 35 (left) and 36 (right). The structure of the ruthenium-based catalyst ("cat") is presented in the centre.

Meyer and collaborators continued to develop their Ru-based systems and demonstrated that upon using fully aqueous conditions and a carbonate/bicarbonate electrolyte system, the singular catalyst $[Ru(tpy)(Mebim\text{-}py)(Solv)]^{2+}$ could anodically catalyse O_2 generation and cathodically catalyse the generation of variable ratios of CO and H_2 with up to 50% energy efficiency. Of interest, the ratios of CO:H_2 were found to be rationally controllable based on the pH of the buffered solution and the value of the applied bias.[36] The ability to tune and vary the ratio of CO:H_2 is specifically important based on its relevancy to the industrial Fischer-Tropsch process. The Fischer-Tropsch process combines ratios of CO and H_2, commonly referred to as syngas, into reduced carbon species: liquid hydrocarbons. Given that H_2 and CO are gases with poor volumetric energy density, efficient conversion of these species into a liquid based fuel would be required, and the Fischer-Tropsch process can accomplish this task. However, the process is not typically selective and is quite sensitive to the ratio of CO and H_2 used as reagents. Therefore, the ability to tune the ratios of CO and H_2 easily affords the possibility to control the selectivity the major product resulting from the Fisher-Tropsch process. The fully synthetic system by Meyer and collaborators highlights an additional advantage of artificial systems, which is increased stability under a large variety of desired conditions. As systems more reminiscent of biological constructs are often less stable to variations of pH or applied potential, they would be poor target to include within a system designed to yield variable ratios of CO and H_2 in a manner similar to that demonstrated by $[Ru(tpy)(Mebim\text{-}py)(Solv)]^{2+}$ (Figure I-9).

One limitation of the Meyer system is that it requires the use of an expensive ruthenium-based catalyst. Nevertheless, in being able to develop a complete system that has no direct analogy to the natural system, Meyer and coll. nicely demonstrate the potential value of fully synthetic molecular based systems.

3.3. Approach chosen and key concepts

3.3.1. The photo-electrochemical model cell

In an effort to directly convert solar energy to fuels, the general system design presented in Figure I-10 is the target that has been chosen by the group here in Collège de France. As has been described previously, a photonanode would use solar energy to split water to O_2, protons and electrons, which would be used to reduce CO_2 to fuels at the cathode. The catalyst at the cathode would consist of discrete molecules that have been immobilised on the cathode. This allows for the study of the CO_2 reduction catalyst in solution homogeneously, with a better control over the chemical and electronic properties as well as system optimisation of the catalyst through ligand variation. The catalyst can then be immobilised on the electrode to obtain the cathode required for the cell.

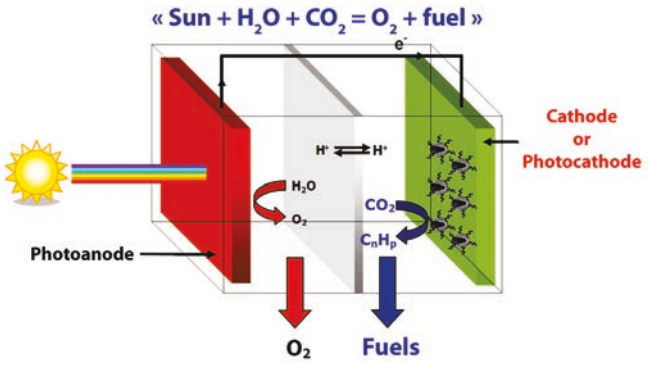

Figure I-10 Schematic representation of a photoelectrochemical cell.

In this work, we will focus on homogeneous molecular catalysts for the reduction of CO_2. We have chosen to study a cathode, not a photocathode, with the understanding that the source of electrons provided to the molecular catalyst could be modified from an electrode to a photosensitiser or a semiconductor to yield a photosensitised catalyst (Figure I-11). We have not considered true and discrete molecular photocatalysts, as they are exceedingly rare and require a single entity that absorbs photons and directly use the energy of these photons to convert a substrate to a product. By decoupling light absorption from catalysis, the complex nature of the excited electronic states of a catalyst can be neglected.

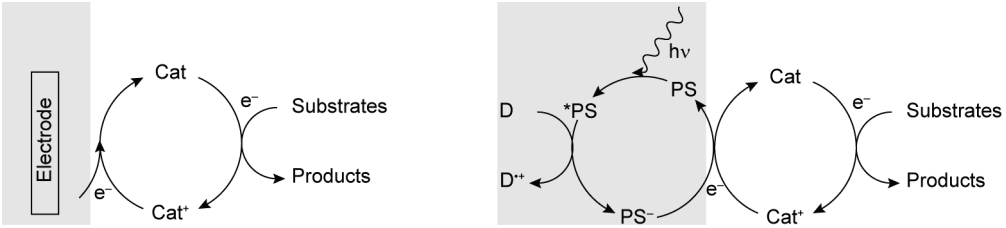

Figure I-11 Schematic representation of an electrochemical and photosensitised catalytic reaction.

3.3.2. What makes a "good" catalyst?

There are several parameters to consider when discussing the merits of a catalyst. Generally, a "good" catalyst should present high activity, high stability, high energetic efficiency, low balance of system cost and the specifically desired selectivity.

The activity of a catalyst is usually determined by calculating the rate constant for the catalytic reaction in conjunction with the turn-over frequency (TOF), which is defined as the number of catalytic cycles that a molecule of catalyst completes per unit of time. The rate constant might prove tricky to determine depending on the conditions and the system. The TOF can more easily be determined by measuring the moles of products of the reaction and dividing by the moles of active catalysts. In a photochemical system where the entirety of the system is illuminated, all of the catalyst molecules in solution participate in the reaction so determination of TOF is straightforward. In an electrochemical cell only the small portion of catalyst added to the solution that which is near the vicinity of the electrode can enter the catalytic cycle at any given point in time. An estimate of this reaction layer must be taken into account to more accurately determine the TOF in these systems. The higher the TOF, the more moles of product are obtained per unit of time.

Stability is the second parameter to monitor when comparing catalysts. The stability of catalysts can depend on a number of parameters, and is sometimes measured in terms of turn-over number (TON). The TON is the average number of catalytic cycles that a particular catalyst molecule enters before complete deactivation of the system, whether through decomposition, deleterious side reactions, product inhibition or other factors. Since stability studies needed to establish the TON of a catalyst might prove time consuming, the stability of the catalyst is tracked through the evolution of its activity over time. In an electrochemical system the evolution of current can be used to track the stability of a catalytic system, as well as the evolution of the formation of products over time as opposed to photo-assisted catalysts where product formation is generally the only tool used to track stability.

The third parameter to consider is the energy requirement for the catalyst to operate at a practical rate. Catalysed reactions usually exhibit high kinetic barriers and slow reaction rates in the absence of catalysts. The extent to which this barrier is modified by an electrocatalyst typically relates to the potential applied to the system. For electrocatalysts, the overpotential is defined as the increase in potential needed, past the thermodynamic potential of the reaction, to overcome the kinetic barrier and achieve the catalytic reaction at a desired rate. The lower the overpotential, the less energy needs to be added into the system to trigger catalysis. For the best catalysts, a small increase in overpotential should result in a large increase of activity. In the case of energy storage reactions, it is worth mentioning that a potential bias should and will always be a prerequisite. For comparing a photo-assisted catalyst to an electrocatalyst, a rough estimate of the potential applied in the photochemical system is given by the redox potential of the photosensitiser.

When considering balance of systems costs, the nature of the system studied might have a larger bearing on the merits of the catalyst than is usually considered. For example, with two identical catalysts, one Rh-based and the other Co-based, there is a 3 orders of magnitude difference in the price from the simple switch between Rh and Co. A slight gain in activity for a Rh-based catalyst might not prove enough to offset the price of using Rh instead of Co. Table I-1 presents the natural abundance in earth's crust and price of the most common transition metals that could be used for CO_2 reduction catalysis.

Table I-1 Price and Natural abundance of transition metals

Metal		Abundance in Earth's Crust[37] (ppm)	Price [38,39] (€/g)
vanadium	V	190	***
chromium	Cr	140	***
manganese	Mn	1100	$1.72 \cdot 10^{-3}$
iron	Fe	63000	$9.99 \cdot 10^{-5}$
cobalt	Co	30	$2.33 \cdot 10^{-2}$
nickel	Ni	90	$1.01 \cdot 10^{-2}$
copper	Cu	68	$5.20 \cdot 10^{-3}$
zinc	Zn	79	$1.46 \cdot 10^{-3}$
molybdenum	Mo	1.1	***
ruthenium	Ru	0.001	$1.63 \cdot 10^{+0}$
rhodium	Rh	0.0007	$2.72 \cdot 10^{+1}$
palladium	Pd	0.0063	$1.84 \cdot 10^{+1}$
silver	Ag	0.08	$5.19 \cdot 10^{-1}$
tungsten	W	1.1	***
rhenium	Re	0.0026	$3.36 \cdot 10^{+0}$
osmium	Os	0.0018	***
iridium	Ir	0.0004	$1.16 \cdot 10^{+1}$
platinum	Pt	0.0037	$3.58 \cdot 10^{+1}$
gold	Au	0.0031	$3.28 \cdot 10^{+1}$

***: data unavailable or the metal is not sold in its pure form (e.g. ferro tungsten).

The abundance of the metals used is also a key factor in terms of scalability, and usually correlates with prices (Table I-1). As a general rule, first-row transition metals are more abundant and cheaper than their second and third row counter parts. The cases of Mo and W are debatable since their natural abundance is "only" an order of magnitude less than Co, Ni, Cu or Zn, but "only" one order of magnitude more than that of silver. This consideration on the nature of the metal centre of the catalyst can be extended to the nature of the ligands chosen. Unless the catalyst is indefinitely stable, a ligand that is complicated, time-consuming and expensive to synthesise will offset the cost benefit of using an abundant cheap metal.

The last factor to consider when determining the merits of a catalyst is its selectivity. The selectivity of the catalyst is defined by the products of catalysis. Several carbon containing products can be envisioned as a result of CO_2 reduction, even without considering carbon-carbon coupling, (eq. I-5 to I-10), alongside H_2 formation from H^+ reduction (eq. I-11). In the following equations, the equilibrium potentials are given *vs.* NHE, in water, at pH 7, at 25°C, and at a pressure of 1 atm ($E_{NHE} = E_{SCE} + 0.24$ V $= E_{Ag/AgCl} + 0.28$ V).

$$CO_2 + 2\,H^+ + 2\,e^- \rightarrow CO + H_2O \qquad E° = -0.53\ V \qquad \text{(I-5)}$$

$$CO_2 + 2\,H^+ + 2\,e^- \rightarrow HCO_2H \qquad E° = -0.61\ V \qquad \text{(I-6)}$$

$$CO_2 + 4\,H^+ + 4\,e^- \rightarrow HCHO + H_2O \qquad E° = -0.48\ V \qquad \text{(I-7)}$$

$$CO_2 + 6\,H^+ + 6\,e^- \rightarrow CH_3OH + H_2O \qquad E° = -0.38\ V \qquad \text{(I-8)}$$

$$CO_2 + 8\,H^+ + 8\,e^- \rightarrow CH_4 + 2\,H_2O \qquad E° = -0.24\ V \qquad \text{(I-9)}$$

$$CO_2 + e^- \rightarrow CO_2^{\bullet -} \qquad E° = -1.90\ V \qquad \text{(I-10)}$$

$$2\,H^+ + 2\,e^- \rightarrow H_2 \qquad E° = -0.42\ V \qquad \text{(I-11)}$$

In a general sense, a catalyst is fully selective if it produces only one product. In the case of an electrocatalysts, more information on the selectivity can be obtained by determining the faradic efficiency. The faradic efficiency is the ratio (in %) of the number of electrons that are used towards making a desired product divided by the total number of electrons that are flowing through the electrode. In a system with 100% faradic efficiency, every electron that is injected in the system leads to productive chemistry and generation of product. For a photo-assisted catalytic system, the determination of the number of electrons transferred by the photosensitiser to the catalyst or other molecules in the system is not straightforward so a measure of the selectivity of the catalyst analogous to a faradic yield is harder to obtain.

With these considerations, we will now survey the literature for molecular homogeneous CO_2 reduction catalysts. For price and simplicity consideration, and given the vastness of this area of chemistry, we will restrict ourselves to homogeneous metals complexes of polypyridyl systems that have been reported to facilitate catalytic CO_2 reduction.

4. Metal-polypyridyl molecular homogeneous CO_2 reduction catalysts: state of the art

4.1. Introduction

In considering a synthetic platform for supporting catalytic centres for CO_2 reduction, the polypyridyl class of ligands offers many advantages. Polypyridyl ligands have been demonstrated to be redox active and could assist in mediating multi-electron transformations. Additionally, polypyridyl ligands are ubiquitous archetypes within inorganic complexes and have generally been shown to be stable and synthetically versatile. These ligands afford the ability to precisely control coordination geometries and electronic structures around a desired metal centre. Therefore, a brief literature review highlighting important precedents and developments of metal-polypyridyl complexes towards CO_2 reduction catalysis will be given.

This section will be divided by metal centre. Starting with the extremely well-studied Ru and Re catalysts, each subsection will present the major reports on the different polypyridyl platforms that have been studied on each metal. The reports will mostly be presented in a chronological manner, focusing on publications that make contributions to the deciphering the structures of active species as well as catalytic mechanisms.

4.2. Non-Abundant or precious metals: 4d and 5d transition metals

4.2.1. Polypyridyl complexes of ruthenium

The $[Ru(bpy)_2(CO)_n(X)_m]^{(2-m)+}$ family of compounds has received much attention as CO_2 reduction catalysts over the past decades. Electrochemical CO_2 reduction catalysed by $[Ru(bpy)_2(CO)_2]^{2+}$ and $[Ru(bpy)_2(CO)Cl]^+$ (see Figure I-12) was initially investigated by Ishida *et al*. in a H_2O/DMF (90:10, v:v) solvent mixture.[40,41] Within these reports, bulk electrolyses at −1.50 V *vs.* SCE yielded several different products depending on the pH of the solution. In slightly acidic conditions (pH = 6) the major products observed were a mixture CO and H_2, but under more basic conditions (pH = 9.5) formate was primarily produced.

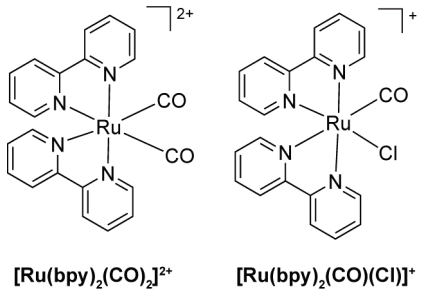

Figure I-12 Structure of the ruthenium polypyridyl catalysts reported by Ishida *et al.* in 1987.

They proposed $[Ru(bpy)_2(CO)(COOH)]^+$ to be the critical selectivity-determining intermediate, forming through the protonation of the CO_2 adduct described as $[Ru(bpy)_2(CO)(CO_2)]^0$ (Figure I-13). Under acidic conditions, $[Ru(bpy)_2(CO)(COOH)]^+$ can be further protonated to yield an

equivalent of H_2O and $[Ru(bpy)_2(CO)_2]^{2+}$. Subsequent two-electron reduction triggers the loss of CO and allows the complex $[Ru(bpy)_2(CO)]^0$ to coordinate a new molecule of CO_2. The formation of H_2 is proposed to arise through a different catalytic cycle, initiated by the protonation of the $[Ru(bpy)_2(CO)_2]^{2+}$ intermediate. In basic conditions, the selectivity determining intermediate, $[Ru(bpy)_2(CO)(COOH)]^+$, is proposed to react with a proton and two electrons to yield $HCOO^-$ and regenerate $[Ru(bpy)_2(CO)]^0$. Of note, this process directly regenerates the $[Ru(bpy)_2(CO)]^0$ intermediate without creating the $[Ru(bpy)_2(CO)_2]^{2+}$ complex that is proposed to be necessary for H_2 generation. This explains the observation of less H_2 being produced under conditions where formate is generated.

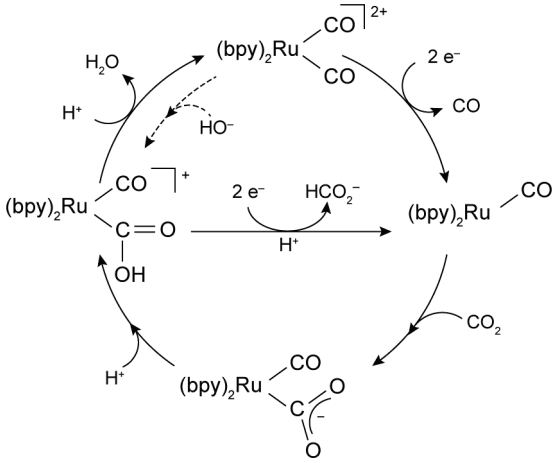

Figure I-13 Mechanism proposed by Ishida *et al.*, see references 40 and 41.

These proposed mechanisms are supported by the changes in the observed product distribution as a function of the pKa of the externally added acid source. As the pKa of the acid source increases the production of formate is greatly enhanced with up to 84.3% of formate reported when using $Me_2NH{\cdot}HCl$ whereas CO and H_2 are favoured in the presence of stronger acids.[40]

Despite these observations, an alternative mechanism for the formation of formate by this class of compounds was proposed by Pugh *et al.*[42] while studying the behaviour of *cis*-$[Ru(bpy)_2(CO)H]^+$ (Figure I-14) as a catalyst of the reduction of CO_2. Upon completion of preparative scale electrolyses of *cis*-$[Ru(bpy)_2(CO)H]^+$ under CO_2 reduction conditions, FTIR spectroscopy was used to identify *cis*-$[Ru(bpy)_2(CO)H]^+$ along with *cis*-$[Ru(bpy)_2(CO)(OC(O)H)]^+$ and *cis*-$[Ru(bpy)_2(CO)(NCCH_3)]^{2+}$ within the solution.

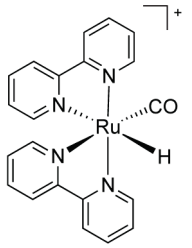

***cis*-[Ru(bpy)$_2$(CO)(H)]$^+$**

Figure I-14 Structure of the Ru-based catalyst studied by Pugh *et al.* (reference 42).

Based on the observation of these additional species in the reaction vessel, they proposed a mechanism of formate production through the direct insertion of CO_2 into the Ru–H bond (Figure I-15). The mechanism proposed by Pugh *et al.* was unique in that it suggested (i) that a Ru–H bond was critical to the production of formate (ii) that no direct CO_2 adduct to a Ru centre was necessary for formate production and (iii) that redox equivalents were stored on the polypyridyl ligands.

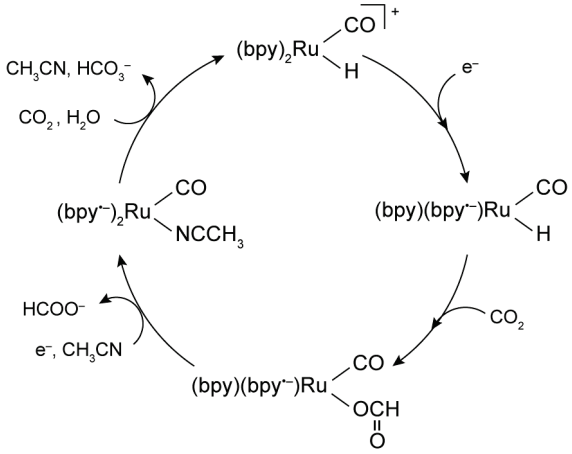

Figure I-15 Mechanism proposed by Meyer in 1991, see reference 42.

These ruthenium bisbipyridyl systems have also been shown to act as catalysts of the photosensitized reduction of CO_2 to formate and CO depending on the conditions, in the presence of $[Ru(bpy)_3]^{2+}$ as a photosensitizer in DMF/H_2O/TEOA (TEOA = triethanolamine) mixtures.[43,44] More recently the selectivity for CO or formate production was investigated as a function of CO_2 pressure and it was shown that CO production varies linearly with CO_2 pressure up to 150 bar, and CO production is enhanced in a biphasic water/DMF supercritical CO_2 mixture. Formate production on the other hand was independent of CO_2 pressure in the 10-150 bar range in water/DMF solutions.[45] These observations support the Ishida-mechanism for CO production through a direct Ru–CO_2 interaction, and support the Pugh-mechanism for formate production through CO_2 insertion into a Ru–H bond.

Elaborating further on Ru-bpy complexes as catalysts of the electrochemical reduction of CO_2, Chardon-Noblat *et al.*[46] demonstrated that *cis*(Cl)-[Ru(bpy)$(CO)_2Cl_2$] and *cis*(CO)-[Ru(bpy)$(CO)_2$(C(O)OMe)Cl] both act as CO_2 reduction electrocatalysts. They proposed that loss of a Cl^- could lead to the formation of a Ru–Ru dimer that could then catalyse CO_2 reduction to

CO alongside traces of formate. Additionally, they reported that *trans*(Cl)-[Ru(bpy)$(CO)_2Cl_2$] led to the formation of a polymeric film of [Ru(bpy)$(CO)_2]_n$ on the electrode, showing that the homogeneous or heterogeneous behaviour of the catalyst can be altered simply through the stereochemistry of the pre-catalyst in solution. [47]

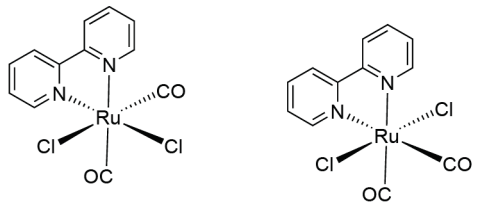

***cis*(Cl)-[Ru(bpy)$(Cl)_2(CO)_2$]** ***trans*(Cl)-[Ru(bpy)$(Cl)_2(CO)_2$]**

Figure I-16 Structure of the pre-catalysts studied by Deronzier and collaborators, reference 46 and 47.

In general, the observation that Ru-polypyridyl complexes act as catalysts for CO_2 reduction yielding primarily CO or formate as a product has resulted in this family of complexes being historically well-studied relative to complexes of other metals. The effects of utilising other polypyridyl ligands, beyond bipyridine, as well as mixing polypyridyl ligands with other ancillary ligands within Ru complexes have been heavily reported. For example, in 1985 Meyer and collaborators reported CO_2 electroreduction using $[Ru(tpy)(dppene)Cl]^+$ (dppene = cis-1,2-bis(diphenylphosphino)ethylene) (Figure I-17, left).[48] The only gaseous product observed after a bulk electrolysis in MeCN at −1.4 V *vs.* SCE for 1 h was CO. Deronzier, Ziessel and Chardon-Noblat reported in 2002 that the electrocatalytic reduction of CO_2 by *cis*- and *trans*-[Ru(tpy)$(CO)Cl_2$] (Figure I-17, right) yielded CO (60% faradic yield) and formate (10% faradic yield) in MeCN solutions containing 20% of water.[49] However, the authors described the catalyst activity to be lower than that of [Ru(bpy)$(CO)_2Cl_2$] complexes.

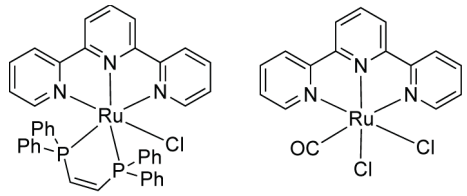

[Ru(tpy)(dppene)(Cl)] **[Ru(tpy)(CO)$(Cl)_2$]**

Figure I-17 Structure of the Ru-terpyridyl catalysts studied by Meyer (reference 48) and Deronzier (reference 49).

Recently, two new Ru-based polypyridyl complexes were assayed as CO_2 reduction catalysts: $[Ru(tpy)(bpy)(Solv)]^{2+}$ (Solv = solvent) and the related $[Ru(tpy)(Mebim\text{-}py)(Solv)]^{2+}$ (Mebim-py = 3-methyl-1-pyridylbenzimidazol-2-ylidene) which have been introduced in the context of a full device in section 3.2 of this chapter (the structures are given again Figure I-18).[50] The catalysts displayed remarkable activity in MeCN at −1.52 V *vs.* NHE. CO was observed as the major product, corresponding to 76% faradic efficiency after 5 h, with detectable traces of CO_3^{2-}/HCO_3^- and $HCOO^-$ (< 20%). The complexes of $[Ru(tpy)(Mebim\text{-}py)(Solv)]^{2+}$ and $[Ru(tpy)(bpy)(Solv)]^{2+}$ were also shown

to be competent proton reduction catalysts in the presence of $H_2PO_4^-$, allowing for the electrocatalytic synthesis of syngas (mixtures of CO and H_2) by electrolysing a CO_2-saturated MeCN solution with variable amounts of $H_2PO_4^-$ in solution.[51]

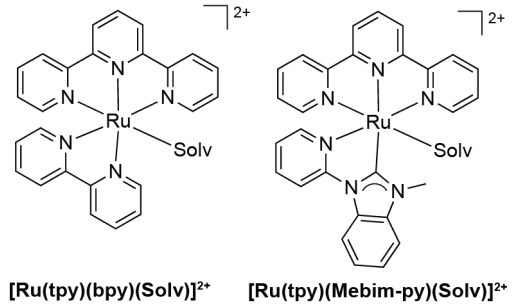

Figure I-18 Structure of the Ru based catalysts studied by Meyer in reference 50 and 51.

Very recently, Ott and collaborators have reported the synthesis of a library of $[Ru(tpy)(N^N)Cl]^+$ complexes (N^N = bipyridine-based ligand) with a variety of different bidentate ligands and assessed the corresponding electrocatalytic activities towards CO_2 reduction. Based on their assignments of the electrochemical features within CVs under N_2 and CO_2 atmospheres, the authors propose the novel hypothesis that the resting state of the catalyst involves a doubly reduced ancillary ligand sphere (Figure I-19).

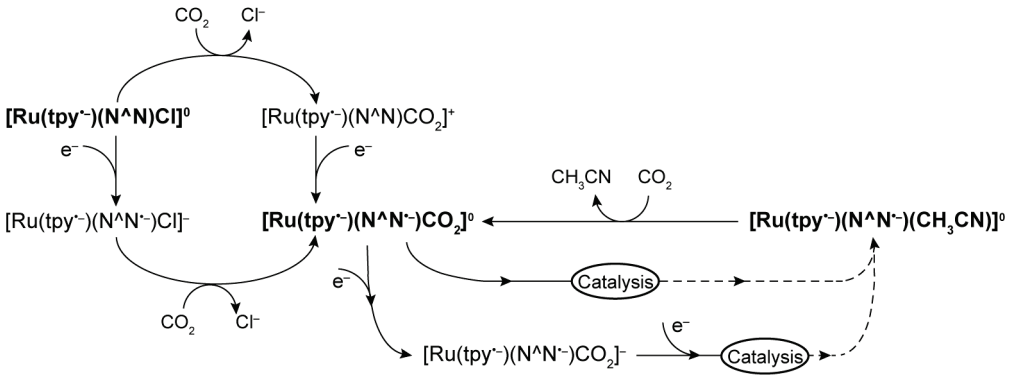

Figure I-19 Mechanism proposed by Ott in 2014 (reference 52).

To enter the catalytic cycles, an initial electron transfer is identified to generate $[Ru(tpy^{\bullet-})(N^N)Cl]^0$. A second reduction occurs which is accompanied by loss of the Cl^- ligand (the ligand loss can precede the electron transfer) to transiently create $[Ru(tpy^{\bullet-})(N^N^{\bullet-})]^0$, which quickly binds CO_2 to afford $[Ru(tpy^{\bullet-})(N^N^{\bullet-})(CO_2)]^0$. From this intermediate, catalysis can proceed via two different pathways. At highly reducing potentials, an additional reduction event is proposed to occur generating $[Ru(tpy^{\bullet-})(N^N^{\bullet-})(CO_2)]^-$ prior to CO_2 reduction to CO, with a subsequent electron required to regenerate the catalytic resting state, $[Ru(tpy^{\bullet-})(N^N^{\bullet-})(CH_3CN)]^0$. At less reducing potentials, direct catalysis is believed to occur from the $[Ru(tpy^{\bullet-})(N^N^{\bullet-})(CO_2)]^0$ intermediate to produce CO, with the regeneration of a $[Ru(tpy^{\bullet-})(N^N^{\bullet-})(CH_3CN)]^0$ intermediate through unspecified steps. Regardless of the pathway, the proposed mechanism by Ott and co-workers is unique in that it

supposes that reduced ancillary ligand spheres exist in the catalytic resting state, facilitating the observed multi-electron transformations.[52]

Despite the vast majority of Ru-polypyridyl systems behaving similarly, there have been reports of alternative products formed during CO_2 reduction catalysis. In 1994 Tanaka and collaborators reported early attempts at using a $[Ru(tpy)(bpy)(CO)]^{2+}$ architecture as a catalyst for the reduction of CO_2 (Figure I-20, left). They observed numerous different products including CO, formate, formaldehyde and methanol, among others.[53,54] In 2006 while investigating this system further, Gibson and collaborators isolated a Ru(tpy)(bpy)CO derivative containing a covalently bound carbonyl between the Ru and the N atom of one of the rings of the tpy ligand (Figure I-20, right). This compound was proposed as a possible intermediate in the mechanism of CO_2 reduction to CO, or other products, by Ru(tpy)(bpy) architectures, however no supporting evidence beyond the existence of this structure has been reported.[55]

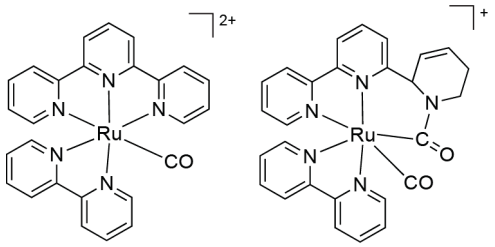

Figure I-20 Structure of the ruthenium catalyst studied by Tanaka in the 1990s (left) and the structure of a potential intermediate characterized by crystallography by Gibson in 2006 (right).

In 1998, Tanaka *et al.* investigated the effect of increasing further the presence of N atoms in the coordination environment by studying the catalytic activity towards CO_2 reduction of the mononuclear complex $[(bpy)_2Ru(dmbbbpy)]^{2+}$ and the binuclear complex $[(bpy)_2Ru(dmbbbpy)Ru(bpy)_2]^{4+}$ (dmbbbpy = 2,2'-bis(1-methylbenzimidazol-2-yl)-4,4'-bipyridine) (see Figure I-21, left).[56] They reported that an electrolysis of $[(bpy)_2Ru(dmbbbpy)]^{2+}$ in CO_2-staurated MeCN led to the formation of formate in the presence of 2.5% of added water in 89% faradic yields. However, in the absence of a proton source (using anhydrous MeCN as the solvent) a faradic efficiency of up to 64% for oxalate is observed. Additionally, the bimetallic species $[(bpy)_2Ru(dmbbbpy)\text{-}Ru(bpy)_2](PF_6)_4$ is reported to have a similar behaviour, with a faradic yield of 90% for formate in the presence of water, but 70% for oxalate in anhydrous solvent. Intriguingly, $[Ru(bpy)_2(btpy)]^{2+}$ (btpy = 2-(2-pyridyl)benzothiazole) was also shown to exhibit catalytic CO_2 reduction activity whereas 1-methylbenzimidazole analogue did not, as demonstrated by Begum and Pickup (see Figure I-21, right).[57] It is noteworthy that these systems seemingly are competent catalysts of the electrochemical reduction of CO_2 despite the absences of an open coordination site for CO_2 coordination. Overall, this study nicely demonstrates the ability to drastically tune product selectivity on the Ru-polypyridyl platform through the presence of H_2O.

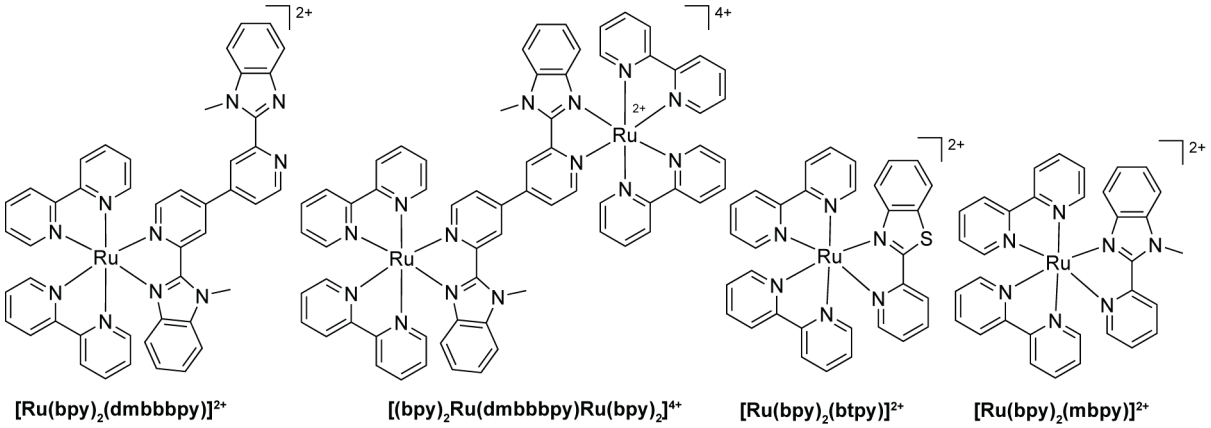

Figure I-21 Structure of the compounds reported by Tanaka in reference 56 and Begum and Pickup in reference 57.

Use of additional reagents has been shown to afford Ru-polypyridyl systems that are capable of reducing CO_2 to other less common products such as ketones. Tanaka and Mizukawa studied CO_2 reduction catalysed by $[Ru(bpy)(napy)_2(CO)_2]^{2+}$ (napy = 1,8-naphthyridine-κN) (see Figure I-22) with $(CH_3)_4NBF_4$ added to the medium.[58]

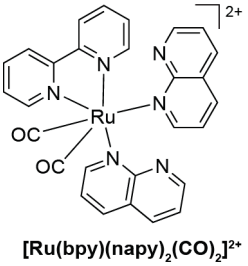

Figure I-22 Structure of the CO_2 reduction catalyst reported by Tanaka and Mizukawa (see reference 58).

They report up to 20% faradic efficiency for production of $CH_3C(O)CH_3$ and CO_3^{2-} according to the reaction:

$$2\ CO_2 + 2\ (CH_3)_4N^+ + 4\ e^- \rightarrow CH_3C(O)CH_3 + CO_3^{2-} + 2\ (CH_3)_3N \qquad \text{(I-12)}$$

Again, this proposed mechanism highlights the ability to vary product selectivity on the Ru-polypyridyl platform through the addition of extrernal reagents other than a direct proton source and provides an example of achieving more chemically complex products from CO_2 reduction through the use of additional reagents.

In summary, Ru-polypyridyl systems have been invaluable in the fundamental mechanistic study of CO_2 reduction catalysis to mostly formate and CO. The synthetic tuneability, general stability and high activity towards the catalysis of CO_2 reduction of this class of compounds have resulted in a wealth of reports in the literature as well as continuing investigations into various aspects of the reactivity.

4.2.2. Polypyridyl complexes of osmium

Building on the successes of the Ru systems, polypyridyl Os complexes have been studied for their properties as CO_2 reduction catalysts. In 1988, Meyer and collaborators reported the electrocatalytic reduction of CO_2 by *cis*-$[Os(bpy)_2(CO)H]^+$ in MeCN solutions.[59] CO was observed as the major product under anhydrous conditions, but up to 25% formate was observed in the presence of water in the MeCN solvent, as confirmed by a later study.[60] Reactivity of the *trans*- derivatives were also reported, and kinetic studies led to a proposed mechanism in which, similar to the analogous Ru system, *cis*-$[Os(bpy)_2(CO)H]^-$ is a key intermediate.

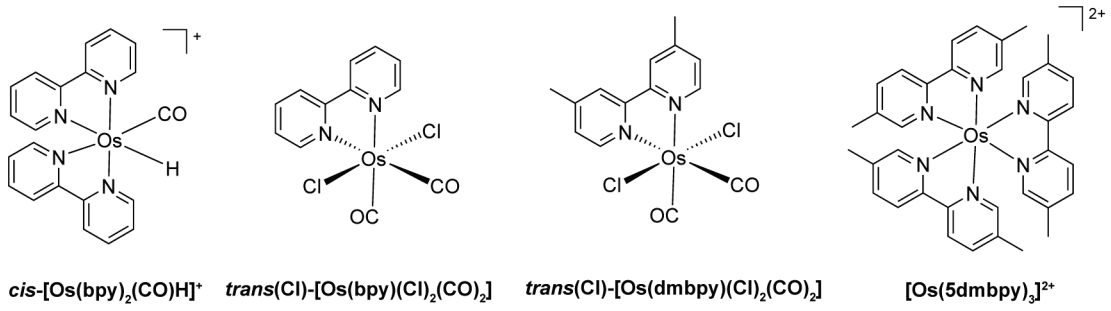

Figure I-23 Structure of Os-based CO_2 reduction catalysts reported in the literature.

Upon investigation of the behaviour of *trans*(Cl)-$[Os(bpy)(CO)_2Cl_2]$, Deronzier, Hartl and Chardon-Noblat showed that this Os complex polymerises on carbon electrodes in a manner related to the behaviour of the Ru derivative, and led to a Os-polymer wire-type catalysts competent for the reduction of CO_2 in aqueous media to CO and formate in 60% and 10% faradic yields respectively.[61] Deronzier and Chauvin subsequently reported the photocatalytic reduction of CO_2 by *trans*(Cl)-$[Os(bpy)(CO)_2(Cl_2)]$ and *trans*(Cl)-$[Os(dmbpy)(CO)_2(Cl_2)]$ in DMF, with 0.1 M $TBAPF_6$ as a supporting electrolyte and with 1 M TEOA as electron donor, yielding CO as the only product.[62] Addition of $[Ru(bpy)_3]^{2+}$ to create a photosensitised system increased the TON observed for CO by 30% after 4.5 h. With a 620 nm cut-off filter, however, Ishitani and collaborators recently reported no activity for the photocatalytic CO_2 reduction by $[Os(5dmbpy)_3]^{2+}$ (Figure I-23, right) in DMF-TEOA solutions with 0.1M 1,3-dimethyl-2-phenyl-2,3-dihydro-1*H*-benzo[*d*]imidazole (BIH) as the electron donor.[63]

Overall, while still in the active stages of development, the behaviour of Os-polypyridyl complexes towards CO_2 reduction closely mimics that of the more-studied Ru analogues.

4.2.3. Polypyridyl complexes of rhodium & iridium

Group 9 metal-polypyridyl complexes of second and third row transition metals were also investigated as catalysts of the electrochemical reduction of CO_2. Bolinger *et al.* initially investigated 2,2'-bipyridine complexes of both Rh and Ir, *cis*-$[M(bpy)_2X_2]^+$ (X = Cl^- or trifluoromethanesulfonate, $^-$OTf) in 1988.[64] Cyclic voltammograms of the complexes presented in Figure I-24 under CO_2 were

reported to give rise to increased cathodic current densities which the authors attribute to catalytic CO_2 reduction.

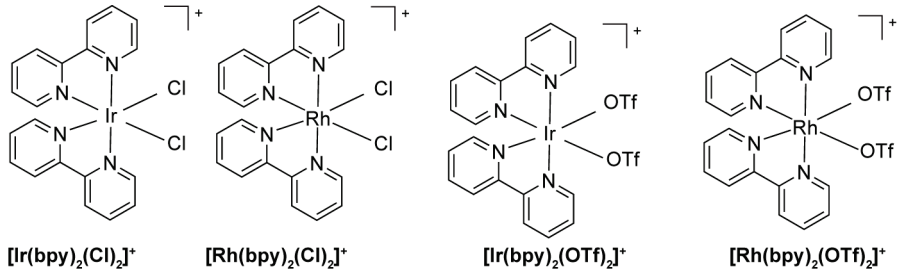

Figure I-24 Scheme of compounds studied by Bolinger *et al.* in 1988 (OTf = trifluoromethanesulfonate).

The Rh complexes were studied further by bulk electrolysis at −1.55 V *vs.* SCE in MeCN and mixtures of H_2 and formate were produced. The faradic yields varied depending on the total charge passed, but did not approach 100%. For example, a faradic yield of about 50% for formate and 20% for H_2 was found after 110 Coulombs were passed. Observations of the formation of a black precipitate during bulk electrolysis, coupled to the disappearance of the bpy-based reduction features by CV, have led the authors to propose a possible degradation by hydrogenation of the bpy ligands.

No added proton source was reported in this study, which led to speculations regarding the source of the requisite proton to lead to the formation of formate. A Hoffmann degradation of the electrolyte salt, [(*n*-Bu)$_4$N](PF$_4$), was proposed as the source of protons, following the reactions:

$$[Rh(bpy)_2]^- + CO_2 \rightarrow [Rh(bpy)_2CO_2]^- \quad \text{(I-13)}$$

$$[Rh(bpy)_2CO_2]^- + (n\text{Bu})_4N^+ \rightarrow [Rh(bpy)_2CO_2H] + H_3CCH_2CH{=}CH_2 + (n\text{Bu})_3N \quad \text{(I-14)}$$

$$[Rh(bpy)_2CO_2H] \rightarrow [Rh^{I}(bpy)_2]^+ + HCOO^- \quad \text{(I-15)}$$

Similar general behaviour of Rh and Ir complexes of the form $[M(bpy)Cp^*X]^+$ (Figure I-25) were reported by Deronzier *et al.* in 1997 for the electrocatalytic reduction of CO_2 in H_2O/MeCN mixtures.[65] The major products observed were formate and H_2 with trace amounts of CO detectable. The ratios of formate to H_2 generated were observed to vary with the applied potential and the water content of the MeCN solution.

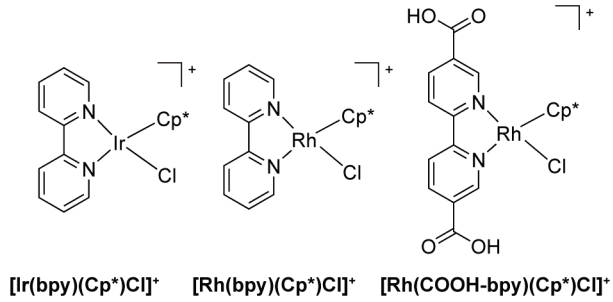

Figure I-25 Ir and Rh CO_2 reduction catalysts reported by Deronzier (left and centre, ref. 65) and Fontecave (right, ref. 66).

Although seemingly forgotten for almost 20 years, these Rh(bpy)Cp*-based catalysts were recently revisited in a homogeneous photosensitised CO_2 reduction system, and their activity for CO_2

reduction to H_2 and formate was confirmed and compared to the activity of the catalyst incorporated into the metal organic framework UIO-67.[66]

Investigation into polypyridyl ligands with greater denticity have been reported, as tridentate polypyridyl complexes of Rh and Ir were also investigated as catalysts for the reduction of CO_2. $Rh(tptz)Cl_3$, $Rh(tpy)Cl_3$ and Rh(tpy)(bpca) (see Figure I-26) were investigated by Paul *et al.* and were reported to catalyse the reduction of CO_2 to formate in DMF at potentials ranging from −1.26 V to −1.44 V *vs.* SCE. [67,68]

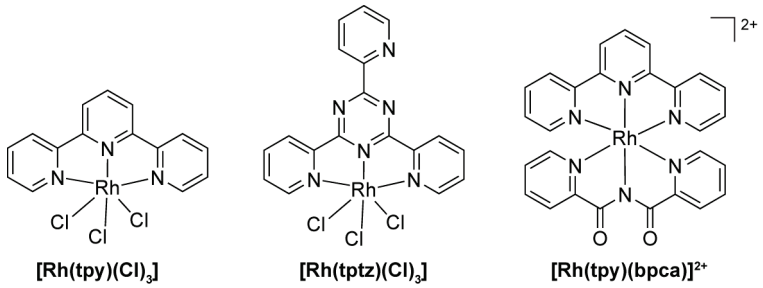

Figure I-26 Structure of the complexes studied by Paul (reference 69 and 70).

Whereas a general observation can be made that Ir and Rh complexes are often more selective for formate production over other potential carbon containing products of CO_2 reduction, this need not always be the case. Interestingly, related complexes of Ir and tpy ligands (Figure I-27) with phenylpyridine-based ligands are reported as photocatalysts and electrocatalysts for the reduction of CO_2 to CO in MeCN solutions, even in the presence of water. [69,70]

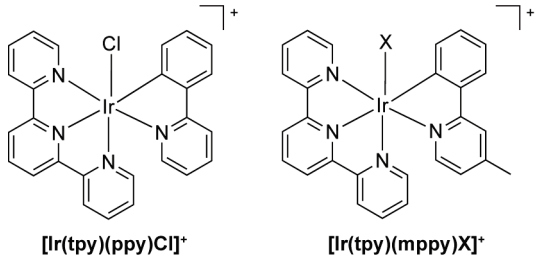

Figure I-27 Structure of the Ir catalysts studied by Ishitani in 2013 (left) and Rieger in 2014 (right, X = Cl^- or I^-).

The proposed mechanism (eq. I-16 to I-19) for the production of CO highlights the redox active nature of the tpy backbone, which allows the storing of reducing equivalents (D = sacrificial electron donor, TEOA):[69]

$$[Ir(tpy)(ppy)Cl] + D + h\nu \rightarrow [Ir(tpy^{\bullet -})(ppy)Cl] + D^+ \quad \text{(I-16)}$$

$$[Ir(tpy^{\bullet -})(ppy)Cl] + H^+ + e^- \rightarrow [Ir(tpy)(ppy)H] + Cl^- \quad \text{(I-17)}$$

$$[Ir(tpy)(ppy)H] + D + h\nu + CO_2 \rightarrow [CO_2\ adduct] + D^+ \quad \text{(I-18)}$$

$$[CO_2\ adduct] + H^+ + e^- \rightarrow [Ir(tpy)(ppy)H] + CO \quad \text{(I-19)}$$

$$[CO_2 \text{ adduct}] + [Ir(tpy^{\bullet -})(ppy)H] \rightarrow \text{Ir dimer} \quad \text{(I-20)}$$

Details regarding the nature of the proposed electron transfers that do not involve light absorption are not clear, but it is speculated to involve disproportionation reactions. The authors also propose a M–H bond to be an intermediate for CO_2 reduction to CO as the product. This is in stark contrast to that which is proposed for Ru-based systems, wherein protonation of a metal-bound CO_2 yields CO, and insertion of CO_2 into a M–H bond affords formate. Finally, this work identifies the formation of an inactive Ir dimer during the course of catalysis (eq. I-20) which limits the overall system activity.

4.2.4. Polypyridyl complexes of rhenium

The most studied Re catalysts for CO_2 reduction are based on the $Re(bpy)(CO)_3X$ class of compounds, that can act as both a photo- and electrocatalyst. Lehn, Ziessel and Hawecker[71,72,73] initially studied this family of compounds in the early 1980s. They reported that $Re(bpy)(CO)_3Cl$ (Figure I-28) reduces CO_2 to CO electrochemically in a DMF/water mixture (90:10, v:v) with Et_4NCl as supporting electrolyte at –1.25 V *vs.* NHE on a glassy carbon electrode. They observed over 90% faradic efficiency for CO production and that catalysis occurs in the one-electron reduction wave at –1.25 V *vs.* NHE, which suggests $[Re^0(bpy)(CO)_3Cl]^-$ is the active catalytic species. One of the drawbacks pointed out by the authors is that if the amount of water in the solvent is increased, the selectivity for CO_2 reduction to CO was decreased in favour of H^+ reduction to H_2. An additional drawback was the relatively low reported TOF of 21.4 h^{-1} at –1.25 V *vs.* NHE for this initial Re-based electrochemical system.

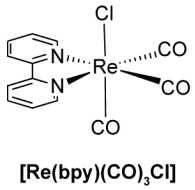

Figure I-28 Structure of $Re(bpy)(CO)_3Cl$ first reported for CO_2 reduction in 1983 by Lehn, Ziessel and Hawecker.

Following these early observations, plenty of bpy-derivatives of $Re(CO)_3(L)Cl$ were assayed as catalysts for CO_2 reduction. These systems are numerous,[74] have been studied extensively, and generally behave in similar fashions. Additional details regarding other derivatives can be found within more comprehensive reviews of the field.[75,76] Within the context of this discussion, landmark studies and unique reports regarding the $Re(bpy)(CO)_3$ class of compounds will be emphasised.

In 1985, Meyer and collaborators studied the electrochemical reduction of CO_2 catalysed by $Re(bpy)(CO)_3Cl$ in MeCN and began proposing mechanistic models.[77] Under an inert atmosphere, the authors report two one-electron electrochemical reductions of $Re(bpy)(CO)_3Cl$. The first reduction event at –1.3 V *vs.* SCE is reversible and was attributed to a reduction of the bpy ligand. The second reduction, around –1.6 V *vs.* SCE, is irreversible and is assigned to a $Re^{I/0}$ metal-centred reduction. Two pathways were proposed for the catalytic reduction of CO_2 to CO and CO_3^{2-}, operating through

either a one- or two-electron initial reduction of the catalyst (Figure I-29). Going down the two-electron reduction path (Figure I-29, right), transient formation of the two-electron reduced $[Re(bpy^{\bullet-})(CO)_3Cl]^{2-}$ complex is claimed to be accompanied by fast loss of a Cl^- ligand and an intramolecular electron transfer from the reduced bpy ligand to the Re centre, to formally yield $[Re(bpy)(CO)_3]^-$. In the one-electron pathway (Figure I-29, left), a slow intramolecular electron transfer in $[Re(bpy^{\bullet-})(CO)_3Cl]^-$resulting in $[Re^0(bpy)(CO)_3Cl]^-$ is required before the slow loss of the Cl^- ligand. This behaviour provides the basis for the difference between the proposed one-electron and two-electron reduction mechanisms depicted in Figure I-29. At applied potentials where the $Re(bpy)(CO)_3Cl$ can be reduced twice, chloride loss is triggered by the two-electron transfer and followed by reduction of CO_2 to CO. At applied potentials where $Re(bpy)(CO)_3Cl$ can only be reduced once, chloride loss proceeds by an intramolecular electron transfer that generated a Re^0 centre capable of interacting with CO_2 in a less reduced state than proposed in the two-electron pathway.

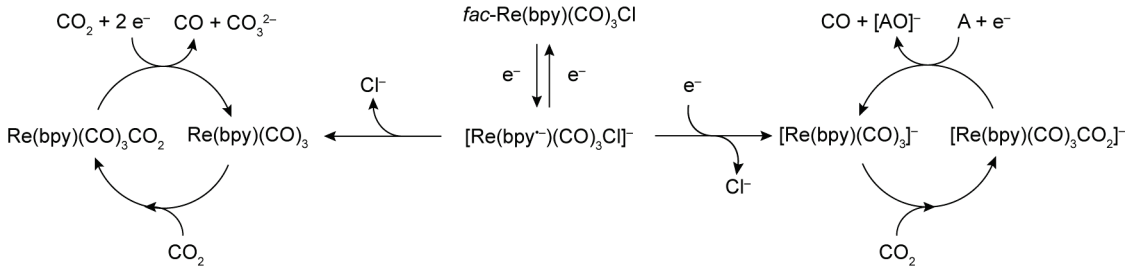

Figure I-29 One- and two-electron pathway mechanisms proposed by Meyer in 1985. "A" is an oxide ion acceptor.

In 1996 Johnson and collaborators studied the electrochemical reduction of CO_2 to CO and CO_3^{2-} catalysed by the $Re(L)(CO)_3X$ class of complexes using IR spectroelectrochemistry.[78] They report that the two-electron reduction to form of $[Re(bpy)(CO)_3]^-$ is necessary for interaction with CO_2 in MeCN. In weakly coordinating solvents such as THF, they observe that the one-electron pathway becomes feasible as solvent exchange with the chloride ligand is more likely. In the case of $Re(dmbpy)(CO)_3Cl$, (Figure I-30, right) the five coordinate Re(I) radical anion $[Re(dmbpy)(CO)_3]^{\bullet-}$ can react with CO_2 directly, even in MeCN, via the one-electron pathway. These spectroscopic results demonstrate that both mechanistic pathways can be operational and are dependent upon solvent conditions as well as the nature of the bipyridyl ligand.

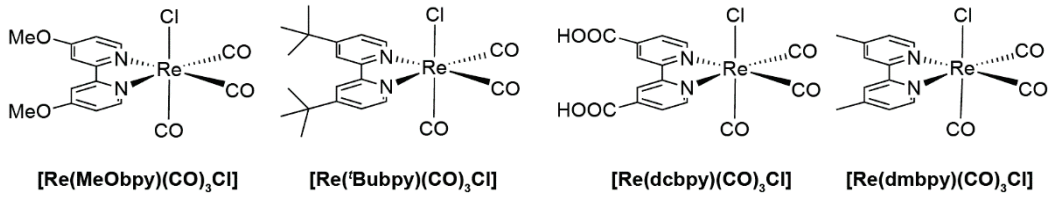

Figure I-30 Figure of the different Re complexes evaluated by Kubiak in 2010 (reference 79) and Johnson in 1996 (reference 78).

More recently, in 2010, Kubiak and coll. reported a systematic study of the ligand variations, using $Re(CO)_3(L)Cl$ complexes (L = bpy, dcbpy, dmbpy, 4,4'-di-tert-butyl-bpy, or 4,4'-dimethoxy-

bpy, see Figure I-30) in MeCN with [TBA]OH (tetrabutylammonium hydroxide) as the supporting electrolyte, and showed the effects of electron donating or withdrawing substituents on the 4,4' position of the bpy ligand on the catalytic activity as observed by cyclic voltammetry.[79] They observed an increased catalytic current for more donating substituents. The best activity, as defined by a calculated turnover frequency corresponding to a measured peak catalytic current, was obtained with the ^{t}Bu-substituted derivative. It was hypothesised that the increased activity originated from the steric strain of the ^{t}Bu functionality, which inhibits the formation of an inactive dimer $[Re^I(L^{\bullet-})(CO)_3]_2$. This was in agreement with IR spectroelectrochemistry data in which, at potentials were Re^I could be reduced to Re^0, $[Re^0(CO)_3(^tBu\text{-}bpy^{\bullet-})]^-$ was identified to be the major species present, but in the case of the parent bpy ligand, the inactive dimer $[Re^I(bpy^{\bullet-})(CO)_3]_2$ was found to be the resting state of the system. Therefore, in the absence of steric strain on the polypyridyl ligand, an inactive dimer forms of the type $[Re^I(L^{\bullet-})(CO)_3]_2$, which apparently inhibits the second electron transfer required for catalysis. This is strong evidence highlighting the potential importance of monomeric active catalysts for this family of Re complexes.

The deactivation pathways of these catalysts were studied in more detail electrochemically in 2012 by Kubiak and collaborators.[80] They report that the inactive dimer $[Re(bpy)(CO)_3]_2$, which is supported by a Re–Re bond, is stable towards one-electron reductions, but that a second reduction event is required to break the metal–metal bond. They postulate that the formation of this dimer under electrochemical reduction of CO_2 constitutes an unproductive pathway that deactivates the catalyst. Further studies on the photochemical deactivation pathways of $Re(dmbpy)(CO)_3Cl$ were undertaken recently by Rieger and collaborators, and have confirmed that the two main photodeactivation pathways involve $[Re(dmbpy^{\bullet-})(CO)_3Cl]^-$, with monovalent Re and a radical anion on the ligand, This structure represents an electronic configuration required for catalysis yet is also susceptible to deactivation through dimerisation.[81]

The effect of adding weak Brönsted acids to related electrochemical Re-based systems has been studied by Wong and collaborators in 1998.[82] The authors report that the rate of electrocatalytic reduction of CO_2 by $[Re(bpy)(CO)_3(py)]^+$ (Figure I-31) in MeCN can be enhanced by increasing the pKa of an external acid source (water, MeOH, trifluoroethanol and phenol). Under the optimised conditions, the authors observed the electrocatalytic reduction of CO_2 to CO in nearly 100% faradic efficiency, and identified an apparent order in protons for the reaction of two.

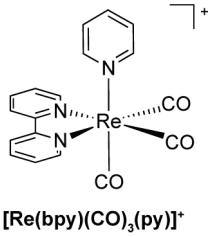

[Re(bpy)(CO)$_3$(py)]$^+$

Figure I-31 Structure of the Re catalyst studied by Wong in 1998.

As these Re-based systems have extensive experimental data available as a guidepost, the mechanism of CO_2 reduction by $Re(bpy)CO_3(X)$ has been thoroughly studied computationally as well. The three major studies focus on explaining the selectivity between CO_2 and water reduction,[83] the influence of weak Brönsted acids,[84] and the differences between the Re system and an analogous Mn-based system.[85] Specifically in regards to mechanistic considerations, DFT analysis indicated that selectivity for CO_2 reduction over H^+ reduction is obtained from the $[Re(bpy)(CO)_3]^-$ structure through an essentially barrier-less interaction with CO_2 as opposed to an approximately 21 kcal/mol unfavourable interaction with H^+ (Figure I-32).[83] The resulting $[Re(bpy)(CO)_3(CO_2)]^-$ intermediate is then computed to be susceptible to a barrier-less protonation to yield $Re(bpy)(CO)_3(CO_2H)$ as an intermediate structure. From this point, another electron transfer is required and subsequent protonation is calculated to be rate limiting. The order of occurrence for this proton transfer and electron transfer appear virtually indistinguishable by the DFT methods used and would likely dependent upon experimental conditions used.

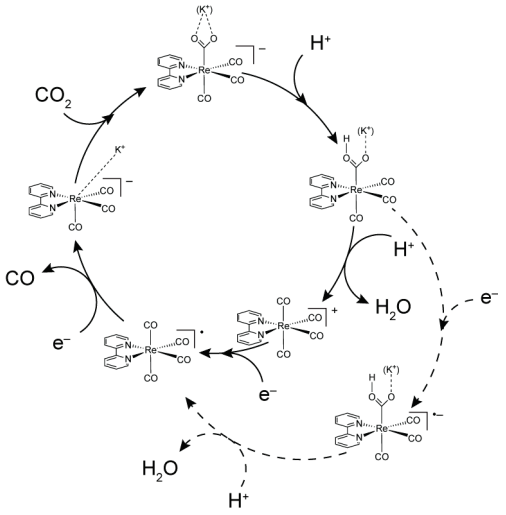

Figure I-32 Mechanism proposed by Kubiak and Carter (reference 83).

Despite significant theoretical efforts, most computed reports involving Re-complexes target the reduction of CO_2 and excess H^+ to CO and H_2O. However, it is experimentally observed that CO_2 reduction catalysed by these classes of compounds often results in the formation of CO and CO_3^{2-} as a result of the electronic disproportionation of two equivalents of the one-electron reduced form of CO_2. Since the generation of $[CO_2]^{\bullet-}$ is thermodynamically unfavourable and requires more reducing potentials than are used experimentally, it is assumed that such a mechanism would likely necessitate a bimetallic disproportionation of two reduced Re-CO_2 complexes. In 2014, to evaluate this bimetallic mechanism, Gilson, Kubiak and collaborators synthesised a modified version of the $[Re(bpy)(CO)_3]^+$ architecture by including substituents in proximity of the active site of the metal capable of hydrogen-bonding (Figure I-33). The ligand scaffold was designed with the view of helping to preassemble two Re-centres in close proximity and promote the electrocatalytic disproportionation of two molecules of CO_2 to CO and CO_3^{2-} pathway as opposed to reducing CO_2 and excess H^+ to CO and water.[86]

Although simultaneously promoting the formation of an inactive dimer was plausible, this synthetic modification resulted in increased activity and supported the role of bimetallic constructs for the formation of CO and CO_3^{2-} from two equivalents of CO_2.

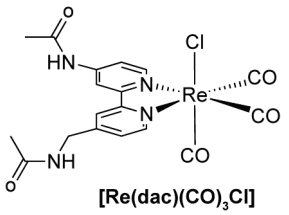

Figure I-33 Structure of the Re catalyst studied by Kubiak in 2014.

Recently, Ishitani and collaborators have made great strides in extending these Re catalysts towards photochemical systems and have reported a supramolecular Ru-Re complex that can photocatalytically reduce CO_2 to formic acid when photolysed in aqueous solution with an ascorbate sacrificial electron donor (Figure I-34).[87] The system also produces a small amount of H_2 and CO (for 25 TON of HCOOH, 4.6 TON of H_2 and 1.2 of CO are observed). This behaviour is strikingly different in that the product observed is formic acid and not CO, even though the same catalyst under irradiation in DMF/TEOA solutions mixed with BNAH yields CO as the only CO_2 reduction product. It is also remarkable that the system can operate in water without producing H_2 as the major product. Ultimately, in aqueous conditions, ligand substitution is observed on the photoactive Ru centre, and is believed to lead to catalyst deactivation.

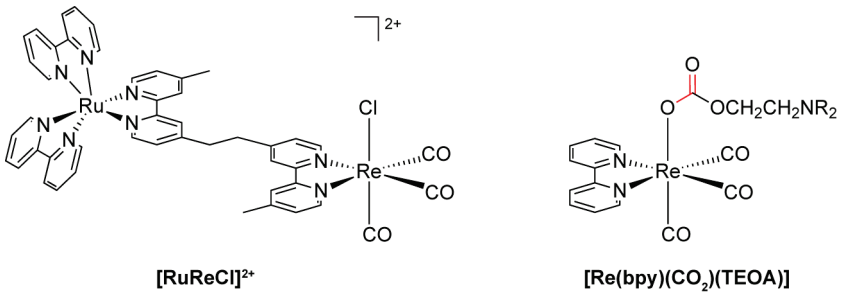

Figure I-34 Schematic representation of the supramolecular Ru-Re system developed by Ishitani in 2015 (left) and structure of the Re-CO_2-TEOA complex proposed in 2013 (right).

Ishitani and Morimoto also reported that the nature of the active catalyst within photosensitised $Re(bpy)(CO)_3(X)$ systems occurring in solution mixtures of DMF/TEOA is a $Re(bpy)(CO)_3(CO_2\text{-TEOA})$ species shown in Figure I-34 (right). The formation of this species was shown to be very effective, and allowed for trapping of low concentrations of CO_2, even in air.[88]

Variations of the system with tpy ligands instead of bpy have also been evaluated but reports are more limited. Efforts indicate that the synthesis of $Re(tpy)(CO)_x$ compounds are not easy, as several attempts to isolate these species have yielded a bidentate tpy ligand chelating the Re centre; $Re(\kappa^2\text{-tpy})(CO)_3Cl$. As an example, the complex $Re(\kappa^2\text{-(phenol-tpy)})(CO)_3Cl$ can be synthesised, in

which a tpy ligand coordinates to the Re only through two pyridines, with the third ring left "dangling", allowing for the coordination of the tricarbonyl motif (Figure I-35, left). Under illumination with a 300 W Xe lamp with an IR filter and a 389 nm cut-off filter, in CO_2-saturated DMSO in the presence of TEOA, the complex was shown to catalyse the photoreduction of CO_2 to CO, albeit at much smaller rates than the parent $Re(bpy)(CO)_3Cl$. Interestingly, no activity was observed photochemically with DMF as a solvent. By electrochemistry, cathodic current was observed to increase under CO_2 reduction conditions in MeCN solutions, but limited additional details are available.[89]

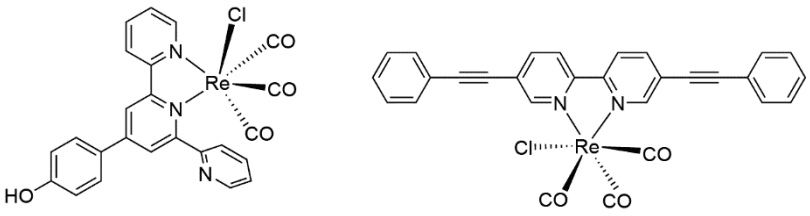

[Re(κ²-(phenol-tpy))(CO)₃(Cl)] [Re(bpebpy)(CO)₃(Cl)]

Figure I-35 Variations on the $Re(bpy)(CO)_3$ framework studied by Li in 1992 (left) and Sariciftci in 2012 (right).

In 2012 another modification to the bpy framework was reported, using the ligand bpebpy (5,50-bisphenylethynyl-2,20-bipyridyl) in the complex *fac*-$(bpebpy)Re(CO)_3Cl$ as a catalyst for the electroreduction of CO_2 to CO (Figure I-35, right).[90] The authors reported a cathodic current increase under CO_2 at –1.75 V *vs.* NHE and a faradic efficiency for CO_2 reduction to CO of 45%.

In summary, reports on Re-polypyridyl complexes as CO_2 reduction catalysts are plentiful and primarily involve a family of complexes with a general structure of $Re(bpy)(CO)_3(X)$. These catalysts are stable and synthetically tuneable, which has afforded the opportunity to evaluate the mechanism of CO_2 reduction in detail. As these systems predominately and selectively produce CO from CO_2 reduction, in depth mechanistic considerations regarding factors governing selectivity for CO over other carbon containing products as well as CO_2 reduction over H^+ reduction are unavailable. Since Re-polypyridyl catalysts have been demonstrated to be quite active in both electrocatalytic and photocatalytic systems, numerous ligand modifications have been reported. However, these modifications predominately involve the electronic tuning of the parent bpy ancillary ligand, with significantly fewer reports towards the use of other polypyridyl structures of higher denticity or different coordination geometries.

4.2.5. Polypyridyl complexes of molybdenum and tungsten

Recently the $[M(bpy)(CO)_3X]$ architecture was extended to Mo and W based catalysts in 2014. $[M(bpy)(CO)_4]$ complexes were developed and assayed as CO_2 reduction catalysts (Figure I-36).[91] Mo- and W-tetracarbonyl complexes with bpy and ^{t}Bu-bpy, reported by Kubiak and collaborators, were shown to be catalysts for the reduction of CO_2 to CO in MeCN, even in the absence of a proton source. The TOF reported appear modest (on average 2 s^{-1}) compared to the ones reported for Re in the

presence of TFE (> 300 s^{-1}). The main product observed during bulk electrolysis is CO, although traces of H_2 are observed as well, usually < 3%. These remain the only examples to date of Mo and W polypyridine-based homogeneous catalysts of the reduction of CO_2.

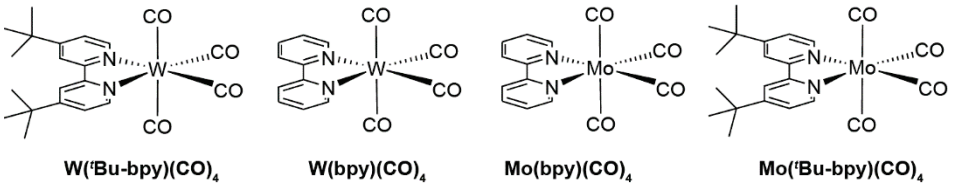

Figure I-36 Structure of the Mo and W complexes studied by Kubiak in 2014 for CO_2 reduction.

4.3. Abundant base metals: 3d transition metals

4.3.1. Polypyridyl complexes of manganese

Following the activity observed with $[Re(bpy)(CO)_3]^+$ catalysts, the Mn-based analogues, $Mn(bpy)(CO)_3Br$ and $Mn(dmbpy)(CO)_3Br$, were synthesised and assessed for CO_2 reduction in 2011 by Deronzier and coll. (Figure I-37).[92] The first reports indicated remarkable activity at potentials of −1.70 V *vs.* $Ag/AgNO_3$, but only in the presence of a proton source (10% of water added to the MeCN solvent). The major product observed was CO, with only traces of H_2 observed after 4 h of bulk electrolysis. However, at longer time points (22 h of electrolysis) the production of H_2 increases to as high as 15% of the total faradic yield.

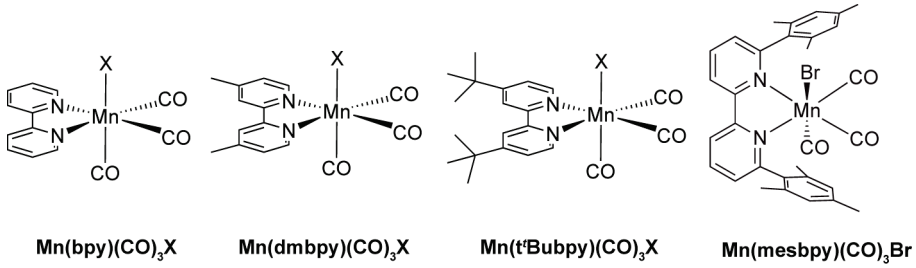

Figure I-37 Structure of the various Mn-based catalysts studied by Deronzier and Kubiak (X = Cl or Br).

Building on this report, the group of Kubiak made strides to understand the influence of protons on the catalytic activity by studying the effect of weak Brönsted acids in solution,[93] as well as the influence of the bulkiness of the substituents on the bpy rings using t^tBubpy and 6,6'-dimesityl-2,2'-bipyridine (mesbpy) as depicted in Figure I-37. As was the case in the analogous Re-systems, they demonstrated a tremendous increase of the activity by inclusion of ligands with more steric strain, and attributed this behaviour to the inhibition of the formation of an inactive Mn-dimer during catalysis.[94] Subsequently, the mechanism was probed by experimental[95,96] and computational[97,98] methods by several groups. The general experimental and theoretical results regarding the mechanism are comparable to the reports involving the analogous Re-systems previously discussed.

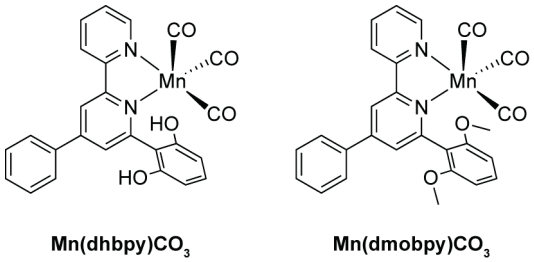

Figure I-38 Structure of the catalysts reported by Gobetto in 2014.

Recently a Mn-based system with a variation on the bpy ligand was tested. The ligands 4-phenyl-6-(1,3-dihydroxybenzen-2yl)-2,2'-bipyridine (dhbpy) with a local proton source, and the related 4-phenyl-6-(1,3-dimethoxybenzen-2yl)-2,2'-bipyridine (dmobpy), which acts as a control without the local proton source, are presented in Figure I-38.[99] The $Mn(dhbpy)(CO)_3Br$ complex was

reported to catalyse the electrochemical reduction of CO_2, even in the absence of an external proton source. In contrast, the methoxy derivative showed no activity under the same conditions. These results confirmed the influence of the alcohol group as an effective local proton source. Interestingly, the inclusion of a local proton source afforded a more complicated mixture of products, with both CO and formate being detected with 70% and 22% faradic efficiency respectively compared to the Deronzier catalyst which selectively produces CO as the only carbon containing product.[92] No further comment has been reported regarding this change in selectivity.

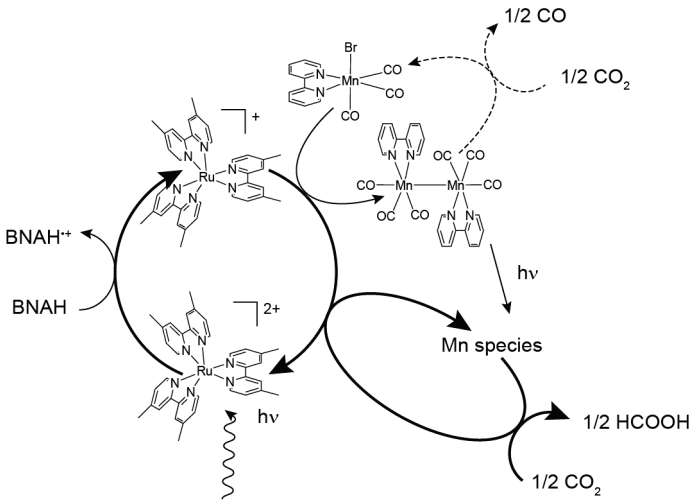

Figure I-39 Proposed catalytic cycle for the photosensitized catalytic reduction of CO_2 to formate and CO by $Mn(bpy)(CO)_3Br$. The main path producing formate is represented in bold arrows.

Given the light sensitivity of the $[Mn(bpy)(CO)_3]^+$ derivatives, photosensitisations with a $[Ru(dmbpy)_3]^{2+}$ proved to be an interesting and unusual case. Whereas direct photosensitisation of the $Mn(bpy)(CO)_3Br$ catalyst would be expected to yield CO as the only product (as observed electrocatalytically), it was shown that irradiation of $Mn(bpy)(CO)_3Br$ leads to the formation of an intermediate during photocatalysis. This intermediate can degrade under irradiation to yield a different Mn-containing catalyst that was reported to be capable of selectively catalysing the reduction CO_2 to formate (Figure I-39).[100] Thus, whereas the directly analogous Re systems give CO as the primary product of CO_2 reduction with very few counter-examples, the Mn-derivatives have already been shown to be capable of producing formate in addition to CO. Although there are currently fewer reports on Mn-bpy catalysts for CO_2 reduction, the studies to date suggest that Mn-bpy platforms are possibly more susceptible to product selectivity tuning via simple system modifications.

4.3.2. Polypyridyl complexes of iron

Surprisingly, very few reports of Fe-polypyridyl catalysts for the reduction of CO_2 exist, even though the Fe-porphyrin family is among the most active homogeneous CO_2 reduction catalysts reported in the literature.[101,102]

Durand and collaborators initially reported the electrocatalytic reduction of CO_2 by $[Fe(phen)_3]^{2+}$ in DMSO at −1.40 V *vs.* SCE with CH_4 as the only gaseous product observed in 1988.[103]

Iron complexes based on phenanthroline derivatives (Figure I-40) were later investigated for their possible electrocatalytic CO_2 reduction activity. $[Fe(dophen)(N\text{-}MeIm)_2]^+$ and the related [Fe(dophen)(Cl)] are reported to be electrocatalysts of the reduction of CO_2 into mixtures of CO, formate, and oxalate in DMF and DMSO. During bulk electrolyses in the absence of an acid source, at –2.0 V *vs.* Fc^+/Fc, formate is the major product. Addition of weak Brönsted acids is reported to increases overall catalytic activity but does not lead to better selectivity, as formate remains the major product but upwards of 40% faradic yield of either H_2 or CO is found.[104]

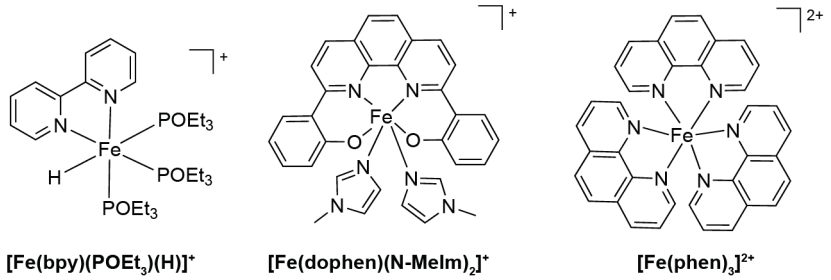

Figure I-40 Structure of Fe catalysts studied by Chen *et al.* in 2010 (left), Pun *et al.* in 2002 (centre) and Durand in 1988 (right).

Preliminary study of the electrocatalytic activity of $[Fe(bpy)(P(OEt_3)_3H]^+$ in MeCN showed current enhancement under CO_2 at an applied potential beyond two reduction features, at about –1.60 V *vs.* Ag/AgCl, suggesting that the two-electron reduced species is a potential CO_2 reduction catalyst. However, no carbon containing products were identified in this study.[105]

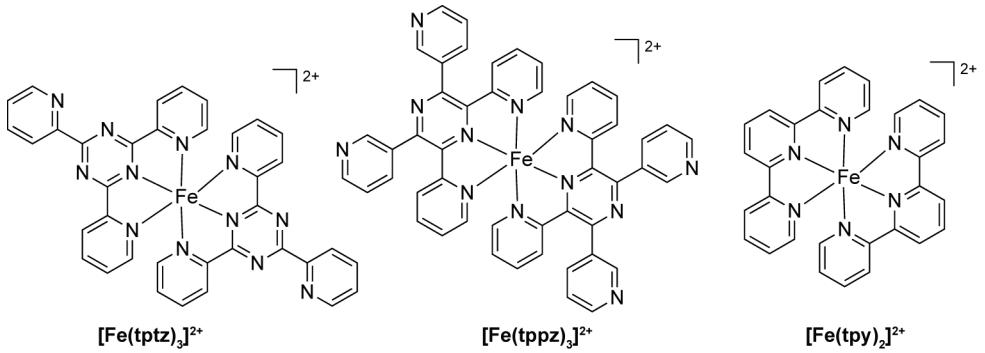

Figure I-41 Fe-based CO_2 reduction catalysts reported by Abruña in the 1990s.

In 1992, Abruña and collaborators reported that the cyclic voltammograms of $[Fe(tppz)_2]^{2+}$, $[Fe(tpy)_2]^{2+}$ and $[Fe(tptz)_2]^{2+}$ (Figure I-41) in DMF (0.1M TBAP as a supporting electrolyte) exhibited current enhancement under CO_2 starting at –1.56, –1.15 and –1.38 V *vs.* SCE respectively. The authors ascribed this behaviour to catalytic activity for the electrochemical reduction of CO_2, however no bulk electrolysis or product analysis was reported.[106] This behaviour was confirmed by the authors in 1994 for $[Fe(tpy)_2]^{2+}$ with an observed current enhancement of 100% at –1.13 V *vs.* SCE in DMF (0.1M TBAP as supporting electrolyte) and 500% at –1.27 V *vs.* SCE. Both electrochemical events are proposed to be ligand-based processes.[107]

On the whole, the general class of Fe-polypyridyl complexes have offered promising preliminary results as potential catalysts of the electrochemical reduction of CO_2. However, there remains a dearth of reports towards understanding the seemingly random trends in product selectivity as well as strategies towards increasing system stability.

4.3.3. Polypyridyl complexes of cobalt

Investigations into the behaviour of Co-polypyridyl complexes as catalysts for CO_2 reduction began with a report by Lehn and Ziessel in 1982.[108] In this initial report, photosensitised systems were evaluated with $[Ru(bpy)_3]^{2+}$ as the photosensitiser in CO_2-saturated solutions of aqueous MeCN (20% H_2O) and TEOA as a sacrificial electron donor. As for a catalyst, no discrete molecular species was pre-synthesised and characterised, but rather variable concentrations of $CoCl_2$ and bpy were added to the mixture and assumed to form Co-bpy complexes in situ (presumed to have the chemical identity $[Co(bpy)_3]^{2+}$). Utilizing a 400 nm cut-off filter, photolyses of these systems resulted in the formation of mixtures of H_2 and CO. Upon varying the ratios of bpy:$CoCl_2$, the general trend was observed wherein larger amounts of additional bpy ligand in solution significantly decreased the amount of CO produced but increased production of H_2. Interestingly, under the same conditions, simply replacing the $CoCl_2$ salt with $RhCl_3$, $NiCl_2$, $CuCl_2$ or K_2PtCl_4 did not result in any observable reduced carbon products. This report was the first indication that Co-polypyridyl complexes could be potentially used in catalytic systems for CO_2 reduction and possibly generated in straightforward *in situ* procedures.

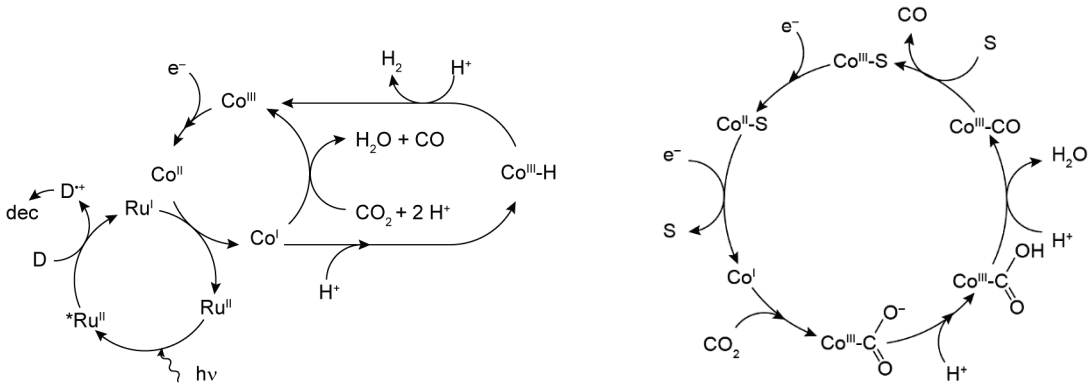

Figure I-42 General mechanism proposed by Lehn in 1986 to explain the two competitive pathways for CO_2 and water reduction (reference 109). The catalytic cycle proposed for CO_2 reduction is detailed on the right, where "S" is a solvent molecule.

A year later, Lehn and Ziessel extended their previous observations to other polypyridyl ligands.[109,110] Using virtually identical conditions as previously reported but replacing the bpy ligand with phen and MeCN by DMF as the solution, mixtures of CO and H_2 were again observed in ratios close to 1:2 (CO:H_2). Isotopic labelling experiments using $^{13}CO_2$ effectively confirmed the source of CO to be CO_2. Subsequently, the mechanism depicted in Figure I-42 was proposed to account for the production of H_2 and CO. Within the mechanism, the authors suggested that a Co^I-polypyridyl complex was the active catalyst, which could either react with a H^+ source or CO_2 in the selectivity determining step. In the case of reaction with H^+, a Co^{III}–H would form and was proposed to be

susceptible to further protonation to yield H_2 and a Co^{III}-polypyridyl complex. If the Co^{I}-polypyridine instead reacts with CO_2, CO was directly produced along with an equivalent of H_2O and a Co^{III}-polypyridyl compound is reformed. While not excessively detailed, this mechanistic proposal directed subsequent investigations of Co-polypyridyl systems. It suggested Co^{I} as being the likely identity of an active catalytic species, as well as the need for open coordination sites for interaction with H^+ or CO_2.

The first pre-synthesised Co-polypyridyl system evaluated as a CO_2 reduction catalyst was $[Co(bpy)_3]Cl_2$ and the investigation was reported by Sutin and co-workers in 1985.[111] Like Lehn and Ziessel, the reaction was studied photochemically with the addition of $[Ru(bpy)_3]^{2+}$ as a photosensitiser. The study was however conducted in aqueous solution with a bicarbonate buffer (pH = 8.5 - 10) instead or the organic solvent. Using spectrophotometry, the authors reported the appearance and subsequent disappearance of $[Co(bpy)_3]^+$. The preparation of $[Co(bpy)_3]^+$ is also reported and afforded the opportunity to monitor the behaviour of the Co(I)-polypyridyl complex towards CO_2. In the dark, the pre-synthesised $[Co(bpy)_3]^+$ is followed by spectrophotometry in the presence of CO_2 as a substrate. The disappearance of $[Co(bpy)_3]^+$ can be directly correlated to the production of CO, alongside H_2 with trace amounts of formate. However, the authors further reported that the CO that is produced further reacts with $[Co(bpy)_3]^+$ and yield the insoluble dimer $[Co(bpy)(CO)_2]_2$ (identified by diagnostic IR features) according to equations I-21 and I-22 (Figure I-43).[111]

$$2\ [Co(bpy)_3]^+ + HCO_3^- + H_2O \rightarrow 2\ [Co(bpy)_3]^{2+} + CO + 3\ HO^- \qquad \text{(I-21)}$$

$$[Co(bpy)_3]^+ + CO \rightarrow ¼\ [Co(bpy)(CO)_2]_2 + bpy + ½\ [Co(bpy)_3]^{2+} \qquad \text{(I-22)}$$

$$[Co(bpy)(CO)_2]_2 + 6\ H^+ \rightarrow 4\ CO + 2\ H_2 + 2\ Co^{2+}(aq) + 2\ bpyH^+ \qquad \text{(I-23)}$$

Of note, the production of CO can be completely quantified via the acidification of the solution (pH = 1), which decomposes the proposed dimeric species and liberates the trapped CO according to the reaction (I-23).

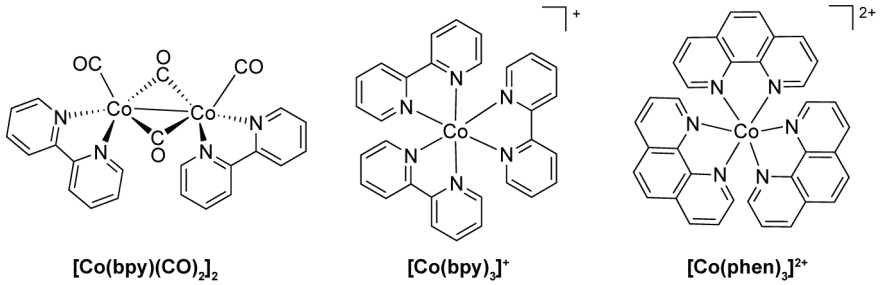

Figure I-43 Structures the catalysts studied by Sutin and of the proposed Co dimer (reference 111).

Despite these initial efforts towards incorporating Co-polypyridyl complexes into photochemical system for CO_2 reduction catalysis, the electrochemistry of Co-polypyridyl complexes under CO_2 reduction conditions was not explored until 1988 by Durand and collaborators.[103] In this

study, the authors reported that cyclic voltammograms of $[Co(phen)_3]^{2+}$ (Figure I-43) in DMSO. Under an N_2 atmosphere, the complex exhibits a metal-based reduction wave at –0.84 V *vs.* SCE (Co^{II}/Co^{I}) and a two-electron feature at –1.53 V *vs.* SCE, which had previously been described as Co^{+1}/Co^{-1} redox event, but has since been reassigned by others as having ligand contribution. Under an atmosphere of CO_2, the authors found significant current enhancement in the region of the electrochemical feature at –1.53 V *vs.* SCE. The current enhancement is attributed exclusively to the reduction of CO_2 to formate, as no CO was observed in this study. The production of CH_4 was also reported, but it is believed to arise from decomposition of the $NaClO_4$ electrolyte salt and the solvent. As the primary catalytic current enhancement occurs within an electrochemical feature that contains significant ligand-reduction character, it is proposed that the loss of a phen ligand can occur at that potential, liberating a coordination site for interaction with CO_2.

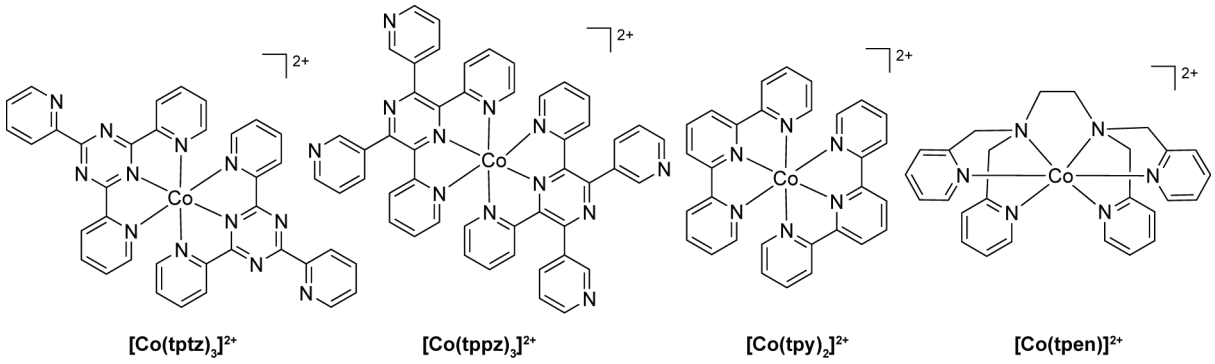

Figure I-44 Structure of the CO_2 reduction catalysts reported by Abruña in the 90s.

Towards assessing Co-polypyridyl complexes with ligands having different denticities, Abruña reported in 1992 observations of current enhancement under CO_2 in the cyclic voltamogramms of $[Co(tptz)_2]^{2+}$, $[Co(tppz)_2]^{2+}$, $[Co(tpy)_2]^{2+}$ and $[Co(tpen)]^{2+}$ (Figure I-44). In DMF solutions with TBAP as the electrolyte, these complexes are reported to catalyse the electrochemical reduction of CO_2 at potentials of respectively –0.93, –1.20, –1.53 and –1.51 V *vs.* SCE.[106] While the characterisation of the activity of complexes is limited to the simple observation of current enhancement under an atmosphere of CO_2, this report indicates a strikingly high degree of versatility of Co-polypyridyl systems as CO_2 reduction catalysts. Taken with the previously described results, there is a general observation of activity for almost any variant of Co-polypyridyl systems. Abruña and collaborators elaborated further on the behaviour of $[Co(tpy)_2]^{2+}$ in solutions in DMF by cyclic voltammetry and electrolyses. In general agreement with previous systems, the cyclic voltammograms indicated that two ligand-based cathodic features could be observed past the $Co^{II/I}$ reduction event, and for both features a current enhancement under CO_2 could be observed of 95% at –1.56 V *vs.* SCE and 820% at –1.91 V *vs.* SCE. In contrast to the previous systems for Co-polypyridyl catalysts however, bulk electrolysis at –1.70 V *vs.* SCE are reported to yield formate as the product of this catalytic process after four equivalents of charge per Co centre were passed.[107]

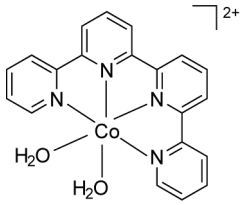

$[Co(qtpy)(OH_2)_2]^{2+}$

Figure I-45 Structure of the Co-based catalyst studied in 1995 by Che and collaborators**.**

A unique variant of a Co-polypyridyl catalyst was synthesised and studied by Che and collaborators in 1995 in which the tetradentate 2,2':6',2":6",2"'-quaterpyridine (qtpy) coordinated a Co centre as depicted in Figure I-45.[112] The resulting complex $[Co(qtpy)(H_2O)_2]^{2+}$ was found to electrocatalytically reduce CO_2 to CO when electrolyzed at –1.70 *vs.* SCE in a DMF solution. However, a brown precipitate was observed during the course of electrolysis, and was assigned to inactive and insoluble Co-carbonate complexes. Subsequent investigations concluded that the catalytic CO_2 reduction activity was due to material derived from the Co-complex that absorbed onto the graphite electrode surface. Independent electrodeposition of a Co-qtpy species on graphite cloth electrode was achieved by electrolysis at –1.65 V *vs.* SCE. The resulting modified electrode was further shown to be competent for CO_2 reduction catalysis in water and DMF, producing CO in 35% faradic yield. Thus, the utilisation of the tetradentate qtpy afforded a Co-species that resulted in a catalytically active material for CO_2 reduction to CO, however it was instable and prone to electrodeposition at reducing potentials.

The use of polypyridyl ligands on a Co centre as a component of a heteroleptic ancillary ligand field for CO_2 reduction electrocatalysts was initially reported by Ogura in 1997.[113] Using $[Co(dmbpy)(PPh_3)_2]^{2+}$ and $[Co(mphen)(PPh_3)_2]^{2+}$ (structures shown in Figure I-46, left and centre) as homogeneous catalysts in an anhydrous CO_2-saturated MeCN solution, electrolyses resulted in the production of CO in 60-80% faradic efficiency. However, when 8% water was added as a co-solvent to the system, the product selectivity shifted to 25-32% faradic yields for CO and 29-43% faradic yields for formate. These results nicely demonstrated the ability of Co-polypyridyl systems to be amenable to significant changes in product selectivity upon inclusion of alternative ligand types.

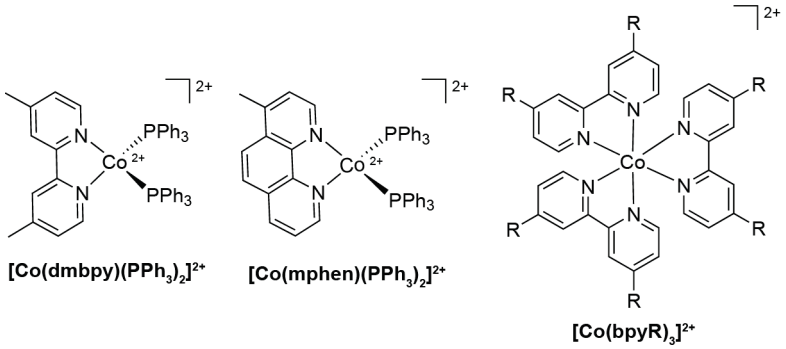

Figure I-46 Structure of the Co-catalysts with heteroleptic ancillary ligand fields studied by Ogura (left and centre) and of the fluorinated $[Co(bpyR)_3]^{2+}$ photosensitised by Hirose in 2010 (right, R = $-C_6H_4-(CH_2)_4(CF_2)_4F$ or $-(CH_2)_2(CF_2)_6F$).

Several noteworthy examples of significantly modified Co-polypyridyl systems have also been reported as CO_2 reduction catalysts. In 2010, Hirose modified the bpy ligand to include fluorinated alkyl chains in the 4,4' positions which afforded complexes of the type $[Co(bpyR)_3]^{2+}$ (depicted in Figure I-46, right) soluble in supercritical CO_2. In supercritical CO_2, under irradiation, at a pressure of 6.8 MPa and a temperature of 35°C, mixing $[Co(bpyR)_3]^{2+}$ with the photosensitiser $[Ru(bpyR)_3]^{2+}$ in the presence of a amine-based sacrificial electron donor resulted in the observation of catalysed CO_2 reduction to CO.[114] Thus, a directed functionalisation of the exceptionally versatile and ubiquitous bpy ligand affords a Co-polypyridyl photocatalytic system that can operate in solvent-free conditions.

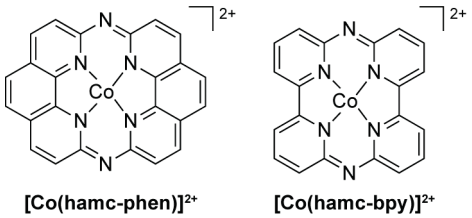

Figure I-47 Cobalt systems with hexaaza-macrocylic ligands developed by Costamagna.

The last class of polypyridyl ligand assayed on a cobalt centre for CO_2 reduction catalysis was investigated by Costamagna and co-workers. They reported Co-polypyridyl systems wherein the polypyridyl ligand was fully conjugated and macrocyclic. Discrete Co complexes of hexaaza-macrocylic ligands derived from the condensation of bipyridines (hamc-bpy) and phenanthrolines (hamc-phen) with structures depicted in Figure I-47 were synthesised and characterised. While no product detection is provided, cyclic voltammetery under CO_2 resulted in cathodic current enhancement which the authors describe as evidence of catalytic CO_2 reduction.[115,116]

In summary, while not exhaustively studied mechanistically, the Co-polypyridyl platform is reported to be a versatile and active catalytic system for CO_2 reduction resulting in primarily CO and H_2 production. Other products have been reported however, and system stability if often limited.

4.3.4. Polypyridyl complexes of nickel

Investigations of Ni-polypyridyl platforms as CO_2 reduction catalysts began in 1987 as Fiorani and collaborators reported the electrochemical reduction of CO_2 catalysed by $[Ni(bpy)_3]^{2+}$.[117] Their report

indicates that, under an inert atmosphere, $[Ni(bpy)_3]^{2+}$ undergoes a two-electron reduction at –1.20 V *vs.* SCE. This reduction event was thought to be accompanied by the loss of a bpy ligand to yield $[Ni(bpy)_2]^0$ as the proposed active catalyst. Cathodic current at a potential beyond –1.20V *vs.* SCE was reported to increase under an atmosphere of CO_2 and was assigned to catalytic CO_2 reduction. The major products detected are reported to be CO and CO_3^{2-}. Stability of this system is found to be limited and two deactivation pathways were identified, with an overall reaction mechanisms presented in eq. I-24 to I-27:

$$[Ni(bpy)_3]^{2+} + 2\ e^- \leftrightarrow [Ni(bpy)_2] + bpy \quad \text{(I-24)}$$

$$[Ni(bpy)_2] + 2\ CO_2 + bpy \rightarrow [Ni(bpy)_3]^{2+} + CO + CO_3^{2-} \quad \text{(I-25)}$$

$$2\ CO + [Ni(bpy)_2] \rightarrow [Ni(bpy)(CO)_2] + bpy \quad \text{(I-26)}$$

$$m\ (CO_3^{2-}) + [Ni(bpy)_3]^{2+} \rightarrow [Ni(bpy)_{3-n}(CO_3^{2-})_m]^{(2-2m)+} + n\ (bpy) \quad \text{(I-27)}$$

The carbonyl and carbonate complexes of Ni-bpy produced during eq. I-26 and I-27 are reported to be inert, and as such represent deactivation pathways of the catalyst. Faradic yields were calculated for this system and are reported to be around 30% for CO. If bound CO molecules trapped in a Ni-carbonyl complex are taken into account, an extra 40-49% faradic yield was reported, thus resulting in upwards of 79% faradic efficiency for total CO production by this system. The faradic yield for total CO_3^{2-} detected was found to be around 90%. Product inhibition and trapping was identified as a problem, and the authors proposed a bulk electrolysis setup with no separation between the working and counter electrode compartment to resolve this issue. In theory, the deactivated $Ni/CO/CO_3^{2-}$ species could diffuse to the counter electrode where oxidation could occur, resulting in the continuous liberation of the bound equivalents of CO. Upon evaluating this reaction setup, no deactivation of the catalyst is observed and a constant stream of CO, as desired, was obtained. However, it should be noted that faradic yields were significantly lower in this cell design and possibly energy storage applications would be hindered by the need to oxidise the catalyst as part of a cycle to liberate the CO.

In 1989, Périchon and collaborators more deeply evaluated the behaviour $[Ni(bpy)_3]^{2+}$ towards the catalysis of the electrochemical reduction of CO_2 using DMF or NMP (*N*-Methyl-2-pyrrolidone) as a solvent system.[118] The authors confirmed the general behaviour of electrochemical reduction of CO_2 to CO catalysed by the Ni-bpy system, but they proposed an alternative reaction mechanism to that which was reported by Fiorani. Like Fiorani, Périchon and collaborators proposed that a $[Ni(bpy)_2]^0$ is initially the active form of the catalyst. Upon generation of $[Ni(bpy)_2]^0$, with an applied potential of –1.2 V *vs.* SCE, a reaction with four equivalents of CO_2 accompanied by a rapid six-electron reduction is proposed to afford a free bpy ligand with two equivalents of CO_3^{2-} and a nickel complex with the stoichiometry $[Ni(bpy)(CO)_2]^0$. While no further comments are made regarding the nature of this

complicated transformation, the authors state that $[Ni(bpy)(CO)_2]^0$ is further reduced by one-electron at –1.6 V *vs.* SCE to yield $[Ni(bpy)(CO)_2]^-$ which is claimed to be capable of performing an electron transfer to CO_2 to transiently yield the radical species $CO_2^{\bullet-}$ and regenerate $[Ni(bpy)(CO)_2]^0$. Two equivalents of the one-electron reduced radical $CO_2^{\bullet-}$ species are then proposed to undergo an electronic disproportionation to generate CO and CO_3^{2-}. An interesting experimental detail is that the authors utilised stoichiometric amounts of Mg^{2+} cations to sequester the carbonate generated as part of the reaction so as to avoid the deleterious side reactions observed by Fiorani and coworkers. In general, the Périchon mechanism for Ni-bpy electrocatalytic reduction of CO_2 is unique in that it proposes the active catalyst to be $[Ni(bpy)(CO)_2]^0$ and that reduction of CO_2 occurs through one-electron reduction and formation of a transient $CO_2^{\bullet-}$ species with minimal direct interaction with a Ni-centre.

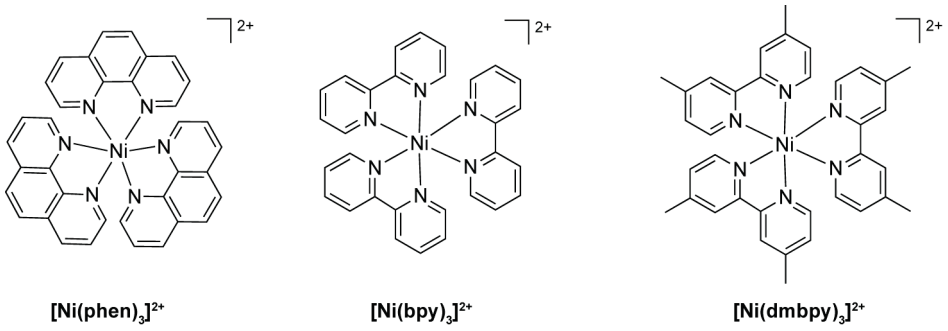

Figure I-48 Ni-based polypyridyl CO_2 reduction catalysts reported containing bpy or phen ligands.

As was the case for cobalt systems, Durand and co-workers extended the scope of polypyridyl ligands of Ni to phen by reporting the electrochemical reduction of CO_2 catalysed by $[Ni(phen)_3]^{2+}$ at a potential of –1.19 V *vs.* SCE in DMSO (0.1M TBAP as the supporting electrolyte). The products reported are CO and trace amounts of CH_4.[103] These results are in agreement with the observations for the related $[Ni(bpy)_3]^{2+}$ system. Of note, the cyclic voltammograms of $[Ni(phen)_3]^{2+}$ are qualitatively identical to that of $[Ni(bpy)_3]^{2+}$, with a two-electron cathodic feature under inert atmosphere that exhibits current enhancement under an atmosphere of CO_2. However, there is a significant difference in the assignment of this feature. Whereas the initial reports for $[Ni(bpy)_3]^{2+}$ identified the two-electron reduction as metal-based, accompanied by ligand loss, Durand and coworkers identify the two-electron reduction feature for $[Ni(phen)_3]^{2+}$ as ligand- and metal-based, accompanied by loss of a ligand. The authors postulate that the reduction of the polypyridyl ligand could be instrumental to the observation of CO_2 reduction catalysis, but further mechanistic considerations are not given.

In a report that ultimately combines the notion of the active species having the structural identity of $[Ni(L)(CO)_2]$ (L= polypyridine) as well as the importance of ligand reduction events to catalysis, Christensen *et al.* studied the behaviour of $[Ni(dmbpy)_3]^{2+}$ and $[Ni(phen)_3]^{2+}$ under electrocatalytic CO_2 reduction conditions via in-situ FTIR.[119] Using IR resonances, the authors directly identify the formation of $[Ni(dmbpy)_2]^0$ and $[Ni(phen)_2]^0$ upon the two-electron reduction of

$[Ni(dmbpy)_3]^{2+}$ and $[Ni(phen)_3]^{2+}$ at –1.3 V *vs.* SCE for both systems. Complexes $[Ni(dmbpy)_2]^0$ and $[Ni(phen)_2]^0$ were further reported to react slowly with multiple equivalents of CO_2 to yield the corresponding $[Ni(L)(CO)_2]$ structures, presumably in a similar mechanism to that proposed by Périchon.[118] Using the carbonyl vibrational frequencies as a spectroscopic handle, the authors observed new frequencies under electrocatalytic conditions. They propose that these IR features are attributed to a resting state of the catalyst that is derived from the further one-electron reduction of the $[Ni(L)(CO)_2]$ complexes to yield a catalytically competent species with a ligand-localised radical anion such as $[Ni(L^{\bullet-})(CO)_2]^-$. The authors further described that decomposition of these species can occur in basic reducing conditions where $[Ni(dmbpy^{\bullet-})(CO)_2]^-$ and $[Ni(phen^{\bullet-})(CO)_2]^-$ react with trace water to yield inactive bimetallic clusters of the proposed structure $[Ni_2(\mu\text{-}H)(CO)_6]^-$.

In conjunction with reports on analogous Co- and Fe-polypyridyl systems, efforts were made towards assessing the activity of Ni-polypyridyl systems with ligands of higher denticity as catalysts of the reduction of CO_2. Abruña and collaborators published in 1992 that cyclic voltamogramms in DMF of Ni complexes of tppz, tpy and tpen (depicted in Figure I-49) display cathodic current increase in the presence of CO_2. The authors attribute the behaviour to electrocatalytic CO_2 reduction at the potentials of –1.54, –1.20 and –1.80 V *vs.* SCE respectively; however no further insights into mechanism or selectivity were reported.[106] Further probing of the $[Ni(tpy)_2]^{2+}$ system in DMF (0.1 M TBAP as a supporting electrolyte) under an atmosphere of N_2 by cyclic voltammetry revealed the presence of three reversible electrochemical features at +1.65, –1.38, and –1.20 V *vs.* SCE.[107] The features at +1.65 and –1.20 V *vs.* SCE are attributed respectively to $Ni^{III/II}$ and $Ni^{II/I}$ metal-centred reductions, however the feature at –1.38 V *vs.* SCE is reported to be ligand-centred. The onset of catalytic current under an atmosphere of CO_2 is shown to occur within the feature at –1.20 V *vs.* SCE. No further information is given, but the assignments by the authors imply that, unlike the systems with bpy and phen ligands, no ligand reduction is required for catalysis in these examples and that generation of a Ni^I centre affords a catalytically active species towards CO_2 reduction.

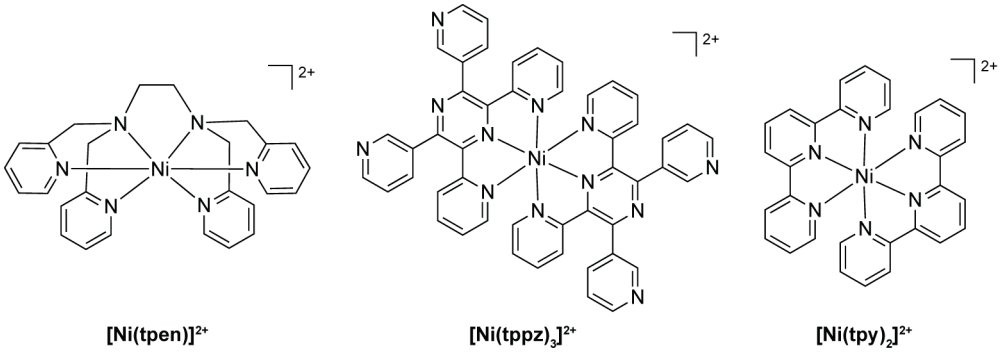

Figure I-49 Ni-based CO_2 reduction catalysts reported by Abruña in the 90s.

The qtpy complexes of nickel were also investigated as potential electrocatalyts for CO_2 reduction. Contrary to that which was reported for the analogous $[Co(qtpy)(OH_2)_2]^{2+}$ complexes, $[Ni(qtpy)(MeCN)_2]^{2+}$ (Figure I-50, left) did not lead to the formation of an electroactive film on glassy

carbon electrodes. Observation of only trace CO is reported after controlled-potential electrolysis of $[Ni(qtpy)(MeCN)_2]^{2+}$ at –1.70 V *vs.* SCE under CO_2.[112] Thus, whereas nickel complexes supported by bidentate and tridentate polypyridyl ligands are found to be catalytically active for CO_2 reduction, tetradentate polypyridyl ligands seemingly behave differently and do not allow for the formation of an active species.

Ni complexes of bpy-based[120] and phen-based[115] hexa-aza-macrocycles (hamc-bpy and hamc-phen) (Figure I-50) have been reported to exhibit electrocatalytic CO_2 reduction in DMF to yield CO and/or formic acid.[116] Further details regarding this chemistry have not been reported, however, observation of CO_2 reduction activity catalysed by these macrocyclic compounds suggests that the lack of activity reported for $[Ni(qtpy)(MeCN)_2]^{2+}$ could be unique and intrinsic to the qtpy ligand.

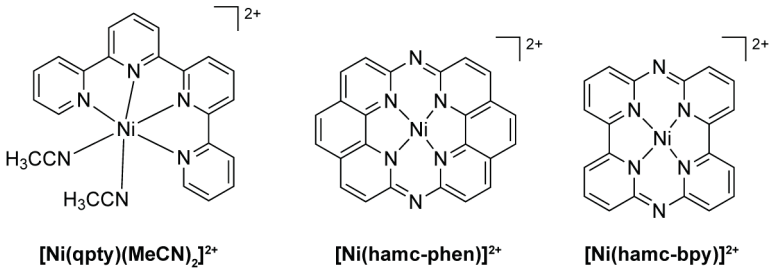

Figure I-50 Ni catalysts with tetradentate ligands studied by Lam et al. (reference 112) and Costamagna (reference 115 and 116).

In 1998, Fujita and coworkers published initial efforts towards evaluating Ni-bpy systems as photocatalysts, as opposed to electrocatalysts.[121] In the absence of an external photosensitiser, the authors reported the results of photolysing solutions of $[Ni(bpy)_3]^{2+}$ in CO_2-saturated MeCN/TEA solutions using a 313 nm cut-off filter. Via UV-vis spectroscopy, the species $[Ni(bpy)_2]^{+}$ was identified as the product of the one-electron reduction of the excited state of $[Ni(bpy)_3]^{2+}$, which implies a rapid loss of a bpy ligand upon reduction. The authors further identify a second reduction event yielding $[Ni(bpy)_2]^{0}$. This formally Ni^0 species is proposed to react with CO_2 to yield CO as the only product. If water is added as a co-solvent, no CO production is observed. While no explanation is directly given for this behaviour, the observations are in agreement with those previously made by Christensen *et al.*[119] Also, in agreement with electrochemical investigations, Fujita and co-workers proposed that the CO produced from CO_2 reduction can lead to the formation of multimetallic and catalytically inactive adducts with $[Ni^{I}(bpy)_2]^{+}$ or $[Ni(bpy)_2]^{0}$. This inhibition explains the sub stoichiometric amounts of CO produced during photocatalysis (0.5 mol of CO produced per mol as starting $[Ni(bpy)_3]^{2+}$). Despite underwhelming catalytic activity, these reports demonstrate the remarkable possibility of directly reducing Ni-polypyridyl species via light absorption in an electronic excited state while showing that the resulting reduced complexes behave similarly to those reported electrocatalytically.

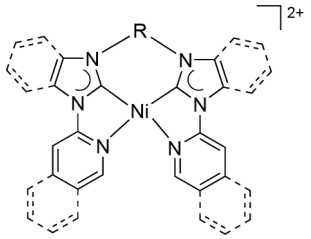

$[Ni(^{R}bimpy)]^{2+}$

Figure I-51 Schematic representation of the Ni catalysts architectures studied by Chang in 2011 and 2013 (R = Me, Et or Pr).

More recently, significant advances on CO_2 reduction using Ni-polypyridyl platforms have been reported by Chang and collaborators using the unique ancillary ligand ^{R}bimpy (R = Me, Et or Pr, depicted in Figure I-51.). The structure of the resulting Ni complexes with ^{R}bimpy is presented in Figure I-51. The authors evaluate these systems under electrocatalytic conditions for CO_2 reduction and report the general production of CO with only trace amounts of H_2 detected. Of note, unlike other Ni-based systems where the CO_2 reduction activity is inhibited by the presence of H_2O, Chang and collaborators are able to observe CO_2 reduction to CO even in the presence of water as a co-solvent. Electro-kinetic studies of this system afforded the determination of TOFs reported in the range from 3.9 h^{-1} to 5.9 h^{-1}. The precise value of the TOF was found to vary based on the nature of the bridge "R" functionality with increased catalytic rates corresponding to increased structural flexibility within the bridge. Furthermore, deactivation of the catalysts was observed to occur at time lengths greater than 2 h in controlled-potential electrolysis conditions.[122] In later work Chang and collaborators extended the π system of the ^{R}bimpy framework creating benzimidazole and isoquinoline moieties (Figure I-51). These new Ni complexes are reported to be incorporated into electro- and photocatalytic systems for CO_2 reduction. Controlled-potential electrolysis in MeCN (0.1M $TBAPF_6$ as the supporting electrolyte) at –1.80 V *vs.* SCE over 8 h yielded 22% of CO in terms of faradic efficiency and trace amounts of CH_4 are also observed. No H_2 formation was found in the first 30 min of the 8 h bulk electrolysis, but at longer time lengths some unspecified amount of H_2 was detected. Additionally, the Ni-complex was successfully integrated into a photochemical system upon treatment with a photosensitiser, Ir(2-phenylpyridine)$_3$, and a sacrificial electron donor, TEA, in a MeCN solution. Similarly to the electrochemical observations, no formation of H_2 is detected in the photosensitised system and TONs as high as 98,000 are reported for the formation of CO.[123]

Upon considering precedent for Ni-polypyridyl systems as CO_2 reduction catalysts, a few general observations can be made. First, the major product is predominantly CO. Second, production of H_2 through H^+ reduction is exceedingly rare, which suggests that Ni-based systems might be ideal candidates for selective reduction of CO_2 over H^+ sources. Third, catalysts are often reported to be inhibited by CO and/or CO_3^{2-}. Finally, the active catalytic species might not necessarily require an entirely polypyridyl ancillary ligand field, but rather a combination of polypyridyl ligands and carbonyl ligands could be optimal. This heteroleptic ligand environment would have some similarities to those ligand fields found within active Re, Ru, Mn, W, and Mo systems.

4.3.5. Polypyridyl complexes of copper

Reports on Cu-polypyridyl complexes as catalysts for CO_2 reduction are limited. However, dinuclear polypyridyl complexes of Cu have been reported in the 1990s as potential catalysts for the electrochemical reduction of CO_2 in MeCN.

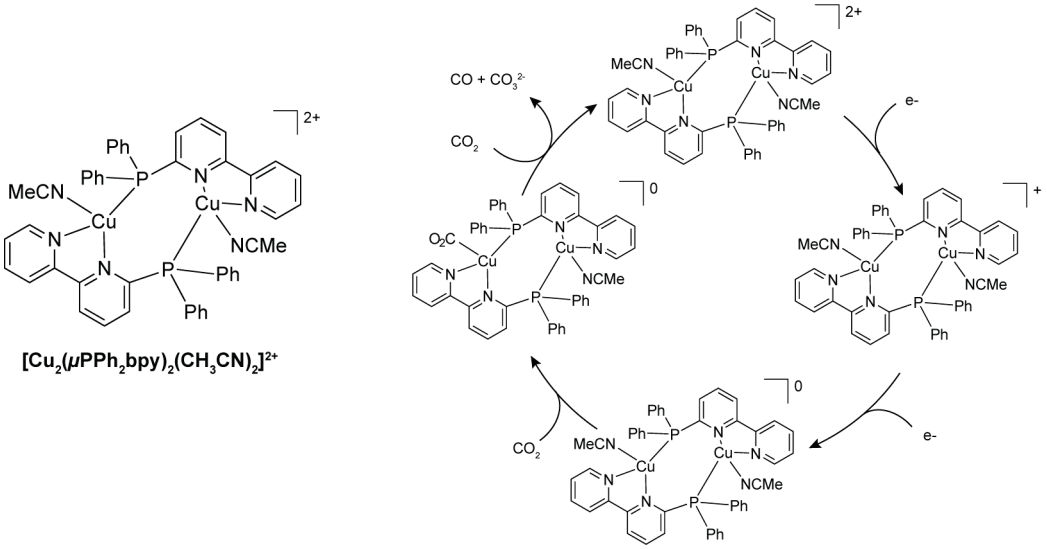

Figure I-52 Structure of the Cu CO_2 reduction catalyst reported by Kubiak and Haines (left) and the proposed mechanism (right).

With initial report of synthesis and activity by Haines and collaborators[124] and further studies by Kubiak and Haines,[125] $[Cu_2(\mu PPh_2bpy)_2(CH_3CN)_2]^{2+}$ (PPh_2bpy = 6-diphenylphosphino- 2,2'-bipyridine) was found to catalyse the production of CO and CO_3^{2-} selectively under CO_2 electroreduction conditions. The mechanism proposed is depicted in Figure I-52, and the relative mechanism and rate constants are described as bearing similarities to those of $[Os(bpy)_2(CO)H]^+$ due to the presence of bpy ligands. The polypyridyl framework is proposed to assist in storing multiple redox equivalents, and to take an active role in catalysis. The authors cite the similar rate constants as well as redox behaviour and potentials of the Cu relative to similar Os catalysts as supporting evidence for mechanistic similarities.

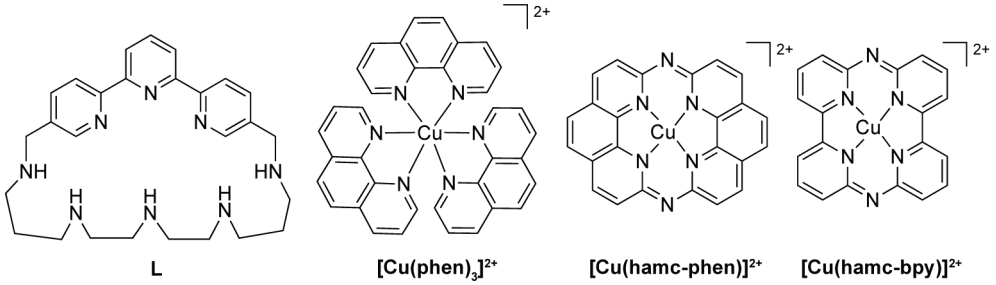

Figure I-53 From left to right: structure of the ligand of the Cu catalyst studied by García-España and of the Cu catalysts studied by Durand and Costamagna.

García-España and collaborators reported the interaction of Cu^{2+} cations with terpyridine derivative ligands, such as **L** in the Figure I-53. These ligands, in pH 5 solution with 0.5 mM Cu^{2+}

exhibit catalytic current enhancement in the presence of CO_2 by cyclic voltammetry which the authors ascribe to CO_2 reduction, but no details as to the nature of the reduction or structure of the catalysts are provided.[126,127,128]

Durand and collaborators mentioned in their 1988 report that cyclic voltammograms of $[Cu(phen)_3]^{2+}$ exhibit cathodic current enhancement under CO_2 within the two electrochemical features assigned to ligand-based reductions at −1.52 and −1.68 V *vs*. SCE respectively. They generally classify this observation as catalytic CO_2 reduction induced by ligand reduction.[103] Building on this work, Costamagna reported a similar behaviour of Cu complexes of hexaaza-macrocylic ligands derived from the condensation of bipyridines (hamc-bpy) and phenanthrolines (hamc-phen), but, while qualitatively similar, no product detection is provided.[115,116]

5. Lessons and Conclusions and Objectives

5.1. Conclusions

Polypyridine-supported metal compounds have been extensively utilised in the catalytic reduction of CO_2, with $[Re(bpy)(CO)_3]^+$ and $[Ru(tpy)(L)(Solv)]^{2+}$, along with variants to these general families of catalysts, being the most efficient and well-studied catalysts.[75,76,129,130] All of these compounds have been shown to catalyze the reduction of CO_2 to carbon monoxide or formate, and in most cases H_2 was observed as well.

Despite the success of such polypyridine-supported noble metal catalysts, fewer examples of first row transition metal polypyridine-based CO_2 reduction electrocatalysts are present in the literature, with the notable exception of $[Mn(bpy)CO_3]^+$ systems. Initial reports exist of observations of activity under CO_2 in reducing conditions for a number of other first-row transition metal complexes, but follow–up mechanistic reports are exceedingly rare, as are confirmations of activity through quantitative product measurements. Product inhibition and ligand degradation is a problem in many of the reported systems.

It is also apparent that two separate waves of study occurred in the field. The first wave, in the 1980s and early 90s, is when most of the initial reports were made, following the work of Lehn, Ziessel, Meyer, Fiorani and Périchon to name a few. The second wave began in the early 2010s and has already generated some exciting results. The Mn-based systems were first reported by Deronzier and collaborators in September 2011, a mere month before the beginning of the PhD work reported in this thesis, and are quickly gaining interest within the CO_2 reduction community. The activity of the [Ru(tpy)(bpy)S] complexes in the context of functional devices developed by Meyer was originally published in October 2011. However, there continues to be a general dearth of reports on of first row transition metal polypyridine-based CO_2 reduction catalysts.

The polypyridyl backbone itself has been demonstrated to be quite advantageous due to its redox active nature and thus should be considered as a non-innocent ligand.[131,132] Multiple equivalents of electrons are able to be stored on such catalysts, which facilitates multi-electron reactivity with CO_2, avoiding the highly energetic one-electron reduction of CO_2 to $CO_2^{\bullet-}$.[133] The reduced polypyridyl rings act as the reservoir of electrons for CO_2 reduction, and the metal centre mediates the transfer of these reducing equivalents to CO_2.

As for the study of Co and Ni complexes as CO_2 reduction electrocatalysts, a common motif that has been shown is the fact that CO molecules (the product of CO_2 reduction) tend to strongly and often irreversibly coordinate to the metal centre. This effect is cited to explain diminished observed faradic yields as well as catalyst deactivation. The lability of the polypyridyl ligand is also a factor to carefully consider, as $[M(bpy)_3]^{2+}$ complexes (M = Co, Ni) are reported to lose a bpy ligand upon one- or two-electron reduction to yield $[M(bpy)_2]^+$ or $[M(bpy)_2]^0$.[111,117] As the complexes are more reduced,

ligand lability will general increase, leading to further ligand losses. Ultimately, in the case of Ni systems, $Ni(CO)_4$ is even reported to form, yet is inactive towards CO_2 reduction.[118,119]

On the other hand, increasing the ligand denticity as a strategy to avoid excessive ligand loss, by substituting the bidentate bpy for the tetradentate quaterpyridine yields Ni and Co complexes that have a very poor activity in the case on Ni, and are prone to polymerisation on electrodes for Co.

However, terpyridine appears to be a compromise, in that no polymerization is observed and that the tridentate nature should coordinate the metal ion more strongly than that which is observed for bpy. The preliminary reports by Abruña and collaborators indicate promising current enhancement under CO_2 in anhydrous DMF with TBAP 0.1M as the electrolyte for Fe, Co and Ni complexes of tpy. These studies were focused more towards the study of electropolymerised films of M-tpy compounds obtained by modifying the tpy ligand with a vinyl function *para* to the central nitrogen. In the course of the studies of these polymerised vinyl-tpy complexes for electrocatalytic CO_2 reduction, product determination is reported to yield different products. In 1989 cobalt-vinyl-terpyridine electropolymerised on platinum gauze electrodes and electrolyzed at −1.2 V *vs.* SCE for 4 h in DMF TBAP 0.1M were reported to yield formic acid in nearly 100% faradic yield as determined using the chromotropic acid test, with trace CO observed by mass spectrometry.[106] The same polymerised films but on glassy carbon electrodes in water, $NaClO_4$ 0.1M, were reported to yield 39% formaldehyde after bulk electrolysis at −1.1 V *vs.* Ag/AgCl, and no CO or formic acid were detectable. Iron versions of these polymerised films are reported to yield 28% of formaldehyde after bulk electrolysis at −1.075 V *vs.* Ag/AgCl, and again no CO or formate was detected.[134] Beyond these reports, no thorough evaluation of first row transition metal tpy-based complexes as CO_2 reduction catalysts exist.

5.2. Objectives

Our aim was to revisit and investigate the activity toward CO_2 of the ubiquitous tpy-metal complexes. The simplicity, low cost, and straightforward synthesis of the terpyridyl motif makes it an ideal candidate as cheap and robust ligand for a CO_2 reduction catalysts. We will concentrate on developing the chemistry on first row transition metals due to considerations regarding natural abundance and cost limitations. Our focus will be on product distribution and factors influencing selectivity for CO_2 reduction to specified products, as well as the competition between H^+ reduction and CO_2 reduction. Once the systems of interest are identified and relevant catalytic activity is characterised, immobilisation on carbon electrodes can be envisioned, to move a step closer to the goal of a cheap cathode for use in the device presented in Figure I-10.

6. References

‡ N. Elgrishi, V. Artero and M. Fontecave, *L'Actualité Chimique*, 2013, **371–372**, 95. Reproduced by permission of the French Chemical Society.

§ Adapted with minor alterations from ‡.

1 Patrick Gerland, Adrian E. Raftery, Hana Ševčíková, Nan Li, Danan Gu, Thomas Spoorenberg, Leontine Alkema, Bailey K. Fosdick, Jennifer Chunn, Nevena Lalic, Guiomar Bay, Thomas Buettner, Gerhard K. Heilig and John Wilmoth, *Science*, 2014, **346**, 234.

2 BP Energy Outlook 2035, www.bp.com/energyoutlook. (Accessed February 2015).

3 International Energy Outlook 2013, *EIA projects world energy consumption will increase 56% by 2040*, http://www.eia.gov/forecasts/ieo/pdf/0484%282013%29.pdf. (Accessed February 2015).

4 *BP Statistical Review of World Energy June 2014*, bp.com/statisticalreview. (Accessed March 2015).

5 J. H. Wood, G. R. Long, D. F. Morehouse, *Long-Term World Oil Supply Scenarios*, www.eia.doe.gov/pub/oil_gas/petroleum/feature_articles/2004/worldoilsupply/oilsupply04. (Accessed 2011).

6 D. P. Trans, D. R. Keeling, *Trends in Atmospheric Carbon Dioxide*, www.esrl.noaa.gov/gmd/ccgg/trends/. (Accessed 2015).

7 *Carbon Dioxide Information Analysis Center*, http://cdiac.olm.gov/trends/emis/tre_glob.html. (Accessed 2011).

8 N. S. Lewis and D. G. Nocera, *Proc. Natl. Acad. Sci. U.S.A.*, 2006, **103**, 15729.

9 T. R. Cook, D. K. Dogutan, S. Y. Reece, Y. Surendranath, T. S. Teets and D. G. Nocera, *Chem. Rev.*, 2010, **110**, 6474.

10 R. Eisenberg and D. G. Nocera, *Inorganic Chemistry*, 2005, **44**, 6799.

11 United Nations Development Program, 2003, *World Energy Assesment Report: Energy and the Challenge of Sustainability*.

12 J. Barber, *Chem. Soc. Rev.*, 2009, **38**, 185.

13 R. Hill and P. R. Rich, *Proc. Natl. Acad. Sci. U.S.A.*, 1983, **80**, 978.

14 J. G. Moura, C. Brondino, J. Trincão and M. Romão, *J. Biol. Inorg. Chem.*, 2004, **9**, 791.

15 M. Leopoldini, S. G. Chiodo, M. Toscano and N. Russo, *Chem. Eur. J.*, 2008, **14**, 8674.

16 J.-H. Jeoung and H. Dobbek, *Science*, 2007, **318**, 1461.

17 H. Dobbek, L. Gremer, R. Kiefersauer, R. Huber, O. Meyer, *Proc. Natl. Acad. Sci. U.S.A.*, 2002, **99**, 15971.

18 G. Steinberg-Yfrach, J.-L. Rigaud, E. N. Durantini, A. L. Moore, D. Gust and T. A. Moore, *Nature*, 1998, **392**, 479.

19 G. Steinberg-Yfrach, P. A. Liddell, S.-C. Hung, A. L. Moore, D. Gust and T. A. Moore, *Nature*, 1997, **385**, 239.

20 A. Parkin, J. Seravalli, K. A. Vincent, S. W. Ragsdale and F. A. Armstrong, *J. Am. Chem. Soc.*, 2007, **129**, 10328.

21 T. Reda, C. M. Plugge, N. J. Abram and J. Hirst, *Proc. Natl. Acad. Sci. U.S.A.*, 2008, **105**, 10654.

22 A. Bassegoda, C. Madden, D. W. Wakerley, E. Reisner and J. Hirst, *J. Am. Chem. Soc.*, 2014, **136**, 15473.

23 A. Majumdar, *Dalton Trans.*, 2014, **43**, 8990.

24 J. Seo, P. G. Williard and E. Kim, *Inorg. Chem.*, 2013, **52**, 8706.

25 J. Seo and E. Kim, *Inorg. Chem.*, 2012, **51**, 7951.

26 S. Groysman and R. H. Holm, *Biochemistry*, 2009, **48**, 2310.

27 J.-M. Lehn, J.-P. Sauvage and R. Ziessel, *Nouv. J. Chim.*, 1980, **4**, 623.

28 M. S. Wrighton, A. B. Ellis, P. T. Wolczanski, D. L. Morse, H. B. Abrahamson and D. S. Ginley, *J. Am. Chem. Soc.*, 1976, **98**, 2774.

29 K. Kalyanasundaram and M. Grätzel, *Angew. Chem.*, 1979, **91**, 759.

30 H. Zhou, X. Li, T. Fan, F. E. Osterloh, J. Ding, E. M. Sabio, D. Zhang and Q. Guo, *Adv. Mater.*, 2010, **22**, 951.

31 K. S. Joya, Y. F. Joya, K. Ocakoglu and R. van de Krol., *Angew. Chem. Int. Ed.*, 2013, **52**, 10426.

32 Michael Grätzel, *Comments Inorg. Chem*., 1991, **12**, 93.

33 S. Y. Reece, J. A. Hamel, K. Sung, T. D. Jarvi, A. J. Esswein, J. J. H. Pijpers and D. G. Nocare, *Science*, 2011, **334**, 645.

34 J. P. Torella, C. J. Gagliardi, J. S. Chen, D. K. Bediako, B. Colón, J. C. Way, P. A. Silver and D. G. Nocera, *Proc. Natl. Acad. Sci. U.S.A.*, 2015, **112**, 2337.

35 Z. Chen, J. J. Concepcion, M. K. Brennaman, P. Kang, M. R. Norris, P. G. Hoertz and T. J. Meyer, *Proc. Natl. Acad. Sci. U.S.A.*, 2012, **109**, 15606.

36 P. Kang, Z. Chen, A. Nayak, S. Zhang and T. J. Meyer, *Energy Environ. Sci.*, 2014, **7**, 4007.

37 http://www.webelements.com/ (Retrieved April 14th 2007).

38 http://www.infomine.com/investment/metal-prices/ (Accessed March 1st 2015).

39 http://www.metalprices.com/ (Accessed March 1st 2015).

40 H. Ishida, H. Tanaka, K. Tanaka and T. Tanaka, *J. Chem. Soc., Chem. Commun.*, 1987, 131

41 H. Ishida, K. Tanaka and T. Tanaka, *Organometallics*, 1987, **6**, 181.

42 J. R. Pugh, M. R. M. Bruce, B. P. Sullivan and T. J. Meyer, *Inorg. Chem.*, 1991, **30**, 86.

43 H. Ishida, T. Terada, K. Tanaka and T. Tanaka, *Inorg. Chem.*, 1990, **29**, 905.

44 J.-M. Lehn and R. Ziessel, *J. Organomet. Chem.*, 1990, **382**, 157.

45 P. Voyame, K. E. Toghill, M. A. Méndez and H. Girault, *Inorg. Chem.*, 2013, **52**, 10949.

46 S. Chardon-Noblat, M.-N. Collomb-Dunand-Sauthier, A. Deronzier, R. Ziessel and D. Zsoldos, *Inorg. Chem.*, 1994, **33**, 4410.

47 S. Chardon-Noblat, A. Deronzier, R. Ziessel and D. Zsoldos, *Inorg. Chem.*, 1997, **36**, 5384.

48 C. M. Bolinger, B. P. Sullivan, D. Conrad, J. A. Gilbert, N. Story and T. J. Meyer, *J. Chem. Soc., Chem. Commun.*, 1985, 796.

49 S. Chardon-Noblat, P. Da Costa, A. Deronzier, S. Maniguet and R. Ziessel, *J. Electroanal. Chem.*, 2002, **529**, 135.

50 Z. F. Chen, C. C. Chen, D. R. Weinberg, P. Kang, J. J. Concepcion, D. P. Harrison, M. S. Brookhart and T. J. Meyer, *Chem. Commun.*, 2011, **47**, 12607.

51 Z. Chen, P. Kang, M.-T. Zhang and T. J. Meyer, *Chem. Commun.*, 2014, **50**, 335.

52 T. A. White, S. Maji and S. Ott, *Dalton Trans.*, 2014, **43**, 15028.

53 H. Nagao, T. Mizukawa and K. Tanaka, *Inorg. Chem.*, 1994, **33**, 3415.

54 K. Toyohara, H. Nagao, T. Mizukawa and K. Tanaka, *Inorg. Chem.*, 1995, **34**, 5399.

55 D. H. Gibson, J. G. Andino and M. S. Mashuta, *Organometallics*, 2006, **25**, 563.

56 M. M. Ali, H. Sato, T. Mizukawa, K. Tsuge, M. Haga and K. Tanaka, *Chem. Commun.*, 1998, 249.

57 A. Begum and P. G. Pickup, *Electrochem. Commun.*, 2007, **9**, 2525.

58 K. Tanaka and T. Mizukawa, *Appl. Organomet. Chem.*, 2000, **14**, 863.

59 M. R. M. Bruce, E. Megehee, B. P. Sullivan, H. Thorp, T. R. O'Toole, A. Downard and T. J. Meyer, *Organometallics*, 1988, **7**, 238.

60 M. R. M. Bruce, E. Megehee, B. P. Sullivan, H. H. Thorp, T. R. O'Toole, A. Downard, J. R. Pugh and T. J. Meyer, *Inorg. Chem.*, 1992, **31**, 4864.

61 S. Chardon-Noblat, A. Deronzier, F. Hartl, J. van Slageren and T. Mahabiersing, *Eur. J. Inorg. Chem.*, 2001, 613.

62 J. Chauvin, F. Lafolet, S. Chardon-Noblat, A. Deronzier, M. Jakonen and M. Haukka, *Chem. Eur. J.*, 2011, **17**, 4313.

63 Y. Tamaki, K. Koike, T. Morimoto, Y. Yamazaki and O. Ishitani, *Inorg. Chem.*, 2013, **52**, 11902.

64 C. M. Bolinger, N. Story, B. P. Sullivan and T. J. Meyer, *Inorg. Chem.*, 1988, **27**, 4582.

65 C. Caix, S. Chardon-Noblat and A. Deronzier, *J. Electroanal. Chem.*, 1997, **434**, 163.

66 M. B. Chambers, X. Wang, N. Elgrishi, C. H. Hendon, A. Walsh, J. Bonnefoy, J. Canivet, E. A. Quadrelli, D. Farrusseng, C. Mellot-Draznieks and M. Fontecave, *ChemSusChem*, 2015, **8**, 603.

67 P. Paul, B. Tyagi, A. K. Bilakhiya, M. M. Bhadbhade, E. Suresh and G. Ramachandraiah, *Inorg. Chem.*, 1998, **37**, 5733.

68 P. Paul, *P. Indian Acad. Sci. (Chem. Sci.)*, 2002, **114**, 269.

69 S. Sato, T. Morikawa, T. Kajino and O. Ishitani, *Angew. Chem. Int. Ed.*, 2013, **52**, 988.

70 R. O. Reithmeier, S. Meister, B. Rieger, A. Siebel, M. Tschurl, U. Heiz and E. Herdtweck, *Dalton Trans.*, 2014, **43**, 13259.

71 J. Hawecker, J. M. Lehn and R. Ziessel, *J. Chem. Soc., Chem. Commun.*, 1983, 536.

72 J. Hawecker, J. M. Lehn and R. Ziessel, *Helv. Chim. Acta*, 1986, **69**, 1990.

73 J. Hawecker, J. M. Lehn and R. Ziessel, *J. Chem. Soc., Chem. Commun.*, 1984, 328.

74 Over 130 unique publications can be found in a cross reference SciFinder search for the substructure Re(bpy) and the words "CO2 reduction"(search performed March 2nd 2015).

75 J.-M. Savéant, *Chem. Rev.*, 2008, **108**, 2348.

76 G. Sahara and O. Ishitani, *Inorg. Chem.*, 2015, DOI: 10.1021/ic50675a.

77 B. P. Sullivan, C. M. Bolinger, D. Conrad, W. J. Vining and T. J. Meyer, *J. Chem. Soc., Chem. Commun.*, 1985, 1414.

78 F. P. A. Johnson, M. W. George, F. Hartl and J. J. Turner, *Organometallics*, 1996, **15**, 3374.

79 J. M. Smieja and C. P. Kubiak, *Inorg. Chem.*, 2010, **49**, 9283.

80 E. E. Benson and C. P. Kubiak, *Chem. Commun.*, 2012, **48**, 7374.

81 S. Meister, R. O. Reithmeier, M. Tschurl, U. Heiz and B. Riege, *ChemCatChem*, 2015, **7**, 690.

82 K. Y. Wong, W. H. Chung and C. P. Lau, *J. Electroanal. Chem.*, 1998, **453**, 161.

83 J. A. Keith, K. A. Grice, C. P. Kubiak and E. A. Carter, *J. Am. Chem. Soc.*, 2013, **135**, 15823.

84 C. Riplinger and E. A. Carter, *ACS Catal.*, 2015, **5**, 900.

85 C. Riplinger, M. D. Sampson, A. M. Ritzmann, C. P. Kubiak and E. A. Carter, *J. Am. Chem. Soc.*, 2014, **136,** 16285.

86 C. W. Machan, S. A. Chabolla, J. Yin, M. K. Gilson, F. A. Tezcan and C. P. Kubiak, *J. Am. Chem. Soc.*, 2014, **136**, 14598.

87 A. Nakada, K. Koike, T. Nakashima, T. Morimoto and O. Ishitani, *Inorg. Chem.*, 2015, **54**, 1800.

88 T. Morimoto, T. Nakajima, S. Sawa, R. Nakanishi, D. Imori and O. Ishitani, *J. Am. Chem. Soc.*, 2013, **135**, 16825.

89 G. Calzaferri, K. Hädener and J. Li, *J. Photochem. Photobiol. A: Chem.*, 1992, **64**, 259.

90 E. Portenkirchner, K. Oppelt, C. Ulbricht, D. A. M. Egbe, H. Neugebauer, G. Knor and N. S. Sariciftci, *J. Organomet. Chem.*, 2012, **716**, 19.

91 M. L. Clark, K. A. Grice, C. E. Moore, A. L. Rheingold and C. P. Kubiak, *Chem. Sci.*, 2014, **5**, 1894.

92 M. Bourrez, F. Molton, S. Chardon-Noblat and A. Deronzier, *Angew. Chem. Int. Ed.*, 2011, **50**, 9903.

93 J. M. Smieja, M. D. Sampson, K. A. Grice, E. E. Benson, J. D. Froehlich and C. P. Kubiak, *Inorg. Chem.*, 2013, **52**, 2484.

94 M. D. Sampson, A. D. Nguyen, K. A. Grice, C. E. Moore, A. L. Rheingold and C. P. Kubiak, *J. Am. Chem. Soc.*, 2014, **136**, 5460.

95 M. Bourrez, M. Orio, F. Molton, H. Vezin, C. Duboc, A. Deronzier and S. Chardon-Noblat, *Angew. Chem. Int. Ed.*, 2014, **53**, 240.

96 D. C. Grills, J. A. Farrington, B. H. Layne, S. V. Lymar, B. A. Mello, J. M. Preses and J. F. Wishart, *J. Am. Chem. Soc.*, 2014, **136**, 5563.

97 C. Riplinger, M. D. Sampson, A. M. Ritzmann, C. P. Kubiak and E. A. Carter, *J. Am. Chem. Soc.*, 2014, **136**, 16285.

98 C. Riplinger, E. A. Carter, *ACS Catalysis*, 2015, **5**, 900.

99 F. Franco, C. Cometto, F. F. Vallana, F. Sordello, E. Priola, C. Minero, C. Nervi and R. Gobetto, *Chem. Commun.*, 2014, **50**, 14670.

100 H. Takeda, H. Koizumi, K. Okamoto and O. Ishitani, *Chem. Commun.*, 2014, **50**, 1491.

101 C. Costentin, S. Drouet, M. Robert and J.-M. Savéant, *Science*, 2012, **338**, 90.

102 C. Costentin, G. Passard, M. Robert and J.-M. Savéant, *Proc. Natl. Acad. Sci. U.S.A.*, 2014, **111**, 14990.

103 T. Comeau Simpson, R. R. Durand Jr., *Electrochim. Acta*, 1988, **33**, 581.

104 S.-N. Pun, W.-H. Chung, K.-M. Lam, P. Guo, P.-H. Chan, K.-Y. Wong, C.-M. Che, T.-Y. Chen and S.-M. Peng, *J. Chem. Soc., Dalton Trans.*, 2002, 575.

105 J. Chen, D. J. Szalda , E. Fujita and C. Creutz, *Inorg. Chem.*, 2010, **49**, 9380.

106 C. Arana, S. Yan, M. Keshavarz-K, K. T. Potts and H. D. Abruña, *Inorg. Chem.*, 1992, **31**, 3680.

107 C. Arana, M. Keshavarz, K. T. Potts and H. D. Abruña, *Inorg. Chimica Acta*, 1994, **225**, 285.

108 J.-M. Lehn and R. Ziessel, *Proc. Natl. Acad. Sci. U.S.A.*, 1982, **79**, 701.

109 J. Hawecker, J.-M. Lehn and R. Ziessel, *J. Chem. Soc., Chem. Comun.*, 1983, 536.

110 R. Ziessel, J. Hawecker and J.-M. Lehn, *Helv. Chim. Acta*, 1986, **69**, 1065.

111 F. R. Keene, C. Creutz and N. Sutin, *Coord. Chem. Rev.*, 1985, **64**, 247.

112 K.-M. Lam, K.-Y. Wong, S.-M. Yang and C.-M. Che, *J. Chem. Soc. Dalton Trans.*, 1995, 1103.

113 A. G. M. Mostafa Hossain, T. Nagaoka and K. Ogura, *Electrochim. Acta*, 1997, **42**, 2577.

114 T. Hirose, S. Shigaki, M. Hirose and A. Fushimi, *J. Fluorine Chem.*, 2010, **131**, 915.

115 J. Costamagna, J. Canales, J. Vargas and G. Ferraudi, *Pure & Appl. Chem.*, 1995, **67**, 1045.

116 M. Isaacs, J. C. Canales, M. J. Aguirre, G. Estiú, F. Caruso, G. Ferraudi and J. Costamagna, *Inorg. Chim. Acta*, 2002, **339**, 224.

117 S. Daniele, P. Ugo, G. Bontempelli and M. Fiorani, *J. Electroanal. Chem.*, 1987, **219**, 259.

118 L. Garnier, Y. Rollin and J. Périchon, *J. Oganomet. Chem.*, 1989, **367**, 347.

119 P. A. Christensen, A. Hamnett, S. J. Higgins and J. A. Timney, *J. Electroanal Chem.*, 1995, **395**, 195.

120 J. Canales, J. Ramirez, G. Estiú and J. Costamagna, *Polyhedron*, 2000, **19**, 2373.

121 Y. Mori, D. J. Szalda, B. S. Brunschwig, H. A. Schwarz and E. Fujita, *Advances in Chemistry*, 1998, **254**, 279.

122 V. S. Thoi and C. J. Chang, *Chem. Commun.*, 2011, **47**, 6578.

123 V. S. Thoi, N. Kornienko, C. G. Margarit, P. Yang and C. J. Chang, *J. Am. Chem. Soc.*, 2013, **135**, 14413.

124 J. S. Field, R. J. Haines, C. J. Parry and S. H. Sookraj, *Polyhedron*, 1993, **12**, 2425.

125 R. J. Haines, R. E. Wittrig and C. P. Kubiak, *Inorg. Chem.*, 1994, **33**, 4723.

126 B. Verdejo, J. Aguilar, E. García-España, P. Gaviña, J. Latorre, C. Soriano, J. M. Llinares and A. Doménech, *Inorg. Chem.*, 2006, **45**, 3803.

127 J. P. Muena, M. Villagran, J. Costamagna and M. J. Aguirre, *J. Coord. Chem.*, 2008, **61**, 479.

128 B. Verdejo, S. Blasco, J. González, E. García-España, P. Gaviña, S. Tatay, A. Doménech, M. T. Doménech-Carbó, H. R. Jiménez and C. Soriano, *Eur. J. Inorg. Chem.*, 2008, 84.

129 Z. Chen, P. Kang, M.-T. Zhang and T. J. Meyer, *Chem. Commun.*, 2014, **50**, 335.

130 J. Qiao, Y. Liu, F. Hong and J. Zhang, *Chem. Soc. Rev.*, 2014, **43**, 631.

131 C. C. Scarborough, K. M. Lancaster, S. DeBeer, T. Weyhermüller, S. Sproules and K. Wieghardt, *Inorg. Chem.*, 2012, **51**, 3718.

132 J. R. Pugh, M. R. M. Bruce, B. P. Sullivan and T. J. Meyer, *Inorg. Chem.*, 1991, **30**, 86.

133 C. Amatore and J.-M. Savéant, *J. Am. Chem. Soc.*, 1981, **103**, 5021.

134 J. A. Ramos Sende, C. R. Arana, J. L. Hernández, K. T. Potts, M. Keshevarz-K and H. D. Abruña, *Inorg. Chem.*, 1995, **34**, 3339.

Chapter II

–

Materials and methods

1. Electrochemical methods

1.1. General Considerations

1.1.1. Introduction

Electrochemistry is a crucial tool utilised in studying the reactivity of catalysts towards electrons and chemical substrates. Using electrochemical techniques, it is possible to oxidise or reduce molecules in a controlled fashion. The unique value of electrochemistry resides in the control offered to the scientist to evaluate and monitor a thermodynamic parameter (the potential, *E*) or a kinetic parameter (the current, *i*), and the relationship between these two fundamental properties, via the turn of a virtual knob. The aim of this section will not be to elaborate on explanations regarding the theory, motivation or execution of general electrochemical techniques. More details on these general subject areas can be found within several seminal and comprehensive books on electrochemistry.[1,2,3] Rather, the goal of this section is to describe the theory and execution of the specific electrochemical techniques employed during the course of study in later chapters. Particular attention will be given to aspects important to the reproducibility of the experiments to be described throughout this dissertation.

The three main electrochemical techniques that will be used and described are cyclic voltammetry (CV), chronoamperometry, and chronopotentiometry. Chronoamperometry and chronopotentiometry can both be viewed as preparative scale electrolysis techniques and will thus be considered together. Here a brief description of the techniques will be given, and the materials used to collect the data will be further described in the following paragraphs.

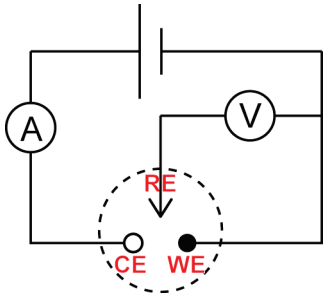

Figure II-1 Simplified schematic representation of a three-electrode setup.

A typical electrochemical setup consists of a three-electrode circuit as described in Figure II-1. It comprises a working electrode (WE), where the current and potential of interest are measured. It is at this electrode that the chemistry under study occurs. The counter electrode (CE) completes the circuit and supports the counter reaction required to balance the chemistry occurring at the WE. The reference electrode (RE) is the third electrode of this system and is used as a reference point to control or measure the applied voltage at the WE. The potentiostat measures the resting potential between the RE and the WE, represented by the presence of a voltmeter on the schematic circuit in Figure II-1, and applies a potential bias between the WE and the CE while recording the current as represented by the

presence of an ammeter in Figure II-1. The reverse, applying a current and recording a potential, is possible as well in most modern commercial potentiostat instruments (*i.e.* galvanostatic functionality).

All cyclic voltammetry data were recorded using either a Bio-Logic SP 300 or a Princeton Applied Research 263A potentiostat. Resistance was compensated to 85% using the ZIR built-in compensation method of the SP 300 Bio-Logic potentiostat. For details on the sources of resistance in electrochemical cells and to understand techniques used to minimise resistance, please refer specifically to page 22 of reference 1, page 24 of reference 2, and page 10 of reference 3.

Cyclic Voltammetry:

During a cyclic voltammetry experiment, a specified range of potentials is scanned at a specified speed, called the scan rate (ν). The potential at the electrode is modified at a constant rate, as described in Figure II-2, left. During this sweep of potential, the electron flow –the current (*i*)– at the electrode is measured over time (Figure II-2, centre). The generalised signal obtained for a reversible one-electron transfer is presented in a cyclic voltammogram: a plot of potential applied versus current measured, at a specified fixed scan rate (Figure II-.2, right).

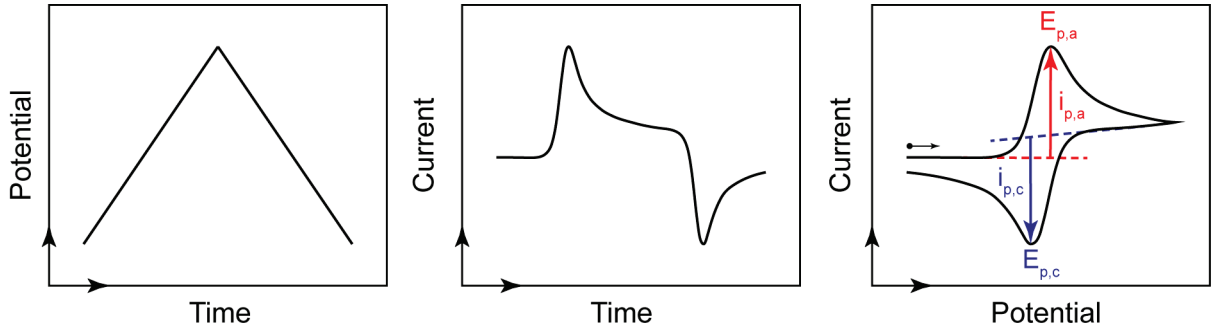

Figure II-2 Evolution of the applied potential over time during a cyclic voltammetry experiments (left), with the resulting current observed over time (centre). Right: current *vs.* potential data presentation called cyclic voltammogram.

In this work, the IUPAC convention is used to report current: anodic currents, corresponding to oxidations, are reported as positive and cathodic currents as negative. To describe electrochemical features such as the one described in Figure II-2, right, peak currents (i_p) and peak potentials (E_p) can be defined as presented in Figure II-2, right. The peak potential corresponds to the potential at which a peak in current is observed. The peak-to-peak separation is the difference in potential observed between the cathodic current and anodic current peaks. The peak current corresponds to the difference between the intensity measured at the peak and the baseline current observed before the peak (or its extrapolation, see Figure II-2). The subscripts “a” and “c” denote the anodic or cathodic nature of the feature. The redox potential of the electrochemical feature can be treated as the $E_{1/2}$ value, corresponds to $(E_{p,a} + E_{p,c})/2$.

Cyclic voltammetry (CV) of homogeneous stable compounds is typically a non-destructive technique. The potential is only applied for a fraction of a second in the vicinity of the working

electrode while the bulk of the solution is unaltered. The diffusion layer is defined as the region in the vicinity of the electrode where the concentrations of species are different from their value in the bulk solution. A simplified schematic representation of concentration profiles of two species Ox and Red (with Red = Ox + e^-) near the vicinity of the electrode is provided in Figure II-3. The top of the figure is taken to be values of higher concentration and the bottom of the figure is taken to be approaching a negligible concentration.

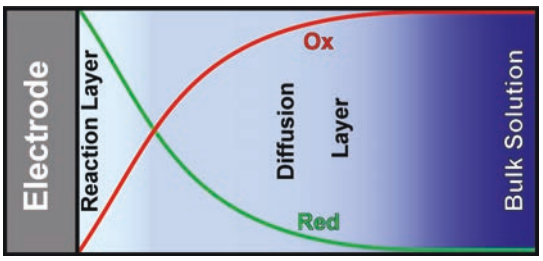

Figure II-3 Schematic representation of concentration profiles near the electrode.

In Figure II-3, the bulk solution is composed of the species Ox. At the electrode, Ox is reduced into Red, and only Red is present at the electrode. A diffusion layer is present between the electrode and the bulk solution, where a gradient of concentration of the species Ox and Red exists. Since the concentrations of Ox and Red reach asymptotic values, the definition of the thickness of the reaction layer is often arbitrary. Nevertheless, the size of the diffusion layer depends on several factors including the diffusion coefficient of the species studied and the scan rate. The largest diffusion layers are obtained for the slowest scan rates, and have lengths on the order of micrometres.[4,2]

Preparative Scale Electrolyses

During preparative scale electrolyses (or bulk electrolyses), either a constant current (chronopotentiometry) or a constant potential (chronoamperometry) is applied over the course of a specified length of time. The goal is generally to observe the behaviour of a chemical system once a thermodynamic (potential) or kinetic (current) parameter is fixed. The most common usage of these techniques is when one seeks to observe and detect large quantities of products resulting from electrocatalytic reactions under different conditions. With a goal to observe products, certain experimental conditions can be used to facilitate the generation of higher concentrations of products, such as the use of higher surface area electrodes and increased reaction times. In contrast to cyclic voltammetry, electrolyses are often viewed as destructive techniques since the nature of the species in the bulk of the solution will likely change over time. Since a likely occurrence is the eventual decomposition of a catalytic species or consumption of substrate, electrolyses are quite useful in obtaining data regarding the relative stability of electrocatalytic systems.

For controlled potential bulk electrolyses, the potential is applied and the current is recorded over time as it evolves freely. The integral of the current, the charge, measured in Coulombs (C), can also be reported and corresponds to the number of moles of electrons that have passed through the

working electrode. For controlled current bulk electrolyses, the current is applied and the potential is recorded over time as it evolves freely. However, since the current is controlled, the total amount of charge passed can also be easily determined based on the parameters of the experiment.

When studying a catalytic reaction by bulk electrolysis, the efficiency of the system in terms of number of electrons injected into the system versus the quantity of product observed, also called faradic efficiency, is often reported. For a system that is perfectly efficient, with a faradic efficiency of 1 (or 100%), every single electron passing through the working electrode is productively used towards the generation of product molecules. To measure the overall efficiency of a system after a long electrolysis, the total number of moles of product generated multiplied by the number of electrons needed to make the product can be divided by the total Coulombs injected into the system.

As for cyclic voltammetry, all preparative scale electrolysis data were recorded using either a Bio-Logic SP 300 or a Princeton Applied Research 263A potentiostat. The current intensity data was typically acquired every 0.02 s and smoothed using an adjacent–averaging method over 10 s.

1.1.2. Solvents and supporting electrolyte

Solvents

The choice of the solvent is dictated by several key aspects. The first and most important consideration is that the electrochemical window accessible with the solvent is wide enough for the reactions under study to be monitored without interference from direct reactivity of the solvent. The electrochemical window of a solvent is defined as the range of potentials between the two potential boundaries where the solvent molecules are reduced and oxidised. Beyond these extremes, the electrochemical activity of solvent dominates the electroactivity of the system as a whole, thus making it impossible to discern discrete electrochemical features relating to the molecules dissolved in the solvent. For example, in DMF with 0.1 M TBAP (tetrabutylammonium perchlorate) and using a Pt working electrode, the electroactive window extends from about −2.8 V to +1.5 V *vs.* SCE.[2]

The second key parameter specific to the study a homogeneous reaction is the solubility of the compounds studied in the solvent chosen. For most of the work presented herein, the catalysts studied are insoluble in water but quite soluble in organic solvents (a typical range of concentrations would be 0.1 - 10 mM).

Finally, for ease of study of the catalytic reactions, it is best to choose a solvent in which the substrate is soluble (here CO_2 and H^+) and where the potential gaseous products are as insoluble as possible. For example, to study the reduction of CO_2 to CO, CO_2 needs to be soluble enough to interact with the catalyst in an appreciable manner, but CO should be as insoluble as possible so as to allow for easy detection in the gaseous phase. The primary solvent chosen for the study is *N*,*N*-dimethylformamide (DMF). The solubility of CO_2 in DMF has been estimated at 0.23 M and that of CO at $9.8 \cdot 10^{-3}$ M at 1 atm and room temperature.[5,6]

Solvents used in this study were purchased from Sigma-Aldrich at ACS reagent grade or higher and used as received. Anhydrous solvents (*N*,*N*-dimethylformamide, *N*,*N*-diethylformamide, 1-methyl-2-pyrrolidinone and acetonitrile) were purchased from Sigma-Aldrich and used as received.

Supporting Electrolyte

The supporting electrolyte facilitates closing the electrochemical circuit with minimal added resistance by allowing for ion mobility within the electrochemical system. As was the case for the solvent, it is important for the supporting electrolyte to be stable towards oxidation and reduction in the range of potentials that are being studied. The concentration of the electrolyte will influence the resistance of the solution, and in this study the electrolyte concentration used is 0.1 M throughout this manuscript unless otherwise noted. The typical supporting electrolyte salt used was tetra-*n*-butylammonium hexafluorophosphate ($TBAPF_6$) and tetra-*n*-butylammonium perchlorate (TBAP). TBAP was used as a standard electrolyte salt in electrochemistry and is available at ≥ 99.0% purity (for electrochemical analysis grade) from Sigma-Aldrich, but concerns over the explosive nature of perchlorates salts have led us to favour $TBAPF_6$ over the later part of this manuscript (Chapter IV and V). $TBAPF_6$ is available at ≥ 99.0% purity (for electrochemical analysis grade) from Sigma-Aldrich and was used without further purification. To vary the nature of the cation, dry $LiClO_4$ was also employed briefly, purchased from Sigma-Aldrich at 99.99% purity, trace metal basis (battery grade).

1.1.3. Gases

All solutions were thoroughly degassed and saturated with inert gas (Ar, N_2) or CO_2 before electrochemical measurements. Gas cylinders were connected to a test-tube containing the electrolyte solution through which gases were bubbled to reach solvent vapour saturation. The sealed test-tube was connected to the electrochemical cell with PTFE tubing, < 1 mm inner diameter, fitted through a septum or through the premade openings in the Teflon caps of the electrochemical cells.

1.2. Electrodes

1.2.1. Working electrodes

The working electrode is to an electrochemist as a reagent is to a synthetic chemist. It has to be stored and handled appropriately. The surface area of the working electrode and the condition of its surface, such as the presence of adsorbed species, will have a significant influence on the measurement.

Carbon electrodes for cyclic voltammetry

All the working electrodes used for cyclic voltammetry experiments are glassy carbon electrodes with a diameter of 1.0, 1.5 or 3.0 mm depending on the experiment, purchased from Bio-Logic. The electrodes are composed of a glassy carbon disk electronically connected to a brass pin that is used to connect to the potentiostat. To control the exposed surface of the glassy carbon, the body of the electrode is covered in the insulating material polyether ether ketone (PEEK) which is stable to organic solvents and acids, leaving only a well-defined glassy carbon disk exposed. The schematic

representation of the glassy carbon used for routine cyclic voltammetry experiments is depicted is Figure II-4.

Figure II-4 Side and bottom view of the schematic representation of the commercial glassy carbon working electrodes used in routine cyclic voltammetry experiments.

Before each measurement in homogeneous solutions, the glassy carbon electrodes were polished with a 1 µm diamond suspension followed by rinsing with water and acetone and finally drying in air. If a deposit formed inadvertently on the electrode during the course of an experiment or in the study of surface-modified electrodes, the glassy carbon electrodes where polished first with 800/2400 and 1200/4000 grit silicon carbide paper, followed by the 1 µm diamond suspension. The electrodes were then rinsed with water and acetone before drying in air as usual.

Mercury electrodes

For bulk electrolysis of homogeneous catalysts, see Chapters III and IV, a pool of liquid mercury (Hg^0) was used as the working electrode. Mercury offers the benefit of being able to reproducibly control the nature, size and purity of the surface of the electrode easily. Hexadistilled mercury (99.999999%) purchased from OPHRAM was used as received and a new pool of mercury was used for each experiment. This ensured a perfectly reproducible surface, in terms of size, nature and state, which allows for appropriate comparison of the current intensities observed in different bulk electrolyses.

Carbon electrodes for bulk electrolysis

Chapter V reports the reactivity of soluble catalysts that are immobilised onto glassy carbon electrode surfaces. While cyclic voltammetry experiments were conducted on the commercially available electrodes described above, bulk electrolyses experiments could not be conducted with the usual pool of mercury as working electrode. Instead 1.4 cm diameter glassy carbon pellets were used as working electrode. The pellets were purchased from OrigaLys and were manufactured to become suitable for use in bulk electrolysis experiments as schematically depicted in Figure II-5.

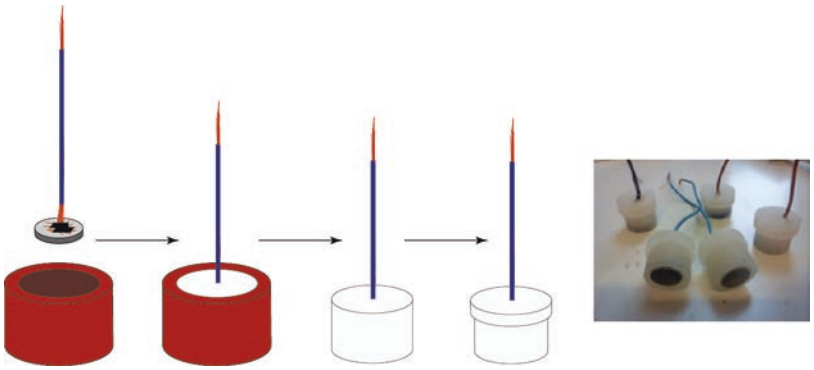

Figure II-5 Schematic representation of the process implemented to obtain glassy carbon WE for bulk electrolysis.[§]

The 1.4 cm diameter glassy carbon pellet is connected to a copper wire with carbon tape and coated with a cold mounting KM-U resin purchased from PRESI in a 30 mm diameter rubber mould. Polymerisation occurs after mixing the two components of the resin. The reaction is exothermic and full polymerisation occurs within 10 minutes at 20 °C. After drying and unmoulding, the resin around the electrode is carved to the appropriate shape (Figure II-5).

The electrical contact between the exposed carbon surface and the copper wire is then tested before the electrode is used for measurements. Prior to use, the electrode is polished as described previously, except no acetone is used. The KM-U resin, which is acrylic based, presents advantages and drawbacks. The main advantage is the ease of use: cold mounting in a rubber mould is easy to implement. The carbon pellet can also be reclaimed and reused easily by soaking the electrode in acetone overnight, at which point the resin swells enough that the carbon pellet can be recovered and reused in a different electrode. However this phenomenon of electrode swelling in the presence of acetone shows the main drawback of this resin: its resistance to organic solvents, although unmatched by other cold mounting resins, is not ideal. The resin will swell quickly if immersed several hours in MeCN, and although it is significantly more resistant to DMF, after 4 h evidence of swelling is observed. By the lack of observation of background electrochemical features, no chemicals appear to leach out of the swollen resin however, making it an appealing candidate as the insulating coating around the carbon electrodes. Nevertheless, each electrode was only used for one experiment before the glassy carbon pellet was reclaimed and reused in a new electrode.

1.2.2. Counter electrodes

The potentiostat increases the potential difference between the counter and working electrodes, in the limit of the compliance, until the potential difference between the WE and RE reaches the specified value. Since the reactions studied and monitored are occurring at the working electrode, it is important for the counter electrode to have a surface area significantly higher than that of the working electrode so that the current intensities are limited by the events at the working electrode. The classical material used for counter electrodes is platinum, since it has a good stability to electrochemical oxidation and reduction. When studying a reduction reaction at the working electrode, it is important to remember that an oxidation reaction is taking place at the counter electrode simultaneously. The reactions studied within this manuscript are mostly reduction reactions that occur in DMF. It is known that at an oxidizing potential in the presence of quaternary amines and at a platinum electrode, the solvent DMF is oxidised to yield liquid products. This means that no interfering production of gases will occur in bulk electrolysis conditions, contrary to reductions in water for example, where O_2 is generally generated at the counter electrode.

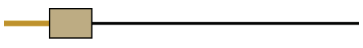

Figure II-6 Schematic representation of the commercial platinum counter electrode used for cyclic voltammetry experiments.

The schematic representation of the commercially available (Bio-Logic) platinum counter electrodes used for cyclic voltammetry experiments is presented in Figure II-6. The electrode is constituted of a platinum wire connected to a brass pin and partially coated with PEEK at the junction between the brass pin and the platinum wire. The platinum counter electrodes were washed in acid, rinsed with water and acetone then air dried before use.

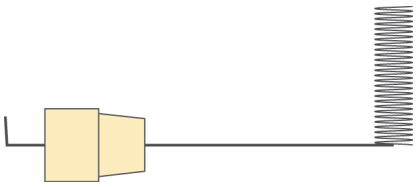

Figure II-7 Schematic representation of the platinum counter electrodes used for bulk electrolysis.

For use in bulk electrolysis cells, platinum counter electrodes were manufactured simply by feeding through a rubber septum a 0.5 mm diameter annealed platinum wire purchased from Alfa Aesar at the highest available purity. The wire is locked in position in the septum by application of an epoxy based resin. The rest of the platinum wire is coiled so as to have a high surface area in a small volume to fit in the bulk electrolysis cell (Figure II-7).

1.2.3. Reference electrodes

In order to provide a stable potential for the regulation of the working electrode (WE) potential, reference electrodes should have a composition that is stable in the experimental conditions, leading to an unvarying resting potential.

Figure II-8 Schematic representation of the commercial reference electrodes used for cyclic voltammetry experiments.

For cyclic voltammetry experiments the reference electrodes used are commercially available Ag/AgCl reference electrodes (RE-1B from Bio-Logic). The electrode has a glass body that contains the silver wire and the 3M NaCl filling solution, which is separated from the solution of the electrochemical cell by a Vycor tip which is maintained in place with a PTFE heat shrink tube as schematically depicted in Figure II-8. The electrical connection to the potentiostat occurs through a brass pin.

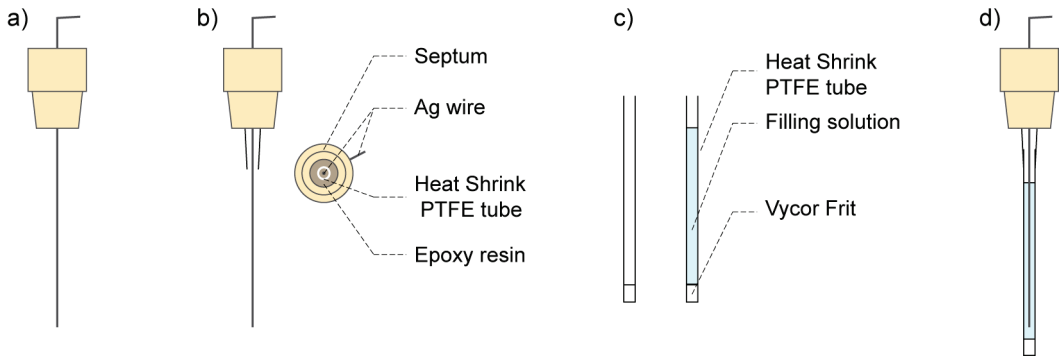

Figure II-9 Schematic representation of the process implemented to make reference electrodes used for bulk electrolysis as described within the text.

Electrodes for use in bulk electrolysis cell were custom made following a modified literature procedure.[1] A 0.5 mm diameter annealed silver wire was purchased from GoodFellow at the highest available purity (99.99%) and fitted through a rubber septum (Figure II-9, a). A portion of heat shrink PTFE tube is affixed to the septum around the silver wire, partially shrunk to obtain a gradient of diameter size, and maintained in place by epoxy glue as depicted in Figure II-9 b.

The silver wire is then cleaned by cycling between –0.3 V and 1.2 V *vs.* Ag/AgCl in H_2SO_4 0.5 M in water in an electrochemical cell by cyclic voltammetry using the silver wire as a working electrode, and a platinum wire counter electrode at 100 mV/s until the scan are superimposable. The silver wire thus cleaned of any oxide is then soaked in a 0.1 M solution of $FeCl_3$ for 20 min to create a AgCl coating layer around the silver core. The silver chloride coating is white and becomes darker in the presence of light. The wire is then rinsed by soaking in deionised water overnight. Meanwhile a heat shrink tube is fitted around a Vycor frit, filled with the filling solution (typically a saturated AgCl with KCl 3 M solution, Figure II-9, c), and fitted through the top of the electrode to seal it (Figure II-9, d).

Vycor frits are used in both the commercial and *house-made* reference electrodes as a way to separate the internal solution from the media of the electrochemical cell because of its modest leak rate and compatibility with the organic solvents used. Ag/AgCl reference electrodes are not typically recommended for use in non-aqueous solvents because of a higher junction potential. However, the reproducibility and stability of the electrode in the condition tested and on the time frames used was satisfactory and as such they were used in this manuscript. For future studies in non-aqueous solvents, a Ag/Ag^+ pseudo-reference electrode can be used, or a salt bridge can be added to the system to further minimize these issues.

As it is, the ferrocenium/ferrocene redox couple (Fc^+/Fc) was used to calibrate the reference electrodes whenever possible, and the potentials in Chapter III and IV are given with respect to this external reference in the exact experimental conditions employed. The experimental conditions will influence the potential of the Fc^+/Fc couple. Table II-1 provides the equivalent of the Fc^+/Fc couple vs. NHE in different solvents.[1]

Table II-1 Potential of the Fc^+/Fc couple in different solvents and vs. different reference electrodes.

Solvent	$E^\circ_{Fc+/Fc}$ in the solvent, V *vs.* NHE	$E^\circ_{Fc+/Fc}$ in the solvent, V *vs.* SCE	$E^\circ_{Fc+/Fc}$ in the solvent, V *vs.* $Ag/AgCl_{sat}$	$E^\circ_{Fc+/Fc}$ in the solvent, V *vs.* Ag/AgCl 3M NaCl
DMF	0.72	0.48	0.53	0.51
MeCN	0.69	0.45	0.50	0.48
H_2O	0.40	0.16	0.21	0.19
DMSO	0.68	0.44	0.49	0.47

Using this external reference as the reference potential for data presentation purposes allows for removing the drifts of potential that might occur with non-saturated Ag/AgCl electrodes over time, as slow evaporation might lead to a more concentrated filling solution, thus causing a drift in the resting potential of the RE. A saturated solution of NaCl or KCl has the advantage of offering a better stability over long periods of time as any evaporative losses would not lead to a change in the concentration of the chloride ions in solution, which is the cause of the modification of the equilibrium potential of the electrode.

1.3. Cells

1.3.1. Cells used in cyclic voltammetry experiments

Cyclic voltammetry experiments were carried out in single compartment cells, using 3 mL or 10 mL glass cells purchased from Bio-Logic. The glass cells were fitted with a Teflon cap with several openings through which either electrodes could be positioned within the cell or gas could be passed into and out of the cell. A schematic representation of the CV cell can be found in Figure II-10.

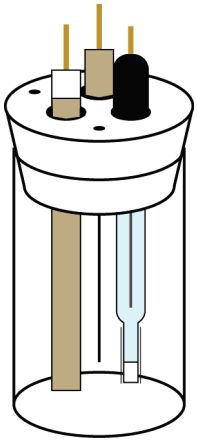

Figure II-10 Schematic representation of an electrochemical cell used for cyclic voltammetry experiments. The typical volume of solution used is 3-10 mL.

1.3.2. Cells used for bulk electrolyses experiments

Beyond the experimental considerations for a standard electrochemical cell, a bulk electrolysis cell must comply with a few extra criteria. First, since the goal is to observe and quantify a large enough concentration of products, the cell needs to be able to accommodate the use of a working electrode with a higher surface area. Second, since the products might be gaseous, the cells must be gas tight to contain those products, and must offer a straightforward way to sample the headspace of the cell with a gas tight syringe to be able to measure those products. Finally, it is often important for some separation to exist between the working and counter electrodes so that the anodic and cathodic reaction products remain separate, at the price of increased cell resistance. It can be important to isolate the chemistry occurring at the counter electrode from the reactions of interest occurring at the working electrode. Cross contamination of products between electrodes can result in many experimental problems, such as artificially lowering faradic efficiency if desired products formed at the WE are re-

oxidised or re-reduced at the CE. Similar considerations must be made for the gaseous atmosphere above the working and counter electrodes, which must be isolated from each other in cases were gases produced at the counter electrode could influence the measurement of gases produced at the working electrode.

Cells with mercury working electrode (used in Chapter III and IV)

In Chapters III and IV, numerous bulk electrolysis experiments are conducted on mercury working electrodes. In order to contain the mercury and to insure a good electrical contact, custom made bulk electrolysis cells were used. The schematic representation of the electrochemical custom made two-compartment cell used for bulk electrolyses on a pool of mercury electrode is depicted bellow (Figure II-11).

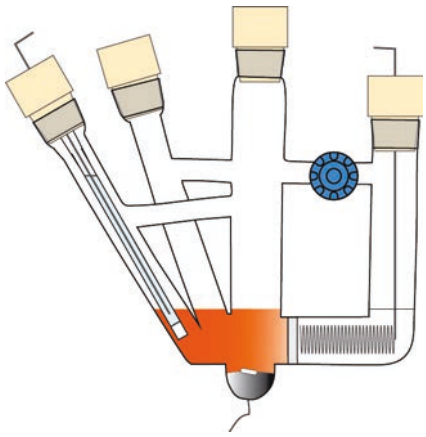

Figure II-11 Schematic representation of the cell used for bulk electrolysis on a mercury working electrode.[‡]

The working compartment (typically 8-10 mL, represented in orange within Figure II-11), on the left, contains the 1.5 cm diameter pool of mercury used as working electrode, connected through the glass with a platinum wire for electrical contact. The reference electrode is separated from the working compartment with a Vycor frit. The working and reference electrodes are separated from the coiled platinum wire counter electrode, on the right, by a porous glass frit (pore diameter 10-16 µm). The solution is constantly stirred throughout the experiments with a small stir bar floating over the pool of mercury. The electrochemical cell is made gas tight with rubber septa (represented in beige within Figure II-11), and the headspace can be sampled through the rubber septa using gas tight syringes for gaseous products analyses. An additional glassy carbon electrode can be fitted through one of the septa for direct cyclic voltammetry experiments of the bulk solution.

Cell used with modified glassy carbon electrodes (used in chapter V)

In Chapter V, bulk electrolysis will need to be conducted on modified glassy carbon electrodes. To accommodate the use of these electrodes, the custom made cell in Figure II-12 was used.

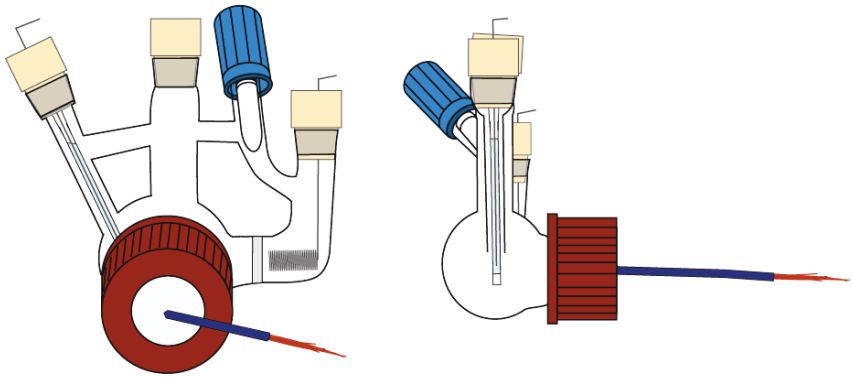

Figure II-12 Front and side view of the schematic representation of the cell used for bulk electrolysis on glassy carbon electrodes.[§]

The working electrode used was a 1.4 cm diameter glassy carbon pellet as described in 1.2.1 of this chapter, separated from the coiled annealed platinum wire counter electrode by a porous frit (pore diameter 10-16 µm). The reference electrode was separated from the working compartment by a Vycor tip. The typical volume of solution used in the working compartment of the cell is 30 mL, and the typical headspace volume is 29 mL. Bulk electrolyses solutions were stirred throughout the experiments via a magnetic stir bar positioned at the bottom of the working electrode compartment.

2. Chemical analysis

2.1. Introduction

As for CO_2 reduction, one needs to carefully detect and quantify the various possible products of the reaction for an accurate representation of catalyst activity. For example, in an iconic survey, Jaramillo and co-workers were able to identify 16 different products in the study of electrochemical CO_2 reduction on copper surfaces.[7] A number of carbon containing molecules need to be considered, as well as the proton reduction product H_2 that is often found as a coproduct in reactions that are not fully selective.

Although natural photosynthesis ultimately transforms CO_2 to carbohydrates, the most common products generated by homogeneous CO_2 reduction catalyst contain fewer than 3 carbon atoms. The most commonly reported products, however, are typically the two-electron reduced and single carbon containing products of CO_2. Of the products, CO is often detected for systems that include molecular catalysts, and is generally obtained alongside H_2. Additionally, liquid formic acid can also be detected as a two-electron reduction product obtained through a unique mechanistic pathway.

Despite the more ubiquitous reports of two-electron reduced products of CO_2 reduction, further reduction can occur and require consideration. However, carbon-carbon bond formations through CO_2 reduction, while not unprecedented, are exceedingly rare and therefore an emphasis is placed on the evaluation of single-carbon containing products. Therefore, if CO_2 is reduced by four-electrons the most likely product is formaldehyde. The most likely six-electron reduced product considered is methanol. Additionally, methane is also evaluated as the fully reduced carbon containing product. Whereas two-electron pathways for CO_2 reduction have much greater precedent, a direct one-electron reduction of CO_2 can occur to yield oxalate through radical coupling and warrants consideration as well.

Finally, other factors to consider when choosing detection methods for CO_2 reduction products include the nature of the solvent (DMF or water), the presence of high concentration of electrolyte salts, the possibility of complex product mixtures, and the presence of the metal complexes used as catalysts.

2.2. Detection of gaseous products

2.2.1. H_2

Given the amount of research efforts that have been directed at developing proton reduction catalysts over the years to produce clean source of hydrogen gas, the methods for detecting hydrogen are well developed. One of the most common methods for hydrogen separation and detection is using a gas

chromatography fitted with a thermal conductivity detector. This is the method that has been utilised within these investigations.

H_2 measurements were performed by gas chromatography on a Shimadzu GC-2014 equipped with a Quadrex column for gas separation, a thermal conductivity detector (TCD) for analyte quantification, and using N_2 as a carrier gas. The standard method calls for heating the column at 100°C with a fixed flow rate of 5 mL/min, with the temperature of the injector fixed at 100°C and 200°C for the TCD. Gas chromatography calibration curves were made by sampling known volumes of pure H_2 gas and H_2 diluted in CO_2 or N_2. The typical volume of gas injected was 50 µL. Although robust, this method is based on the idea that H_2 can be first separated from other gases in the headspace by column, and then that the thermal conductivity of H_2 is different enough from the carrier gas that is has a strong signal on the detector. Given the experimental setup in the lab, with N_2 as the carrier gas and the Quadrex column, it is important to remember that Ar cannot be used as an inert atmosphere during bulk electrolysis because its retention time in the conditions tested and on the Quadrex column is too similar to H_2 and obscures the interpretation of H_2 measurements. The sample complications exist for CO and O_2, as these gases are not efficiently separated from H_2 in the method used. However, the sensitivity of the TCD to CO and O_2 in the conditions used is generally too low to perturb the measurement when a controlled atmosphere is maintained in the experimental setup. Nevertheless great care should be taken to avoid O_2 contamination of the reaction vessel or of the syringe to insure an accurate measure of H_2. Similarly, in an electrochemical experiment, it is critical to ensure that the nature of the reaction occurring at the counter electrode will not prevent accurate H_2 measurement.

Given these preoccupations, a mass spectrometer detector, one that is sensitive to the actual mass of the analytes, would have been useful to unequivocally identify H_2, O_2, CO and other gases even if quantification might prove more challenging.

2.2.2. Gaseous carbon containing products

CO was measured using a Shimadzu GC-2010 Plus gas chromatography, fitted with a Restek Shin Carbon column, helium as the carrier gas, a methanizer and a flame ionisation detector (FID). The typical method used imposes a temperature of 100°C to the column, for 13 min, at a fixed pressure in the column of 250 kPa, with a purge flow of 3 mL/s, a split ratio of 4 and temperatures of 390°C for the injector and the methanizer, and 280°C for the FID. In these conditions CO is detected at about 1.2 min and CO_2 at about 3.7 min. Other small gaseous carbon containing gases, such as CH_4, typically elute between the CO and CO_2 peaks.

Since the sensitivity of the FID to CO is low, but the sensitivity to CH_4 is high, the stream of gases once separated on the column is passed through a methanizer, which burns the stream of gases, turning CO and CO_2 in CH_4. This way the sensitivity of the FID to CO is greatly augmented and renders its use possible routinely even with the low concentration of CO that are produced in bulk

electrolyses. It is worth noting that in the conditions used, in the absence of a mass spectrometer detector, the unequivocal identification of the source of the carbon atom during CO production cannot be obtained through labelling experiments.

Gas chromatography calibration curves were obtained by sampling known volumes of pure CO gas and CO diluted in CO_2 or N_2. The calibration curve, although stable on the short time scale (couple of weeks), was observed to drift over long periods of time, or after particular experiments. The sensitivity and the calibration curve depend mainly on the state of the methanizer. If unusual volatile products are injected and polymerise onto the methanizer, its efficiency for methanizing CO and CO_2 will decrease, leading to a different sensitivity, and thus a different value for the calibration curve. Nevertheless, with frequent checks of the calibration curves, using this instrument present no major problems. A quick handle on the state of the methanizer, and thus the calibration curve, is given by the area of the CO_2 peak. Since most experiments are conducted under 1 atm of CO_2, the area of the CO_2 peak should stay constant for a given volume of gas injected, which gives a quick visual measure of the state of the methanizer.

2.3. Detection of products in solution

2.3.1. Charged carbon containing products

Formate and oxalate are the two main carbon containing products that are under consideration as anionic products. Although formate detection methods are numerous, not many are selective and adapted to the range of products that are present in the reaction mixture of a CO_2 reduction reaction.

If the concentrations are sufficiently high, and the reaction medium is amenable to it, ^{1}H and ^{13}C NMR are a valuable technique to measure the concentrations of formate or formic acid. This method also allows for the verification of the origin of the carbon atom, using $^{13}CO_2$ and monitoring the increase in ^{13}C signal or lack thereof. Since the systems used in this manuscript result from electrochemical experiments, which imply a large quantity of salt, and using paramagnetic transition metal complexes, ^{13}C and ^{1}H NMR were not suitable for routine measurements of formate concentrations.

The method chosen instead is based on the conductivity of formate ions in solution, using ionic exchange chromatography (IC). The instrument elutes ions based on their affinity to an ion exchange column and detects their presence based on their conductivity. In general ion separation relates to both the charge and size of the ion.

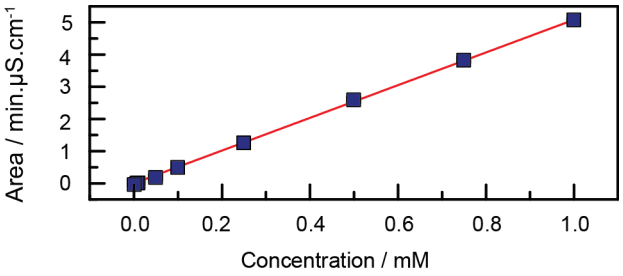

Figure II-13 Calibration curve for the determination of formate concentration in solution. The equation of the linear fit, in red, is y = 5.0794x, with R^2 = 0.9998.

Formate and oxalate concentrations were determined using a Metrohm 883 Basic IC plus ionic exchange chromatography instrument, using a Metrosep A Supp 5 column and a conductivity detector. A typical measurement requires the sampling of 1 mL of solution, followed by a 100 fold dilution in deionised 18 MΩ/cm water and injection of 20 µL into the instrument. The eluent is a 1 mM $NaHCO_3$ / 3.2 mM Na_2CO_3 water solution. With a flow rate of 0.7 mL/min, the typical elution time of formate is 6.5 min. The calibration curve (Figure II-13) was obtained by injecting HCOONa solutions of known concentration and measuring the area of the resulting formate peak. The sensitivity is mainly dependent on the conductivity and was extremely stable over time. The baseline, elution times and measured conductivity were observed to be sensible to the exact concentration of the buffer solution, so great care should be taken when changing the buffer solution.

Caution is also necessary when determining formate concentrations if DMF is being employed as a solvent. Great care must be taken to separate the counter electrode from the working electrode during bulk electrolyses, as formate appears to be generated at the counter electrode, possibly through a one-electron oxidation of DMF followed by hydrolysis. It is also worth noting that with the standard method parameters, all small organic acids elute at extremely close time points, meaning that, for example, acetic acid should not be employed as an acid source in a system where formate detection is needed.

2.3.2. Formaldehyde

Formaldehyde detection is challenging in the context of CO_2 reduction since detection methods need to be not only very sensitive but also extremely selective considering that the reaction mixture containing formaldehyde might also contain other CO_2 reduction products such as formate or methanol, as well as carbonates in the solution. It is tempting to think of oxidizing formaldehyde to formate and detect the resulting formate by IC, given that the amount of formate will be routinely measured by IC. However this technique requires oxidants that are not too powerful to avoid oxidizing formate, which would then be lost as CO_2, rendering this approach difficult to reproduce quantitatively. This is even without considering possible products of side oxidation events in the conditions used. For example, DMF, which is routinely used as a solvent for electrochemical studies

for its good solubilizing properties and stability in reducing conditions, is susceptible to oxidations, which, in the presence of water, leads to its hydrolysis into formate.

Another possible analytical method is the use of liquid injection into GC/FID instruments to detect formaldehyde; however the sensitivity of this detection method did not appear to be sufficient given the slow nature of the systems under study. An additional consideration is the question of contamination of the liner of the GC by electrolyte salts on a regular basis, so that a method to remove the electrolyte without perturbing the formaldehyde concentration would have had to be developed.

Finally, chemical coupling methods were tested to obtain a highly coloured molecule which could then be detected by UV-vis directly or detected after separation on an HPLC instrument. It has been previously reported that chromotropic acid (1,8-dihydroxynaphthalene-3,6-disulfonic acid) can react according to an unidentified reaction to form a highly coloured purple species that is easily identifiable by UV-vis at 575 nm.[8] However, this reaction requires heating at 100°C for several minutes in concentrated sulfuric acid. This leads to strong concerns about the selective nature of the reaction, as these very harsh conditions can lead to numerous side reactions in the solution, including on the metal complexes that might be present. It is therefore not surprising that this method proved unselective and not suitable for the reaction conditions that are used routinely. This became apparent as the reaction generated a gaseous product, and through the inconsistency of the measurements obtained.

To overcome these challenges, the Nash test was evaluated as a possible detection method due to the more gentle reaction conditions required, the extremely high selectivity for reactivity with formaldehyde, and the compatibility with the presence of solvents typically used for electrochemistry. Formaldehyde reacts with the Nash reagents to form a yellow species with an extinction coefficient of about $8 \cdot 10^3$ M^{-1} cm^{-1} at 412 nm. Detection by UV-Vis is straightforward, and the method can be improved by HPLC if a detection limit as low as 0.1 µM is required.[9]

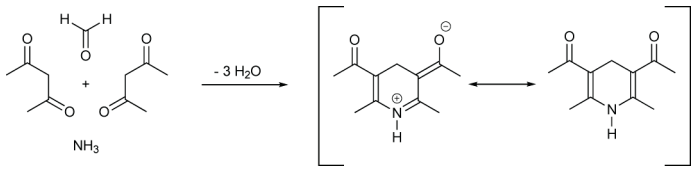

Figure II-14 Schematic representation of the Nash reaction.

Nash reagent stock solution is prepared by adding 7.5 g of ammonium acetate, 150 µL of acetic acid and 100 µL of 2.4-pentanedione to deionised water to obtain 50 mL. This solution can be kept in the dark at –20 °C for at least 5 days. During a Nash test, formaldehyde reacts with the ammonium and the acetylacetonate to yield the yellow dye, as depicted in Figure II-14.

The Nash test first calls for a 10 fold dilution of the samples to be able to measure concentrations of formaldehyde in the 0 - 2.5 mM range within the reaction mixture, since the

solubility of the Nash yellow dye is 0.250 mM in water. The dilution is done in deionised water. Typically, 100 µL of the solution to be tested (DMF) is mixed with 900 µL of deionised water to obtain 1 mL of solution that is placed in an Ependorph. 200 µL of Nash stock solution is added, and the mixture is heated to 51°C for 20 min, followed by cooling for 3 min at room temperature in a water bath, at which point the solution is transferred to a 1 cm cuvette and the absorbance of the solution is measured at 412 nm. To take into account the background absorbance of the electrolyte at 412 nm, the same procedure is applied to another 100 µL of solution to be tested, except 200 µL of deionised water are added instead of the 200 µL of Nash solution. The only false positive known to the Nash test is acetaldehyde.

To obtain calibration curves in the conditions that are used for bulk electrolyses, a stock solution of formaldehyde in water (33.3 mM) was purchased from Sigma-Aldrich (Formaldehyde IC Standard, Aldrich). The 1 mL solutions of various known formaldehyde concentration in DMF/H_2O (95:5; v:v) TBAP 0.1M mixtures were prepared and analysed according to the method described above.

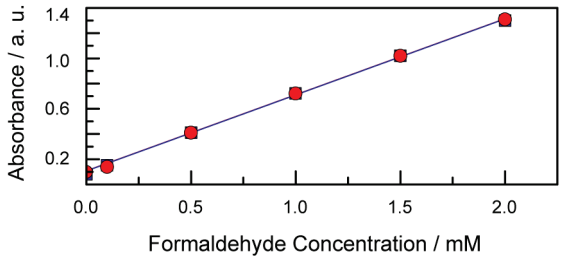

Figure II-15 Comparison of the response to the Nash test as observed in a quartz (blue squares) and plastic (red circles) cuvette of solutions of DMF/H_2O (95:5; v:v) TBAP 0.1M, with various concentrations of formaldehyde. The equations of the linear fits are virtually identical, with a slope of 0.604 mM^{-1} correlation coefficients of 0.999 in both cases.

The calibration curve obtained is independent of the nature of the cuvette used (PMMA plastic or quartz), allowing for routine use of disposable plastic cuvettes as shown in the left part of Figure II-15.

The reproducibility of this method was evaluated by varying all the solutions involved (Figure II-16). Test n°1 and Test n°2 were done using the same batch of electrolyte (DMF/H_2O, 95:5 volumetric ratio, TBAP 0.1 M) but different formaldehyde stock solutions, which tests the accuracy of the dilution as well as the reproducibility of the Nash reaction test. Test n°3 was done changing all the solutions, including the Nash stock solution. These three tests are summarised in the Figure II-16 and led to the decision that the calibration value used for the subsequent formaldehyde measurements is 0.60 a.u per mM of formaldehyde, corresponding to the slope of the linear fits. The second conclusion is that the electrolyte influences slightly the background absorbance value, which is reflected in the y-axis at x = 0. Thus the electrolyte used in the electrochemical experiments will have to be tested with the Nash solution systematically to obtain a corrected value of background absorbance.

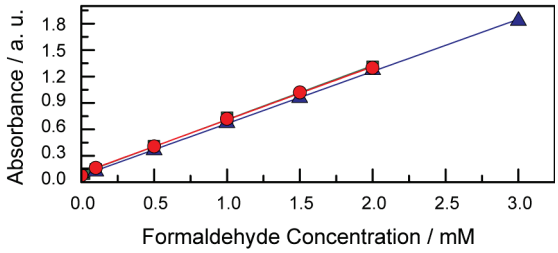

Figure II-16 Reproducibility tests. Slopes of the linear fits are as follows: Test n°1 (red circles), y = 0.613x + 0.098, R^2 = 0.9994; Test n°2 (green squares), y = 0.592x + 0.074, R^2 = 0.9999; Test n°3 (blue triangles), y = 0.603x + 0,104, R^2 = 0.9996.

The accuracy of the method at lower formaldehyde concentrations was also evaluated, and the results are shown in Figure II-17. It appears that the accuracy is enough to measure concentration as low as 0.5 mM. Should lower concentrations be measured, two methods could be used to obtain a better accuracy: either not diluting the sample 10-fold prior to reaction with Nash reagent, or injecting the sample into the HPLC to separate the actual Nash dye from unreacted molecules or from the background signals.

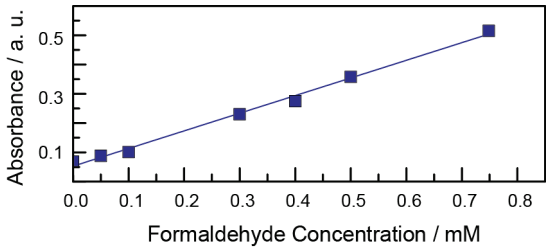

Figure II-17 Results of the Nash tests at lower formaldehyde concentrations. The equation of the linear fit is y = 0.603x + 0.053 and R^2 = 0.995.

The influence of the presence of a coloured metal complex in solution on the absorbance measured was also tested. The orange $[Co(tpy)_2](PF_6)_2$ complex was used for this study. Solutions of DMF/H_2O (95:5; v:v) TBAP 0.1 M were prepared, with 1 mM $[Co(tpy)_2](PF_6)_2$ and 1 mM formaldehyde. On one sample the Nash test was performed as described previously (Test n°4). On a second sample, the same steps were implemented (dilution, addition of 200 µL of Nash solution, heating at 51°C for 20 min, then cooling at RT and detection at 412 nm) but the 200 µL of Nash solution were replaced with 200 µL of deionised water (Test n° 5). The results are presented in Figure II-18.

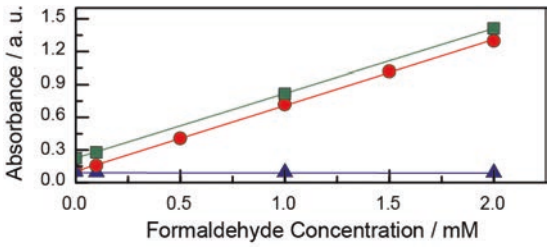

Figure II-18 Effect of the presence of $[Co(tpy)_2](PF_6)_2$ on the results of Nash tests. Green squares: Test n° 4 (y = 0.60x + 0.22, R^2 = 0.9998), red circles: Test n°1 from Figure II-16 (y = 0.61x + 0.098, R^2 = 0.9994) and blue triangles: Test n° 5 (y = −0.0016x + 0.0909, R^2 = 0.9519).

The slope of the calibration curve is unaffected, but the y value at x = 0 is modified; indicating that a "blank" measurement will have to be performed every time, by replacing the 200 µL Nash solution with 200 µL deionised water. It is thus possible to determine the formaldehyde concentration of solutions containing $[Co(tpy)_2](PF_6)_2$ using the previously determined calibration curve, taking into accoun the background absorbance of the $[Co(tpy)_2](PF_6)_2$ complex, as well as the background reactivity of the electrolyte to the Nash solution as determined previously. Several solutions of known formaldehyde concentrations in the electrolyte containing 1 mM $[Co(tpy)_2](PF_6)_2$ were made. They were divided into two portions, and were both subjected to the conditions of the Nash test, except in one of them the Nash solution is replaced with deionised water. The difference of absorbance of the two solutions is reported in Table II-2 (second column).

Table II-2 Results of the Nash test on 5 samples of different formaldehyde concentration containing each 1 mM Co-tpy in DMF/H_2O (95:5; v:v), TBAP 0.1 M. The background absorbance of the electrolyte (after Nash reaction) is b = 0.120.

Actual H_2CO Concentration / mM	*Measured* ΔAbs / a. u.	*Calculated* H_2CO Concentration / mM
0.00	0.139	0.03
0.10	0.182	0.10
1.00	0.718	1.00
1.00	0.717	1.00
2.00	1.314	1.99

With these absorbance differences, the it is possible to calculate the concentration of formaldehyde using the equation: $[H_2CO] = (\Delta Abs - b)/ 0.60$. The results presented in the third column of Table II-2 indicate that an accurate determination of the concentration of formaldehyde in solutions containing $[Co(tpy)_2](PF_6)_2$ is possible.

The next parameter to be tested was the influence of time, by measuring repeatedly at different time intervals the concentration of a standard solution of formaldehyde at 1.00 mM in DMF/H_2O (95:5; v:v) TBAP 0.1 M. Performing the Nash test immediately after making the solution, at t = 0, gave a concentration of 1.01 mM. The same analysis repeated after leaving the components of the Nash test (the dye) to react further at room temperature for 2 h gave a formaldehyde measurement of 1.03 mM. This shows that once the Nash test has been performed (the reaction heated in the presence

of the Nash reagents), the solution should be analysed promptly by UV-Vis as errors on the order of 1% could be otherwise introduced.

The second important parameter pertaining to time is the duration in which a formaldehyde solution of a given concentration can be left at room temperature before performing the Nash reaction without disturbing the formaldehyde concentration; and the length of time that the Nash stock solution can be kept in the dark before degrading. To test those factors, 1 mM formaldehyde solutions in DMF/H_2O (95:5; v:v) TBAP 0.1 M were made and analysed by the Nash after varying periods of time. Results indicate that Nash stock solutions once made are stable at room temperature at least 3 days. However, samples containing formaldehyde should be analysed quickly, as after three days the calculated formaldehyde concentrations were observed to increase significantly. Therefore, an efficient use of the Nash test is required in order to avoid possibly false positive Nash tests suggesting greater levels of formaldehyde than were actually generated.

The influences of other parameters on the detection of formaldehyde were tested as well. The possible interference of formate on the measurement of formaldehyde was tested by performing a Nash test on 1 mL of electrolyte saturated with [HCOO]Na. The absorbance measured of 0.074 compared to the absorbance measured of the blank of 0.070 leads to the calculation of an observed concentration of formaldehyde of (0.074 – 0.070)/0.60 = 0.0001 mM, *i.e.* 0.00 mM. The presence of formate will not lead to a false positive on the measurement of formaldehyde.

Lastly, to consider the possibility of measuring even smaller concentrations of formaldehyde, 1 mL of electrolyte containing 0.10 mM formaldehyde was saturated with $MgSO_4$ and NaCl. These salts were chosen because they when added to $[Co(tpy)_2](PF_6)_2$ solutions, they allow for precipitation of the complex. Since the complex absorbs light, it might be beneficial to perform a separation via precipitation prior to analysis in order to get more accurate measurement on a small concentration of formaldehyde. After the Nash test was performed on this solution, an absorbance of 0.158 was measured, to compare to the 0.096 observed in the blank. This leads to a calculated formaldehyde concentration of (0.158 – 0.096)/0.60 = 0.1033 mM, *i.e.* 0.10 mM. Therefore, it is possible to precipitate out the catalyst without interfering with the formaldehyde measurement, should absorbance of the catalyst be a problem.

Throughout this manuscript, formaldehyde concentrations were determined using the Nash colorimetric test as described above, using a Shimadzu UV-1800 instrument. We observed that post-electrolyses solutions containing DMF and $[Co(tpy)_2](PF_6)_2$ must be analysed for formaldehyde quickly as re-oxidation in air led to increasing amounts of formaldehyde being produced, which is attributed to the reaction of DMF with a Co^{III} generated through the reaction of Co^{II} with O_2.

2.3.3. Methanol

Methanol presence was assessed using a Shimadzu GC-2010 Plus gas chromatography fitted with a ZB-WAX Plus column, Helium as a carrier gas and a flame ionisation detector. MeOH presence was also assessed through ^{1}H NMR spectroscopy on a Brücker 300 MHz Instrument when possible.

3. References

‡ N. Elgrishi, M. B. Chambers, V. Artero and M. Fontecave, *Phys. Chem. Chem. Phys*, 2014, **16**, 13635–13644. Reproduced with minor modifications by permission of the PCCP Owner Societies.

§ N. Elgrishi, S. Griveau, M. B. Chambers, F. Bedioui and M. Fontecave, *Chem. Commun.*, 2015, **51**, 2995–2998. Reproduced with minor modifications by permission of the Royal Society of Chemistry.

1 *Handbook of Electrochemistry*, C. Zoski Ed., Elsevier, 2006.

2 *Electrochemical Methods: Fundamentals and Applications*, A. J. Bard and L. R. Faulkner Eds., John Wiley & Sons inc., 2000.

3 J.-M. Savéant, *Elements of Molecular and Biomolecular Electrochemistry: An Electrochemical Approach to Electron Transfer Chemistry*, John Wiley & Sons, Interscience 2006.

4 IUPAC, Compendium of Chemical Terminology, 2nd ed. (the "Gold Book") (1997). Online corrected version: http://goldbook.iupac.org/D01725.html (accessed February 2015).

5 C. Costentin, M. Robert and J.-M. Saveant, *Chem. Soc. Rev.*, 2013, **42**, 2423.

6 M. M. Taqui Khan, S. B. Halligudi and S. Shukla, *J. Chem. Eng. Data*, 1989, **34**, 353.

7 K. P. Kuhl, E. R. Cave, D. N. Abram and T. F. Jaramillo, *Energy Environ. Sci.*, 2012, **5**, 7050.

8 P. W. West and B. Sen, *J. Anal. Chem.*, 1956, **153**, 12.

9 S. B. Jones, C. M. Terry, T. E. Lister and D. C. Johnson, *Anal. Chem.*, 1999, **71**, 4030.

Chapter III

–

Evaluation of CO_2 reduction by first row transition metal complexes of the ubiquitous terpyridyl ligand

Based on the work reported in: N. Elgrishi, M. B. Chambers, V. Artero and M. Fontecave, *Physical Chemistry Chemical Physics*, 2014, **16**, 13635–13644.

1. Introduction

The development of new energy storage technologies is central to solving the challenges facing the widespread use of renewable energies, namely their dilution and intermittent nature.[1,2] Batteries and hydrogen production are potential solutions which have been extensively investigated, but typically suffer from poor graviometric energy densities for the former and poor volumetric energy densities for the latter.[3] A more attractive option is the reduction of carbon dioxide (CO_2) into carbon-based fuels, combining higher graviometric and volumetric energy densities. This can be accomplished either directly through the generation of formic acid, methanol and higher hydrocarbons, or indirectly via the formation of carbon monoxide, which can be used as a feedstock chemical for the synthesis of alkanes through the Fischer-Tropsch process. Moreover, CO_2 reduction presents the advantage of providing a global carbon neutral energy system, fitting into existing infrastructure and facilitating energy transport.[4]

This process can be achieved within an electrochemical cell in which electricity derived from renewable energy sources is converted into chemical energy.[5] However, the electroreduction of CO_2 generally requires the presence of catalysts and the application of large overpotentials, since the reactions involve multiple electrons. Furthermore it suffers from limited selectivity since a mixture of the products mentioned above are generally obtained, together with hydrogen (H_2), derived from the parallel reduction of protons required for activation of CO_2. Molecular compounds have proven to be beneficial to the understanding of structure-activity relationships and the optimization of electrocatalytic systems.[6,7,8] A challenging goal is the development of selective, efficient and cheap catalysts. Cost limitation would require the combination of simple and robust ligands with first row transition metals.

Polypyridyl ligands, such as bipyridine (bpy) and terpyridine (tpy), are common ligands in coordination chemistry and molecular catalysis as they generally generate stable well-defined complexes.[9,10] As a consequence they have been frequently studied in the context of CO_2 electroreduction in organic solvents, most often acetonitrile (CH_3CN) or *N*,*N*-dimethylformamide (DMF), in the presence of a source of protons.[11] Such systems are capable of undergoing multiple reductions and thus storing multiple redox equivalents both in the ligand and in the metal ion.[12,13] Surprisingly, few studies have been reported using synthetic metal-polypyridyl complexes with first row transition metals. Indeed, the best reported catalysts are based on Re,[14,15,16] Rh[17,18,19] and Ru,[20,21] using mostly bpy and only in a few cases tpy ligands. Recently, [Mn(bpy-R)$(CO)_3$Br] (where bpy-R = substituted 2,2′-bipyridines) complexes were reported as electrocatalysts for the reduction of CO_2 to CO with reasonable efficiency, selectivity and stability.[22,23]

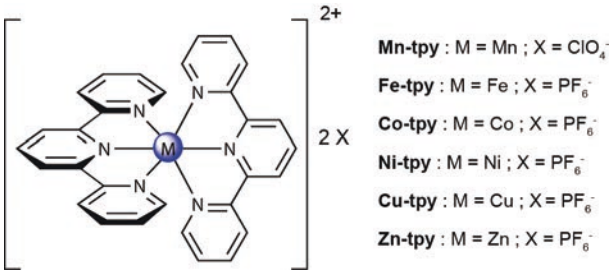

Figure III-1 Schematic depiction of the compounds studied.[‡]

In this chapter we report on our investigation of $[M(tpy)_2]^{2+}$ systems, with M = Co, Ni, Zn, Mn, Cu, Fe (noted **M-tpy** in the following, see Figure III-1) for CO_2 reduction in solution. These systems were studied at the end of the 80's by Abruña and collaborators almost exclusively in a different context, namely that of electrodes modified with electropolymerised films of vinyl-tpy-M complexes.[24,25,26,27,28] Although the initial reports indicate a possible activity of the **Cr-tpy** derivatives,[28] we focused our attention on late transition metals.

2. Cyclic voltammetry

For cyclic voltammograms reported within Chapter III, data was collected using a glassy carbon electrode with a diameter of 3 mm in a 10 mL CV electrochemical cell described in Chapter II.

2.1. Zn-tpy

To glean insight into the behaviour of the tpy ligand on metallic centres, **Zn-tpy** was first investigated to help the attribution of electrochemical features. The typical voltammograms of a 2 mM solution of **Zn-tpy** exhibits two reversible electrochemical features, at –1.68 and –1.81 V *vs.* Fc^+/Fc (Figure III-2).

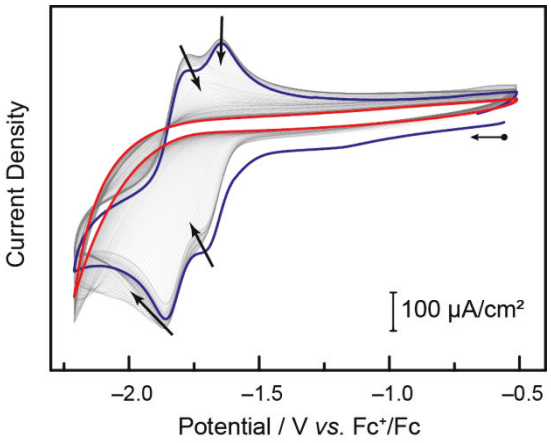

Figure III-2 Cyclic voltammograms of a 2 mM N_2-saturated solution of **Zn-tpy** and its evolution as the number of scans is increased. The first scan is shown in blue and the 100th scan, indicative of complete passivation, is shown in red.[§]

Since the reduction of Zn^{II} to Zn^{I} is not likely to occur under these conditions, the two waves are assigned to ligand-based reduction processes, and this attribution will prove useful in the study of other metal-tpy compounds. More generally, these results suggest that tpy reduction events can be expected to occur in potential ranges around –1.6 V to –2.0 V *vs.* Fc^+/Fc in the conditions commonly used within this work. In specific regards to **Zn-tpy**, it has to be noted that a passivation of the glassy carbon electrode was observed as the number of scans was increased in these conditions (Figure III-2).

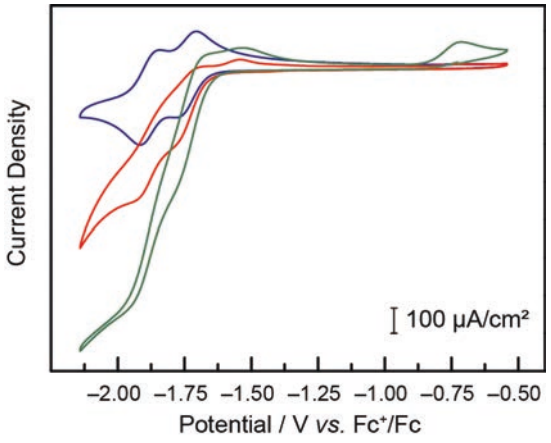

Figure III-3 Typical cyclic voltammograms at 100 mV/s of a 1 mM solution of **Zn-tpy** in DMF/H_2O (90:10, v:v) under argon (blue, only the third scan is presented), CO_2 (red, only the third scan is presented), and under CO_2 after the addition of over 20 mM excess tpy ligand (green, only the third scan is presented). [§]

Upon addition of CO_2 and saturation of the solution, and after polishing of the electrode, the two electrochemical features from the blue trace of Figure III-3 become irreversible (red trace Figure III-3) and the intensity of the corresponding cathodic peaks significantly increase. As shown in Figure III-3, the intensity of the cathodic peaks is further increased upon addition of an excess of free tpy ligand (Figure III-3, green trace). When the same solution, containing excess tpy, is saturated with Ar, the two waves of **Zn-tpy** become reversible once more, with no visible contribution of additional equivalents of tpy to the current observed (identical to the blue trace of Figure III-3).

The redox inert nature of Zn makes it unlikely to mediate multi-electron transformations to a substrate, even when redox equivalents are stored within the ancillary ligand platform. Since Zn-catalysed CO_2 reduction is unlikely, as is a tpy catalysed CO_2 reduction activity, and no cathodic current increase is observed by free tpy under CO_2 in the potential range studied by CV, this unique behaviour of **Zn-tpy** under CO_2 is noteworthy and will be elaborated on later in this chapter.

2.2. Co-tpy

The cyclic voltammogram of a 2 mM Ar-saturated solution of **Co-tpy** in a DMF/H_2O (95:5, v:v) mixture with 0.1 M TBAP displays two reversible one-electron electrochemical features in the –0.5 V to –2.3 V *vs.* Fc^+/Fc range (Figure III-4, I and II).

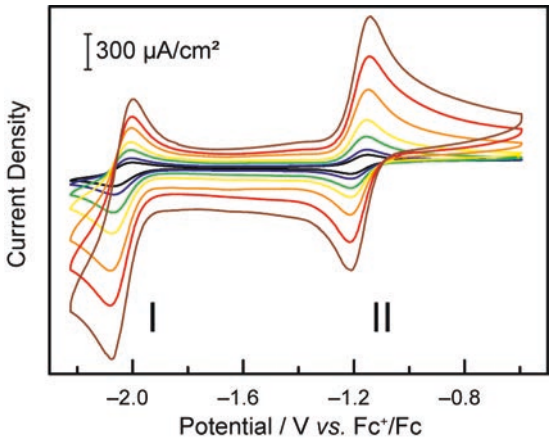

Figure III-4 Cyclic voltammograms of a 2 mM solution of **Co-tpy** under argon at 10 (black), 20 (blue), 50 (green), 100 (yellow), 250 (orange), 500 (red) and 1000 (brown) mV/s.[§]

The first feature, at –1.17 V *vs.* Fc^+/Fc, is a reversible metal-based process, assigned to a Co^{II}/Co^{I} reduction (Figure III-4, II). This system is diffusion controlled, with a difference between the potential of the anodic and cathodic peaks (peak-to-peak separation) of about 60 mV at slow scan rates (59 to 64 mV in the 10-100 mV/sec range). The peak-to-peak separation then increases as the scan rate is further increased to reach a separation of 77 mV at a scan rate of 500 mV/sec. The plots of i_{pc} and i_{pa} *vs.* $v^{1/2}$ are linear and the i_{pa}/i_{pc} ratio is close to unity in the 10-500 mV/sec scan rate range (Figure III-5). This feature was used to determine the diffusion coefficient using the Randles-Sevick equation. A diffusion coefficient of $3.7 \cdot 10^{-6}$ cm²/s was calculated. The second electrochemical feature, at –2.03 V *vs.* Fc^+/Fc, is attributed to a one-electron ligand-based reduction (Figure III-4, I). This couple is mostly

reversible, with a peak-to-peak separation of about 66 mV for scan rates in the 10-50 mV/sec range. This value increases to 91 mV at 1 V/s. Plots of i_{pc} and i_{pa} versus $\nu^{1/2}$ are linear over the range of scan rates studied, and the i_{pa}/i_{pc} value is close to 1 which denotes chemical reversibility (Figure III-5).

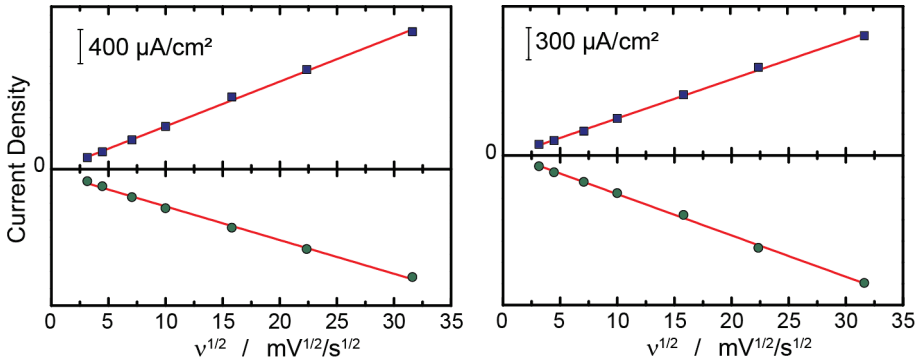

Figure III-5 i_{pc} (green circles) and i_{pa} (blue squares) curves *vs.* the square root of scan rate ($\nu^{1/2}$) for both of the electrochemical features (I: left; II: right) of **Co-tpy** under inert atmosphere.[§]

As the potential range interrogated was increased to include more anodic potentials, just beyond 0 V *vs.* Fc^+/Fc, a third feature at –0.17 V *vs.* Fc^+/Fc is observed and is attributed to the Co^{III}/Co^{II} couple (Figure III-6, III). If the potential window scanned is increased to more cathodic potentials values, an electrochemically irreversible wave is observed with a peak potential of –2.46 V *vs.* Fc^+/Fc (Figure III-6).

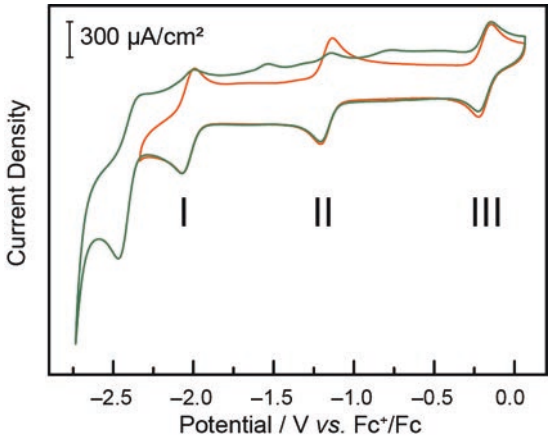

Figure III-6 Cyclic voltammograms of a **Co-tpy** solution under N_2 atmosphere in the 0.06 to –2.33 V potential range (orange) and the same solution scanned to –2.73 V (green). Only the third scan is shown in the latter case, as more scans led to degradation.[§]

This wave is accompanied by the apparition of two anodic features at –1.54 and –0.76 V *vs.* Fc^+/Fc as well as a decrease in the intensity of the anodic waves of the Co^{II}/Co^{I} and $tpy/tpy^{\bullet-}$ couples. While investigating the more negative potential ranges, as the number of scans is increased, the intensity of the anodic features of these two peaks continues to decrease. This additional irreversible feature at –2.46 V *vs.* Fc^+/Fc is attributed to a second ligand-based reduction and appears to lead to decomposition pathways. Therefore, the potential ranges have always been controlled in the following work so as to avoid reaching this deleterious reduction feature.

When the same solution was saturated with CO_2, no difference was observed in the metal-based processes (Figure III-7, II and III). However, a strong enhancement of the cathodic current was observed in the ligand-based reduction process, with an onset at –1.80 V *vs.* Fc^+/Fc as can be seen in Figure III-7. The current increases over 4-fold, from –0.33 to –1.51 mA/cm² (at –2.23 V, for a scan rate of 100 mV/s), and is stable over time. The wave becomes irreversible, with no anodic return-wave observed in the range of scan rates studied (10-1000 mV/sec, data presented in Figure VI-1 of the Appendix). It is thus assigned to catalytic CO_2 reduction, which was confirmed by controlled-potential electrolysis experiments.

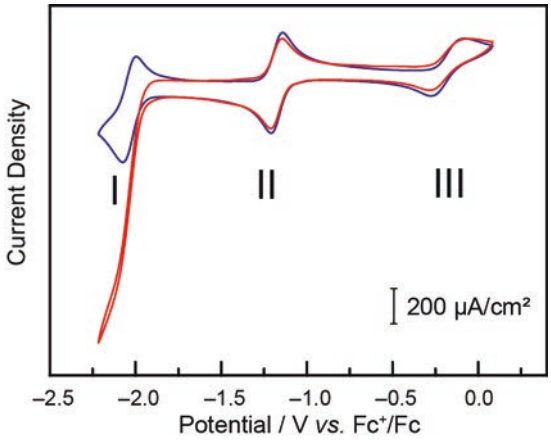

Figure III-7 Typical cyclic voltammograms of 2 mM solutions of **Co-tpy** under argon (blue) and CO_2 (red) atmospheres at 100 mV/s in DMF/H_2O (95:5, v:v) with 0.1 M TBAP.[§]

Similar results, under inert and CO_2-saturated atmospheres, were obtained when synthetic $[Co(tpy)_2]^{2+}$ complexes are replaced by a 1:2 mixture of the corresponding metal salt and the terpyridyl ligand, respectively. Of note, minimal current is observed in the potential range studied in the absence of cobalt salt or tpy ligand. Accordingly, no current increase is observed under CO_2 when the carbon electrode is tested in pristine electrolyte solution after a 30 min controlled-potential electrolysis at –2.23 V *vs.* Fc^+/Fc followed by rinsing of the electrode, confirming the homogeneous nature of the catalytic process.

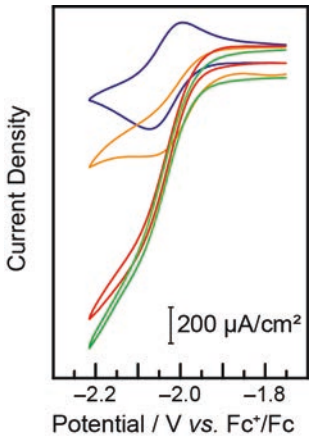

Figure III-8 Ligand-based reduction region of the CVs at 100 mV/s of 2 mM solutions of **Co-tpy** under argon (blue) and under CO_2 (red) in DMF/H_2O (95:5, v:v) and under CO_2 in anhydrous DMF (orange), and DMF/H_2O (90:10, v:v) (green).

The influence of the presence of a proton source in the form of water was briefly investigated. In anhydrous DMF, the cathodic current increase attributed to CO_2 reduction is minimal (Figure III-8, yellow). When the same experiment is repeated in the presence of 5% (Figure III-8, red) or 10% (Figure III-8, green) water by volume, the intensity of the cathodic catalytic peak is increased. Since the current increase between 5% and 10% water added was minimal, the concentration of 5% of water by volume in DMF was kept and used in the rest of this study.

2.3. Ni-tpy

In an analogous manner to **Co-tpy**, the behaviour of **Ni-tpy** was analysed by cyclic voltammetry in DMF/H_2O (95:5, v:v) solutions with 0.1 M of TBAP. The cyclic voltammograms of a 2 mM solution of **Ni-tpy** under inert atmosphere display features at –1.62 and –1.88 V *vs.* Fc^+/Fc (Figure III-9, II and III).

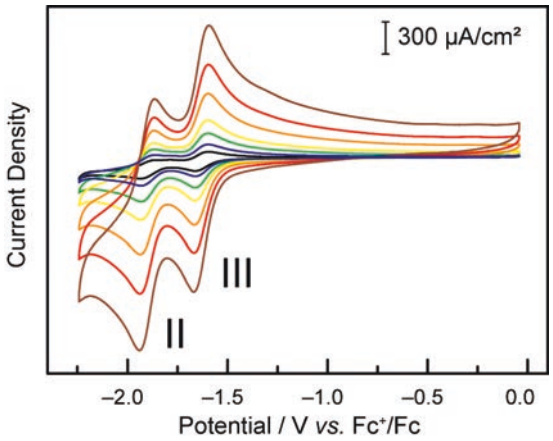

Figure III-9 Top: cyclic voltammograms of a 2 mM N_2-saturated solution of **Ni-tpy** at 10 (black), 20 (blue), 50 (green), 100 (yellow), 250 (orange), 500 (red) and 1000 (brown) mV/s.[§]

By analogy to that which was observed in the case of **Zn-tpy**, both features are assigned to ligand-based electrochemical processes. This is further supported by recent studies on the electronic structure of Ni-monoterpyridine and $[Ni(tpy)_2]^{2+}$ compounds.[29,30] Peak-to-peak separation of both features are close to 60 mV (62 and 65 mV respectively at 100 mV/s) and the plots of i_{pc} and i_{pa} *vs.* $\nu^{1/2}$ (Figure III-10) are linear in the scan range studied (10-1000 mV/s), consistent with the notion that both peaks are diffusion controlled and exhibit electrochemical and chemical reversibility. Given the proximity in terms of potential of the electrochemical features, an accurate measurement of the values of i_a with respect to i_c is more challenging as the measured current does not reach a diffusion controlled regime before the onset of the next feature. For this reason there exists a discrepancy in the reported values of i_c and i_a, and a deviation from 1 for values of i_{pc}/i_{pa} for those features is observed.

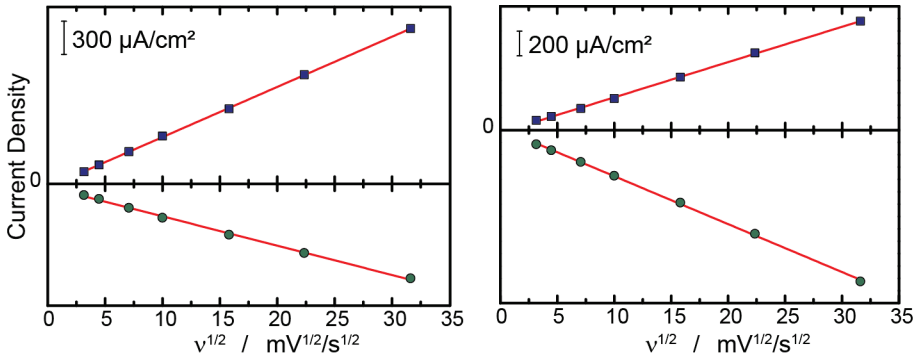

Figure III-10 i_{pc} (green circles) and i_{pa} (blue squares) curves *vs.* the square root of scan rate for the ($\nu^{1/2}$) for both of the electrochemical features (II: left; III: right).[§]

Under CO_2-saturated conditions, the two electrochemical features lose reversibility (significantly attenuated anodic return features are observed) and the intensity of the corresponding cathodic peaks increase over 2-fold, suggesting possible electrocatalytic behaviour. A third irreversible catalytic cathodic wave is observed at lower potentials (–2.15 V *vs.* Fc^+/Fc), which is absent under Ar (Figure III-11, I).

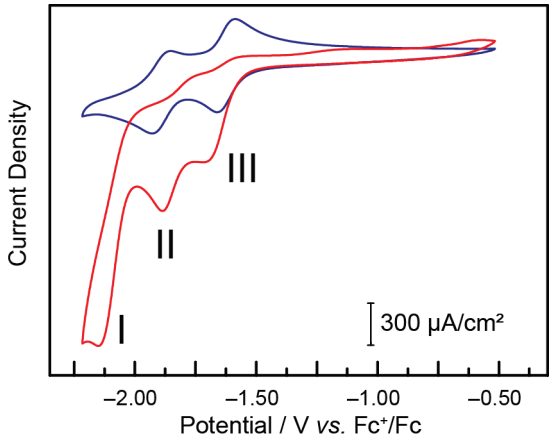

Figure III-11 Typical cyclic voltammograms of 2 mM solutions of **Ni-tpy** under argon (blue) and CO_2 (red) atmospheres at 100 mV/s.[§]

It is to be noted that the behaviour of **Ni-tpy** under CO_2-saturating conditions appears more complicated than that of **Co-tpy**, as evidenced by the noticeable positive shift of the feature II under CO_2, as well as the appearance of feature I.

2.4. Cu-tpy, Fe-tpy and Mn-tpy

2.4.1. Cu-tpy

Evidence for deposition behaviour on glassy carbon electrode under CO_2 was observed during cyclic voltammetry experiments of 2 mM **Cu-tpy** solutions in DMF with 5% H_2O (Figure III-12).

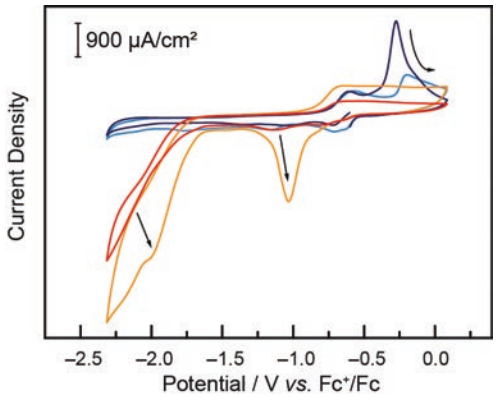

Figure III-12 Cyclic voltammograms of a 2 mM solution of **Cu-tpy** at 100 mV/s under argon (dark blue: scan 1; light blue: scan 38) and under a CO_2 atmosphere (red: scan 1; orange: scan 38).[§]

As more scans are acquired under inert atmosphere (blue), the oxidative CV signal around 0.25 V evolves, from the dark blue signal in Figure III-12 during the first scan to the light blue signal after 38 scans. Remarkably, the signal presents little to no change in the region scanned below −0.8 V. Under CO_2, a strong cathodic current enhancement is observed during the first scan (Figure III-12, red trace), and as more scans are acquired, the onset potential for catalysis appears to diminish as the current enhancement is exacerbated. Concurrently, a cathodic peak grows with a peak potential of about −1.05 V. This behaviour is explained by a deposition of a more catalytically competent entity on the surface of the electrode. This heterogeneous behaviour has been subsequently extensively studied elsewhere and has been recently reported by Artero, Fontecave and co-workers.[31] With similar ligand scaffolds, it has been determined that the deposition process yields chemically complex particles likely based on a mixture of Cu^0/CuO. These particles have been shown to be capable of CO_2 reduction in organic solvents with activity strongly dependent upon the nature of the Cu-complex precursor.

2.4.2. Fe-tpy and Mn-tpy

Typical cyclic voltammograms of **Fe-tpy** and **Mn-tpy** are shown respectively in the left and right panels of Figure III-13 below, in the same conditions as used previously. The behaviour of **Fe-tpy** is extremely reminiscent of that of **Zn-tpy** under argon, confirming the attribution of the electrochemical features as both ligand-based events. The cyclic voltammograms of **Mn-tpy** are more complex, and lead to questioning the stability of the complex in the conditions tested.

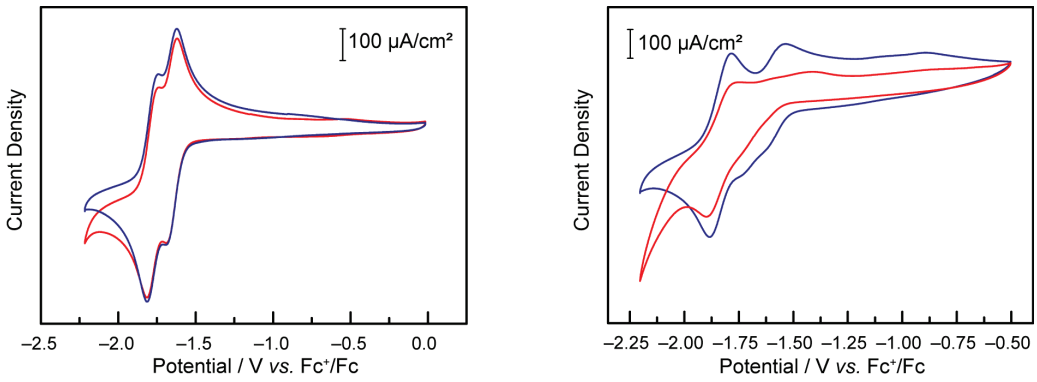

Figure III-13 Cyclic voltammograms under argon of 2 mM solutions of **Fe-tpy** (left) and **Mn-tpy** (right) at 100 mV/s (blue) and CO_2 (red) atmospheres.[§]

Under the conditions used, *i.e.* CO_2-saturated conditions, in DMF/H_2O (95:5) with TBAP 0.1 M as supporting electrolyte on a glassy carbon electrode, no strong current enhancement was observed by cyclic voltammetry when compared to the signal observed under an inert atmosphere. This suggests a lack of electrocatalytic activity in the conditions tested and these complexes were not investigated further in the context of this work. This lack of electrocatalytic reduction feature under CO_2 is in disagreement with previous reports as far as **Fe-tpy** is concerned, since H. Abruña and co-workers report observing catalytic CO_2 reduction in the same conditions as the ones tested here at the potential of the more positive of the two ligand-based reduction waves.[26] Although this behaviour has not been observed in the context of this work, the **Fe-tpy** features were observed to be very sensitive to the presence of air, which could suggest catalytic O_2 reduction.

2.5. Conclusions

The central role of ligand reduction in mechanisms postulated for polypyridyl CO_2 reduction catalysts highlights the importance of understanding the reduction potential assignments within the cyclic voltammetry experiments. The assignments of the waves in the cyclic voltammograms of the **M-tpy** complexes are the subject of multiple differing interpretations. Originally, in the case of **Ni-tpy** the two reduction waves (Figure III-9, III and II) were assigned as metal-based and ligand-based, respectively.[26,27] We have found, by comparison with **Zn-tpy**, that the waves would be better described as both being ligand-based. In contrast, in the case of **Co-tpy**, reduction of the ligand occurs at potentials more negative than those required to generate the Co^I species.

Co-tpy and **Ni-tpy** are confirmed as potential candidates for CO_2 reduction, which will have to be verified by bulk electrolysis and product analysis. **Zn-tpy** exhibits an unexpected behaviour, and will be studied further. **Cu-tpy** leads to deposition onto the carbon electrode, and the heterogeneous compound appears to exhibit activity, which will not be studied further in the context of this thesis. **Fe-tpy** does not appear to be a desirable candidate in the conditions tested. The behaviour of **Mn-tpy** is more complex, and although it will not be the focus of this study, a revaluation of this system might prove fruitful in the future. Since the completion of this body of work, studies on $[Mn(tpy)(CO)_3]^+$ has confirmed that the complex can release CO upon reduction, building upon Mn-bpy$(CO)_3$ as a CO_2 reduction catalyst.[32]

3. Controlled-potential electrolyses

In order to assess the catalytic activity of the various **M-tpy** complexes under study and to characterise the catalysed reaction, controlled-potential electrolysis of CO_2-saturated DMF/H_2O (95:5, v:v) with 0.1 M TBAP solution of each complex were carried out. Quantitative analyses of CO and H_2 formation were achieved by gas chromatography, formaldehyde (HCHO) formation by a colorimetric assay and formic acid (HCOOH) formation by ion-exchange chromatography coupled to a conductimeter, as described in Chapter II. The presence of methane was assessed through gas chromatography, of methanol by ^{1}H and ^{13}C NMR and of oxalate by ionic exchange chromatography. Formaldehyde, methane, methanol and oxalate could not be detected in any of the following experiments.

3.1. Co-tpy

3.1.1. Evolution of charge and current

Controlled-potential electrolysis at –2.03 V under CO_2 in the presence of 10 mL of a 2 mM solution of **Co-tpy** yields sustained current over the course of 3 hours (Figure III-14, blue trace). During the first hour of the electrolysis, a decrease in the current is observed while the first 1.93 C are exchanged. This charge of 1.93 C corresponds to about $2 \cdot 10^{-5}$ moles of electrons and is attributed to the first quantitative one-electron reduction of Co^{II} to Co^{I} prior to the formation of the catalytic species. After the first 1.93 C are passed, the current reaches the steady value of –0.39 mA and remains constant for the remainder of the experiment.

Cyclic voltammograms of the bulk solution after a 3 h electrolysis exhibit the same features as that of **Co-tpy**, but the open circuit potential was more negative than –1.17 V, confirming that most of the **Co-tpy** species in solution was formally Co^{I} and pointing at the stability of the system.

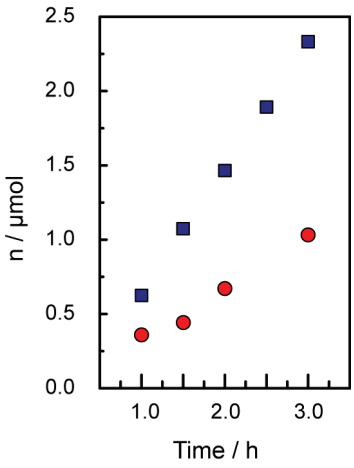

Figure III-14 Total moles of H_2 (red circles) and CO (blue squares) measured in the headspace during the electrolysis of a 2 mM solution of **Co-tpy** at –2.03 V *vs.* Fc^{+}/Fc under a CO_2 atmosphere.[§]

The controlled-potential electrolyses resulted in the exclusive formation of CO and H_2. In some cases trace amounts of formate are also detected, always < 3% of the charge passed, but are attributed to deleterious reactions of DMF. The production of CO and H_2 by **Co-tpy** was constant over

time in the region where the current densities are stable and corresponds to 17% faradic yield (12% for CO and 5% for H_2).

In the absence of **Co-tpy**, a steady low background current of 19 µA was observed, with background levels of CO ($1.6 \cdot 10^{-8}$ moles) and H_2 ($< 6 \cdot 10^{-7}$ moles) being formed after 3 h. Electrolysis of **Co-tpy** for 3 h in N_2-saturated solution, in the absence of CO_2, resulted in a continuous decrease of the current to reach the levels observed without catalyst. At the end of the 3h electrolysis, 3.31 C were passed, corresponding to slightly under 2 equivalents of electrons per **Co-tpy** molecule in solution. Background levels of CO and H_2 were detected during this experiment. In the absence of water the overall behaviour of the system was conserved, with a decrease of the current as the first 1.93 C are passed, followed by a steady current during the rest of the experiment (Figure III-15). However the value of the current was lower, as well as the faradic yields and fewer moles of CO were observed (Figure III-15). These experiments combined indicate that CO_2 reduction in this system requires the **Co-tpy** complex, CO_2, and a proton source such as water.

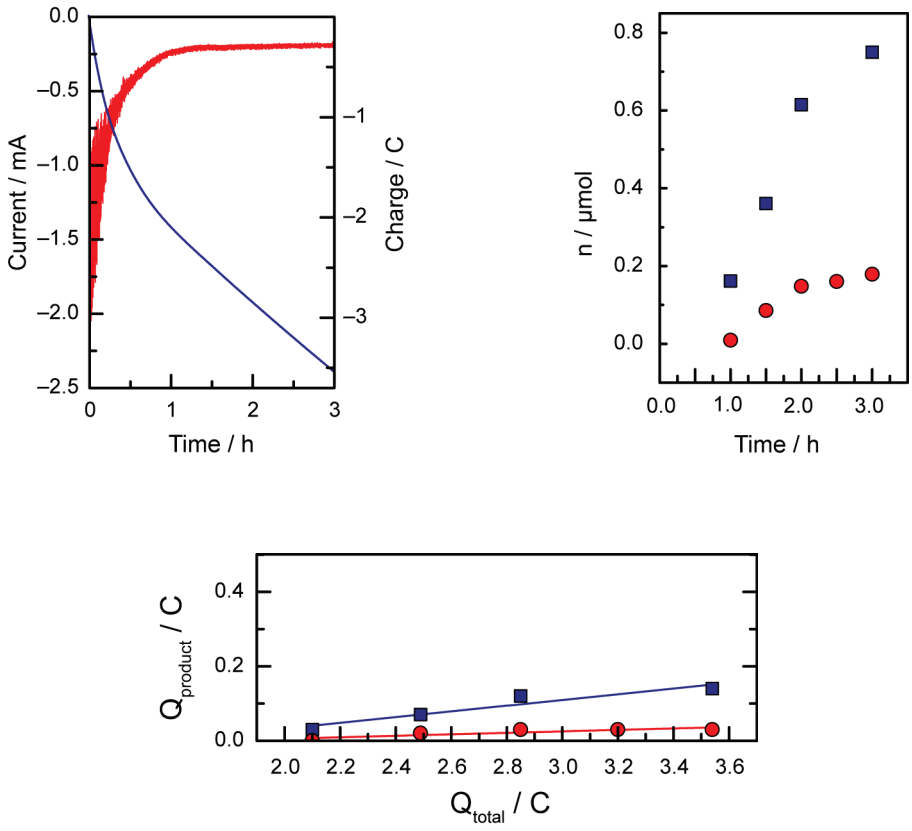

Figure III-15 Current (top left, red) and charge (top left, blue) measured during a controlled-potential electrolysis of a 2 mM **Co-tpy** CO_2-saturated solution in 10 mL of anhydrous DMF, with 0.1 M of TBAP as supporting electrolyte. Total moles of CO (blue squares) and H_2 (red circles) measured in the headspace during the electrolysis (top right) and charge corresponding to the products measured (assuming $2e^-$ for CO of H_2 production) *vs.* the total charge passed during the electrolysis (bottom). The slope of the linear fit, corresponding to the faradic efficiency, is 8% for CO (blue squares) and 2% for H_2 (red circles).[§]

The same bulk electrolyses experiments performed in CH_3CN as the primary solvent yielded comparable results, with the exception that some precipitate was observed. Following that which has been reported by Meyer and co-workers on analogous Ru polypyridyl systems, this precipitate is being tentatively assigned to be the result of reduced complex-carbonate/bicarbonate salts.21 No evidence of precipitation was observed in DMF and thus, in order to limit side phenomena, DMF was used as the primary solvent for the studies reported herein. Since DMF can be subject to hydrolysis to yield formate or formaldehyde that is not derived from CO_2 reduction,[33] great attention was paid to the product analysis in control experiments.

3.1.2. Exploring selectivity as a function of applied potential

The influence of the applied potential on product distribution was investigated by varying the applied potential in controlled-potential electrolysis experiments. Five different potentials were tested, in the range of –1.93 to –2.23 V *vs.* Fc^+/Fc. At all applied potentials tested, the current densities decrease during the first 30 minutes to 1 h (depending on the potential) corresponding in each case to about 1.93 C before reaching a steady current density (Figure III-16, charge presented in the Appendix in Figure VI-2).

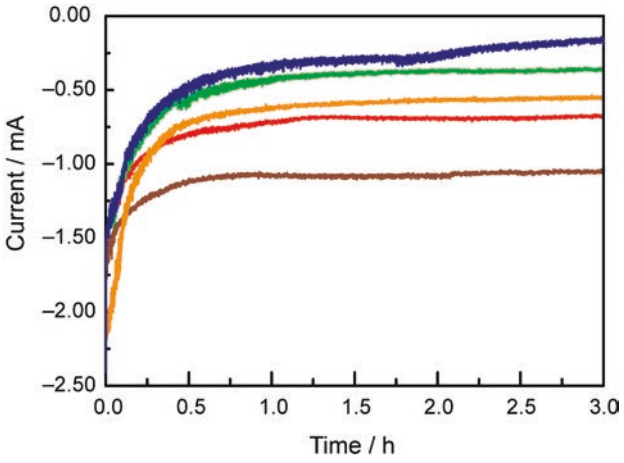

Figure III-16 Current measured during controlled-potential electrolyses of 2 mM **Co-tpy** CO_2-saturated solutions at different applied potentials (blue: –1.93 V, green: –2.03 V, orange: –2.08 V, red: –2.13 V and brown: –2.23 V). Bulk electrolyses were performed in 10 mL of DMF/H_2O (95:5, v:v), with 0.1M TBAP.[§]

The stable current densities values increase upon decreasing the applied voltage (from –0.29 mA at –1.93 V to –1.28 mA at –2.23 V). The only products observed were CO and H_2 at the five different potentials applied. The charge attributed to CO and H_2 (assuming two electrons are needed in both cases) as a function of the total charge passed during the 3 h of controlled-potential electrolysis is given in Figure III-17 at the five potentials tested.

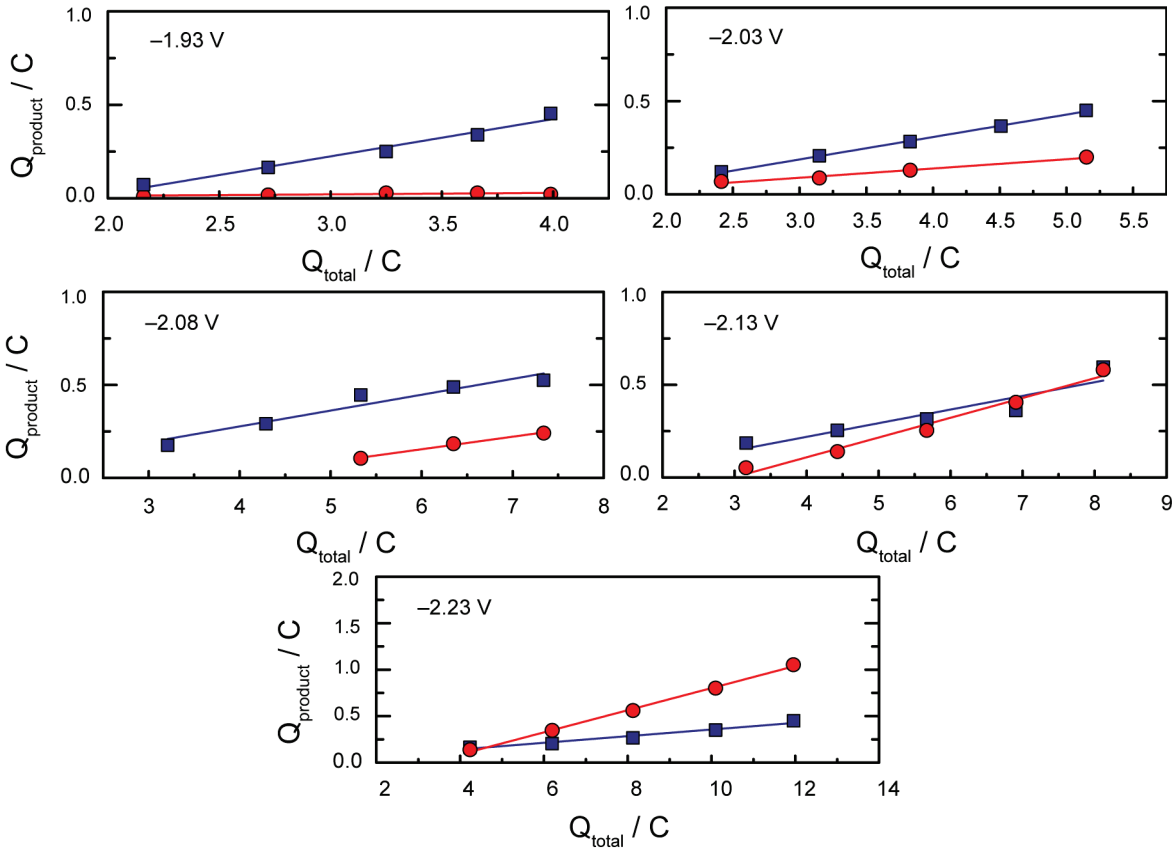

Figure III-17 Charge corresponding to the products measured (CO: blue squares, H_2: red circle) *vs.* the total charge passed during the electrolyses of 2 mM **Co-tpy** CO_2-saturated solutions at the different applied potentials specified on the Figures.[§]

The faradic efficiency for CO or H_2 production is given by the slopes of the linear fits. As the overpotential is increased, the faradic efficiency for CO production drops from 20% at –1.93 V to 12% at –2.03 V, 9% at –2.08 V, 7% at –2.13 V to reach 3% at –2.23 V. At the same time, the faradic efficiency for H_2 production rises from 1% at –1.93 V to 5% at –2.03 V, 7% at –2.08 V, 11% at –2.13 V and finally 12% at –2.23 V. The combined faradic efficiency going towards CO and H_2 was between 16-21%, with little variation as the applied potential was varied.

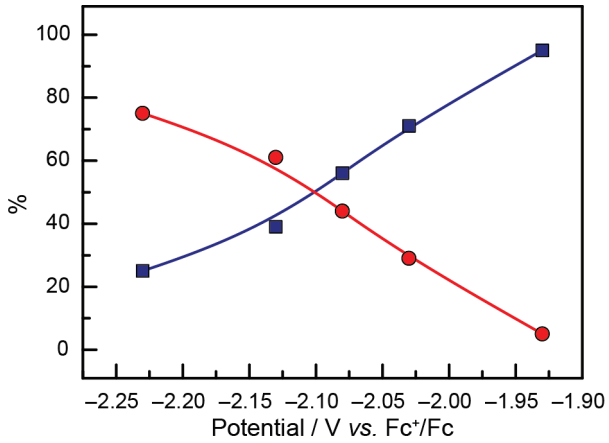

Figure III-18 Evolution of the proportions of CO (blue squares) and H_2 (red circles) among the products observed for CO_2 reduction by **Co-tpy** with the applied potential during controlled-potential electrolyses (lines drawn to guide the eye).[§]

The proportions of CO and H_2 produced during controlled-potential electrolyses (CPE) vary as a function of the applied potential, as can be seen in Figure III-18. The relative amounts of H_2 and CO formed vary with the applied voltage, with the highest CO:H_2 ratio value of 20 obtained at –1.93 V. The CO:H_2 ratio decreases to 0.3 as the applied potential was lowered to –2.23 V *vs.* Fc^+/Fc, thus allowing a simple control of the produced CO/H_2 mixture by the potential applied during electrolysis.

3.2. Ni-tpy

As shown by the cyclic voltammetry experiments, the onset potential for electroreduction of CO_2 catalysed by the **Ni-tpy** system is less negative than in the **Co-tpy** system. Thus, electrolyses can be carried out at applied potentials as low as –1.72 V, more than 200 mV less negative than that required for electroreduction of CO_2 catalysed by **Co-tpy**.

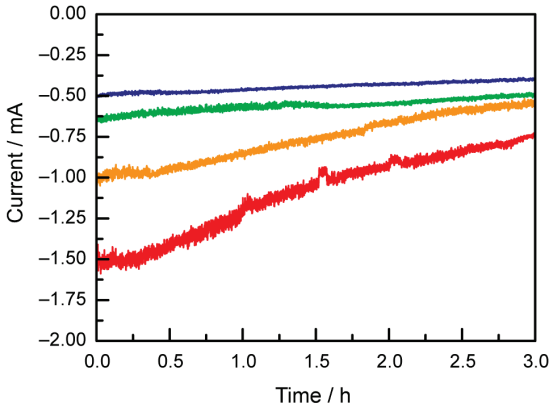

Figure III-19 Current measured during CPE of 2 mM **Ni-tpy** CO_2-saturated solutions at: –1.72 V (blue), –1.76 V (green), –1.89 V (orange) and –2.14 V (red). CPE were performed in 10 mL of DMF/H_2O (95:5, v:v), with 0.1M TBAP.[§]

The current obtained during CPE of 2 mM **Ni-tpy** DMF/H_2O (95:5, v:v) solutions at the four applied potential from –1.72 to –2.14 V are significantly less stable that what was observed for **Co-tpy** (Figure III-19 and VI-3 of the Appendix). No "stabilisation" phase is observed, as expected from the CVs, since the first electrochemical feature already exhibits current enhancement under CO_2.

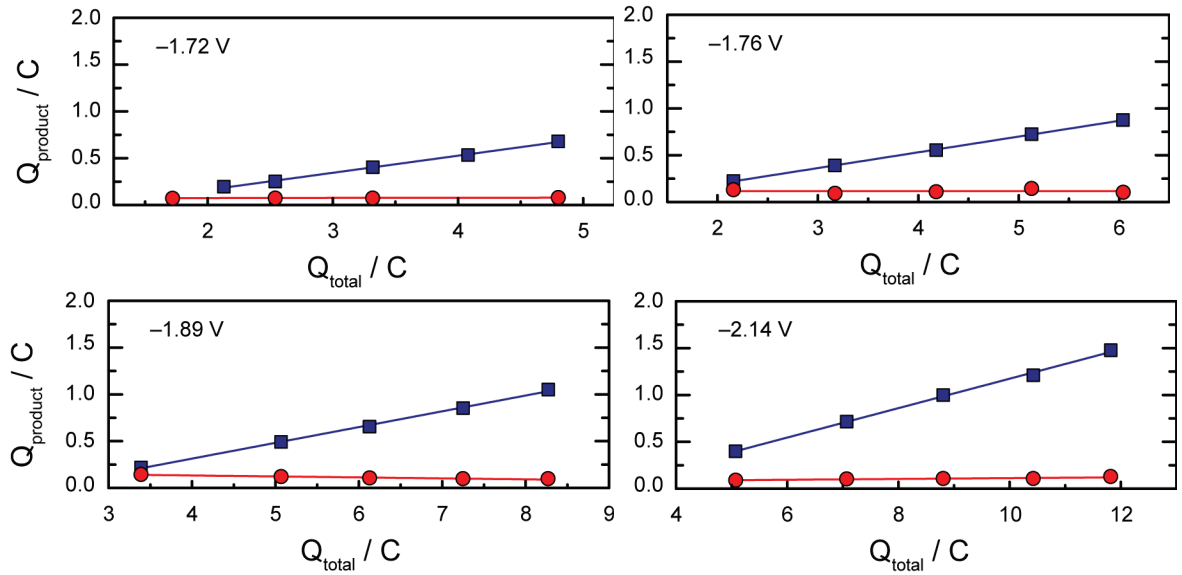

Figure III-20 Charge corresponding to the products measured (CO: blue squares, H_2: red circle) *vs.* the total charge passed during the electrolyses of 2 mM **Ni-tpy** CO_2-saturated solutions at the potentials specified in the Figures.[§]

During the four controlled-potential electrolyses, the only product detected was CO. The plots of the charge corresponding to the amount of CO and H_2 produced (assuming two electrons are required in both cases) as functions of the total charge passed in the system are given in Figure III-20. The slope of these plots give a faradic efficiency for H_2 production of 0% regardless of the potential applied, and a faradic efficiency for CO production of 18% at –1.72 V, 17% at –1.76 V and –1.89 V and 16% at –2.14 V *vs.* Fc^+/Fc.

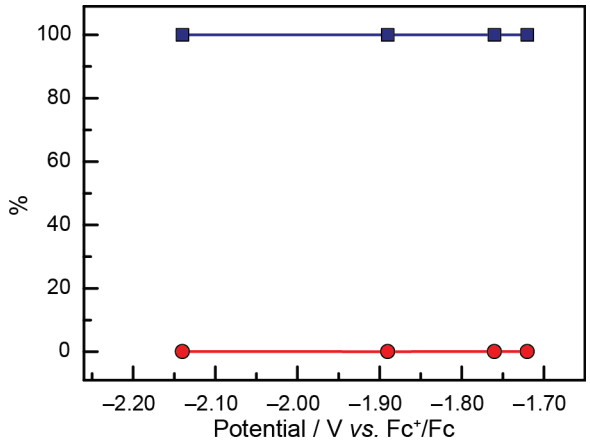

Figure III-21 Evolution of the proportions of CO (blue squares) and H_2 (red circles) among the products observed for CO_2 reduction by **Ni-tpy** (b) with the applied potential during controlled-potential electrolyses (lines drawn to guide the eye).[§]

As in the case of **Co-tpy**, a total faradic yield of around 20% was obtained with no effect of varying the applied potential. Figure III-21 gives a visual representation of the selectivity of **Ni-tpy** for CO_2 reduction to CO over water reduction to H_2 as a function of applied potential. **Ni-tpy** is selective for CO_2 reduction to CO over H_2 production at all the four potential in the window tested, from –1.72 to –2.14 V.

3.3. Comparing Ni-tpy and Co-tpy

A direct comparison of the electrochemical behaviour of **Co-tpy** and **Ni-tpy** offers some insights into the nature of **M-tpy** electrocatalytic reduction of CO_2 and some factors that correlate to differences in selectivity. The most striking difference between the two systems is the assigned oxidation states of the metal centres during onset of catalysis. For **Co-tpy**, CVs of the bulk solution during electrolyses indicate that resting state of the catalytic cycle comprises Co^I cations. On the other hand, for **Ni-tpy** no metal-based reduction can be observed via CV suggesting that an oxidation state of Ni^{II} is best assigned within the catalytic cycle.

These assignments have implications on the electronic structure of the catalytic species and point to a possible significant difference between the Co- and Ni-based catalysts and strongly impact the possible operative mechanistic pathways. Co^I centres have been shown to lead, upon reaction with protons, to the formation of a Co^{III}-H which would then be implicated in H_2 evolution,[34,35,36,37,38,39] which has been demonstrated in related polypyridyl cobalt complexes as well.[40,41,42] This is in stark

contrast with the Ni-based system, since a Ni^{IV}-H resulting from the protonation of a Ni^{II} centre is unlikely to form in the conditions of the experiment.[43,44,45,46] This would explain the distinct difference in reactivity of the two catalytic systems in terms of product distribution, since metal hydrides are required for H_2 evolution but are not necessarily needed for CO_2 reduction, and are often not invoked in the specific case of CO_2 reduction to CO. Thus, as confirmed herein, **Co-tpy** is more susceptible than **Ni-tpy** to proton reduction, in parallel to conversion of CO_2 into CO.

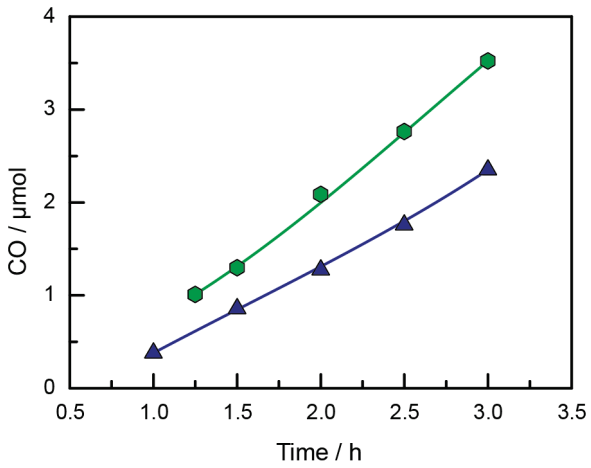

Figure III-22 Comparison of the number of moles of CO produced by **Ni-tpy** (green hexagons) and **Co-tpy** (blue triangles) during the course of 3 h electrolyses at –1.72 V for **Ni-tpy** and –1.93V for **Co-tpy**. Carbon monoxide generation by the **Ni-tpy** system is better in these conditions than for **Co-tpy**, even at a 200 mV less overpotential (lines drawn to guide the eye).[§]

The two systems are compared in Figure III-22, in terms of CO production, which shows that under similar conditions CO production is more efficient in the case of the **Ni-tpy** system. Even with an overpotential 200 mV lower in the case of **Ni-tpy**, more µmoles of CO are produced relative to **Co-tpy**. The last key difference between the **Co-tpy** and **Ni-tpy** systems has been highlighted previously, namely the lack of stability if the current obtained during controlled-potential electrolyses of **Ni-tpy** compared to **Co-tpy**.

4. Understanding the faradic yields: hunting for side reactions

Despite the observation of electrocatalytic activity for **Co-tpy** and **Ni-tpy** towards CO_2 reduction, the low faradic yields (typically <20%) left unanswered the origins of the remaining charge passed. The identification of factors contributing to the low faradic yields would afford opportunities to optimize the efficiency of the system. Therefore, we were motivated to explore the effects on faradic yields of a variety of parameters relevant to the experimental setup as well as the chemical system.

4.1. Influence of general parameters

Several routes were explored to account for the low faradic efficiency going towards CO_2 reduction products. Given its apparent better stability, the **Co-tpy** system was chosen for this study.

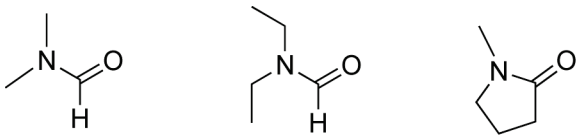

Figure III-23 Chemical structure of DMF (left), DEF (centre) and NMP (right).

First the influence of solvent was investigated. To reduce reactivity of the methyl groups of DMF, *N*,*N*-diethylformamide (DEF) was tested as a solvent and 1-methyl-2-pyrrolidinone (NMP) was tested to reduce the potential interference from reaction with the carbonyl group. These solvent variations lead to similar faradic yields for CO and H_2 production (Figure III-24).

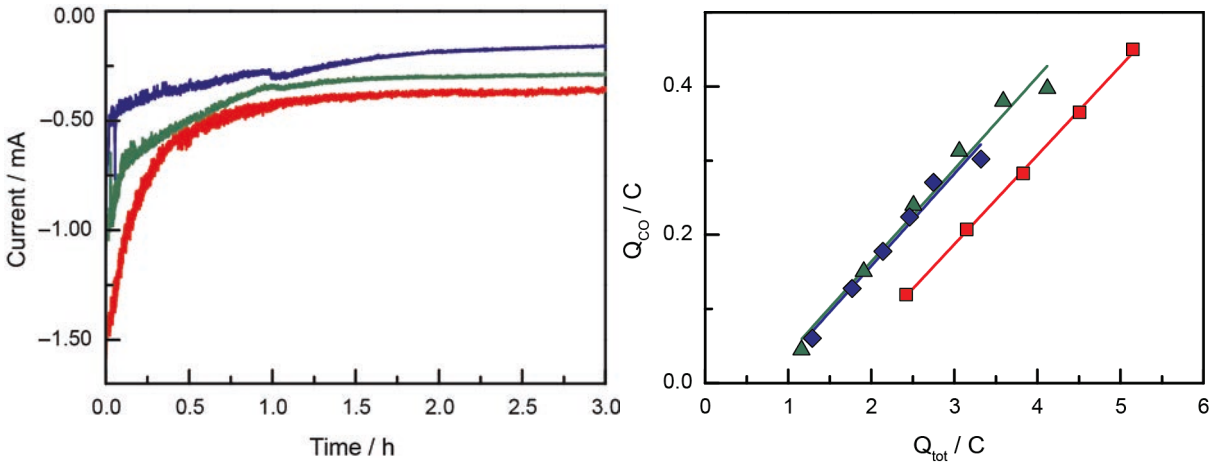

Figure III-24 Current (left) measured during controlled-potential electrolyses of **Co-tpy** CO_2-saturated solutions at –2.03 V using *N*,*N*-diethylformamide (DEF) (green, 1 mM **Co-tpy**), 1-methyl-2-pyrrolidinone (NMP) (blue, 1 mM **Co-tpy**) and DMF (red, 2 mM **Co-tpy**) as primary solvent. Charge corresponding to the CO produced (in DMF: red squares, DEF: green triangles and NMP: blue diamonds) *vs.* the total charge passed during the electrolyses. The slope of the linear fits, corresponding to the faradic efficiency, is 12% in the three cases.[§]

The influence of the electrolyte on the low faradic yields was also investigated. Sequential modifications of the cation from TBA^+ to Li^+ and of the anion from ClO_4^- to PF_6^- also led to similar faradic efficiency. Since **Co-tpy** is also known for O_2 reduction catalysis, the influence of potential O_2 leaks in the system during bulk electrolysis was investigated by performing the experiment in a N_2 filled glovebag. No significant influence on faradic yields was observed. All these results are

consistent with the speculation that the low faradic efficiencies for CO_2 reduction results from reactivity of the **Co-tpy** system under these conditions.

4.2. Electrolysis of free terpyridine

As variations of parameters not specific to the catalysts did not affect the faradic yields significantly, attention was given the chemical structure of the catalyst itself. Specifically, the behaviour of the terpyridyl ligand was investigated in order to identify possible deleterious side reactions intrinsic to terpyridine within the standard catalytic conditions employed.

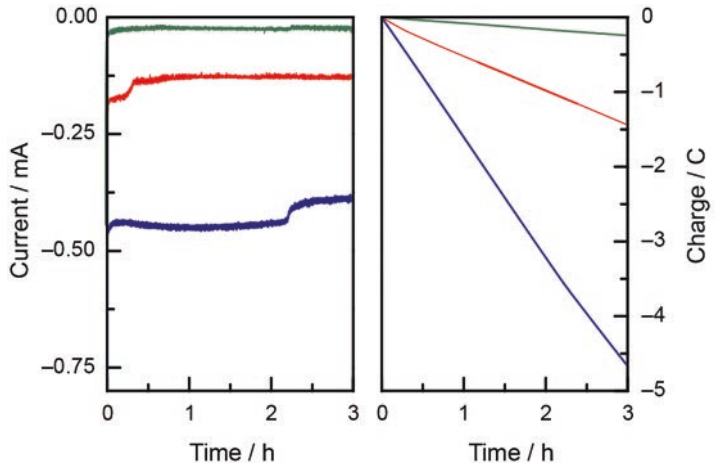

Figure III-25 Current (left) and charge (right) measured during controlled-potential electrolyses of 4 mM terpyridine solutions. Electrolyses carried out at –2.03 V under Ar (green) and CO_2 (red) and at –2.23 V under CO_2 (blue).[§]

Bulk electrolyses of 4 mM solutions of terpyridine at –2.03 V or at –2.23 V *vs.* Fc^+/Fc under CO_2 lead to significant steady currents (–0.13 mA at –2.03 V and –0.45 mA at –2.23 V), contrary to what is observed under inert atmosphere (Figure III-25). However, no CO_2 reduction products or H_2 can be detected in these experiments. This suggests the possibility that tpy transformation is a significant side reaction during catalysis that limits faradic efficiencies.

A possible source of reactivity on the terpyridyl ligand is an *N*-carboxylation. Literature precedents suggest that in DMF, under CO_2, at reducing potentials, *N*-heteroaromatic cycles can undergo *N*-carboxylation reactions to yield compounds that can be trapped by addition of alkylating agents.[47]

4.3. Zn-tpy to catalyse side reactions

To experimentally probe the hypothesis of tpy being involved in side reactions during electrolyses of **M-tpy** complexes, we investigated **Zn-tpy** as a diamagnetic version of the system during both electroreduction and photoreduction of CO_2, with the aim of using ^1H NMR spectroscopy to get some insight into the production of tpy-derived compounds. The paramagnetic nature of the cobalt and nickel based systems precluded investigations of degradation pathways through ^1H NMR, but the diamagnetic nature of Zn^{II} allowed us to probe these side reactions. Assuming that Zn^{II} catalyses the

same side reactions with tpy than that responsible for the low faradic efficiencies observed for **Ni-tpy** and **Co-tpy** under CO_2-saturated conditions, the **Zn-tpy** system was studied further.

4.3.1. Electrochemically

In a first series of experiments a 5 mM **Zn-tpy** solution was electrolysed at –2.15 V vs. Fc^+/Fc during 4.5 h in CO_2-saturated conditions with 0.1 M $LiClO_4$ as supporting electrolyte instead of TBAP to avoid the possibly distracting ^1H NMR signals of the TBA^+ cation.

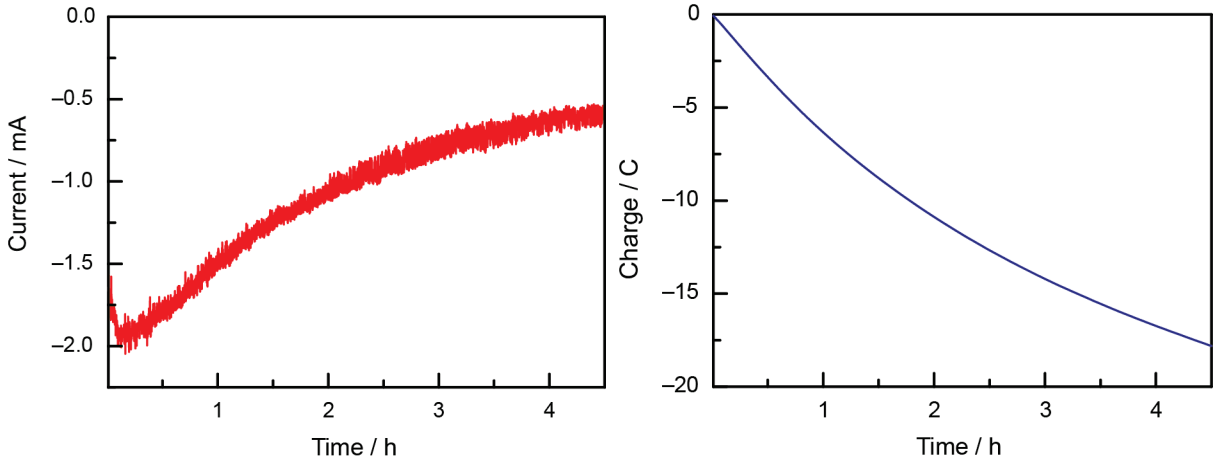

Figure III-26 Current (Top left) and charge (Top right) measured during controlled-potential electrolyses of 5 mM **Zn-tpy** CO_2-saturated solutions at –2.15 V.[§]

A current of about –1.8 mA is obtained, which slowly decreases, as in the **Ni-tpy** case, to reach about –0.8 mA after 3 h (Figure III-26). Notably, no corresponding CO_2 reduction products or H_2 could be detected.

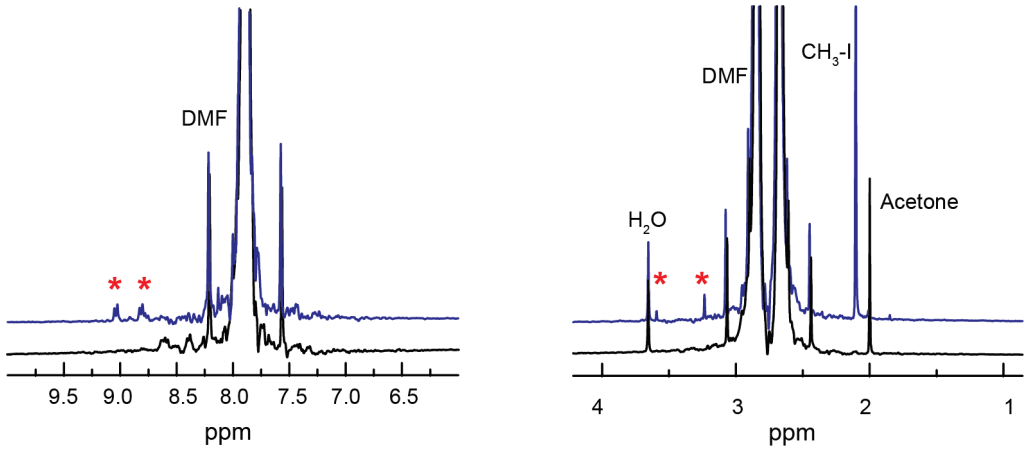

Figure III-27 The aliphatic (right) and aromatic (left) regions of ^1H NMR spectra before the addition of CH_3I (black) and after reaction with CH_3I (blue) are presented here. The spectra have been referenced to the aldehyde proton of DMF (7.9 ppm). The red stars mark the appearance of new peaks after reaction with CH_3I.[§]

After 4.5 h of controlled-potential electrolysis, the experiment is stopped, but the cell is kept sealed and under vigorous stirring. 200 µL of iodomethane (3.2 mmol) was added trough the septum of

the electrochemical cell and the solution was stirred at room temperature for 1.5 h. After 1.5 h, 0.5 mL of the solution is syringed out of the cell and the ^{1}H NMR of the resulting solution, presented in Figure III-27, is consistent with a carboxylation reaction on the terpyridyl ligand. This approach, although successful, was not investigated further however due to safety concerns over the combined presence of iodomethane and mercury.

4.3.2. Photochemically

Photochemical reduction was considered as it provides the opportunity to generate larger concentrations of such compounds more rapidly since the bulk of the solution is reacting at any given point in time, as opposed to the electrochemical system where catalysis occurs in a localised reaction layer near the electrode. In a second series of experiments **Zn-tpy** was photolysed in the presence of CO_2 and $[Ru(bpy)_3]^{2+}$ as the photosensitiser in MeCN/TEOA (triethanolamine, the sacrificial electron donor).

Photochemical Reactions were performed using a 300 W, high pressure Xe arc lamp (Oriel Instruments). The beam was passed through an infrared filter, a collimating lens, a filter holder equipped with a 415 nm band pass filter, and an iris. Samples were prepared in a 1 cm path length quartz cuvette (Starna) which was placed in a temperature controlled cuvette holder (Quantum Northwest) maintained at 20°C with a circulated water bath. Sample preparation involved the use of a 5:1 volumetric ratio of acetonitrile-d_3 to triethanolamine. This solvent system was chosen due to practical considerations regarding deuterated solvent accessibility. The solvent mixture was used to prepare a 4.0 mM stock solution of $Ru(bpy)_3Cl_2(H_2O)_6$ and a 2.0 mM stock solution of **Zn-tpy**. For photolysis including **Zn-tpy**, two samples were made in tandem, each of which included 0.4 mL of the **Zn-tpy** stock solution mixed with 0.4 mL of the $Ru(bpy)_3Cl_2(H_2O)_6$ stock solution within the quartz cuvette. The resulting 0.8 mL solution (2.0 mM $Ru(bpy)_3Cl_2(H_2O)_6$ and 1.0 mM **Zn-tpy**) was saturated with CO_2 via vigorous bubbling of CO_2 through the solution for 15 minutes through a cuvette cap with a septum. One of the samples prepared was then photolysed for 6 h while the other was placed in the dark for the same length of time. Upon completion the reaction mixtures were pipetted from the quartz cuvette into an NMR tube for analysis via ^{1}H NMR. Photolysis samples including only $Ru(bpy)_3Cl_2(H_2O)_6$ were prepared and treated in an analogous manner with the 0.4 mL of **Zn-tpy** stock solution being replaced by 0.4 mL of the solvent mixture. The resulting solutions were analysed by ^{1}H NMR (Figure III-28).

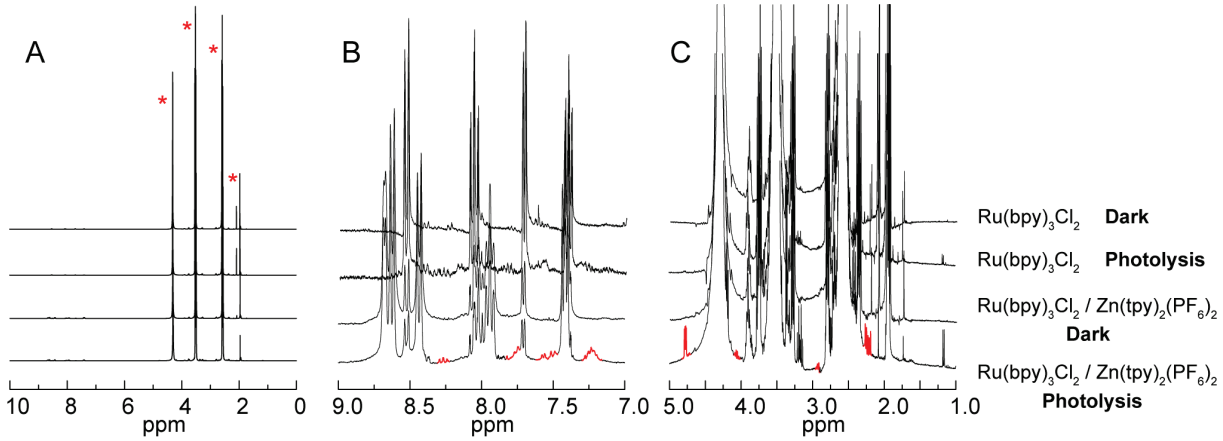

Figure III-28 ^{1}H NMR spectra for the photolysis of experiments of 1.0 mM **Zn-tpy** in the presence of 2.0 mM $Ru(bpy)_3Cl_2(H_2O)_6$ in a CO_2-saturated 5:1 volumetric ratio of acetonitrile-d_3 to triethanolamine. From top to bottom, the spectra represent $Ru(bpy)_3Cl_2(H_2O)_6$ in the dark; $Ru(bpy)_3Cl_2(H_2O)_6$ photolysed for 6h; both $Ru(bpy)_3Cl_2(H_2O)_6$ and **Zn-tpy** in the dark; and both $Ru(bpy)_3Cl_2(H_2O)_6$ and **Zn-tpy** photolysed for 6h. (a) The full spectra are shown with the intense peaks associated with TEOA marked by *. (b) Aromatic resonances are shown with peaks only observed post-photolysis of **Zn-tpy** presented in red. (c) Aliphatic resonances are shown with peaks only observed post-photolysis of **Zn-tpy** presented in red.[§]

The ^{1}H NMR spectrum shows the presence of protons in the aliphatic region which are not originating from TEOA degradation pathways. This suggests a loss of aromaticity on the pyridine rings of the ligands and direct transformation of tpy. All of these observations further support ligand degradation pathways as contributing to the low faradic efficiencies of the reaction of **M-tpy** with CO_2.

4.3.3. Conclusions

Together, the electrochemical and photochemical experiments with **Zn-tpy** under an atmosphere of CO_2 indicate that reactivity of the terpyridyl ligand does occur. Given that no other parameters have been identified as relevant to the faradic yield, tpy reactivity is likely a significant contributing factor to the low faradic yields towards CO_2 reduction for the **Co-tpy** and **Ni-tpy** systems. This provides a promising strategy for developing more efficient second generation catalysts in the future, despite being unable to unequivocally assign the nature of the tpy reactivity. Higher efficiencies can likely be achieved either by tuning the ligand environment to enhance CO_2 reactivity (and outcompete the deleterious reactions) of by modifying the ligand environment to either sterically hinder or electronically disfavour the deleterious reactions.

5. Probing the mechanisms of CO_2 reduction by Co-tpy

5.1. Order in catalyst

The initial assessment of the order of the catalytic reaction in **Co-tpy** was carried out by cyclic voltammetry. CO_2-saturated solution of **Co-tpy** at different concentrations in DMF/H_2O (95:5, v:v) with 0.1 M TBAP as supporting electrolyte were analysed by cyclic voltammetry, and the catalytic peak current was recorded. The resulting value, corrected for the capacitive current, is given in Figure III-29 as a function of the concentration of **Co-tpy**. The linear fit suggests that the reaction is first-order in catalyst under the conditions tested.

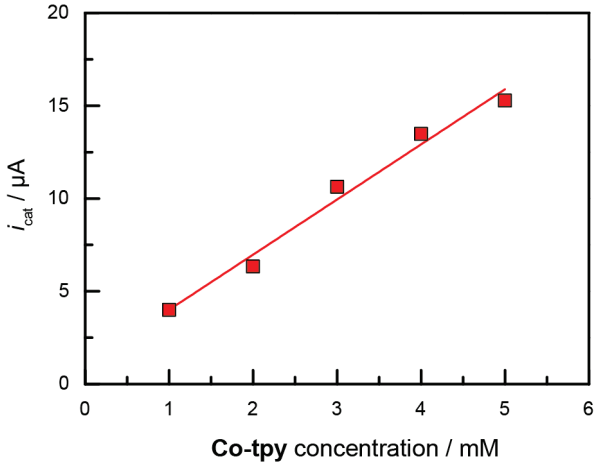

Figure III-29 Variation of i_{cat} with the concentration of **Co-tpy** in CO_2-saturated solutions during cyclic voltammetry experiments at 50 mV/s. The working electrode used was 1 mm diameter glassy carbon electrode, the counter electrode was a platinum wire, and the reference electrode was a Ag/AgCl, 3M KCl reference electrode. The solvent system used was DMF/H_2O (95:5, v:v), with 0.1M of TBAP as supporting electrolyte. The correlation coefficient of the linear fit (red) is 0.98.[§]

Controlled-potential electrolyses experiments were also used to gain an insight into the mechanism. Bulk electrolysis at a fixed applied potential of –2.03 V *vs.* Fc^+/Fc were carried out on solutions of **Co-tpy** at different concentrations in order to assess the order of **Co-tpy** under steady state conditions as opposed to fast time scales previously probed by CV experiments. The faradic yields for CO and H_2 production were constant in the range of concentration tested. The potential was also varied in a step-wise manner after the initial stabilisation of the current, to measure the stable current values observed as a function of the applied potential. In an effort to obtain activation controlled conditions, the solution above the pool of mercury was stirred as vigorously as possible without disrupting the surface of the mercury electrode. Current values were corrected for the values observed in a solution without **Co-tpy**, at each given potential. The slope of the linear fits, corresponding to the apparent order in cobalt under bulk electrolyses conditions, is given in the table.

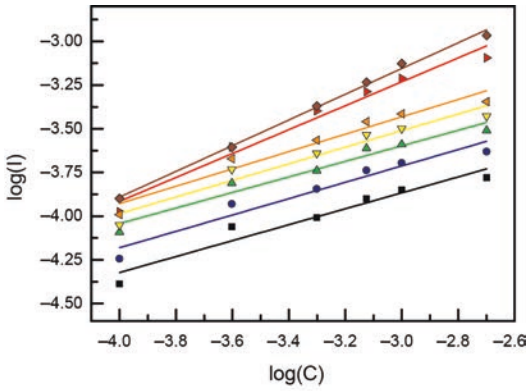

Applied potential	Apparent order in Cobalt	correlation coefficient
–1.97 V	0.46	0.93
–1.99 V	0.47	0.93
–2.02 V	0.44	0.95
–2.04 V	0.47	0.93
–2.07 V	0.50	0.94
–2.17 V	0.68	0.97
–2.27 V	0.74	0.99

Figure III-30 Plot of the log(current(A)) *vs.* the log(concentration(mol/L)) obtained in 6 controlled-potential electrolyses of **Co-tpy** CO_2-saturated solutions at different concentrations of **Co-tpy** where the potential was first held at –2.03 V until the current reached the plateau region and then varied in a step manner every 30 min and the plateau current at each potential was recorded (brown diamonds: –2.27 V, red triangles: –2.17 V, orange triangles: –2.07 V, yellow triangles: –2.04 V, green triangles: –2.02 V, blue circles: –1.99 V, black squares: –1.97 V).[§]

The results, as shown in Figure III-30, indicate that under steady-state bulk electrolysis conditions the apparent order in cobalt was 0.5 at the five potentials tested in the –1.97 V to –2.07 V potential range. The order then increased to 0.74 as the potential applied was further decreased to reach –2.27 V. It has to be noted that the current stability was diminished at this negative potential value. Of importance, the order in **Co-tpy** was found to be 1 under the fast time scale conditions of a CV experiment but was found to definitely be less than 1 (likely 0.5) under steady state conditions. This difference is attributed to an inhibition process that occurs under steady state conditions and will be elaborated upon later.

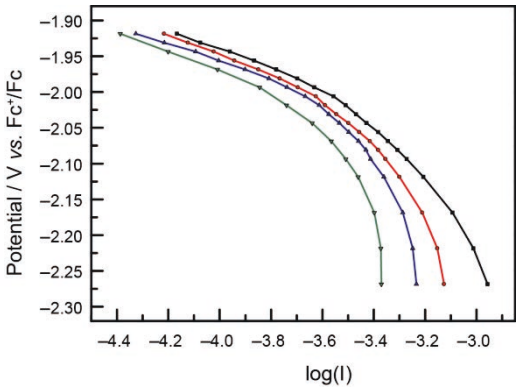

Figure III-31 Plot of applied potential *vs.* log(current(A)) extracted from the experiments described in Figure III-30 (black squares: 2 mM, red circles: 1 mM, blue triangles: 0.75 mM and green triangles: 0.5 mM of **Co-tpy**). At all **Co-tpy** concentrations, the slope of the linear fit (not represented) of the –1.9 V to –2.1 V region is ~135 mV/dec).[§]

A plot of potential *vs.* the log of the total current, analogous to a Tafel plot, at various catalyst concentrations was extracted from the experimental bulk electrolysis data. The data are shown in Figure III-31. At all concentrations, linearity was observed over a short range of potentials from –1.9 V to –2.1 V with a slope of 135 mV/dec. As the potential is stepped to more negative values, the slope increases rapidly to reach values > 1 V/dec. This supports either a chemical rate determining step or mass transport limitation to the apparent kinetics. The lack of a pre-equilibrium electron transfer step inhibits our ability to utilize electrochemistry to probe further into mechanistic aspects of electrocatalytic reduction of CO_2 by **Co-tpy**.

5.2. Nature of the active catalyst

Since there are no available coordination sites for interaction with CO_2 in $[Co(tpy)_2]^+$, it was assumed that a catalytic species different from the starting complex was generated during bulk electrolysis resulting from either de-coordination of a pyridine ring of tpy or complete loss of a tpy ligand. In order to assess the ligand-to-metal stoichiometry of the catalytically relevant species, a methodology used by Sauvage and Lehn[48] in the study of CO_2 photoreduction by the analogous $[M(bpy)_n]^{m+}$ complexes was followed, in which the efficiency of the catalysis, during bulk electrolyses, was assessed while the tpy:Co ratio was varied by combining tpy with $CoCl_2$ salt. Figure III-32 presents the evolution of the observed current during these controlled-potential bulk electrolyses. The evolution of the charge is presented in Figure VI-4 of the Appendix.

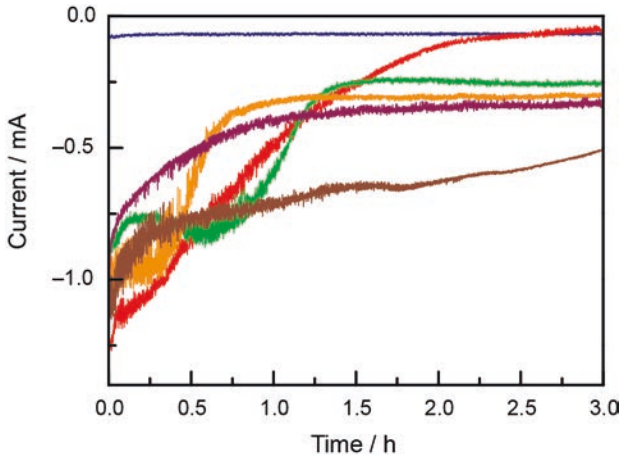

Figure III-32 Current measured during controlled-potential electrolyses of CO_2-saturated solutions at –2.03 V of: 2 mM tpy (blue), 2 mM $CoCl_2$ (red), 2 mM tpy and 2 mM $CoCl_2$ (yellow), 4 mM tpy and 2 mM $CoCl_2$ (purple), 1 mM tpy and 2 mM $CoCl_2$ (green) and a mixture of 2 mM $CoCl_2$, 2 mM tpy and 2mM bpy (brown).[‡]

Additionally, the amount of CO and H_2 produced during these controlled-potential bulk electrolyses was measured and the results, in terms of charge attributed to the formation of CO and H_2 *vs.* total charge passed are given in Figure III-33. The results in terms of the faradic efficiency for CO production are summarized in Table III-1.

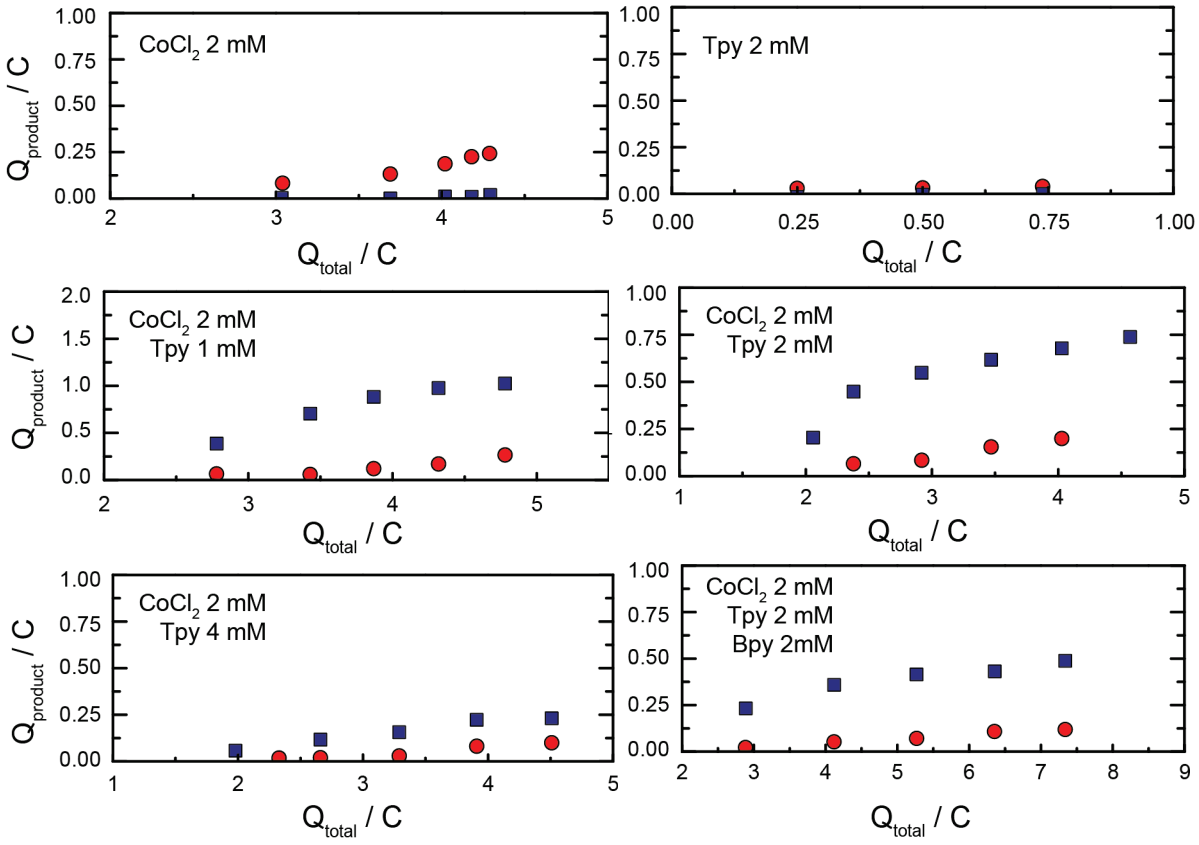

Figure III-33 Charge corresponding to the products measured (CO: black squares, H_2: red circle) *vs.* the total charge passed during the electrolyses at –2.03 V of the solutions described.[§]

At –2.03 V *vs.* Fc^+/Fc, solutions of 2 mM $CoCl_2$ appear to exhibit electrocatalytic activity. This system is highly unstable, as the current intensity continuously decreased down to baseline levels during the 3 h electrolysis, and produced almost exclusively H_2 with only traces of CO. This is attributed to the formation of a Co^0 solid which can be rendered electrochemically inert via amalgamation with the mercury, thus explaining the constant drop in current densities. When solutions of terpyridine are electrolyzed at –2.03 V under CO_2, a steady current is observed but no CO or H_2 could be detected.

Table III-1 influence of the relative concentrations (mM) of tpy, $CoCl_2$ and bpy and of time on CO faradic yields ($\%_{CO}$) observed during bulk electrolyses at –2.03 V *vs.* Fc^+/Fc.

tpy	bpy	$CoCl_2$	$\%_{CO}$ 1-2 h	$\%_{CO}$ 2-3 h
4	0	2	7	6
2	0	2	38[a](76[b])	11
2	2	2	8	3
2	0	0	0	0
1	0	2	46	16
0	0	2	1	4

[a:] Measured between minutes 45 and 90 of electrolysis.[b.] Measured between minutes 45 and 60 of electrolysis.[§]

When a tpy:Co ratio of 2:1 is used, the behaviour observed is similar to that of pre-synthesised $[Co(tpy)_2]^{2+}$ with a faradic yield for CO production stable over time and a current (purple trace, Figure III-32) stabilising after enough electrons are passed to reduce all the Co^{II} to Co^{I}.

As the tpy:Co ratio is decreased, faradic efficiencies for CO production are increased, with the highest recorded value of 76% during the beginning of the electrolysis of a 1:1 Co/tpy mixture. The currents observed, and the faradic yields for CO, are not as stable as for the 2:1 ratio. CO production appears more efficient at early time points and decreases over time to reach levels comparable to that which is observed for the 2:1 ratio. The currents follow the same trends, and stabilise to values smaller than that of the 2:1 system. One explanation would be that, based on the behaviour of $CoCl_2$ (red trace in Figure III-32), free Co centres not coordinated by tpy are being reduced to an inactive Co^0 solid state. An equilibrium is reached as no more free Co centres exist, at which point the composition of the solution is closer to the 2:1 system, with the corresponding lower faradic yields for CO production. These results tend to suggest a catalytic species composed of at most 1 equivalent of terpyridine per cobalt centre.

5.3. Mechanism

To allow for direct interaction between CO_2 and the metal centre, the ability of the system to liberate a coordination site is crucial. This is achieved in Ru-based catalysts[49] by the exchange of a solvent molecule for CO_2, in $[M(bpy)_3]$ compounds by the prior loss of a bpy ligand[50] and in the case of $[Re(bpy)(CO)_3Cl]$ the opening of a coordination site through loss of the Cl^- ligand is triggered by bpy reduction.[51] Similarly, we propose that ligand reduction triggers the loss of the second (neutral) terpyridyl ligand, as has been proposed for analogous cobalt-based systems.[52]

The proposed mechanism for **Co-tpy** is depicted in Figure III-34, where solvent, electrolytes, or other Lewis bases complete the coordination sphere around the cobalt. We propose that the $[Co^{II}(tpy)_2]^{2+}$ compounds acts as the pre-catalyst. Upon reduction of first Co^{II} to Co^{I} and then tpy to $tpy^{\bullet-}$, a neutral terpyridyl ligand is lost, generating a catalytically active species with a stoichiometry of one tpy per Co. In steady state bulk electrolysis conditions however, we propose that a resting state dimeric species forms where two $[Co^{I}(tpy)]$ centres are bridged, possibly by carbonates or carbonyl groups, as has been reported in analogous structures in the literature.[53,54,55,56,57,58] The carbonates could possibly originate either from a CO_2/water equilibrium or as an outcome of CO formation. The necessity for this dimer to break apart, liberating the Co-monoterpyridine catalyst, is supported by the apparent order of 0.5 observed in these conditions, as well as the observation from the Tafel data of a chemical limiting step. By analogy with reported mechanism for CO formation on related polypyridyl compounds, we propose the substitution of CO_2 for a solvent molecule in the $[Co^{I}(tpy^{\bullet-})]$ entity, which then reacts with a second CO_2 molecule and H^+ to yield a Co-CO intermediate, which eventually releases CO and HCO_3^-. This mechanism for CO generation likely can be extended to **Ni-tpy**, however the two catalytically relevant reduction events for the catalyst would be primarily ligand based.

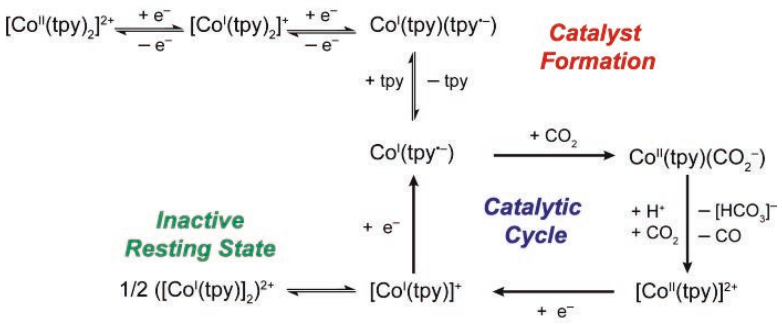

Figure III-34 Proposed mechanism for CO_2 reduction to CO by **Co-tpy**.[‡]

An alternate pathway, paralleling CO and H_2 formation, explains the low faradic yield. It is likely that the reduction of the tpy ligand renders it highly susceptible to further reactions, such as carboxylations,[47] or possibly hydrogenation,18 which compete with CO and H_2 formation. Previous reports in the case of noble metal-based systems have also pointed to such a parallel process that might explain the low faradic yields.[17,]18 However it seems that the late first row transition metals are less efficient in avoiding these reactions as faradic yields for CO + H_2 are significantly lower in that case.

6. Conclusions

We have shown that homoleptic terpyridine complexes of nickel and cobalt are competent catalysts for the electrocatalytic reduction of CO_2 to CO as the exclusive carbon containing product. The catalysis is observed to begin by reduction of a tpy ligand for both the **Ni-tpy** and **Co-tpy** systems. The systems differ in that the resting state of the **Co-tpy** catalyst is assigned to be monovalent cobalt whereas the resting state of the **Ni-tpy** catalyst is assigned to be divalent nickel. The higher valent nickel catalyst is proposed to be unable to generate intermediate nickel-hydrides required for hydrogen generation in the conditions used and thus exhibits remarkable selectivity for CO_2 reduction to CO over proton reduction. The lower valent cobalt catalyst is found to generate gaseous mixtures of CO and H_2, the ratio of which can be tuned upon varying the applied voltage. Indeed, at the least negative potentials electrolysis generated CO almost exclusively, while decreasing the potential resulted in a drop of the CO:H_2 ratio, with a CO:H_2 value of 1 at about –2.1 V. Decomposition of the polypyridyl ligand has been hypothesised to be the primary pathway which limits overall faradic efficiency, even though the intrinsic catalytic activity for the cobalt based system is comparable to that which has been reported for other polypyridyl metal catalysts.[59]

7. References

‡ N. Elgrishi, M. B. Chambers, V. Artero and M. Fontecave, *Phys. Chem. Chem. Phys.*, 2014, **16**, 13635–13644. Reproduced by permission of the PCCP Owner Societies.

§ Adapted with minor alterations from ‡.

1 N. S. Lewis and D. G. Nocera, *Proc. Natl. Acad. Sci.*, 2006, **103**, 15729.

2 T. Faunce, S. Styring, M. R. Wasielewski, G. W. Brudvig, A. W. Rutherford, J. Messinger, A. F. Lee, C. L. Hill, H. deGroot, M. Fontecave, D. R. MacFarlane, B. Hankamer, D. G. Nocera, D. M. Tiede, H. Dau, W. Hillier, L. Wang and R. Amal, *Energy Environ. Sci.*, 2013, **6**, 1074.

3 T. R. Cook, D. K. Dogutan, S. Y. Reece, Y. Surendranath, T. S. Teets and D. G. Nocera, *Chem. Rev.*, 2010, **110**, 6474.

4 H. Arakawa, M. Aresta, J. N. Armor, M. A. Barteau, E. J. Beckman, A. T. Bell, J. E. Bercaw, C. Creutz, E. Dinjus, D. A. Dixon, K. Domen, D. L. DuBois, J. Eckert, E. Fujita, D. H. Gibson, W. A. Goddard, D. W. Goodman, J. Keller, G. J. Kubas, H. H. Kung, J. E. Lyons, L. E. Manzer, T. J. Marks, K. Morokuma, K. M. Nicholas, R. Periana, L. Que, J. Rostrup-Nielson, W. M. H. Sachtler, L. D. Schmidt, A. Sen, G. A. Somorjai, P. C. Stair, B. R. Stults and W. Tumas, *Chem. Rev.*, 2001, **101**, 953.

5 J. L. Inglis, B. J. MacLean, M. T. Pryce and J. G. Vos, *Coord. Chem. Rev.*, 2012, **256**, 2571.

6 M. Rakowski DuBois and D. L. DuBois, *Acc. Chem. Res.*, 2009, **42**, 1974.

7 E. E. Benson, C. P. Kubiak, A. J. Sathrum and J. M. Smieja, *Chem. Soc. Rev.*, 2009, **38**, 89.

8 A. J. Morris, G. J. Meyer and E. Fujita, *Acc. Chem. Res.*, 2009, **42**, 1983.

9 A. Winter, G. R. Newkome, U. S. Schubert, *Chem. Cat. Chem.*, 2011, **3**, 1384.

10 C. Kaes, A. Katz and M. W. Hosseini, *Chem. Rev.*, 2000, **100**, 3553.

11 J.-M. Savéant, *Chem. Rev.*, 2008, **108**, 2348.

12 C. C. Scarborough, K. M. Lancaster, S. DeBeer, T. Weyhermüller, S. Sproules and K. Wieghardt, *Inorg. Chem.*, 2012, **51**, 3718.

13 M. Wang, J. England, T. Weyhermüller and K. Wieghardt, *Inorg. Chem.*, 2014, **53**, 2276.

14 J. Hawecker, J.-M. Lehn and R. Ziessel, *J. Chem. Soc., Chem. Commun.*, 1984, 328.

15 T. Yoshida, K. Tsutsumida, S. Teratani, K. Yasufuku and M. Kaneko, *J. Chem. Soc., Chem. Commun.*, 1993, 631.

16 J. M. Smieja and C. P. Kubiak, *Inorg. Chem.*, 2010, **49**, 9283.

17 C. Caix, S. Chardon-Noblat and A. Deronzier, *J. Electroanal. Chem.*, 1997, **434**, 163.

18 C. M. Bolinger, N. Story, B. P. Sullivan and T. J. Meyer, *Inorg. Chem.*, 1988, **27**, 4582.

19 P. Paul, B. Tyagi, A. K. Bilakhiya, M. M. Bhadbhade, E. Suresh and G. Ramachandraiah, *Inorg. Chem.*, 1998, **37**, 5733.

20 H. Nagao, T. Mizukawa and K. Tanaka, *Inorg. Chem.*, 1994, **33**, 3415.

21 Z. Chen, C. Chen, D. R. Weinberg, P. Kang, J. J. Concepcion, D. P. Harrison, M. S. Brookhart and T. J. Meyer, *Chem. Commun.*, 2011, **47**, 12607.

22 M. Bourrez, F. Molton, S. Chardon-Noblat and A. Deronzier, *Angew. Chem. Int. Ed.*, 2011, **50**, 9903.

23 J. M. Smieja, M. D. Sampson, K. A. Grice, E. E. Benson, J. D. Froehlich and C. P. Kubiak, *Inorg. Chem.*, 2013, **52**, 2484.

24 A. R. Guadalupe, D. A. Usifer, K. T. Potts, H. C. Hurrell, A.-E. Mogstad and H. D. Abruña, *J. Am. Chem. Soc.*, 1988, **110**, 3462.

25 H. C. Hurrell, A. L. Mogstad, D. A. Usifer, K. T. Potts and H. D. Abruña, *Inorg. Chem.*, 1989, **28**, 1080.

26 C. Arana, S. Yan, M. Keshavarz-K, K. T. Potts and H. D. Abruña, *Inorg. Chem.*, 1992, **31**, 3680.

27 C. Arana, M. Keshavarz, K. T. Potts and H. D. Abruña, *Inorg. Chim. Acta*, 1994, **225**, 285.

28 J. A. Ramos Sende, C. R. Arana, L. Hernandez, K. T. Potts, M. Keshevarez-K and H. D. Abruña, *Inorg. Chem.*, 1995, **34**, 3339.

29 G. D. Jones, J. L. Martin, C. McFarland, O. R. Allen, R. E. Hall, A. D. Haley, R. J. Brandon, T. Konovalova, P. J. Desrochers, P. Pulay and D. A. Vicic, *J. Am. Chem. Soc.*, 2006, **128**, 13175.

30 C. Hamacher, N. Hurkes, A. Kaiser, A. Klein and A. Schüren, *Inorg. Chem.*, 2009, **48**, 9947.

31 T. N. Huan, E. S. Andreiadis, J.Heidkamp, P. Simon, E. Derat, S. Cobo, G. Royal, H. Dau, V. Artero and M. Fontecave, *J. Mater. Chem. A.*, 2015, **3**, 3901.

32 J.-D. Compain, M. Bourrez, M. Haukka, A. Deronzier and S. Chardon-Noblat, *Chem.Commun.*, 2014, **50**, 2539-2542

33 A. Paul, D. Connolly, M. Schulz, M. T. Pryce and J. G. Vos, *Inorg. Chem.*, 2012, **51**, 1977.

34 J. L. Dempsey, J. R. Winkler and H. B. Gray, *J. Am. Chem. Soc.*, 2010, **132**, 16774.

35 J. L. Dempsey, J. R. Winkler and H. B. Gray, *J. Am. Chem. Soc.*, 2009, **132**, 1060.

36 J. L. Dempsey, B. S. Brunschwig, J. R. Winkler and H. B. Gray, *Acc.Chem. Res.*, 2009, **42**, 1995.

37 T. Lazarides, T. McCormick, P. Du, G. Luo, B. Lindley and R. Eisenberg, *J. Am. Chem. Soc.*, 2009, **131**, 9192.

38 M. M. Roubelakis, D. K. Bediako, D. K. Dogutan and D. G. Nocera, *Energy Environ. Sci.*, 2012, **5**, 7737.

39 V. Artero, M. Chavarot-Kerlidou and M. Fontecave, *Angew. Chem. Int. Ed.*, 2011, **50**, 7238.

40 R. Ziessel, J. Hawecker and J.-M. Lehn, *Helvetica Chimica Acta*, 1986, **69**, 1065.

41 C. V. Krishnan, N. Sutin, *J. Am. Chem. Soc.*, 1981, **103**, 2141.

42 C. Creutz, H. A. Schwarz, N. Sutin, *J. Am. Chem. Soc.*, 1984, **106**, 3036.

43 Z. Han, L. Shen, W. W. Brennessel, P. L. Holland and R. Eisenberg, *J. Am. Chem. Soc.*, 2013, **135**, 14659.

44 J. Yang, S. E. Smith, T. Liu, W. G. Dougherty, W. A. Hoffert, W. S. Kassel, M. Rakowski Dubois, D. L. Bubois and M. Bullock, *J. Am. Chem. Soc.*, 2013, **135**, 9700.

45 A. D. Wilson, R. H. Newell, M. J. McNevin, J. T. Muckerman, M. Rakowski Dubois and D. L Dubois, *J. Am. Chem. Soc.*, 2006, **128**, 358.

46 J. Y. Yang, R. Morris Bullock, W. J. Shaw, B. Twamley, K. Fraze, M. Rakowski Dubois and D. L. Dubois, *J. Am. Chem. Soc.*, 2009, **131**, 5935.

47 P. Fuchs, U. Hess, H. H. Holst and H. Lund, *Acta Chemica Scandinavica B*,1981, **35**, 185.

48 J.-M. Lehn and R. Ziessel, *Proc. Nati. Acad. Sci. USA*, 1982, **79**, 701.

49 Z. Chen, P. Kang, M.-T. Zhang and T. J. Meyer, *Chem. Commun.*, 2014, **50**, 335.

50 S. Daniele, P. Ugo, G. Bontempelli and M. Fiorani, *J. Electroanal. Chem.*, 1987, **219**, 259.

51 B. P. Sullivan, C. M. Bolinger, D. Conrad, W. J. Vining and T. J. Meyer, *J. Chem. Soc., Chem. Commun.*, 1985, 1414.

52 D. Chen, P.-L. Fabre and O. Reynes, *Electrochimica Acta*, 2011, **56**, 8603.

53 G. Fachinetti, T. Funaioli and P. F. Zanazzi, *J. Chem. Soc., Chem. Commun*., 1988, 1100.

54 E. Fujita, D. J. Szalda, C. Creutz and N. Sutin, *J. Am. Chem. Soc.*, 1988, **110**, 4870.

55 J. Nath, D. Kalita and J. B. Baruah, *Polyhedron*, 2011, **30**, 2558.

56 T. Duangthongyou, C. Phakawatchai and S. Siripaisarnpipat, *J. Mol. Struct.*, 2011, **987**, 101.

57 K. Dimitrou, K. Folting, W. E. Streib and G. Christou, *J. Am. Chem. Soc.*, 1993, **115**, 6432.

58 S. Bhaduri, N. Y. Sapre and A. Basu, *J. Chem. Soc., Chem. Commun*., 1986, 197.

59 C. Costentin, M. Robert and J.-M. Savéant, *Chem. Soc. Rev.*, 2013, **42**, 2423.

Chapter IV

–

CO_2 reduction selectivity over H^+ reduction by **Co-tpy**

Based on the work reported in: N. Elgrishi, M. B. Chambers and M. Fontecave, *Chemical Science*, 2015, DOI: 10.1039/C4SC03766A.

1. Introduction

In general, catalysts for CO_2 reduction are often plagued by lack of selectivity due to the numerous possible CO_2 reduction carbon-containing products, as well as the constant competition with proton reduction to H_2. The lack of selectivity would subsequently require additional purification and isolation processes in order to obtain the particular product of interest, resulting in increased total system costs. Among various classes of catalysts, molecular ones offer the possibility to synthetically finely tune their structure and reactivity and allow for a deeper understanding of underlying mechanistic pathways, thus paving the way to the rational design of more selective catalysts.[1,2,3] This molecular approach has been favoured recently, with a shift to the study of first row transition metals combined with simple cheap ligands.[4,5,6,7,8,9,10] However, while most studies have been dealing mainly with catalytic efficiency using empirically selective catalysts,[11,12] through comparison of a variety of metal-ligand combinations, rational optimisation of the selectivity for a particular product has been generally unexplored in molecular CO_2 reduction catalytic systems.

As demonstrated within Chapter III, our studies of molecular systems for CO_2 reduction began with a re-evaluation of the CO_2 reduction chemistry of metal-terpyridine catalytic systems. We have reported that the cobalt (**Co-tpy**) and nickel based catalysts can reduce CO_2 to CO and that in the case of cobalt a mixture of H_2 and CO is produced.[13] The proportions of H_2 produced were shown to be easily tuneable through the modulation of the applied potential during bulk electrolysis, motivating our desire to understand the parameters allowing this tuneability. This initial observation suggests that the rate limiting step for H_2 production and CO_2 reduction are distinctive due to the different responses to applied potential. Different rate limiting transition states suggests that modification to affect one would not necessarily have the same effect on the other. We thus sought to investigate the possibility of enhancing selectivity for CO production through the rational inhibition of the hydrogen evolution reaction (HER), with a goal of enhancing the faradic yields observed for CO_2 reduction to CO. While seemingly backwards at first, the strategy of suppressing the H_2 evolution reaction in order to increase faradic efficiencies for a more chemically challenging reduction has recently been proposed in the course of the study of CO reduction on oxide-derived nanocrystalline copper and lead electrodes in water, but has yet to be extended to molecular-based catalytic systems.[14,15]

Polypyridyl cobalt complexes have recently received renewed interest as electrocatalysts for proton reduction[16,17,18] although precedent is scarce for mononuclear cobalt-terpyridine systems catalyzing the HER. To our knowledge the only two previous reports of such systems consist of H_2 evolution from $[Co(tpy)_2]^{2+}$ embedded in a nafion® membrane in water[19] and a recent report on a Co(tpy)(phen) catalyst grafted on an electrode for H_2 evolution from water.[20]

It is practically challenging to study and optimise CO_2 reduction independent of concomitant proton reduction as CO_2 reduction typically involves a proton source. Thus in an attempt to better understand the underlying chemical principle leading to the controlled production of a CO/H_2 ratio of products, we decided to focus first on understanding the hydrogen evolution reaction as catalysed by **Co-tpy**, independently of CO_2 reduction. To this end, the proton reduction reaction was studied independently as the *foot-of-the-wave analysis* (*FOWA*) was performed on **Co-tpy** as well as on cobalt systems bearing substituted terpyridyl ligands (**Co-tpyY$_2$X**) to allow for tuning of the electronics of the complex.

2. Cobalt-terpyridine complexes as catalysts for hydrogen evolution

2.1. Structure and synthesis

The structure of the compounds studied is presented in Figure IV-1. Compounds **1-5** are composed of a cobalt(II) centre coordinated to two substituted terpyridyl ligands. The modifications of the electronic structure occur through substituent groups placed *para* to the nitrogen atoms so as to minimize perturbation of the steric properties of the compounds around the cobalt atom.

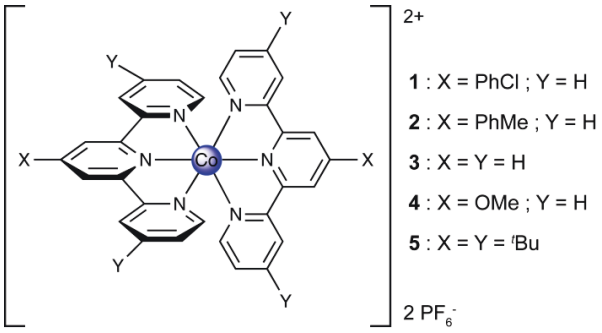

Figure IV-1 Chemical structure of the compounds studied.‡

Due to the ubiquitous nature of tpy ligands, and their ease of synthesis and their recent usage as ligands on cobalt to be used as electron mediators in the $Co^{II/III}$ wave in dye sensitised solar cells, a wide variety of tpy derived ligands are available commercially, and the synthesis of many more have been reported following several routes.[21,22,23,24,25] 4'-(4-chlorophenyl)-2,2':6',2"-terpyridine (tpyPhCl), 4,4',4"-tri-*tert*-butyl-2,2':6',2"-terpyridine (tpyT^{t}Bu), 4'-(4-methylphenyl)-2,2':6',2"-terpyridine (tpyPhMe) and 2,2':6',2"-terpyridine (tpy) of the highest purity available were purchased from Sigma-Aldrich and used as received for this study. 4'-methoxy-2,2':6',2"-terpyridine (tpyOMe) was synthesised from the commercially available 4'-chloro-2,2':6',2"-terpyridine according to a literature procedure, as were compounds **1-5** .[26,27,28]

2.2. Characterisation under argon by cyclic voltammetry

All cyclic voltammetry data presented within Chapter IV was collected using a glassy carbon electrode with a 3 mm diameter, as described in Chapter II.

Under an inert atmosphere of argon in anhydrous DMF, compounds **1-5** exhibited the CVs at 50 mV/s scan rate presented in Figure IV-2. In the interrogated potential range, all of the compounds exhibited two reversible, diffusion-controlled one-electron waves.

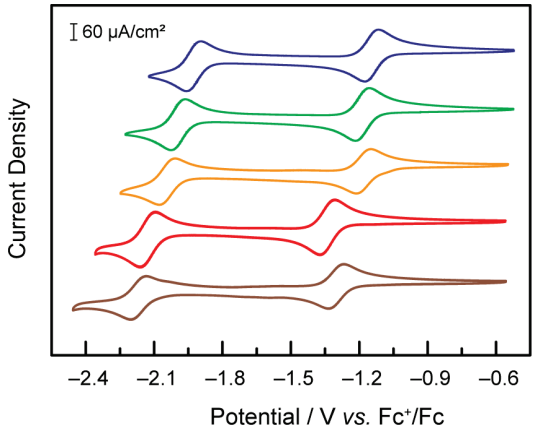

Figure IV-2 Cyclic voltammograms under Ar at 50 mV/s of 1 mM solutions of compounds **1** (— blue), **2** (— green), **3** (— orange), **4** (— red) and **5** (— brown) in DMF, $TBAPF_6$ 0.1M, on a glassy carbon electrode.‡

The first feature is attributed to a $Co^{II/I}$ metal-based reduction, ranging from –1.14 V for **1** to –1.34 V *vs.* Fc^+/Fc for **4.** The redox potentials follow a behaviour consistent with the trend in Hammett parameter of the substituent noted "X" in Figure IV-1, indicating that the electronic density on the metal is dictated more strongly by the substituent on the *para* position of the central pyridyl ring in $[Co(tpyY_2X)_2]^{2+}$ as can be seen from the correlation observed between the redox potentials and the sigma Hammet parameter for the substituent X (Figure IV-3).

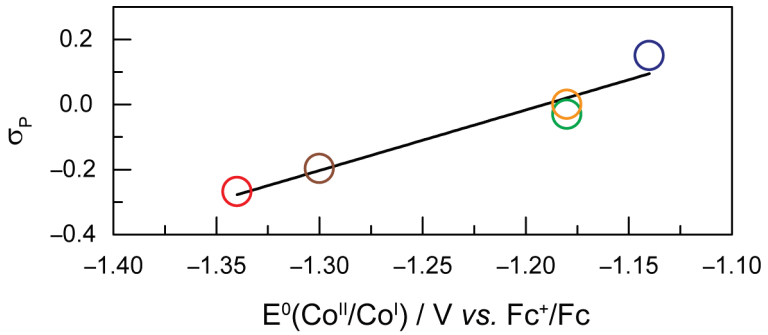

Figure IV-3 Standard potential observed for the Co^{II}/Co^{I} couple for compounds **1** (blue), **2** (green), **3** (yellow), **4** (red) and **5** (brown) in DMF, $TBAPF_6$ 0.1M as a function of the Hammett parameter of the substituent present on *para* position of the central pyridyl ring.‡

The second feature is assigned to a ligand-based reduction, ranging from –1.92 V for **1** to –2.17 V *vs.* Fc^+/Fc for **5**. If the parent compound with unsubstituted terpyridyl ligands, **3**, is taken as a reference point for comparison, as expected the ligand-based reductions are found at more positive potentials for complexes with more electron-withdrawing substitutions on the terpyridine, (**1** *vs.* **3**). Conversely, the more electron-donating substituents give rise to more negative ligand-based reductions (**4** and **5** *vs.* **3**). The presence of a phenyl ring allowing for electron delocalisation explains the relative reduction potentials of **2** *vs.* **3** while also highlighting that Hammett parameters, derived from substitution rates on aryl rings, are useful tools to estimate the electron affinity of a system but are not expected to perfectly correlate to reduction potential variations. The correlation between electron affinity and reduction potential is summarised by the linear trend observed in Figure IV-4

plotting the redox potential of the second electrochemical event as a function of the average sigma parameter of the 3 substituents on the ligands (1 X and 2 Y in scheme 1).

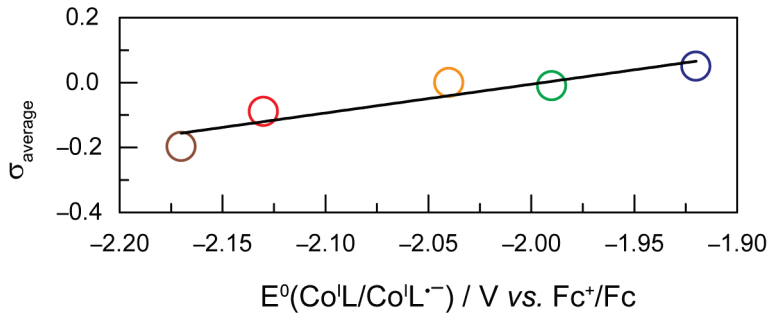

Figure IV-4 Standard potential observed for the $Co^{I}L/Co^{I}L^{\bullet-}$ couple for compounds **1** (blue), **2** (green), **3** (yellow), **4** (red) and **5** (brown) in DMF, $TBAPF_6$ 0.1M as a function of the average Hammett parameters of the substituent present on the *para* position of the three pyridyl ring.[‡]

2.3. Activity towards H^+ reduction

To study the HER independently from CO_2 reduction, in organic media, proton reduction by **1-5** was studied in DMF with acetic acid as the proton source. Acetic acid was chosen as the proton source for its relatively low pKa in organic media (13.5 in DMF), and for its highly negative reduction potential on a bare glassy carbon electrode in organic solvents,[29] allowing for the study of **Co-tpyY$_2$X** on glassy carbon by CV to be virtually unaffected by background H^+ reduction at the electrode. Since it is known that variable amounts of water affect the HER on glassy carbon electrode in organic solvent in the presence of acetic acid, a strictly anhydrous DMF solvent was chosen for this study.[29,30]

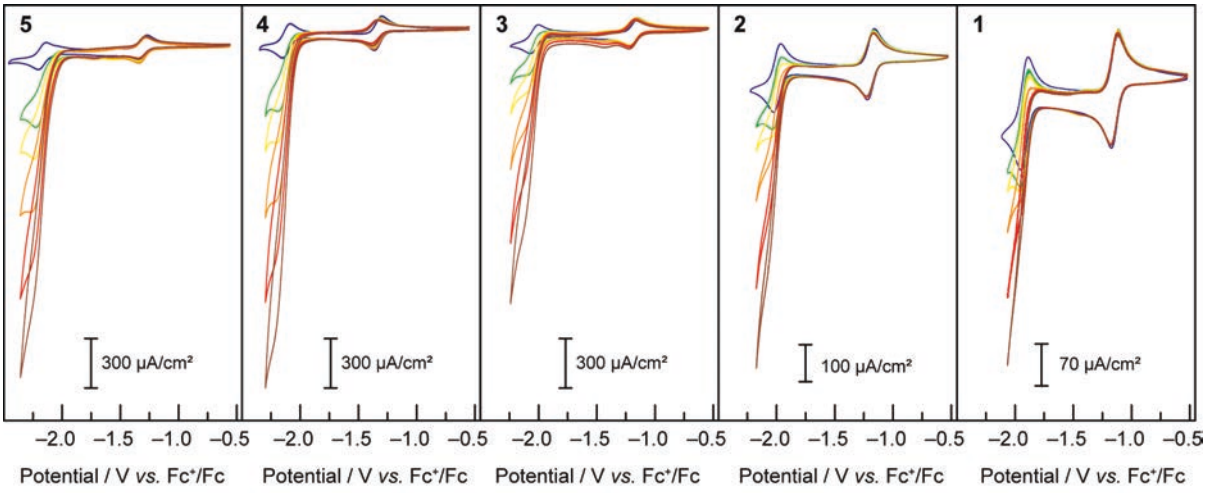

Figure IV-5 Cyclic voltammograms under Ar at 50 mV/s of 1 mM solutions of compounds **1-5** in DMF, $TBAPF_6$ 0.1M, on a glassy carbon electrode with 0 (— blue), 5 (— green), 10 (— yellow), 20 (— orange), 40 (— red) and 60 (— brown) mM of acetic acid.[‡]

When treated with increasing amounts of acetic acid, compounds **1**-**5** exhibit the voltammograms presented in Figure IV-5. Contrary to the metal-based reduction where minimal effect is found, the ligand-based reduction showed an enhancement of the cathodic current accompanied by a loss of reversibility, with the cathodic current increasing with the increase of acetic acid concentration. Electron-deficient compound **1** was observed to have the least current enhancement upon treatment with acetic acid whereas **4** and **5** appeared to be the most active. A clear trend was observed in which more cathodic current enhancement was found with cobalt complexes of more electron-donating terpyridyl ligands. As the scan rate is increased (50, 100, 250, 500, 750 and 1000 mV/s) the behaviour persists, with the catalytic current showing very little dependence on scan rate. Enhancing the nucleophilicity of the Co complex by ligand modification thus results in the expected shift of redox couples to more negative potentials and in a greater overpotential being required for proton reduction. At the same time protonation is favoured, thus enhancing the catalytic activity in the presence of a proton source.

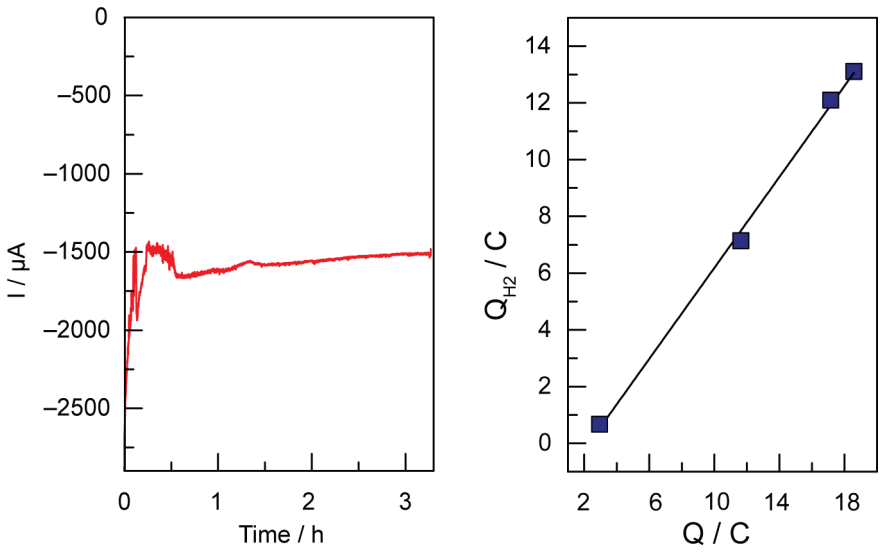

Figure IV-6 Left: Current (red) measured during a controlled-potential electrolysis of a 2 mM DMF solution of **3** at –2.03 V *vs.* Fc^+/Fc with 2 M acetic acid. Right: Charge corresponding to the amount of H_2 (Q_{H2}, blue squares) measured in the headspace during bulk electrolysis *vs.* the total charge passed during the electrolysis. The slope of the linear fit, corresponding to the faradic efficiency, is 80%.[§]

The aforementioned behaviour is attributed to catalytic proton reduction to H_2, as confirmed by the bulk electrolysis of **3** under similar conditions. The 8 mL DMF solution of 2 mM of **3**, with 0.1 M of $TBAPF_6$ as supporting electrolyte and 2 M acetic acid was N_2-saturated prior to electrolysis. The bulk electrolysis cell, described in Chapter II, uses a 1.5 cm diameter pool of mercury as the working electrode. The experiment yielded a constant generation of H_2 as the only product observed in over 80% Faradic yield (Figure IV-6), as quantified by gas chromatography.

2.4. On the nature of the active species: mono- or bis-terpyridine?

The initial complex under consideration is $[Co(tpy)_2](PF_6)_2$ with a full coordination sphere, theoretically unsuitable for substrate binding and activation. Indeed, although there exists one report of a relevant pyridyl-coordinated cobalt complex with a coordination number greater than 6, cobalt complexes of such high coordination numbers remain exceedingly rare.[31] Therefore, to generate an open coordination site through which catalysis can proceed, two options exist: a) de-coordination and rotation of either one or two peripheral pyridyl rings or b) loss of an entire terpyridyl ligand. Whereas both processes have been speculatively included within catalytic cycles, we favour catalysis occurring through an active species comprising of only one terpyridyl ligand due to precedent for a similar structure in an analogous system.[32]

The ability of $[Co(tpy)_2]^{2+}$ to liberate a tpy ligand, in a reaction depicted in equation (IV-1), has been studied previously and has been shown to have a strong dependence on the nature of the solvent.[33,34]

$$[Co(tpy)_2]^{2+} \underset{k_a}{\overset{k_d}{\rightleftarrows}} [Co(tpy)]^{2+} + tpy \qquad \text{(IV-1)}$$

The rate constant for the forward reaction (equation IV-1) has been measured recently in different solvents, and was shown to be $k_d = 3.2\ 10^{-2}\ s^{-1}$ in conditions similar to those utilised for catalysis within this report (DMF as the solvent).[35] Upon reduction of Co^{II} to Co^{I}, the lability should increase and the loss of a tpy ligand should become easier.

Independently synthesised $Co(tpy)Cl_2$,[36] obtained as a green powder and characterised by single crystal XRD, loses its green colour as soon as it is dissolved in a solvent such as DMF and disproportionate following equation (IV-2). Although the bisterpyridyl complex is clearly favoured, this precedent clearly suggests the kinetic viability of a monoterpyridyl complex, especially upon further reduction.

$$[Co(tpy)_2]^{2+} + Co^{2+} \underset{k_{a'}}{\overset{k_{d'}}{\rightleftarrows}} 2\,[Co(tpy)]^{2+} \qquad \text{(IV-2)}$$

In an attempt to glean insights into the redox potential of a possible Co-monotpy species in DMF and identify possible electrochemical features, the evolution of the CV features of various proportions of cobalt dichloride and terpyridine were analysed in order to manipulate the equilibrium presented in equation (IV-2).

CVs of a 2 mM solution of terpyridine in DMF under argon were initially collected. No signal is observed in the potential range scanned (Figure IV-7, black). $CoCl_2$ was then added to this solution to obtain a solution of 2 mM terpyridine with 1 mM of $CoCl_2$ (Figure IV-7, blue). Under these conditions, similar to those of our catalytic assays, the cyclic voltammograms were found to be

identical to those collected with pre-synthesised $[Co(tpy)_2]^{2+}$. Subsequently, additional $CoCl_2$ was added to the electrochemical cell in order to shift the equilibrium depicted in eq. IV-2 towards a possible Co-monotpy complex.

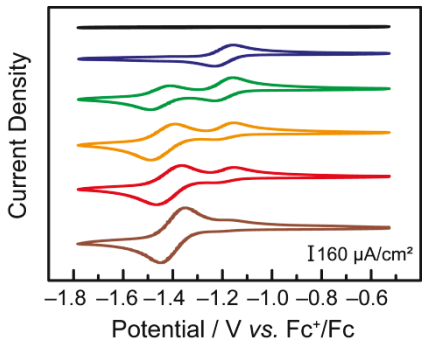

Figure IV-7 Cyclic voltammograms under Ar at 100 mV/s in DMF, $TBAPF_6$ 0.1M, on a glassy carbon electrode of a solution of 2 mM tpy (— black) and 2 mM tpy with added 1 mM (— blue), 2 mM (— green), 3 mM (— orange), 4 mM (— red) and 10 mM (— brown) of $CoCl_2$.[‡]

A new electrochemical feature could be observed at −1.40 V *vs.* Fc^+/Fc when a ratio of $CoCl_2$:tpy of 2:2 was obtained (Figure IV-7, green). We have assigned the new electrochemical feature found at −1.40 V *vs.* Fc^+/Fc as the $Co^{II/I}$ couple associated with a Co-monotpy given that it can neither be attributed to $Co(tpy)_2$, $CoCl_2$ nor tpy itself (Figure IV-8, left). Upon further addition of $CoCl_2$, the new electrochemical feature was observed to increase in intensity while the $[Co(tpy)_2]^{2+}/[Co(tpy)_2]^+$ feature decreased in intensity.

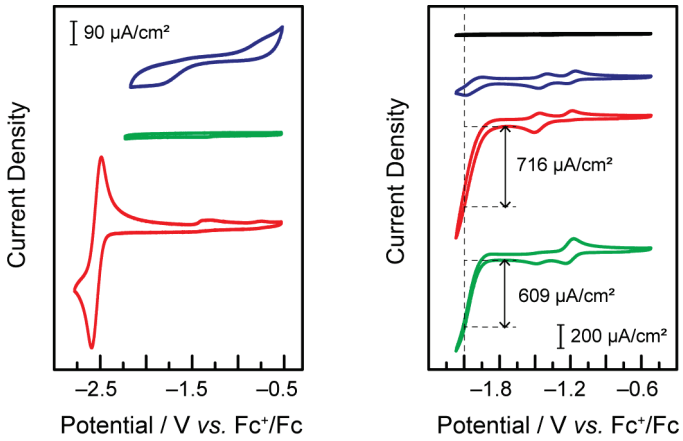

Figure IV-8 Cyclic voltammograms under Ar at 100 mV/s in DMF, $TBAPF_6$ 0.1M, on a glassy carbon electrode. Left: 1 mM $CoCl_2$ (— blue), 2 mM tpy (— green), 2 mM tpy in a wider potential range (— red). No wave is observed in the −1.40 V *vs.* Fc^+/Fc region. Right: 1 mM tpy (— black). To this solution, 1 mM $CoCl_2$ is added (— blue), followed by 40 mM of acetic acid (— red), and finally 1 mM tpy (— green).[§]

Under conditions of the greatest excess of $CoCl_2$ relative to terpyridine tested (10:2), the small feature assigned to Co-bisterpyridine was still present in the mixture, as seen by the presence of the anodic feature of the $[Co(tpy)_2]^{2+}/[Co(tpy)_2]^+$ couple. This further shows that the preferred state is Co-

bistpy, and is consistent with our observation that $Co(tpy)_2$ is the only observable species in the bulk during catalysis under similar conditions.[13]

A similar experiment was conducted under catalytic conditions, where the height of the catalytic peak was monitored as different ratios of tpy and $CoCl_2$ were added (Figure IV-8, right). A catalytic peak was observed even in proportions of Co/tpy of 1:1. This alone does not discriminate between an active species of 2 or 1 tpy per cobalt since as noted above, 1:1 mixtures of Co and tpy will disproportionate to form a part of Co-bisterpyridine. However, when a second equivalent of terpyridine was added, the catalytic current decreased by 15% (Figure IV-8, right). Should Co-bisterpyridine be the active catalyst, the addition of the 2nd equivalent of tpy would be expected to increase the catalytic current observed. Since the reverse is observed, this experiment supports the idea of an active catalyst containing less than 2 tpy per cobalt centre.

From this, and based on our previous study of CO_2 reduction by **Co-tpy**, we conclude that it is likely that the active catalyst for the reduction of protons to hydrogen is comprised of one tpy per cobalt centre.

2.5. Possible mechanisms - Quantification of the catalytic activity for hydrogen evolution by 1-5

2.5.1. Mechanisms

A few potential mechanisms are described below with the initial assumptions that all electron transfers occur at the electrode and a heterolytic mechanism is operative. The two main heterolytic mechanisms are schematically depicted in Figure IV-9, without taking into account the localisation of the electrons in the complex (*ie*: the species formally denoted Co^0 could also be $Co^I L^{\bullet -}$). In the ECEC mechanism on the left, Co^I is reduced to Co^0, which undergoes protonation to form a Co^{II}–H. This hydride is not sufficiently hydridic to be protonated efficiently and is reduced to a formally Co^I–H. Subsequent protonation of the hydride yields H_2 and Co^I. The second mechanism, on the right, is an EECC mechanism, where the Co^{II} species is sequentially reduced twice to generate a Co^0 which can be protonated to form a Co^{II}–H. In that case the latter is nucleophilic enough to react with a second proton thus forming H_2 and Co^{II}.

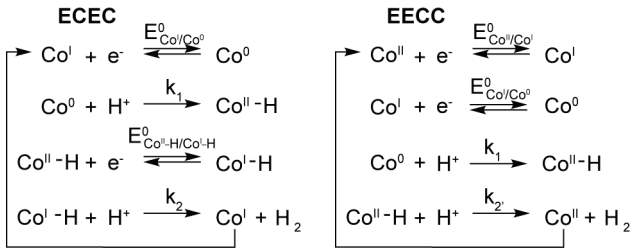

Figure IV-9 ECEC and EECC schematic mechanisms for H_2 evolution by **1-5**.‡

2.5.2. Determination of rate constants/quantification of catalytic activity

To quantify the rates by which the HER occur for compounds **1**-**5** using cyclic voltammetry, the *foot-of-the-wave* analysis (*FOWA*) developed by Savéant et al. was performed.[37] *FOWA* was preferred to the i_c/i_p analysis that has been classically used in the literature[38,39,40] because of the shape of the CVs observed. In the absence of the classical *S*-shaped curve with a fixed plateau current and overlapping forward and backward traces, the CVs near the peak are mostly under the influence of other factors, such as substrate consumption and diffusion. To circumvent this and estimate the rate constant for the HER, the CV is modelled near the foot of the wave, where these factors play a smaller role and the shape of the CV is dominated by the catalytic reaction.

It has to be noted that the rate constants determined by means of the *FOWA* here represent intrinsic rate constants in the hypothetical scenario where the catalysis is not limited by any side phenomena such as substrate consumption. As such, they are most likely overestimations of the observed rate constant in bulk electrolyses, where the side phenomena and mass transport might have a greater influence. Towards direct application of electrocatalytic systems, these practical factors need to be carefully considered and optimized; often through the engineering of cell design and electrode surface area. However, in the context of evaluating intrinsic catalytic activity, the *FOWA* provides insights towards convenient benchmarking of catalytic behaviour that can be later incorporated into optimally engineered systems, if desired.

For a reversible homogeneous diffusion controlled one-electron transfer, such as the features observed in DMF in the absence of acetic acid (Figure IV-2), the current at the peak is given by the Randles-Sevick equation:

$$i_p^0 = 0.4463FSC_P^0\sqrt{\frac{F\nu D}{RT}} \qquad \text{(IV-3)}$$

S: Surface area of the electrode

C_p^0: Concentration of P in the bulk solution

D: Diffusion coefficient

ν: Scan rate

F: Faraday's constant

For a multi-step catalytic reaction following the two mechanisms depicted in Figure IV-9, namely an EECC and a ECEC (where the second reduction event is easier than the first) where all electron transfers occur at the electrode, the expression of the current is given by the following equation[41,42]:

$$i = \frac{2FSC_P^0\sqrt{Dk_{obs}}}{1+e^{\left[\frac{F}{RT}\left(E-E^0_{Co^I/Co^0}\right)\right]}} \qquad \text{(IV-4)}$$

where k_{obs} is the apparent rate constant and $E^0_{Co^I/Co^0}$ is the standard potential of the redox couple triggering catalysis.

Since the surface of the electrode used is constant, and assuming that the diffusion coefficient of the complexes involved in the catalytic cycle are comparable, dividing (IV-4) by the equation of i_p^0 (IV-3) for the ligand-based reduction feature allows for a straightforward determination of k_{obs} without prior need for the determination of the diffusion coefficient or the electrochemically accessible surface of the electrode:

$$\frac{i}{i_p^0} = \frac{2\sqrt{k_{obs}}}{0.4463}\sqrt{\frac{RT}{Fv}} \times \frac{1}{1+e^{\left[\frac{F}{RT}\left(E-E^0_{Co^I/Co^0}\right)\right]}} \qquad \text{(IV-5)}$$

Plotting i/i_p^0, with current values corrected for capacitive currents, as a function of $1/\left(1+exp\left[\frac{F}{RT}\left(E-E^0_{Co^I/Co^0}\right)\right]\right)$ near the foot of the wave gives a linear function at a given scan rate. As a representative example, Figure IV-10 shows the CV data for proton reduction by **3** at 500 mV/s and for a concentration of acetic acid of 60 mM (left) and the corresponding FOWA (right). The replotting of the data, in orange, is fitted linearly near the foot of the wave. The linear fit (red), has a slope of 8.084.

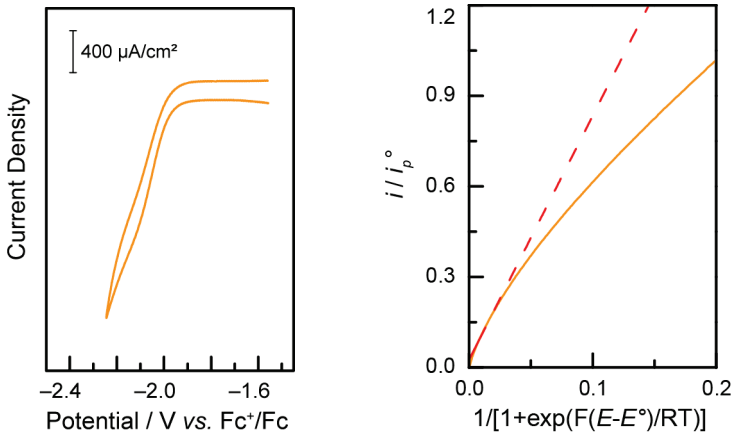

Figure IV-10 Sample *FOWA* of the catalytic activity of **3** for H_2 evolution, using data presented in Figure VI-5 of the Appendix at 500 mV/s and a concentration of acetic acid of 60 mM. The experimental data (orange) is fitted linearly near the foot of the catalytic wave.[§] The slope of the linear fit (red) is: slope = 8.0841 with R^2=0.998.

The observed rate constant k_{obs} can then be extracted from the slope of the linear fit using the equation:

$$slope = \frac{2\sqrt{k_{obs}}}{0.4463}\sqrt{\frac{RT}{Fv}} \qquad \text{(IV-6)}$$

For both mechanisms considered here $k_{obs} = k_1 \times C_A^0$ with k_1 the rate constant for the hydride formation reaction and C_A^0 the concentration of acid in the bulk solution. In the example of Figure IV-10, this gives a second-order rate constant k_1 of:

$$k_1 = \frac{slope^2 (0.4463)^2 Fv}{4RT} \times \frac{1}{C_A^0} = 1056\ M^{-1}.s^{-1} \qquad \text{(IV-7)}$$

In the case of compounds **1-5**, the rate constants were determined using the *FOWA* with a concentration of acetic acid of 60 mM and the analysis was repeated at 6 different scan rates in the 0.05 - 1 V/s range. The results are shown in Figure IV-11 (left).

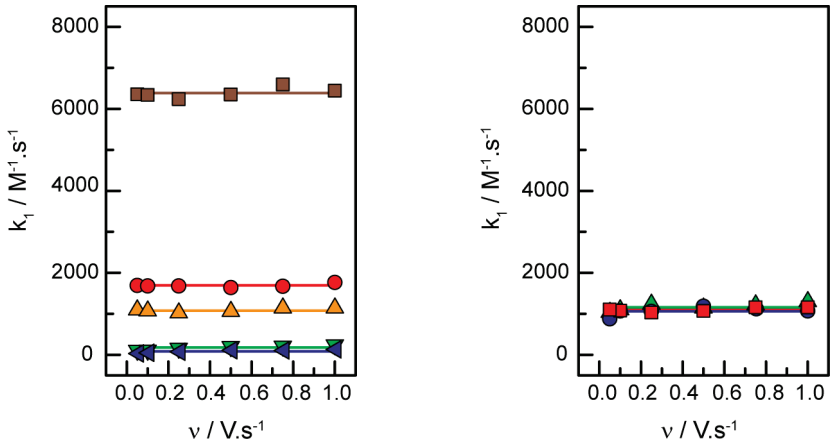

Figure IV-11 Left: k_1 values obtained through the *FOWA* of compounds **1** (— blue), **2** (— green), **3** (— orange), **4** (— red) and **5** (— brown) at different scan rates. Right: Values for k_1 for H^+ reduction obtained through the *FOWA* of compounds **3** using the data obtained with 20 (— green), 40 (— blue) and 60 (— red) mM of acetic acid at different scan rates. The CVs used are presented in Figure VI-5 through Figure VI-9 of the Appendix.‡

As expected, the rate constants are independent of scan rate (Figure IV-11, left). In the case of compound **3**, the same analysis was performed at 40 and 20 mM of acetic acid with scan rates of 0.05 - 1 V/s and the rate constant was shown to be independent of acid concentration as expected (Figure IV-11, right). The average of the values obtained at the 6 different scan rates tested was used as k_1: 6400 $M^{-1}.s^{-1}$ for **5**, 1700 $M^{-1}.s^{-1}$ for **4**, 1100 $M^{-1}.s^{-1}$ for **3**, 200 $M^{-1}.s^{-1}$ for **2** and 100 $M^{-1}.s^{-1}$ for **1** (the cyclic voltammetry data used is presented in Figure VI-5 through Figure VI-9 of the Appendix).

2.5.3. Evaluation of the rate determining step and catalytic Tafel plots

The mechanistic models proposed within Figure IV-9 imply two possible rate determining steps (RDS). The first possible RDS is the protonation of a Co^0 centre to yield a Co^{II}–H and is governed by the rate constant k_1. This is the second-order rate constant that was calculated using the *FOWA*. The second possibility is that the RDS is the protonation of a Co–H to yield H_2, which proceeds at a rate constant defined as k_2 or $k_{2'}$. Rate limiting electron transfer is not considered as electron transfer is assumed to be fast.

As described above, the *FOWA* affords a direct measurement of k_1 but does not provide information in regards to k_2 or the rate constant for the RDS (k_{cat}). Cyclic voltammograms are often used to estimate k_{cat} through comparison between catalytic plateau current (i_c) and the peak current in the absence of substrate (i_p^0). In both mechanisms considered in Figure IV-9, the catalytic plateau

current i_c is given by the following equation,[42,41] where k_{cat} is the rate constant of the rate determining step ($k_{cat} = k_1$ or k_2) :

$$i_c = 2FSC_P^0\sqrt{D}\sqrt{[H^+]}\sqrt{k_{cat}} \quad \text{(IV-8)}$$

Dividing (IV-8) by (IV-3) affords the theoretical value for i_c/i_p^0, given by the following equation:

$$\frac{i_c}{i_{p^0}} = \frac{2}{0.4463}\frac{\sqrt{RT}}{\sqrt{F\nu}} \times \sqrt{[H^+]} \times \sqrt{k_{cat}} \quad \text{(IV-9)}$$

As the experimental CVs for compounds **1-5** do not provide a catalytic plateau current that can be interpreted with a high degree of quantitative accuracy, we sought an alternate method to differentiate between k_1 and k_2 as the rate constant for the RDS. Given that k_1 is experimentally determined, using k_1 as k_{cat} we can estimate a maximum value for i_c/i_p^0 using equation IV-9. Additionally, setting the condition that if k_2 is the RDS, then $k_1 >> k_2$, we can estimate that a maximum value of k_2 is approximately $k_1/10$. Therefore, we can calculate a maximum theoretical value for i_c/i_p^0 in the scenario wherein k_2 is the RDS by substituting $k_1/10$ for k_{cat} into equation IV-9. Using **3** as an example, these estimates were made in Figure IV-12 with various scan rates analysed. The maximum i_c/i_p^0 values for $k_1 = k_{cat}$ is shown in red and the maximum i_c/i_p^0 values for $k_2 = k_{cat}$ is shown in blue. For illustrative purposed, if $k_2 = k_1/20 = k_{cat}$, the resulting i_c/i_p^0 values are shown in green.

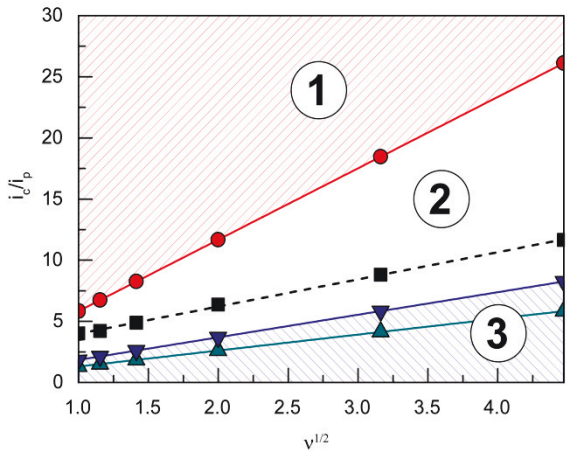

Figure IV-12 Theoretical values for i_c/i_p^0 for **3** in the presence of 60 mM acetic acid and various scan rates plotted using equation IV-9. Red circles represent values were $k_{cat} = k_1 = 1100$ $M^{-1}sec^{-1}$. Blue triangles represent values were $k_{cat} = k_2 = k_1/10 = 110$ $M^{-1}sec^{-1}$. Green triangles represent values were $k_{cat} = k_2 = k_1/20 = 55$ $M^{-1}sec^{-1}$.[‡]

There are three distinct regions in the plot, as labelled in Figure IV-12. Region 1 includes all values of i_c/i_p^0 that are theoretically impossible to obtain as they are greater than the maximum possible values based on $k_1 = k_{cat}$. Region 2 represents values of i_c/i_p^0 that are indicative of k_1 being rate limiting, as they are below the maximum theoretical values for $k_{cat} = k_1$ but above the maximum theoretical values for $k_{cat} = k_2$. Region 3 represents values of i_c/i_p^0 where no statement can be made regarding the

nature of the rate determining step, as values are both below the maximum theoretical values for $k_{cat} = k_1$ and $k_{cat} = k_2$.

With the theoretical boundary conditions calculated, we then estimated the experimental i_c/i_p^0 values for **3** at various scan rates. Of note, since no catalytic plateau is observed, these measurements are likely underestimates. The experimental i_c/i_p^0 data is plotted in Figure IV-12 as a dashed black line and clearly fall within Region 2. Upon comparing the experimental data to the theoretical boundaries established for $k_1 = k_{cat}$ and $k_2 = k_{cat}$, it is clearly observed that the empirical i_c/i_p^0 values are greater than the maximum theoretical values for $k_2 = k_{cat}$. Additionally, the empirical data is less than the theoretical maximum values for $k_1 = k_{cat}$. Given that the data is likely an underestimate, these results strongly suggest that the RDS is governed by k_1 and that the RDS is the protonation of the Co^0 complex.

Now that k_1 has been established as rate limiting, insights regarding turnover frequencies (TOF) values can then be derived from the second order rate constants numbers using the equation: $TOF_{max} = k_1 C_A^0$. Thus maximum intrinsic turnover frequency (TOF_{max}) are given in Figure IV-13 for a concentration of acetic acid of 1 M. Comparison of the five complexes confirms that the more electron-donating the substituent, the better the catalyst is at hydrogen evolution from acetic acid in DMF in terms of maximal turnover frequency. If the protonation of a cobalt centre is invoked in the mechanism for hydrogen evolution, the Lewis basicity of the cobalt centre would be dictated by the electronic density on the metal centre. As more electron-donating substituents are included within the ligands, the electronic density on the metal is expected to increase, yielding a metal centre more reactive towards protonation.

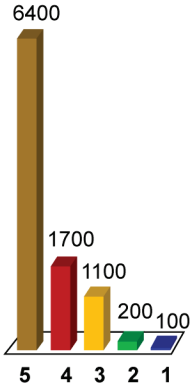

Figure IV-13 TOF_{max} (in s^{-1}) for an acid concentration of 1 M corresponding to the k_1 values obtained through the *FOWA* of compounds **1** (— blue), **2** (— green), **3** (— orange), **4** (— red) and **5** (— brown) at different scan rates.‡

In an effort to benchmark the activity of the complexes towards proton reduction and to afford the ability to more generally compare the activity of **1**-**5** to other systems in the future, a catalytic Tafel plot was generated (Figure IV-14). The catalytic Tafel plot has been recently proposed by Savéant *et al.* as an efficient way to compare catalysts without having to depend so heavily on cell geometries used for bulk electrolyses.[43] It consists of a plot of the log of TOF as a function of overpotential. As

has been demonstrated elsewhere,[42] the turnover frequency depends on the applied potential following equation (IV-10):

$$TOF = \frac{TOF_{max}}{1+exp\left[\frac{F}{RT}\left(E-E_{1/2}\right)\right]} \quad \text{(IV-10)}$$

where $E_{1/2}$ is the redox potential of the event triggering catalysis, here $E_{1/2} = E^0_{Co^I/Co^0}$. In order to take into account the overpotential $\eta = E^{0,ap}_{H^+/H_2} - E$, with $E^{0,ap}_{H^+/H_2}$, the apparent redox potential for the reduction of the acid under consideration in the solvent studied, (IV-10) can be reformulated as :

$$TOF = \frac{TOF_{max}}{1+exp\left[\frac{F}{RT}\left(E^{0,ap}_{H^+/H_2} - \eta - E^0_{Co^I/Co^0}\right)\right]} \quad \text{(IV-11)}$$

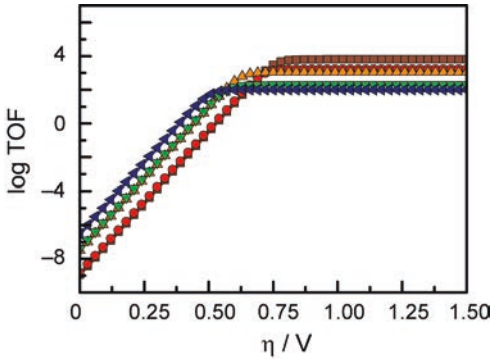

Figure IV-14 Catalytic Tafel plot. Turnover frequency for the evolution of hydrogen from 1 M acetic acid in DMF catalysed by **1** (— blue), **2** (— green), **3** (— orange), **4** (— red) and **5** (— brown) as a function of overpotential.[‡]

The log of equation (IV-11) gives the equation of the catalytic Tafel plot. The catalytic Tafel plot can be generated from three parameters: TOF_{max}, $E^0_{Co^I/Co^0}$ and $E^{0,ap}_{H^+/H_2}$. We have previously determined $TOF_{max} = k_1 C_A^0$ for a specifically chosen concentration of acetic acid, $C_A^0 = 1$ M, (Figure IV-13). $E^0_{Co^I/Co^0}$ is determined from CVs in the absence of substrate (Figure IV-2, ligand-based feature). $E^{0,ap}_{H^+/H_2}$ can be calculated using the following thermodynamic relationship (IV-12):

$$E^{0,ap}_{H^+/H_2} = E^0_{H^+/H_2} - 0.059 \times pK^{solvent}_{acid} \quad \text{(IV-12)}$$

with $E^0_{H^+/H_2}$ the thermodynamic potential for the reduction of protons to hydrogen in the solvent chosen. Following previously reported values, under our conditions $E^0_{H^+/H_2} = -0.62$ V *vs.* Fc^+/Fc, and $pK^{DMF}_{acetic\ acid} = 13.5$.[44] These values are used to calculate $E^{0,ap}_{H^+/H_2} = -1.42$ V *vs.* Fc^+/Fc.

This catalytic Tafel plot representation allows for easy interpretation of the catalytic activity, and exemplifies the trade-off between overpotential and TOF of a catalytic system. While there only are a few examples of hydrogen evolution catalysts that have been studied using the *FOWA* analysis so far,[45,43] we believe that this report of catalytic Tafel behaviour will prove useful for future comparative purposes as more catalytic Tafel plots are reported. As a point of comparison, the best reported

homogeneous hydrogen evolution catalysts to date have TOF_{max} values at 1 M acid concentration reported to be in the 1.3 10^3 to 4 10^5 s^{-1} range.[43]

2.5.4. Conclusions

We have established that **1-5** can catalyse the HER in anhydrous DMF in the presence of acetic acid as a proton source. The corresponding rate constants have been determined, and we have shown that increasing the electron donating substituents on the tpy ligand leads to increased rate constants for H_2 evolution, at the penalty of overpotential, as summarised by the catalytic Tafel plot. The catalyst exhibiting the lowest rate constant for H_2 evolution is **1**, with the more electron withdrawing substituents on the tpy ligand. We will now study CO_2 reduction catalysed by **1-5** in conditions similar to those used in Chapter III. The focus of this study is to observe the effect or lack thereof of the different substituents on the selectivity of CO_2 reduction to CO over H^+ reduction to H_2.

3. Study of complexes 1-5 as catalysts for CO_2 reduction to CO

3.1. Assessment of the potential activity through cyclic voltammetry

3.1.1. Observations in cyclic voltammetry

Compounds **1-5** were then assayed for CO_2 reduction, in CO_2-saturated DMF, with 5% of added water as a proton source to mimic the conditions of Chapter III in which mixtures of CO and H_2 were generated using compound **3** as a catalyst. The cyclic voltammograms, in Figure IV-15, show that compounds **1**, **2**, **4** and **5** behaved as compound **3**[13]: two reversible one-electron diffusion-controlled waves under an inert atmosphere, as observed previously in dry DMF, and a strong cathodic current enhancement of the ligand-based reduction feature accompanied by loss of reversibility in CO_2-saturated solutions. As shown in Chapter III, this corresponds to a catalytic process producing a mixture of CO and H_2, which is potentially overlapped, at least in controlled-potential electrolyses conditions, with competitive reaction on the ligand. It is noteworthy that the differences between catalysts **1-5** in terms of cathodic currents enhancements under CO_2 are much less pronounced than that which was observed in the case of proton reduction.

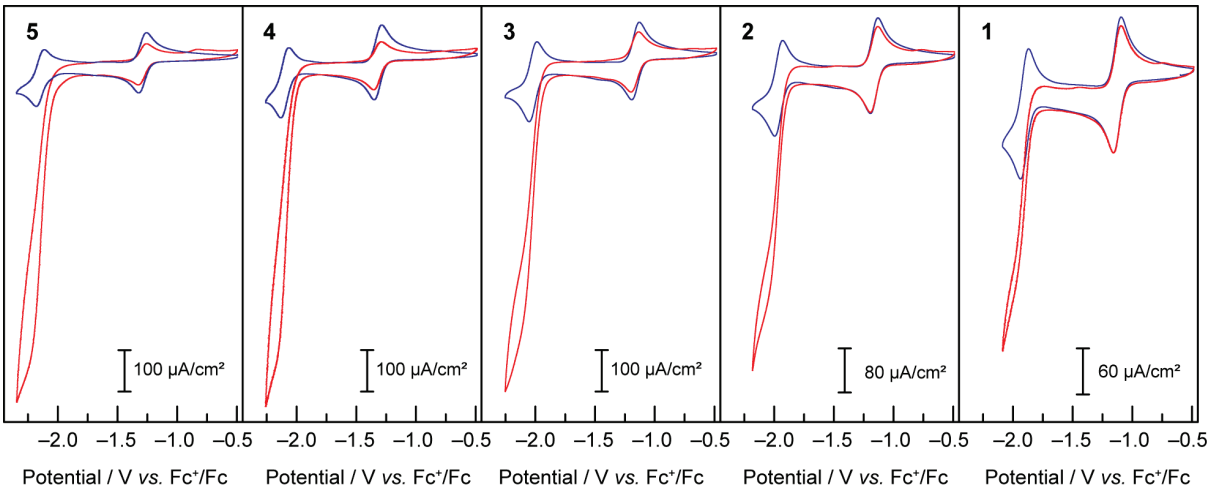

Figure IV-15 Cyclic voltammograms under Ar (— blue) and CO_2 (— red) at 50 mV/s of 1 mM solutions of compounds **1-5** in DMF/H_2O (95:5), $TBAPF_6$ 0.1M.‡

As observed during the study of the HER, complexes bearing more electron-donating groups on the ligands exhibit higher current enhancements, as well as a shift of the catalytic activity to more reducing potentials.

3.1.2. FOWA-type analysis

To evaluate the range of the relative rate constants for CO_2 reduction for **1-5**, the *FOWA* was performed on CVs at different scan rates for each catalyst under catalytic conditions. The goal was to obtain an estimate of the maximal possible rate for the CO_2 reduction catalytic process. The *FOWA* was performed in an analogous manner to that presented in the study of the HER and yields a second order rate constant for the reaction of a Co^0 centre with CO_2. The results of the *FOWA* (Figure IV-16,

based on the CV data presented in Figure VI-10 and Figure VI-11 of the Appendix) indicate a range of second-order rate constants across the series from below 50 $M^{-1}.s^{-1}$ for **1** to over 350 $M^{-1}.s^{-1}$ for **5**. As expected when the assumptions of the *FOWA* are met, these rate constants are virtually invariant with respect to scan rate (Figure IV-16).

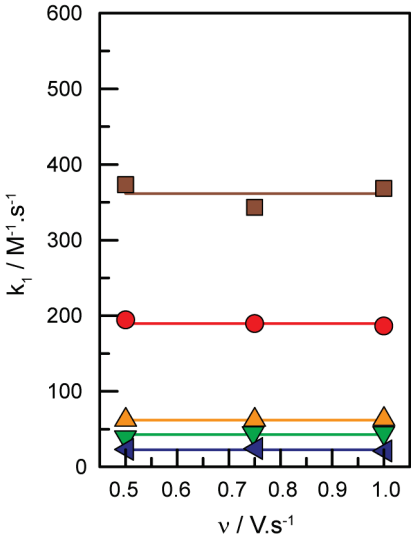

Figure IV-16 Estimated k_1 values obtained through the FOWA of compounds **1** (— blue), **2** (— green), **3** (— orange), **4** (— red) and **5** (— brown) at different scan rates under CO_2-saturating conditions using the CVs presented in Figure VI-10 and Figure VI-11 of the Appendix.‡

The pseudo-first order rate constant for CO_2 reduction to CO can be obtained by multiplying the second order rate constants (62 $M^{-1}.s^{-1}$ for **3**) by the concentration of CO_2 in DMF, 0.23 M.[46] A pseudo-first order rate constant of 14.3 s^{-1} is obtained for **3**. In an effort to compare the activity to other values reported in the literature, of particular interest is the activity of the catalyst at zero overpotential. Under the experimental conditions used, one can estimate a maximum turnover frequency of about $4.0 \cdot 10^{-10}$ s^{-1} at zero overpotential for the production of CO by **3**. This value is within an order of magnitude to that which has been reported for other polypyridyl-based CO_2 reduction catalysts of various transition metals. For example, the related Ru(tpy)(bpy)(S_{olv}) complex has a reported maximum turnover frequency at zero overpotential of $1.6 \cdot 10^{-10}$ s^{-1} and the value of $2.0 \cdot 10^{-9}$ s^{-1} is reported for Mn(dmbpy)$(CO)_3$Br.[46] In this calculation, the CO/CO_2 reduction potential in a DMF/water solvent mixture is estimated to be –1.41 V *vs.* Fc^+/Fc, as the CO/CO_2 potential is reported to be –0.690 V *vs.* NHE[46] and the Fc^+/Fc potential is reported to be 0.720 V *vs.* NHE in DMF.[47] The catalytic cyclic voltammograms of **3** display substantial current enhancement with an applied potential of –2.08 V *vs.* Fc^+/Fc, which represents an applied overpotential of 0.67 V. This overpotential can be factored into the TOF calculation and a TOF within the catalytic wave was determined to be 101 s^{-1}.

Of importance, these values are upper estimates of the rate constants for CO_2 reduction due to the presence of multiple electrochemical processes occurring within the catalytic feature of the CVs.

These results give a quantitative description of the greater effect that electronic tuning of the ligand sphere has on proton reduction rates relative to CO_2 reduction rates, as the rate constants for H_2 evolution from acetic acid for the same catalysts series vary from 100 to over 6000 $M^{-1}.s^{-1}$. In both cases, electron withdrawing groups also decrease the overpotential for the onset of catalysis, albeit at the expense of observed current densities.

3.2. Bulk electrolysis

3.2.1. Current and stability

To compare the activity of these compounds for the reduction of CO_2, bulk electrolyses were performed with a fixed applied current. The traditional constant potential bulk electrolyses would have forced to change the kinetics of the systems, since applying a given fixed potential to the different catalysts would result in different currents being passed. In order to control the kinetics of the system, a constant current of −300 µA was applied for 4 hours to 8 mL of 1 mM CO_2-saturated solutions of compounds **1-5** in DMF/H_2O (95:5) with 0.1 M of $TBAPF_6$ as supporting electrolyte (the electrochemical cell used is described in Chapter II).

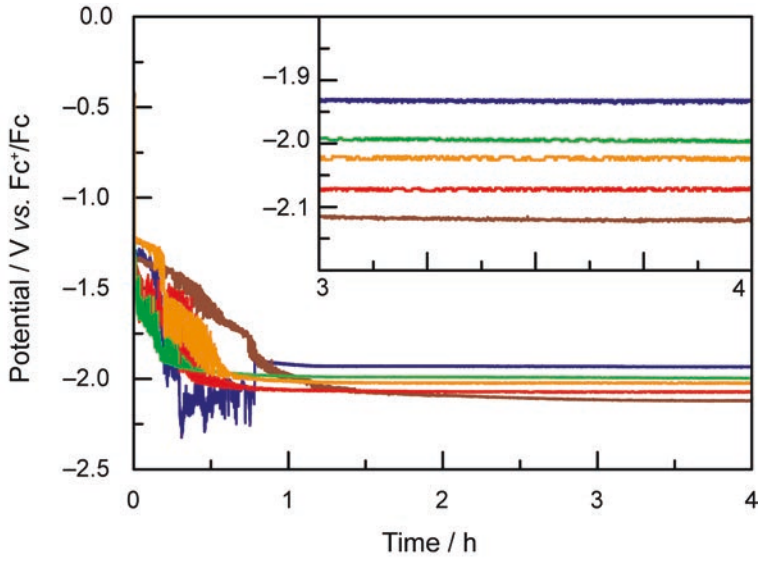

Figure IV-17 Potential observed during the bulk electrolysis of compounds **1** (— blue), **2** (— green), **3** (— orange), **4** (— red) and **5** (— brown) at a constant applied current of i = –300 µA.[‡]

Over the course of the experiment, the potential at the working electrode slowly decreased as all the Co^{II} was reduced to Co^{I} (0.77 C, 43 min), at which point a steady potential was observed, which remained constant throughout the rest of the experiment (Figure IV-17). As expected, the more negative the potential of the ligand-based reduction, the more negative the potential at which the system equilibrated.

3.2.2. Product detection and selectivity

As was the case for a previous report involving compound **3**, the only gaseous products observed were CO and H_2.[13] Since a constant current was applied during the experiments, the number of coulombs

passed over time was fixed and the absolute moles of product observed correlates directly to the faradic yields. The systems can thus be compared in terms of faradic yields or moles of product formed alike (Figure IV-18). The faradic efficiencies for these products are given in Figure IV-19.

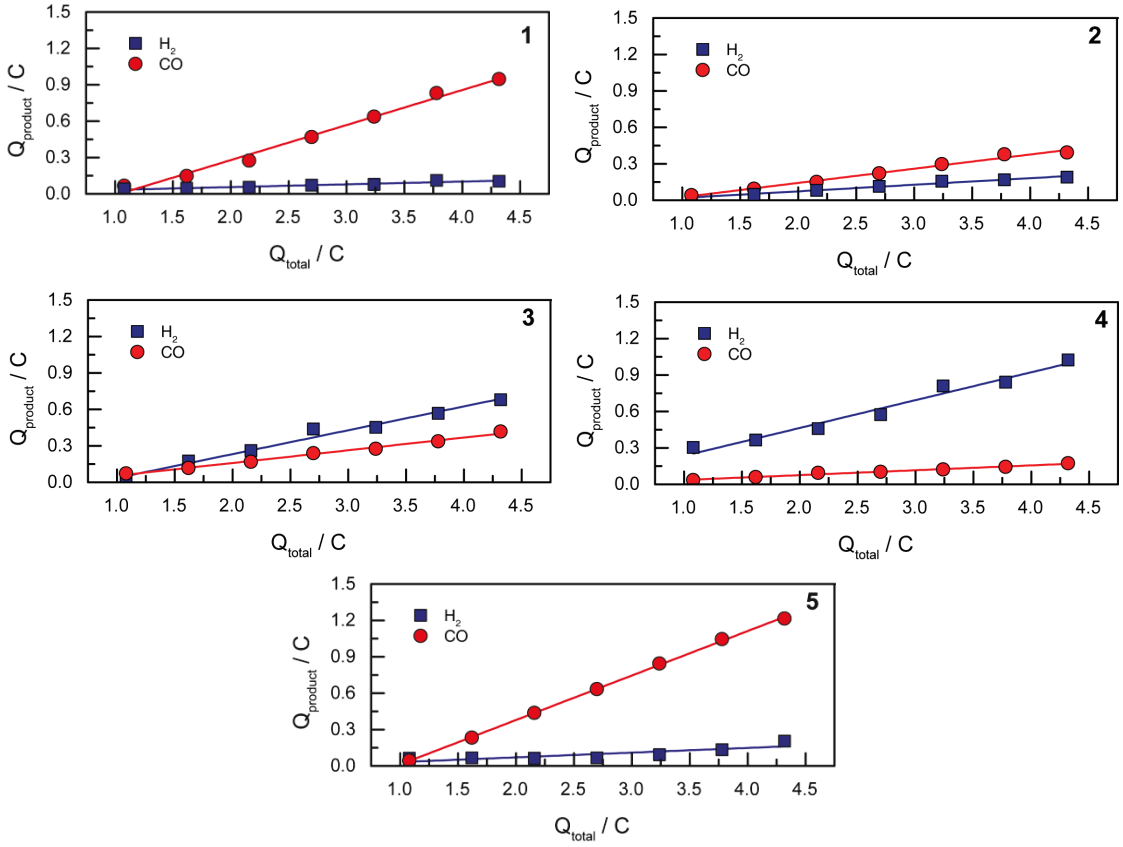

Figure IV-18 Charge corresponding to the products measured (H_2: blue squares, CO: red circle) *vs.* the total charge passed during the electrolyses of **1**-**5** as described in Figure IV-17. The slopes of the linear fits, corresponding to the faradic efficiencies, are given in Figure IV-19.‡

When considering only complexes **1**-**4**, the catalysts that exhibited the lowest activity towards H_2 evolution from acetic acid in DMF were found to be the most selective compounds for CO production over H_2 evolution under CO_2 reduction conditions. From compound **4** to compound **1**, the faradic efficiency for CO production rose from 4 % to 31 %, while the efficiencies for H_2 evolution dropped from 23 % for **4** to 2 % for **1**. The strategy of tuning the electronics of the system to turn off hydrogen production thus yielded the desired results, with compound **1** being the most selective CO_2 reduction catalyst. Interestingly, **5** exhibits a different behaviour, with 37% faradic efficiency for CO_2 reduction to CO, and only 4% of the charge going towards H_2 evolution. Catalyst **5** does not appear to follow the same trends as **1**-**4**, and the combined faradic efficiency for CO+H_2 in these conditions is over 40%. This behaviour was studied further and will be discussed below (*vide infra*).

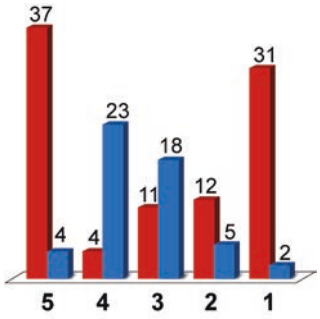

Figure IV-19 Faradic yields (in %) for CO (red) and H_2 (blue) during the bulk electrolysis of 1 mM solutions of compounds **1-5** under CO_2 in DMF/H_2O (95:5), $TBAPF_6$ 0.1M with an applied current of 300 µA during 4 h.‡

We have previously shown using catalyst **3** that the ratios of H_2 to CO obtained in CO_2 reduction catalytic conditions can be tuned by varying the applied potential.[13] More specifically, increasing the overpotential favours H_2 production with respect to CO_2 reduction by increasing the total amount of H_2 generated but virtually unaltering the amount of CO generated. Interestingly, considering only complexes **1-4**, we show here a similar qualitative behaviour wherein increasing the electron density on the metal centre, now using tpy-derived ligands with increasing electron-donating properties, results in enhanced H_2 production thereby decreasing the ratio of CO:H_2 generated. Thus, in this particular case, increasing the reducing power of the system, while accelerating both reactions, has a greater effect on H^+ reduction than on CO_2 reduction in a similar manner as increasing the applied potential of a single system enhanced the amount of H_2 generated while having little effect on the total amount of CO generated.

3.2.3. Thoughts on mechanism

Our present data suggests a monoterpyridyl cobalt complex $Co^I(tpy^{\bullet-})$ as the active catalytic intermediate, with product selectivity depending on the competition between reaction with H^+ or CO_2 (Figure IV-20). This is consistent with the data from Chapter III where a 1:1 ration of $CoCl_2$:tpy yielding the highest faradic yields for CO production.

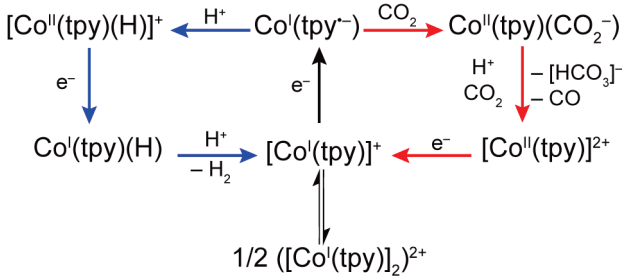

Figure IV-20 proposed mechanisms for CO_2 and H^+ reduction by **Co-tpy**.‡

Understanding the reason for electron-enriched tpy ligands affecting the two reactions so differently requires deep theoretical characterisation of the electronic structure of the intermediate species as well as the activation energies of the reactions in both cases which are currently under investigation. However, we suggest that, to a first approximation, differences in coulombic repulsion of transition states can be invoked to explain the larger variations found in $Co^I(tpy^{\bullet-})$ interactions with H^+ relative to interactions with CO_2 upon changes in electronic structure of the ligand field. In

considering proton reduction, the critical interaction is between a positively charged H^+ atom and an electron-rich cobalt centre. As the cobalt centre is made less electron-rich through the incorporation of more electron-withdrawing tpy ligands, the coulombic repulsion between the cobalt centre and the H^+ should be increased resulting in a higher activation barrier. In contrast, as CO_2 is a neutral substrate, there should be minimal effect on the activation barrier between the cobalt centre and CO_2 attributable to the cobalt centre becoming less electron-rich. While simply a first approximation, electronic repulsion forces have proven to significantly contribute to activation barriers for other reactions fully characterised by high level density functional theory.[48]

Whereas **1**-**4** clearly correlated to the aforementioned trend between proton reduction rate constants and selectivity for CO_2 reduction, **5** surprisingly varied from the trend. The tpy ligand within **5**, which includes three ^{t}Bu groups, is the most electron-rich ligand of the series under study and as a consequence afforded the highest rates of H^+ reduction (Figure IV-11). Yet **5** only exhibited a faradic yield of 4% for H_2 evolution under CO_2 reduction conditions, despite its tremendous activity for hydrogen evolution from acetic acid in DMF. Along with this very small faradic efficiency for H_2 production, **5** also exhibits the highest activity towards CO_2 reduction to CO. It is tempting to consider that this is related to a steric effect as the functionalisation of **5** is unique relative to the other complexes under study, with all three pyridyl rings of the tpy ligand modified with larger ^{t}Bu substituents. We have previously proposed a mechanism for CO_2 reduction by **3** implying the formation of inactive dimeric species in the electrocatalytic reaction layer, in agreement with an apparent order in catalyst **3** of 0.5 in bulk electrolysis under electrocatalytic conditions.[13] It is thus proposed that increased steric hindrance provided by ^{t}Bu substituents on the tpy ligand disfavours the formation of the inactive dimer and thus greatly increases the concentration of the catalytically active mononuclear $Co^I(tpy^{\bullet-})$ intermediate. Accordingly, under CO_2 reduction conditions, the reaction order in **5** was observed to be much closer to a traditional first order (Figure IV-21).

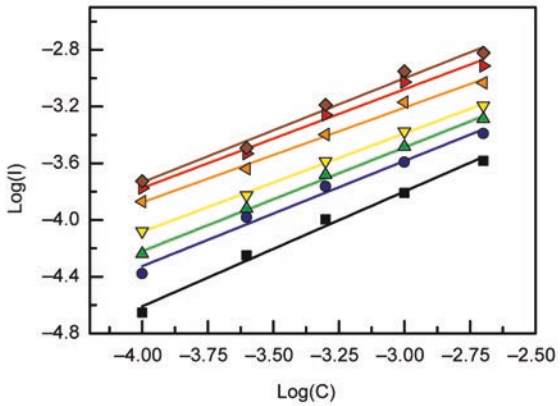

Figure IV-21 Plot of the log(current(A)) *vs.* the log(concentration(mol/L)) obtained in 5 controlled-potential electrolyses of **5** CO_2-saturated solutions at different concentrations of **5** where the potential was first held at –2.14 V *vs.* Fc^+/Fc until the current reached the plateau region and then varied in a step manner and the plateau current at each potential was recorded (brown diamonds: –2.29 V, red right triangles: –2.24 V, orange left triangles: –2.19 V, yellow down triangles: –2.14 V, green top triangles: –2.11 V, blue circles: –2.09 V, black squares: –2.06 V).[‡]

To obtain a reasonable estimate to the reaction order of **5**, while making an effort to reach conditions close to activation controlled, the solution above the pool of mercury was stirred as vigorously as possible without disrupting the surface of the mercury electrode. Current values were corrected for the values observed in a solution without **5**, at each given potential. The slope of the linear fits, corresponding to the apparent order in **5** under bulk electrolyses conditions, is given in Table IV-1 below. Despite the efforts to be in conditions as close to activation control as possible in the setup, we cannot rule out a small contribution of diffusion limited conditions, which would contribute to an apparent order smaller than in reality. Keeping this in mind, the data is more representative of a behaviour that is 1st order in catalyst.

Table IV-1 Apparent order in **5** under bulk electrolyses conditions at different applied potentials.[§]

Applied potential	Apparent order in Cobalt	correlation coefficient
–2.29 V	0.73	0.980
–2.24 V	0.70	0.982
–2.19 V	0.67	0.990
–2.14 V	0.69	0.997
–2.11 V	0.73	0.996
–2.09 V	0.74	0.981
–2.06 V	0.81	0.987

However, simply increasing the concentration of a Co-monoterpyridine intermediate can only affect product selectivity if the dimeric species can also participate in a selectivity determining step. As mentioned before, the primary selectivity determining step is the relative interaction between $Co^{I}(tpy^{\bullet-})$ and either an equivalent of CO_2 or an equivalent of H^+. The observation of steric hindrance affecting selectivity by disfavouring H^+ reduction suggests that the dimeric species can directly enter a proton reduction cycle via protonolysis. While speculative, this observation of a steric effect on product selectivity is unprecedented for CO_2 reduction. Typically, the inclusion of functional groups within a ligand sphere to increase steric hindrance has been shown to increase overall rates of catalysis by either disfavouring the formation of inactive species or increasing the overpotential, but has not been shown to affect product selectivity. Despite falling outside the scope of the current investigation, this report of the unexpected role of steric strain on product selectivity within the **Co-tpy** system clearly indicates a more complex reaction scheme relevant to selectivity and is motivation to continue to interrogate the role of steric hindrance on selectivity in the future.

4. Conclusions

In summary, we have reported the catalytic competency of catalysts **1**-**5** towards two reactions: the reduction of protons to H_2, and the parallel reduction of CO_2 and water to a mixture of CO and H_2. Utilising preparative scale electrolysis and the *foot-of-the-wave* analysis on cyclic voltammograms, the faradic yields for proton reduction and corresponding rate constants have been reported. A general trend is observed wherein faster rate constants are obtained with more electron rich ancillary ligands field, however at the expense of larger overpotentials.

We have similarly evaluated the faradic yields and rate constants for CO_2 reduction for the same series of catalysts and have observed a correlation between higher faradic yields for CO production with lower proton reduction rate constants. This represents the first report of a molecular system for which the selectivity towards CO_2 reduction can be rationally optimized through disfavouring the HER. In agreement with this observation, utilizing the *foot-of-the-wave* analysis, we have demonstrated that electronic modifications to the ancillary ligand field have a much smaller effect on rate constants for CO_2 reduction relative to rate constants for proton reduction. The less dramatic effect found for CO_2 reduction rate constants upon ligand modifications validates the proposed strategy of "turning off" proton reduction in order to gain enhanced selectivity for carbon containing products for molecular CO_2 reduction systems. Whereas transition state electronic repulsion arguments can be made to justify these results, a more thorough theoretical evaluation is currently under pursuit. Finally, we have also observed a novel steric effect on product selectivity through the inclusion of multiple ^{t}Bu functional groups within the polypyridyl ligands. Future work will be focused on better understanding this unique relationship between steric hindrance and product selectivity. We believe that these results and strategy validation are valuable to the rapidly growing area of molecular CO_2 reduction catalysts development.

5. References

‡ N. Elgrishi, M. B. Chambers and M. Fontecave, *Chem. Sci.*, 2015, DOI: 10.1039/C4SC03766A. Reproduced by permission of the Royal Society of Chemistry.

§ Adapted with minor alterations from ‡.

1 M. Rakowski DuBois and D. L. DuBois, *Acc. Chem. Res.*, 2009, **42**, 1974.

2 E. E. Benson, C. P. Kubiak, A. J. Sathrum and J. M. Smieja, *Chem. Soc. Rev.*, 2009, **38**, 89.

3 A. J. Morris, G. J. Meyer and E. Fujita, *Acc. Chem. Res.*, 2009, **42**, 1983.

4 S. N. Riduan, Y. Zhang and J. Y. Ying, *Angew. Chem. Intl. Ed.*, 2009, **48**, 3322.

5 C. Federsel, A. Boddien, R. Jackstell, R. Jennerjahn, P. J. Dyson, R. Scopelliti, G. Laurenczy and M. Beller, *Angew. Chem. Intl. Ed.*, 2010, **49**, 9777.

6 C. Costentin, S. Drouet, M. Robert and J.-M. Saveant, *Science*, 2012, **338**, 90.

7 M. Bourrez, F. Molton, S. Chardon-Noblat and A. Deronzier, *Angew. Chem. Intl. Ed.*, 2011, **50**, 9903.

8 J. D. Froehlich and C. P. Kubiak, *Inorg. Chem.*, 2012, **51**, 3932-3934.

9 J. Agarwal, T. W. Shaw, C. J. Stanton, G. F. Majetich, A. B. Bocarsly and H. F. Schaefer, *Angew. Chem. Intl. Ed.*, 2014, **53**, 5152.

10 M. L. Clark, K. A. Grice, C. E. Moore, A. L. Rheingold and C. P. Kubiak, *Chem. Sci.*, 2014, **5**, 1894.

11 J. A. Keith, K. A. Grice, C. P. Kubiak and E. A. Carter, *J. Am. Chem. Soc.*, 2013, **135**, 15823.

12 J. M. Smieja, E. E. Benson, B. Kumar, K. A. Grice, C. S. Seu, A. J. M. Miller, J. M. Mayer and C. P. Kubiak, *Proc. Natl. Acad. Sci. U. S. A*, 2012, **109**, 15646.

13 N. Elgrishi, M. B. Chambers, V. Artero and M. Fontecave, *Phys. Chem. Chem. Phys.*, 2014, **16**, 13635.

14 C. W. Li, J. Ciston and M. W. Kanan, *Nature*, 2014, **508**, 504–507.

15 C. H. Lee and M. W. Kanan, *ACS Catal.*, 2015, **5**, 465.

16 A. Call, Z. Codola, F. Acuna-Pares and J. Lloret-Fillol, *Chem. Eur. J.*, 2014, **20**, 6171.

17 M. Nippe, R. S. Khnayzer, J. A. Panetier, D. Z. Zee, B. S. Olaiya, M. Head-Gordon, C. J. Chang, F. N. Castellano, J. R. Long, *Chem. Sci.*, 2013, **4**, 3934.

18 S. Varma, C. E. Castillo, T. Stoll, J. Fortage, A. G. Blackman, F. Molton, A. Deronzier, M.-N. Collomb, *Phys. Chem. Chem. Phys.*, 2013, **15**, 17544.

19 T. Abe and M. Kaneko, *J. Mol. Cat. A*, 2001, **169**, 177.

20 X. Chen , H. Ren , W. Peng , H. Zhang , J. Lu and L. Zhuang, *J. Phys. Chem. C*, 2014, **118**, 20791.

21 A. O. Adeloye and P. A. Ajibade, *Molecules*, 2014, **19**, 12421.

22 G. Koyyada, V. Botla, S. Thogiti, G. Wu, J. Li, X. Fang, F. Kong, S. Dai, N. Surukonti, B. Kotamarthi and C. Malapaka, *Dalton Trans.*, 2014, **43**, 14992.

23 D. M. Chang, D. Y. Kwon and Y. S. Kim, *Mol. Cryst. Liq. Cryst.*, 2013, **585**, 91.

24 K. C. D. Robson, B. D. Koivisto, A. Yella, B. Sporinova, M. K. Nazeeruddin, T. Baumgartner, M. Grätzel and C. P. Berlinguette, *Inorg.Chem.*, 2011, **50**, 5494.

25 J. Husson and M. Knorr, *J. Heterocyclic Chem.*, 2012, **49**, 453.

26 R. S. Gaddie, C. B. Moss and C. M. Elliott, *Langmuir*, 2013, **29**, 825.

27 P. Salvatori, G. Marotta, A. Cinti, E. Mosconi, M. Panigrahi, L. Giribabu, M. K. Nazeeruddin and F. De Angelis, *Inorg. Chim. Acta*, 2013, **406**, 106.

28 J. Chambers, B. Eaves, D. Parker, R. Claxton, P. S. Ray and S. J. Slattery, *Inorg. Chim. Acta*, 2006, **359**, 2400.

29 B. D. McCarthy, D. J. Martin, E. S. Rountree, A. C. Ullman and J. L. Dempsey, *Inorg. Chem.*, 2014, **53**, 8350.

30 A.E. King, Y. Surendranath, N. A. Piro, J. P. Bigi, J. R. Long and C. J. Chang, *Chem. Sci.*, 2013, **4**, 1578.

31 K. A. Gheysen, K. T. Potts, H. C. Hurrell and H. D. Abruna, *Inorg. Chem.*, 1990, **29**, 1589.

32 D. Inoki, T. Matsumoto, H. Nakai and S. Ogo, *Organometallics*, 2012, **31**, 2996.

33 H. P. Bennetto and E. F. Caldin, *J. Chem. Soc. A*, 1971, 2191.

34 J. Prasad and N. C. Peterson, *Inorg. Chem.*, 1969, **8**, 1622.

35 I. M. Henderson and R. C. Hayward, *J. Mater. Chem.*, 2012, **22**, 21366.

36 F. Habib, O. R. Luca, V. Vieru, M. Shiddiq, I. Korobkov, S. I. Gorelsky, M. K. Takase, L. F. Chibotaru, S. Hill, R. H. Crabtree and M. Murugesu, *Angew. Chem. Intl. Ed.*, 2013, **52**, 11290.

37 C. Costentin, S. Drouet, M. Robert and J.-M. Savéant, *J. Am. Chem. Soc.*, 2012, **134**, 11235.

38 S. Kal, A. S. Filatov and P. H. Dinoflo, *Inorg. Chem.*, 2014, **53**, 7137.

39 G. P. Connor, K. J. Mayer, C. S. Tribble and W. R. McNamara, *Inorg. Chem.*, 2014, **53**, 5408.

40 J. P. Bigi, T. E. Hanna, W. H. Harman, A. Chang and C. J. Chang, *Chem. Commun.*, 2010, **46**, 958.

41 E. S. Rountree, B. D. McCarthy, T. T. Eisenhart and J. L. Dempsey, *Inorg. Chem.*, 2014, **53**, 9983.

42 C. Costentin and J.-M. Savéant, *ChemElectroChem*, 2014, **1**, 1226.

43 V. Artero and J.-M. Savéant, *Energy Environ. Sci.*, 2014, **7**, 3808.

44 V. Fourmound, P.-A. Jacques, M. Fontecave and V. Artero, *Inorg. Chem.*, 2010, **49**, 10338.

45 D. J. Graham and D. G. Nocera, *Organometallics*, 2014, ***33***, 4994.

46 C. Costentin, M. Robert and J.-M. Saveant, *Chem. Soc. Rev.*, 2013, **42**, 2423.

47 S. Creager, in *Handbook of Electrochemistry*, ed. C. G. Zoski, Elsevier, Amsterdam, 1st edn, 2007, ch. 3, pp. 101.

48 L.-P. Wang, Q. Wu and T. Van Voorhis, *Inorg. Chem.*, 2010, **49**, 4543.

Chapter V
–
Electrode functionalisation with a terpyridyl ligand: preparation, metallation and catalysis

Based on the work reported in: N. Elgrishi, S. Griveau, M. B. Chambers, F. Bedioui and M. Fontecave, *Chemical Communications*, 2015, **51**, 2995–2998.

1. Introduction

Heterogeneous catalysis is often favoured industrially due to more facile product isolation and catalyst regeneration and recovery.[1,2,3] However, mechanistic studies of catalytic processes are more common for homogeneous systems as molecular compounds afford the opportunity to more easily design and tune the coordination environment of the catalyst and due to the availability of common solution phase *in situ* spectroscopic techniques.[4,5,6,7,8,9] To reconcile these two approaches, homogeneous catalysts are often immobilised on heterogeneous supports.[10,11,12,13,14,15,16,17]

In a case wherein the solid support is a conductive surface, this strategy provides access to modified electrodes with the activity of the particular grafted molecule. Such procedures have been implemented for a wide variety of catalysts using a range of specific techniques, from electro-polymerisation of phenanthroline[18] or vinyl[19,20] or pyrrole[21,22] functional groups, to phosphonates[23,24] or thiols groups[25], pi-stacking interactions between a pyrene motif and a carbon electrode[26,27] or diazotisation,[28,29,30,31,32,33] to name a few. A few relevant examples of polypyridyl complexes immobilised on carbon electrodes are represented in Figure V-1. While successful, one common limitation of these techniques is that the entire catalytic entity must be synthesised prior to immobilisation. Therefore, beyond this primary synthetic effort, the scope of activity for each modified electrode is restricted to only the specific reactivity of each molecular motif. Immobilisation of catalysts **A**[27] and **E**[18] had the explicit purpose of studying H^+ reduction, catalysts **B**[19], **D**[28], **F**[20] and **G**[27] for CO_2 reduction, and **C**[26] for the study of the functionalisation of single-walled carbon nanotubes.

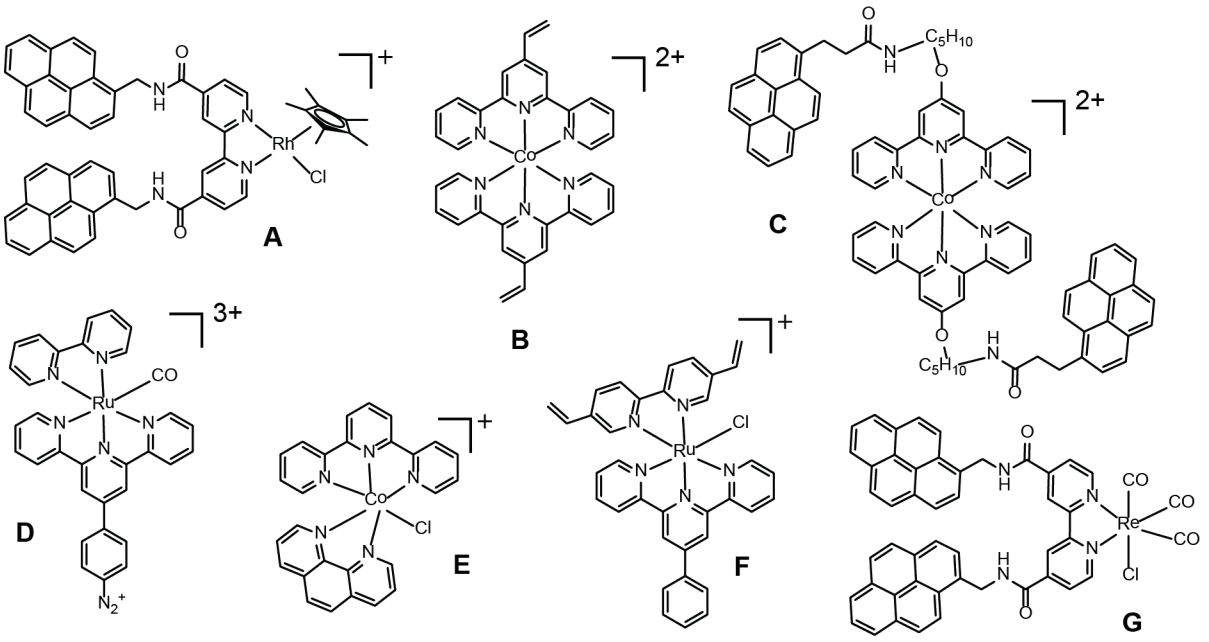

Figure V-1 Relevant examples of immobilised polypyridyl catalysts. The immobilisation techniques used are π-stacking (**A**, **C**, **G**), electropolymerisation (**B**, **E** and **F**) and electrografting of a diazonium group (**D**).

Here a new perspective of this strategy was investigated: grafting a versatile ligand first, followed by reversible metal incorporation required for catalysis. This presents the advantage of potentially being able to functionalise the electrode with a wide range of different metals for different purposes.

The terpyridine (tpy) motif is present in numerous catalysts for the reduction of H^+, CO_2, O_2, NAD^+ just to name a few of interest to the energy landscape, not to mention water oxidation.[34,35,36,37,38,39,40,41,42] We have previously studied tpy motifs on first row transition metals for their ability to reduce CO_2 to CO in DMF solutions as well as H^+ to H_2 and numerous observations pointed to the active catalyst comprising of only one tpy ligand per cobalt atom.[43,44] We thus sought to functionalise a glassy carbon electrode by electrografting of a diazotised version of the tpy ligand, and pursue subsequent metallation to study its catalytic activity towards proton and CO_2 reduction. This theoretically would also offer the added benefit of having an easily accessible Co-monoterpyridine entity, with little possibility for the ligands to rearrange themselves to recreate Co-bisterpyridine entities.

Recent work by F. Bedioui and collaborators interrogated different electrode modification methods, with a focus on the merits of each one, using the grafting of a ferrocene motif as an electrochemical probe.[45] Four paths for the immobilisation of ferrocene were studied, as depicted in Figure V-2. The results showed that based on the intensity of the ferrocene redox signal in the cyclic voltammograms of the final electrode, the strategy "A" and "R" gave the biggest signal, with about 4 layers for route A and about a monolayer for route R.

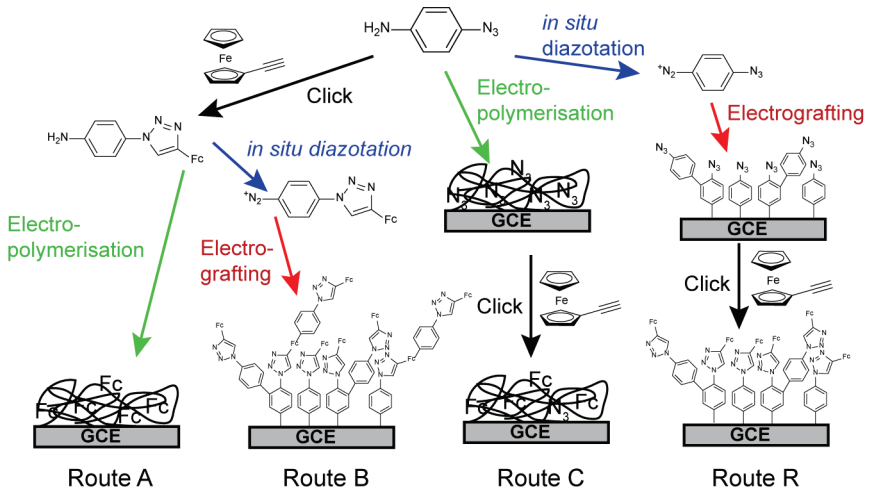

Figure V-2 Four grafting routes proposed for the immobilisation of Fc on a glassy carbon electrode, adapted from ref 45.

With these results in mind, our goal is to obtain a modified carbon electrode containing grafted tpy ligands, so that a metallation with any metal can be attempted. This strategy, if successful, will allow for the easy study of a wide range of tpy-metal complexes for a wide variety of reactions and applications, without further tedious synthetic steps.

2. Functionalisation of carbon electrodes

2.1. Click chemistry

Taking advantage of the experience of our collaborators, one strategy chosen to obtain a layer of tpy ligands on the surface of a glassy carbon electrode was the electrografting of a small molecule (N_3-Ph-N_2^+) onto a glassy carbon electrode, followed by click chemistry of a modified tpy ligand, and subsequent metallation. The strategy is depicted in Figure V-3 and is akin to route "R" in Figure V-2 except for the diazotisation which is performed here in a separate step.

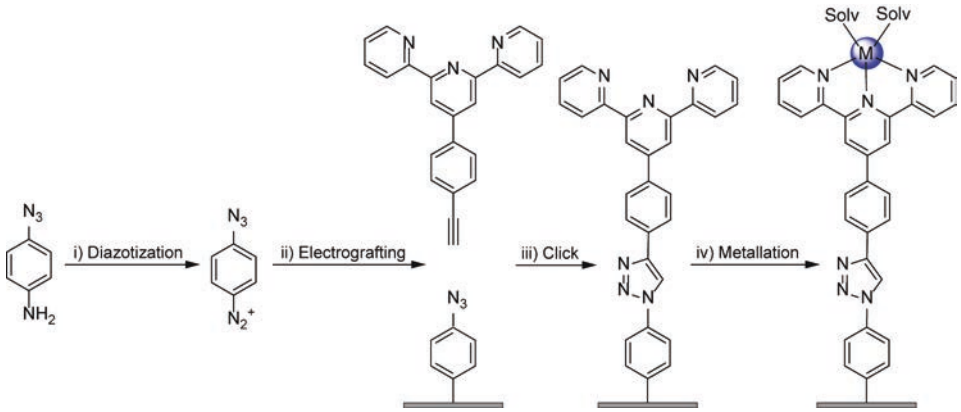

Figure V-3 Proposed synthetic scheme for the preparation of the modified electrodes through click chemistry in 4 steps: i) $NaNO_2$, HBF_4/H_2O, 0°C, 15 min. ii) Cyclic voltammetry, MeCN, $TBAPF_6$ 0.1M, Ar, 1 mM of $[N_2^+PhN_3]BF_4$, 2 cycles from +0.5 to –0.7 V *vs.* Ag/AgCl, 50 mV/s, glassy carbon electrode. iii) Soaking in 10 mM tpy-Ph-CC in $EtOH/H_2O$ (2:1), RT, 72 h, shielded from light under Ar with CuI or $CuSO_4$ and ascorbic acid. iv) Soaking in a DMF solution of 75 mM $CoCl_2$.

The diazotised N_2^+-Ph-N_3 was synthesised and electrografted onto a glassy carbon electrode following standard protocol. The alkyne, 4'-(4-ethynylphenyl)-2,2':6',2"-terpyridine (tpy-Ph-CC) was then synthesised following a literature procedure[46], and several conditions were tested to attempt the click chemistry reaction catalyzed by copper. The reaction was attempted in the dark under an inert atmosphere at room temperature in the presence of an equivalent of CuI or $CuSO_4$ and ascorbic acid. Despite the different attempts, no evidence for the click reaction occurring was gathered, probably due to the fact that the method employed for the click chemistry utilised a non-activated alkyne, at a heterogeneous interface, and was performed at ambient temperature. With these unfavourable conditions combined, this strategy proved unsuccessful. Should this strategy be tested again, attempts at heating the reaction, as well as synthesizing a different terpyridine bearing an activated alkyne, like a cyclooctyne, should be considered.

2.2. Amine electropolymerisation

Another successful method for the grafting of small molecules on the surface of an electrode is the oxidative electropolymerisation of aniline groups, as seen in route A of Figure V-2.

Instead of electopolymerising NH_2-Ph-N_3 followed by a new attempt at the click chemistry reaction, since the click chemistry step was unsuccessful in the previous strategy, an aminated version

of terpyridine, tpy-Ph-NH_2 was considered to try a direct electrolpolymerisation of the ligand on the glassy carbon electrode. The simplified reaction scheme of the oxidative electropolymerisation of amines is presented in the right part of Figure V-4 (right). The aminated ligand, presented in Figure V-4 (left), was synthesised following a literature procedure.[47]

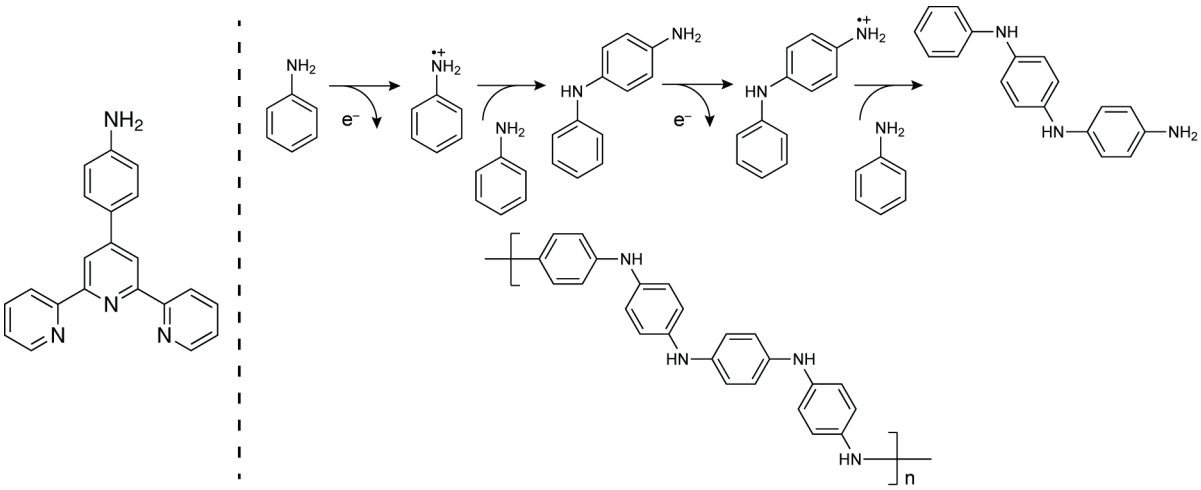

Figure V-4 Aminated version of the terpyridyl ligand used for oxidative polymerisation (left) and simplified oxidative polymerisation mechanism of anilines (right).[48]

Polymerisation onto a carbon electrode was then attempted by soaking a polished 1 mm diameter carbon electrode in a 3 mL tpy-Ph-NH_2 saturated solution of MeCN containing 0.1 M $TBAPF_6$ as the supporting electrolyte in an electrochemical cell. A cycling voltammetry experiment was conducted, at 100 mV/s for 10 scans, in the potential range of −0.2 V to +1.2 V *vs.* Ag/AgCl. A stable and consistent oxidative wave is observed in each scan which, by analogy of the polymerisation of NH_2PhN_3 observed in ref 45, appears to correspond to the oxidative polymerisation event (Figure V-5).

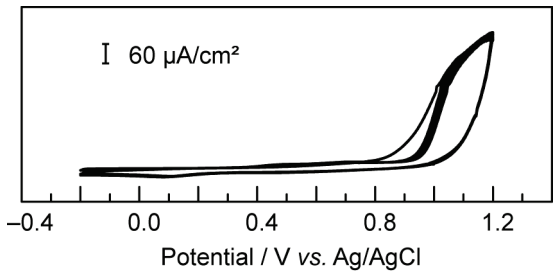

Figure V-5 Cyclic voltammograms of the electropolymerisation procedure: 100 mV/s in MeCN, 10 scans.

Although the film appears stable in MeCN, and was successfully metallated with cobalt to yield a stable film with well-defined electrochemical features (see Figure VI-12 of the Appendix), any attempt at soaking the film, metallated or not, in DMF resulted in film instability. One possibility is that the polymer formed at the surface on the electrode, although insoluble in MeCN and thus stable at the surface of the electrode, gets solubilised in DMF, detaches itself from the electrode and diffuses into the bulk solution.

As our aim was to study CO_2 reduction and proton reduction by the modified electrode in DMF, we have not further pursued this grafting technique, although the film obtained could be suitable for other reactions in MeCN, or even proton reduction in water. One might think of oxidation reactions too, given the well-defined $Co^{II/III}$ couple observed which gives a measurable handle on the system.

2.3. Diazonium electrografting

Having the aminated version of the ligand in hands, the diazotisation followed by electrografting strategy depicted in Figure V-6 was employed.

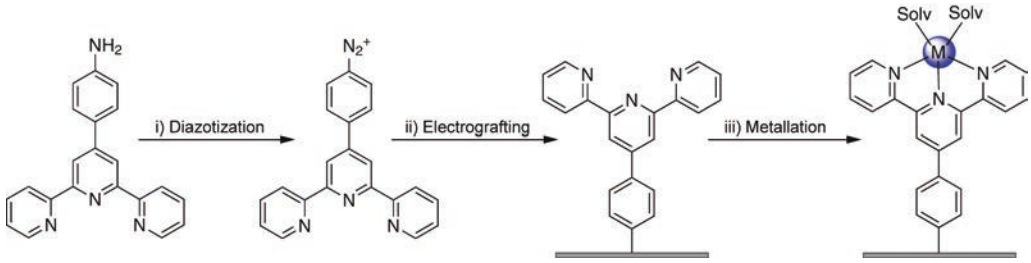

Figure V-6 Simplified synthetic scheme for the preparation of the modified electrodes in 3 steps: i) $NO(BF_4)$, MeCN/Sulfolane (1:1), –40°C, 40 min, Ar, shielded from light. ii) Cyclic voltammetry, MeCN, $TBAPF_6$ 0.1M, Ar, shielded from light, 10 cycles from +0.8 to –0.4 V *vs.* Ag/AgCl, 50 mV/s, glassy carbon electrode. iii) Soaking in a DMF solution of 75 mM $CoCl_2$.[§]

The diazonium salt of the terpyridyl ligand was synthesise according to a recently published procedure by reacting with $NO(BF_4)$ in a MeCN/sulfolane (1:1) solution at –30°C for 40 min. The product is isolated as a dark red powder with characterisation data consistent with that reported in the literature. [49]

The dark red powder of $[tpy\text{-}Ph\text{-}N_2]BF_4$ (2.8 mg for 3 mL of solvent) was dissolved in MeCN with 0.1M of tetrabutylammonium hexafluorophosphate ($TBAPF_6$) as supporting electrolyte in single compartment electrochemical cell. The cell was fitted with a Ag/AgCl reference electrode, a platinum counter electrode, and the solution is shielded from light and degassed with argon. A bare freshly polished 1 mm diameter glassy carbon electrode was immersed in the solution and electrografting was achieved through cyclic voltammetry. The potential was cycled from +0.80 V to –0.40 V *vs.* Ag/AgCl at 50 mV/s until the cyclic voltammograms were super-imposable as seen Figure V-7 (10 scans). In this potential window, a reduction event occurs starting at +0.50 V *vs.* Ag/AgCl during the first scan, corresponding to the reduction of the diazonium group. This liberates N_2 and generates a radical that is believed to react with the glassy carbon electrode, yielding a modified surface. The resulting organic layer was shown to be insulating in the potential window scanned, and thus the grafting process ended as the electrode was completely covered (Figure V-7).

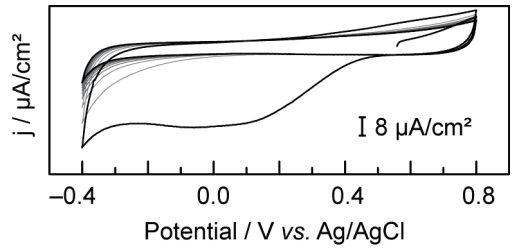

Figure V-7 Cyclic voltammograms of the electrografting procedure: 50 mV/s in MeCN, 10 scans. The first and last scans are in black, cycles 2-9 are in grey for clarity.[§]

The grafted electrode was rinsed by immersion in DMF and H_2O for 10 minutes each and characterised by cyclic voltammetry in DMF with $TBAPF_6$ as supporting electrolyte (0.1 M). The electrode presented no signal in the potential window interrogated (+0.60 V to –1.50 V) under argon and was virtually indistinguishable from a bare polished electrode under these conditions (Figure V-8).

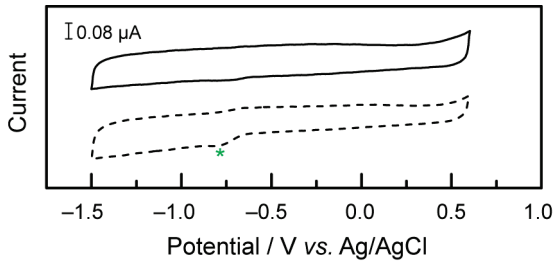

Figure V-8 Cyclic voltammograms under Ar in DMF, $TBAPF_6$ 0.1M, of a bare (top, — solid black line) and a modified (bottom, --- dashed black line, the green star * indicates residual O_2) glassy carbon electrode at 100 mV/s.[‡]

To assess the presence of an insulating grafted layer, the electrode was immersed in a 5 mM solution of $K_4[Fe(CN)_6]$ in 0.1 M KCl as supporting electrolyte and CVs recorded before and after the grafting process. The results are shown in Figure V-9. A grafted layer was indeed present on the grafted electrode, as evidenced by the silencing of the redox signal of the probe ferrocyanide compared to the signal observed on the bare electrode.

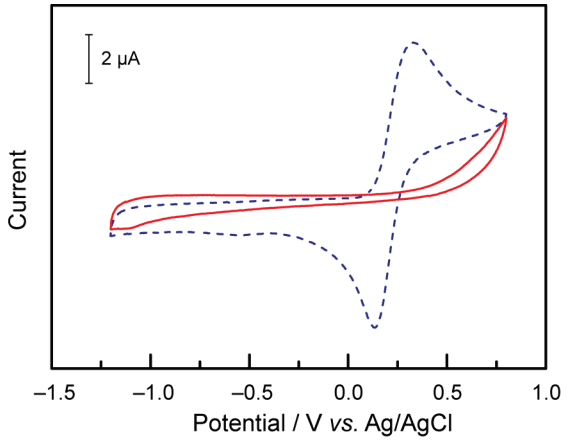

Figure V-9 Cyclic voltammograms under Ar at 100 mV/s in a 0.1 M KCl solution of 5 mM of $K_4[Fe(CN)_6]$ on: a bare polished glassy carbon electrode (----blue) and a tpy-modified glassy carbon electrode (— red).[‡]

Atomic force microscopy imaging further supports the fact that a grafted layer is present on the surface of the carbon electrode after the grafting and rinsing procedures as seen in Figure V-10. On the right is the grafted electrode, which exhibits a smoother profile than that of the polished glassy carbon electrode.

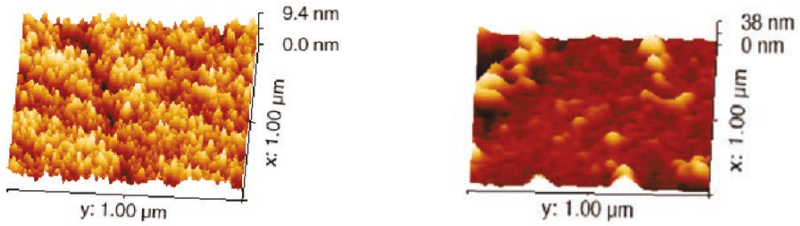

Figure V-10 Atomic Force Microscopy Images of a bare polished glassy carbon electrode (left) and of a glassy carbon electrode modified by electrografting of the tpy ligand (right).

Of note, *in situ* diazotisation followed by immediate electrografting was investigated and is way of obtaining the desired tpy-modified electrodes by analogy with paths B and R in Figure V-2. However, since the diazonium salt of the ligand was observed to be stable in the freezer in the dark for several months, this *in situ* diazotisation method was not further pursued as it was more cumbersome.

2.4. Conclusion

After a screening of three techniques to immobilise a tpy ligand onto a glassy carbon electrode, a tpy-modified electrode of satisfactory apparent stability was obtained through the electrografting of the diazotised version of a NH_2-Ph-tpy ligand.

3. Metallation of modified electrodes

3.1. Metallation with cobalt

The tpy-modified electrode obtained through electrografting was metallated by immersion in a DMF solution of $CoCl_2$ at a concentration of 75 mM 3 h at room temperature. The electrode was subsequently thoroughly rinsed in DMF and H_2O for 15 minutes each. The electrode was then characterised by cyclic voltammetry, and exhibited several redox events in the window scanned, none of which were present in the ligand modified electrode (Figure V-11).

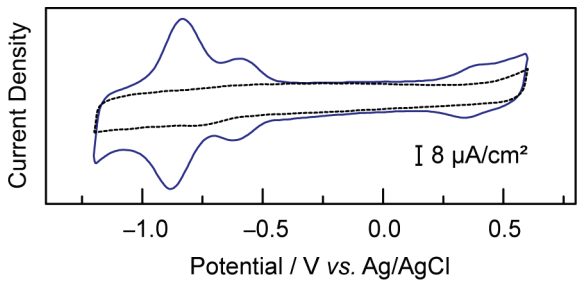

Figure V-11 Cyclic voltammograms in DMF solutions containing 0.1 M of $TBAPF_6$ as supporting electrolyte, under Ar, at 100 mV/s of a bare glassy carbon electrode (---black dashed line) and the grafted electrode metallated with cobalt (— blue line).‡

The features at –0.61 and +0.37 V are attributed to a $Co(tpy)_2^{II/I}$ and $Co(tpy)_2^{III/II}$ respectively by comparison to the features observed in a $Co(tpy)_2$ homogeneous solution.[43] The feature at –0.86 V is attributed to a cobalt monoterpyridine feature, again by analogy with the homogenous system.[44] This claim is further supported by the observation of a pre-feature during the first scan of a modified electrode metallated with $CoCl_2$ when rinsed with DMF and not water (Figure V-12). This pre-feature is consistent with the liberation of the chloride ions in solution, and replacement with solvent molecules as has been described in similar system.[20,27]

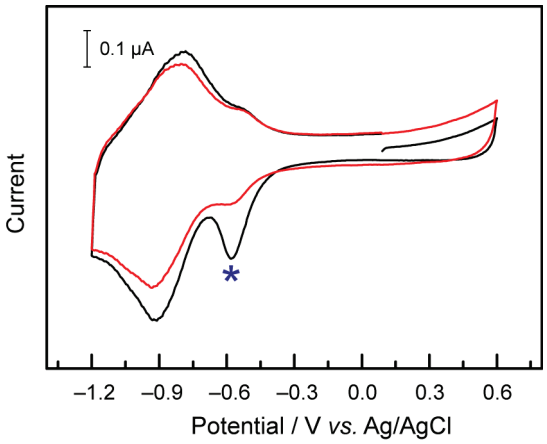

Figure V-12 Cycles 1 (black) and 2 (red) of the cyclic voltammograms under Ar at 100 mV/s in DMF, $TBAPF_6$ 0.1 M of a modified glassy carbon electrode after metallation by $CoCl_2$ and rinsing in DMF (but not water) showing the feature attributed to chloride liberation (***** blue star).‡

To verify that the electrochemical features correspond to surface-bound species the scan rate was varied from 50 to 1000 mV/s in cyclic voltammetry experiments (Figure V-13).

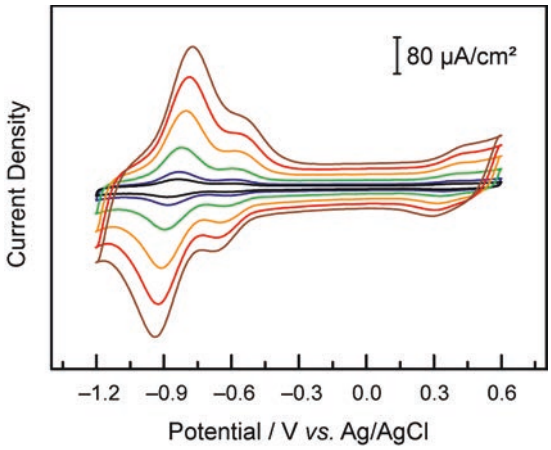

Figure V-13 Cyclic voltammograms under Ar in DMF, $TBAPF_6$ 0.1 M, of a glassy carbon electrode modified with the tpy ligand and freshly metallated with $CoCl_2$ and rinsed at 50 (— black), 100 (— blue), 250 (— green), 500 (— orange), 750 (— red) and 1000 (— brown) mV/s.

The electrochemical features indeed correspond to surface-bound species, as evidenced by the fact that i) they are observed in a pristine electrolyte solution with the modified electrode, ii) their intensity varies linearly with the scan rate applied (Figure V-14).

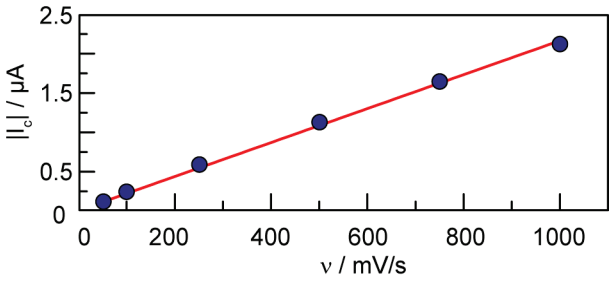

Figure V-14 Absolute value of the cathodic current observed on the peak at –0.86 V and its linear evolution with scan rate (correlation coefficient: 0.999).‡

The area of the peaks observed in the cyclic voltammograms is linked to the charge exchanged. Knowing the scan rate and the geometrical area of the electrode, the cyclic voltammograms allow for easy estimation of the density of cobalt atoms on the surface. Using the data at 100 mV/s, an estimated surface coverage of $5 \cdot 10^{-10}$ mol/cm² was obtained, corresponding to close to a monolayer. This further shows the advantage of this grafting method, since an apparent monolayer is easily obtained.

3.2. Metallation with nickel

Having decoupled the events of ligand grafting and metallation, it is possible to envision metallation with a wide range of different metals. Since nickel showed promising CO_2 reduction activity in Chapter III, metallation was tried with nickel as a proof of concept. A tpy-modified electrode was

metallated with nickel by soaking in a 75 mM DME·$NiCl_2$ adduct DMF solution overnight followed by rinsing in H_2O and DMF for 15 min each.

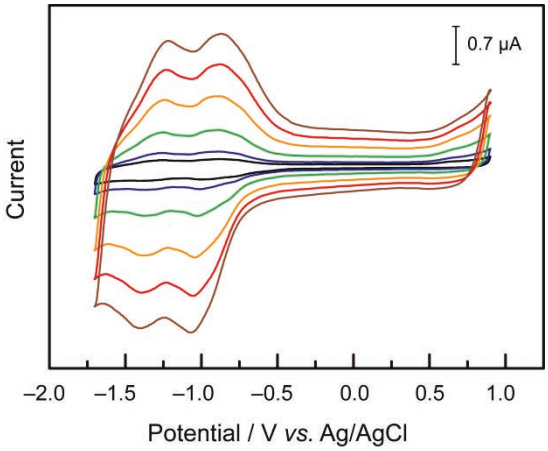

Figure V-15 Cyclic voltammograms under Ar in DMF, $TBAPF_6$ 0.1 M, of a glassy carbon electrode modified with the tpy ligand and freshly metallated with $NiCl_2$ and rinsed at 50 (— black), 100 (— blue), 250 (— green), 500 (— orange), 750 (— red) and 1000 (— brown) mV/s.‡

The Ni-metallated tpy-modified electrode was then characterised by cyclic voltammetry at 100 mV/s in DMF with 0.1 M of $TBAPF_6$ as supporting electrolyte (Figure V-15). Two electrochemical features are observed in the window scanned. These features are reminiscent of the ones observed in homogeneous solutions (see Chapter III), and are both believed to be ligand based features. The species responsible for the features are confirmed as surface bound by the fact that they are observed in pristine solution of electrolyte, but more importantly the absolute value of the cathodic current of the peak at −1.07 V exhibits a linear evolution with scan rate, as opposed to the evolution with the square root of scan rate traditionally observed for homogeneous electron transfer events (Figure V-16).

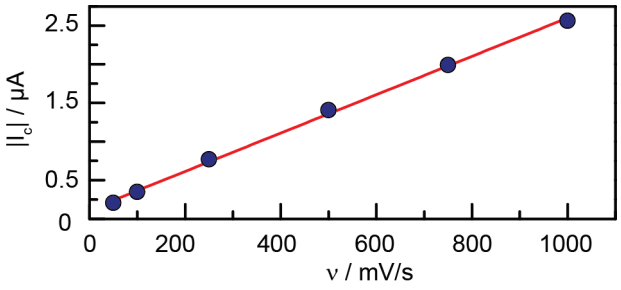

Figure V-16 Absolute value of the cathodic current observed on the peak at –1.07 V and its linear evolution with scan rate (correlation coefficient: 0.998).§

3.3. Electrode recycling

Another benefit of having decoupled the grafting and metallation processes is that the tpy-modified electrodes can be tested for their recyclability. Taking advantage of known coordination chemistry principle, it is possible to envision de-metallating the tpy-modified electrodes to recover the original

tpy-modified electrode. Exposing the metallated electrode to a solution containing a chelating agent should allow for straightforward de-metallation, aided by the thermodynamic driving force of the equilibrium between the solution of chelating agent and the relatively few metal ions present on the surface of the electrode.

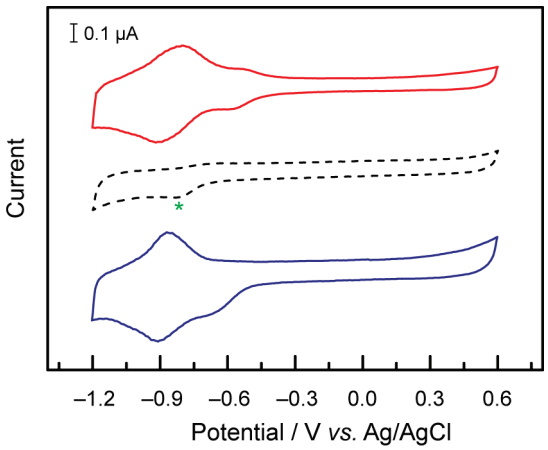

Figure V-17 Cyclic voltammograms at 100 mV/s under Ar in DMF, $TBAPF_6$ 0.1 M, of a tpy-modified glassy carbon electrode and freshly metallated with $CoCl_2$ and rinsed (— red). The same electrode after immersion in a solution of 50 mM ethylenediaminetetraacetic acid solution in water at pH 10 for 3 h (--- black, the green star * indicates residual O_2) and after re-metallation with $CoCl_2$ and rinsing (— blue).[‡]

To test this possibility, a cobalt-metallated tpy-modified glassy carbon electrode was soaked in a 50 mM solution of ethylenediaminetetraacetic acid (EDTA) in water at pH 10. After 3 hours in the EDTA solution, the pristine tpy-modified electrode is recovered (Figure V-17) and can be re-metallated at will. In order to probe the state of the recovered modified electrode, cobalt was re-introduced, and the peaks attributed to cobalt complexes showed that over 95% of the intensity of the original features were recovered, which demonstrates that the grafted layer of tpy ligand was not irreversibly modified by the de-metallation procedure.

4. Catalytic assays

4.1. Reduction of H^+

Having obtained the modified electrodes, we next assayed the derivatives with cobalt for their catalytic properties towards the reduction of protons to hydrogen. When 4.3 mM of acetic acid was added to a DMF solution containing 0.1 M $TBAPF_6$ as supporting electrolyte, a strong cathodic current increase was observed starting at −1.06 V *vs.* Ag/AgCl, with an 11-fold increase in intensity at −1.40 V *vs.* Ag/AgCl compared to the behaviour observed in the absence of acid, or in the presence of acid with a bare polished glassy carbon electrode. This suggests catalytic proton reduction by the modified electrode (Figure V-18).

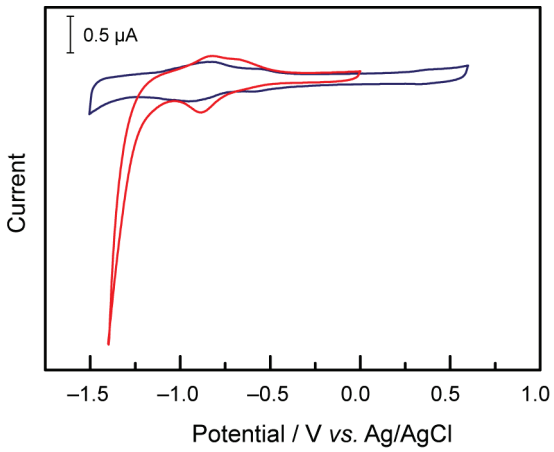

Figure V-18 Cyclic voltammograms in DMF, $TBAPF_6$ 0.1 M, of a glassy carbon electrode modified with the tpy ligand freshly metallated with $CoCl_2$ under Ar (— blue) and with added 4.3 mM acetic acid (— red), at 100 mV/s.‡

To confirm the identity of the catalytic process, a 1.4 cm diameter glassy carbon electrode was grafted with the tpy ligand, metallated with cobalt, and tested in bulk electrolysis conditions. Under N_2, a solution of 0.1 M acetic acid in DMF, with 0.1 M $TBAPF_6$ as supporting electrolyte was electrolyzed at −1.50 V *vs.* Ag/AgCl. A current density of 300 µA/cm² was observed and was sustained during the 3 hours that the experiment lasted (Figure V-19), during which time a steady production of H_2 was observed (Figure V-20a).

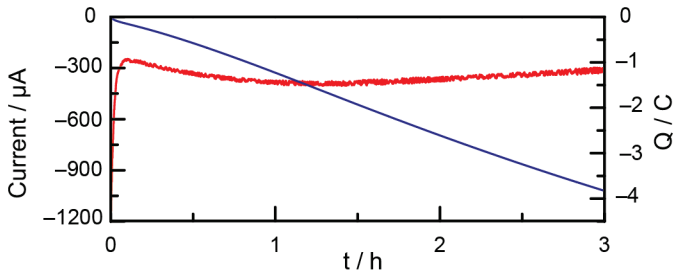

Figure V-19 Current (red) and charge (blue) measured during a controlled-potential electrolysis of cobalt-metallated tpy-modified glassy carbon electrode in DMF at −1.50 V *vs.* Ag/AgCl, in the presence of 0.1 M acetic acid and 0.1 M $TBPF_6$ as supporting electrolyte. The solution was N_2-saturated prior to electrolysis, and the set-up is described in Chapter II.§

The presence of H_2 was confirmed by GC measurements. This production of H_2 represented 6 µmol/h for the 1.4 cm diameter electrode corresponding to an apparent turnover number (TON) of 24 000 when the electrolysis was stopped (3 h). Of note, the activity was still sustained at the end of the experiment and by no mean is this TON implied to be a maximum. The turnover frequency (TOF) obtained from this experiment was 2.2 s^{-1}. The faradic yield for H_2 production obtained during the bulk electrolysis as given in Figure V-19b is ≥ 90%, confirming H_2 production as the main reduction event.

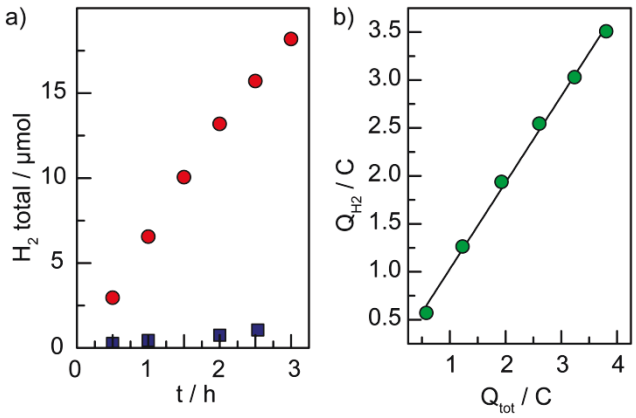

Figure V-20 a) Total amount of H_2 produced during a bulk electrolysis at –1.50 V of a modified (● red circles) and bare (■ blue squares) glassy carbon electrode from a DMF solution with 0.1 M $TBAPF_6$ as supporting electrolyte and 0.1 M acetic acid as proton source. b) Total charge accounted for by the H_2 produced *vs.* total charge passed in the bulk electrolysis of the modified electrode (● green circles). The correlation coefficient is 0.996, and the faradic yield for H_2 production, given by the slope of the line, is 90% ± 5%.[‡]

One of the advantages of immobilizing homogeneous catalysts onto the surface of electrodes is the possibility to diversify the nature of the solvents that can be used, including water. To test the possibility of utilizing a Co-tpy modified electrode as a catalyst for H^+ reduction from neutral water, a tpy-modified cobalt-metallated electrode was immersed in a phosphate buffer at pH 7 in water under argon. As the electrode was scanned to negative potentials, an 18-fold increase in cathodic current was observed at –1.50 V compared to a bare glassy carbon electrode (Figure V-21).

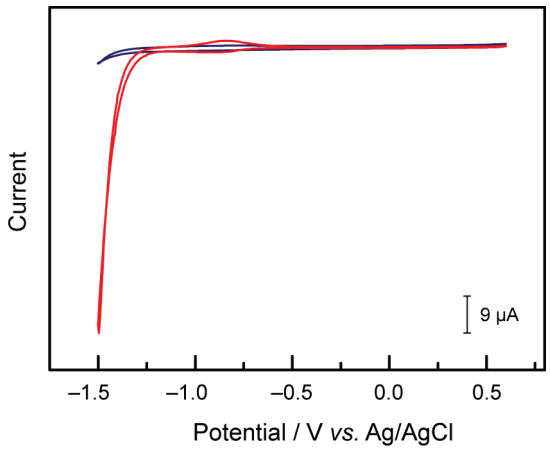

Figure V-21 Comparison of the cyclic voltammograms under Ar in water in a phosphate buffer (pH = 7) of a tpy-modified glassy carbon electrode after metallation with $CoCl_2$ (— red) and a polished bare glassy carbon electrode (— blue).[‡]

To reach the same current intensities on a bare glassy carbon electrode, a potential about 370 mV more negative has to be applied, confirming the activity of the electrodes modified with Co-tpy as catalysts for the reduction of protons in phosphate buffer (Figure V-22). No controlled potential electrolyses have been conducted in water using these modified glassy carbon electrodes yet, but they represent an interesting future research direction.

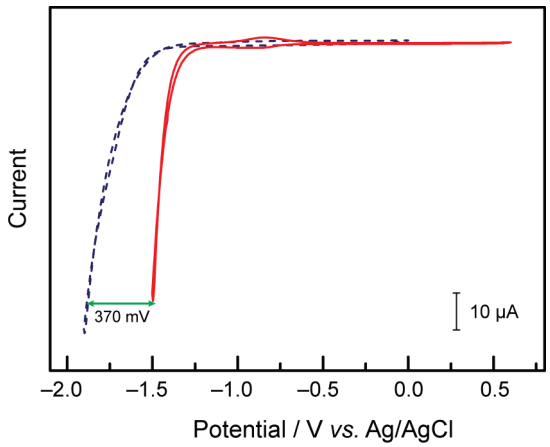

Figure V-22 Comparison of the cyclic voltammograms under Ar in water in a phosphate buffer (pH = 7) of a tpy-modified glassy carbon electrode after metallation with $CoCl_2$ (— red) and a polished bare glassy carbon electrode (---blue). To reach comparable current intensities to the modified electrode, the bare electrode has to be scanned to ~ 370 mV more negative.[‡]

4.2. Reduction of CO_2

The cobalt-metallated tpy-modified electrodes were also assayed for their activity towards CO_2 reduction in DMF solutions containing 0.1 M of $TBAPF_6$ as supporting electrolyte by cyclic voltammetry. A strong cathodic current enhancement was observed under CO_2 compared to argon as was observed for the corresponding homogeneous catalysts, with an onset at –1.12 V *vs.* Ag/AgCl (Figure V-23).[43,44] However, an anodic feature was also observed under CO_2 at –0.69 V *vs.* Ag/AgCl. This feature was not observed in homogeneous solutions, and is not observed on a bare glassy carbon electrode.

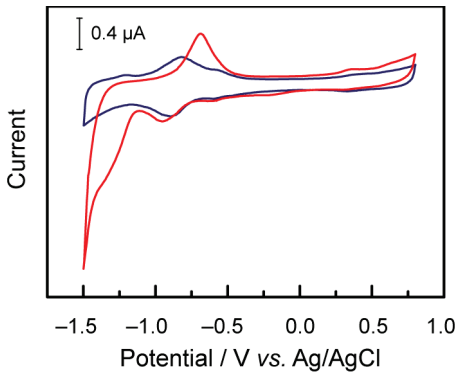

Figure V-23 Cyclic voltammograms in DMF, $TBAPF_6$ 0.1 M, of a glassy carbon electrode modified with the tpy ligand freshly metallated with $CoCl_2$ under Ar (— blue) and CO_2 (— red) at 100 mV/s.

To assess the identity of this anodic feature, a cobalt-metallated tpy-modified electrode was exposed to an atmosphere of CO in the same conditions (Figure V-24). A similar anodic feature was observed, confirming the tentative assignment of this feature as a Co-CO adduct.‡

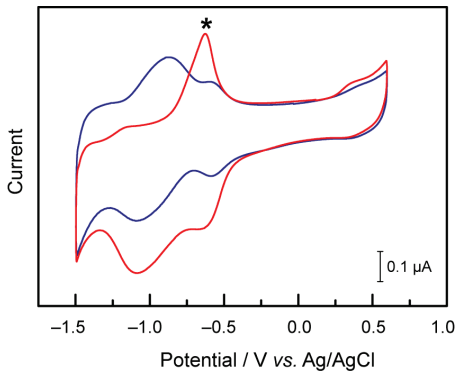

Figure V-24 Cyclic voltammograms in DMF, $TBAPF_6$ 0.1 M, of a glassy carbon electrode modified with the tpy ligand freshly metallated with $CoCl_2$ under Ar (— blue) and CO (— red) at 100 mV/s showing the new anodic peak at −0.63 V (***** black star).

The activity of Co-metallated tpy-modified electrodes as catalysts for the reduction of CO_2 was assessed through bulk electrolyses at −1.50 V *vs.* Ag/AgCl in DMF under CO_2 with 0.1M added $TBAPF_6$ as supporting electrolyte. No extra source of water was added to the electrolyte, as the CV features were not apparently affected by added water. It has to be noted that the anhydrous nature of the DMF solvent used in this instance cannot be guaranteed. The 1.4 cm diameter tpy-modified glassy carbon electrode metallated with cobalt exhibited a rapid decrease of current during the first 30 minutes of bulk electrolysis to reach baseline levels. During those 30 minutes, 55 nmol of CO were produced, corresponding to a TON of 70 per cobalt atom on the electrode (Figure V-25).‡

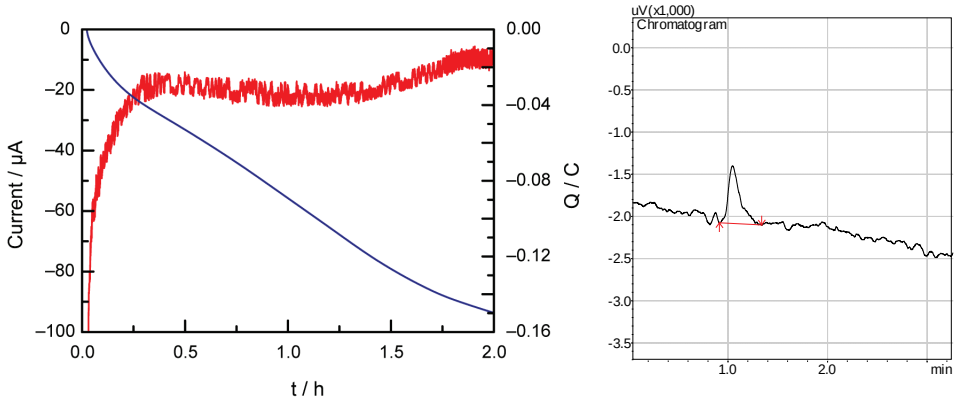

Figure V-25 Left: Current (red) and charge (blue) measured during a controlled-potential electrolysis of cobalt-metallated tpy-modified glassy carbon electrode in DMF at −1.50 V *vs.* Ag/AgCl, in the presence of 0.1 M $TBPF_6$ as supporting electrolyte. Right: First 3 minutes of the chromatogram obtained after a GC injection of 100 µL of headspace after 2 h of bulk electrolysis showing the small CO response peak corresponding to 55 nmoles produced in the bulk electrolysis cell.‡

The confirmation of the CO_2 reduction catalytic activity of the Co-metallated tpy-modified electrodes for the electroreduction of CO_2 to CO allows to speculate further on the differences between

the homogeneous and immobilised Co-tpy catalysts. The presence of the anodic feature in the CVs, which was not observed in the study of homogeneous CO_2 reduction by Co-tpy (Chapter III and IV) indicated a fundamental difference in the catalytic behaviour after immobilisation on the electrode. This behaviour appears to indicate that the release of CO by the catalysts immobilised on the glassy carbon electrode is hindered compared to the homogeneous catalyst. Additionally, the stability of the immobilised catalyst appears much attenuated compared to the homogeneous system since the currents drop to baseline levels within 30 minutes. In agreement with the initial hypothesis for the homogeneous system that the catalyst can become inactive, these results further indicate that a product inhibition pathway could be operative, in the manner reported by Sutin during the study of the related $[Co(bpy)_3]^{2+}$.[50]

Interestingly, the difference of behaviour observed after immobilisation could point to a potential role for the second tpy ligand in homogeneous solutions. It has been shown that the $[Co(tpy)_2]^{2+}$ pre-catalysts that are put in solution are not likely the structure of the active catalysts, but rather it is proposed that a tpy ligand can be dynamically lost, thereby freeing coordination sites for interaction with substrates within the reaction layer in the vicinity of the electrode. However, in the bulk of the solution the resting state species is $[Co(tpy)_2]^{+}$, indicating that once the complex has reacted and the product is released, the free tpy ligand re-coordinates the cobalt cation. The lack of an oxidative feature corresponding to the release of H_2 observed in CV under proton reduction conditions could be explained if it is assumed that a stronger bond exists between a CO-Co than a H_2-Co. It would also explain the CO release feature being observed in immobilised catalysts and not homogeneously. In homogeneous solutions, the second free tpy ligand and its chelating effect will help release the CO molecule, whereas in the case of immobilised systems the possibility of re-coordination by a second tpy molecule to assist in the release of CO is unlikely.

5. Conclusions and perspectives

In summary, the simple preparation of glassy carbon electrode functionalised with terpyridine, a common stable and cheap polypyridyl ligand with broad applications has been described. The strategy of decoupling the grafting and metalation processes allows a versatility of the end uses of such modified electrodes through reversible metallation with a variety of metal ions, here non-noble cobalt and nickel ions, to obtain immobilised catalysts. Specifically, the cobalt-modified electrode displays excellent stability and electrocatalytic performances during proton reduction into hydrogen, in both organic and aqueous solvents. Despite the modest activity for CO_2 reduction and limited stability, it is comparable to that which has been recently reported for rhenium-modified electrodes[27]. However, the electrode is one of the very rare examples of glassy carbon electrodes functionalised with non-noble catalysts for CO_2 reduction[51] and provides an interesting basis for future optimisation.

6. References

‡ N. Elgrishi, S. Griveau, M. B. Chambers, F. Bedioui and M. Fontecave, *Chem. Commun.*, 2015, **51**, 2995–2998. Reproduced by permission of the Royal Society of Chemistry.

§ Adapted with minor alterations from ‡.

1 D. J. Cole-Hamilton, *Science*, 2003, **299**, 1702.

2 L.-N. He, J.-Q. Wang and J.-L. Wang, *Pure Appl. Chem.*, 2009, **81**, 2069.

3 M. P. Conley and C. Coperet, *Top. Catal.*, **2014**, *57*, 843.

4 E. E. Benson, C. P. Kubiak, A. J. Sathrum and J. M. Smieja, *Chem. Soc. Rev.*, **2009**, *38*, 89.

5 H. Dau, C. Limberg, T. Reier, M. Risch, S. Roggan and P. Strasser, *ChemCatChem*, 2010, **2**, 724.

6 C. Brandt, R. van Eldik, *Chem. Rev.*, 1995, **95**, 119.

7 W. von Philipsborn, *Chem. Soc. Rev.*, 1999, **28**, 95.

8 T. S. Teets and D. G. Nocera, *Chem. Commun.*, 2011, **47**, 9268.

9 R. B. King, *J. Organomet. Chem.*, 1999, **586**, 2.

10 P. McMorn and G. J. Hutchings, *Chem Soc. Rev.*, 2004, **33**, 108.

11 Z. Wang, G. Chen andK. Ding, *Chem Rev.*, 2009, **109**, 322.

12 S. Minakata and M. Komatsu, *Chem. Rev.*, 2009, **109**, 711.

13 T. Matsumoto, M. Ueno, N. Wang, and K. Shu. *Chem. Asian J.*, 2008, **3**, 196.

14 H. C. L. Abbenhuis, *Angew. Chem. Intl. Ed.*, 1999, **38**, 1058.

15 M. Pagliaro, V. Pandarus, R. Ciriminna, F. Beland, P. Demma Cara, *ChemCatChem*, 2012, **4**, 432.

16 N. End, K.-U. Schoening, *Top. Curr. Chem.*, 2004, **242**, 241.

17 A. Le Goff, V. Artero, B. Jousselme, P. D. Tran, N. Guillet, R. Metaye, A. Fihri, S. Palacin and M. Fonteacve, *Science*, 2009, **326**, 1384.

18 X. Chen, H. Ren, W. Peng, H. Zhang, J. Lu and L. Zhuang, *J. Phys. Chem. C*, 2014, **118**, 20791.

19 H. C. Hurrell, A.-L. Mogstad, D. A. Usifer, K. T. Potts and H. D. Abruna, *Inorg. Chem.*, 1989, 28, 1080.

20 D. P. Harrison, A. M. Lapides, R. A. Binstead, J. J. Concepcion, M. A. Méndez, D. A. Torelli, J. L. Templeton and T. J. Meyer, *Inorg. Chem.*, 2013, **52**, 4747.

21 S. Cosnier, A. Deronzier and N. Viachopoulos, *J. Chem. Soc., Chem. Commun.*, 1989, 1259.

22 N. P. Rodriques, J. Obirai, T. Nyokong and F. Bedioui, *Electroanalysis*, 2005, **17**, 186.

23 M.-A. Haga, T. Takasugi, A. Tomie, M. Ishizuya, T. Yamada, M. D. Hossain and M. Inoue, *Dalton Trans.*, 2003, 2069.

24 M. K. Coggins, M. A. Mendez, J. J. Concepcion, R. A. Periana and T. J. Meyer, *J. Am. Chem Soc.* 2014, **136**, 15845.

25 M. Maskus and H. D. Abruna, *Langmuir*, 1996, **12**, 4455.

26 E. W. McQueen and J. I. Goldsmith, *J. Am. Chem. Soc.*, 2009, **131**, 17554.

27 J. D. Blakemore, A. Gupta, J. J. Warren, B. S. Brunschwig and H. B. Gray, *J. Am. Chem. Soc.*, 2013, **135**, 18288.

28 Y. Tsukahara, T. Wada and K. Tanaka, *Chem. Lett.*, 2010, **39**, 1134.

29 B. Jousellme, G. Bidan, M. Billon, C. Goyer, Y. Kervella, S. Guillerez, E. A. Hamad, C. Goze-Bac, J.-Y. Mevellec and S. Lefrant, *J. Electroanal. Chem.*, 2008, **621**, 277.

30 J. C. Swarts, D. Laws and W. E. Geiger, *Organometallics*, 2005, **24**, 341

31 A. Yesildag and D. Ekinci, *Electrochimica Acta*, 2010, **55**, 7000.

32 A. A. Tregubov, K. Q. Vuong, E. Luais, J. J. Gooding and B. A. Messerle, *J. Am. Chem. Soc.*, 2013, **135**, 16429.

33 M. Coates, S. Griveau, F. Bedioui and T. Nyokong, *Electoanalysis*, 2012, **24**, 1833.

34 Z. Chen, C. R. K. Glasson, P. L. Holland and T. J. Meyer, *Phys. Chem. Chem. Phys.*, 2013, **15**, 9503.

35 J. Wang, S. Li, G. Zhu, W. Zhao, R. Chen and M. Pan, *J. Power Sources*, 2013, **240**, 381.

36 T. Abe and M. Kaneko, *J. Mol. Cat. A.*, 2001, **169**, 177.

37 S. Masaoka and K. Sakai, *Chem. Lett.*, 2009, **2009**, 182.

38 Z. Chen, C. Chen, D. R. Weinberg, P. Kang, J. J. Concepcion, D. P. Harrison, M. S. Brookhart and T. J. Meyer, *Chem Commun.*, 2011, **47**, 12607.

39 J. Limburg, J. S. Vrettos, H. Chen, J. C. de Paula, R. H. Crabtree and G. W. Brudvig, *J. Am. Chem. Soc.*, 2001, **123**, 423.

40 T. Yoshida, K. Tsutsumuida, S. Teratani, K. Yasufuku and M. Kaneko, *J. Chem. Soc., Chem Commun.* 1993, 631.

41 P. Paul, B. Tyagi, A. K. Bilakhiya, M. M. Bhadbhade, E. Suresh and G. Ramachandraiah, *Inorg. Chem.*, 1998, **37**, 5733.

42 A. Winter, G. R. Newkome and U. S. Schubert, *ChemCatChem*, 2011, **3**, 1384.

43 N. Elgrishi, M. B. Chambers, V. Artero and M. Fontecave, *Phys. Chem. Chem. Phys.*, 2014, **16**, 13635.

44 N. Elgrishi, M. B. Chambers and M. Fontecave, *Chem. Sci.*, 2015, **6**, 2522.

45 M. Coates, H. Elamari, C. Girard, S. Griveau, T. Nyokong and F. Bedioui, *J. Electroanal. Chem.*, 2012, **670**, 79.

46 E. C. Constable, C. E. Housecroft, S. L. Kokatam, E. A. Medlycott and J. A. Zampese, *Inorg. Chem. Comm.*, 2010, **13**, 457.

47 A. C. Durrell, G. Li, M. Koepf, K. J. Young, C. F.A. Negre, L. J. Allen, W. R. McNamara, H.-e. Song, V. S. Batista, R. H. Crabtree, G. W. Brudvig, *J. Catal.*, 2014, **310**, 37.

48 I. Y. Sapurina and M. A. Shishov (2012). *Oxidative Polymerization of Aniline: Molecular Synthesis of Polyaniline and the Formation of Supramolecular Structures, New Polymers for Special Applications*, Dr. Ailton De Souza Gomes (Ed.), ISBN: 978-953-51-0744-6,

49 Y. Pan, B. Tong, J. Shi, W. Zhao, J. Shen, J. Zhi and Y. Dong, *J. Phys. Chem. C*, 2010, **114**, 8040.

50 F. R. Keene, C. Creutz and N. Sutin, *Coord. Chem. Rev.*, 1985, **64**, 247.

51 S. A. Yao, R. E. Ruther, L. Zhang, R. A. Franking, R. J. Hamers and J. F. Berry, *J. Am. Chem. Soc.*, 2012, **134**, 15632.

Chapter VI

–

Epilogue

1. Conclusions and perspectives

For this project, the aim was to select likely CO_2 reduction catalysts as targets, and study their mechanism, selectivity, and eventually immobilising them onto carbon electrodes.

Chapter III reported the homogeneous CO_2 reduction properties of first row transition metal bis-terpyridine systems. We have clarified preliminary reports[1,2,3] that homoleptic terpyridine complexes of nickel and cobalt were competent catalysts for the electrocatalytic reduction of CO_2 to CO as the exclusive carbon containing product. However, no activity was observed for the iron and manganese derivatives in the conditions tested, and the copper derivative proved unstable under CO_2 and led to decomposition on the electrode. The **Co-tpy** and **Ni-tpy** systems were investigated further and it was shown that CO_2 reduction catalysis is triggered by a ligand based reduction in both cases, but involved a divalent nickel for **Ni-tpy** as opposed to a monovalent cobalt for **Co-tpy**. The divalent nickel system led to the exclusive formation of CO, with no detectable H_2 formed. This striking selectivity is thought to result from the requisite yet unfavourable formation of a Ni^{IV} hydride complex in a mechanism to catalyse the reduction of protons to H_2. This is in stark contrast to that which is observed for **Co-tpy** in which the lower valent cobalt catalyst was found to generate gaseous mixtures of CO and H_2. However, the selectivity for the production of H_2 or CO was easily tuneable through the application of a different overvoltage during controlled-potential electrolyses. Higher proportions of CO in the H_2:CO mixture were observed to correlate to the application of lower overvoltages. This ease of tuning is greatly valuable in the context of the Fisher-Tropsh process which requires syngas (mixtures of CO and H_2) of specific ratios depending on the products to be synthesised. Overall, the faradic efficiencies were lower than expected, with a potential deactivation pathway proposed to be dominated by ligand decomposition events, such as *N*-carboxylation of the terpyridine ligand. This behaviour of low faradic yields on cobalt and nickel polypyridyl complexes are not unprecedented; with the related $M(bpy)_n$ catalysts having been shown to enter several deactivation pathways, one of which being cause by slow product release.[4,5,6] Other polypyridyl-based catalysts with low faradic yields were hypothesised to suffer from ligand degradation.[7,8] Overall, despite low faradic yields, the apparent stability of the current observed during bulk electrolysis of **Co-tpy** under CO_2, coupled to the cheap nature of the metal, the ubiquitous nature of the ligand, and the selectivity properties prompted further studies on the mechanisms of the catalyst.

In Chapter IV, to begin to evaluate factors governing the selectivity of between formation of H_2 and CO, H^+ reduction catalysed by a class of cobalt terpyridine complexes was first studied in the absence of CO_2. Surprisingly given the ubiquitous nature of terpyridine ligands and the natural abundance of cobalt, no study existed on the homogeneous proton reduction catalysis by **Co-tpy** before this work. We reported that the **Co-tpy** family are competent H^+ reduction catalysts in DMF,

producing H_2 in nearly quantitative faradic yields. Simple modifications of the electronic properties of the terpyridine ligand were observed to have a tremendous effect on the rate constants for H^+ reduction as determined using the *foot-of-the-wave* analysis developed by Savéant and collaborators in 2012.[9] The more donating the substituents on the terpyridine ligand the higher the rate constants were for H^+ reduction, at the expense of the greater overpotentials required for catalysis. Using this observation, we set out to increase the selectivity of the **Co-tpy** family for CO_2 reduction to CO over H^+ reduction to H_2 by "turning off" the H^+ reduction pathway. Using the electronically tuned ligands cobalt complexes, controlled current electrolyses ender CO_2 were performed and resulted in lower faradic yields for H^+ reduction to H_2 observed for the catalysts with the lower rate constants for H^+ reduction. Similarly, the faradic efficiencies for CO_2 reduction to CO by these complexes were increased for the complexes bearing ligands with withdrawing groups, thus validating the strategy of turning off the H^+ reduction pathway in order to increase selectivity for CO_2 reduction to CO. In the course of this study, the effect of steric strain on catalysis with a ^{t}Bu substituted terpyridine ligand was also observed, and led to the highest faradic yields for CO production with minimal H_2 evolution despite the donating nature of the substituents. This is hypothesised to arise from the disfavouring of the formation of a potentially inactive dimer. Lastly, the study of the H_2 evolution reaction confirmed hints observed in Chapter III that the active catalyst for proton and CO_2 reduction comprises of less than two tpy ligands per cobalt centre. This has led us to think about new ways to force the system to reach a cobalt monoterpyridine (Co-monotpy) state.

One method to achieve a monoterpyridine state was pursued in Chapter V, in which the simple preparation of glassy carbon electrodes functionalised with the terpyridine ligand was investigated. By decoupling the grafting and metallation steps, it was possible to obtain cobalt-metallated terpyridine-functionalized glassy carbon electrodes with mostly Co-monotpy catalysts at the surface of the electrode. These modified electrodes were shown to be competent and stable catalysts for the electrocatalytic reduction of H^+ to H_2 in DMF, and the immobilisation process allowed the systems to be tested in different conditions, including in water at neutral pH. The electrodes were assayed for electrocatalytic CO_2 reduction, and were shown to produce CO, albeit with a modest activity and stability. Their activity and stability pointed to the potential limitations of the system but despite these issues they proved to be on par with recently reported Re-based modified electrodes[10] and represent one of the rare examples of non-noble metal catalysts for CO_2 reduction grafted onto a carbon electrode.

A major difference observed during the study of CO_2 reduction by **Co-tpy** on the grafted electrodes was the new oxidation feature in CVs attributed to a CO–Co adduct. The presence of this feature coupled to the sluggish nature of the grafted system for CO_2 reduction suggested the notion that CO release is a limiting factor of catalysis. The absence of this feature in homogenous catalysis, and the apparent stability of the activity of the catalyst together pointed to a major difference between the homogeneous and grafted systems. It also suggested that the possibility of a $[Co(tpy)_2]^+$ resting

state in the homogeneous system might be beneficial for catalysis, as the chelating effect of the second tpy ligand around the cobalt could help trigger the CO release, thus accelerating the catalysis.

This comparison and its conclusions are only preliminary but they point to the power of immobilising homogeneous catalysts. Not only can other solvents and conditions be assayed with fewer restrictions, the comparison between the homogeneous and immobilised systems can help design the next generation catalysts. For example, should the importance of the second free tpy ligand prove correct, and knowing from Chapter III the reactive nature of that second free tpy ligand, a few guiding principles could be put forth for the synthesis of new ancillary ligand platforms.

First a new ligand platform could be proposed that includes hemi-labile functionalities that feature the possibility of 1, 2 or 3 extra coordination sites. This would offer the possibility of providing active sites to bind CO_2 but also would re-coordinate to promote the release CO. One could cite the recent example developed by Reisner to improve the catalytic activity of Cobaloximes for proton reduction as an inspiration for hemi-labile ligand design (Scheme VI-1, left).[11]

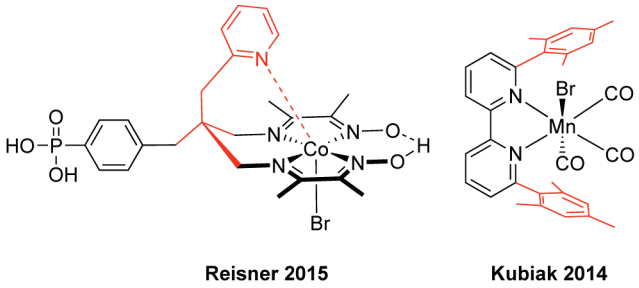

Scheme VI-1 Inspirations for next generation ligand designs taken from recent reports by Reisner[11] and Kubiak[12].

The second modification of the ancillary ligand platform to envision is based on the observations from Chapter III and IV of the fact that the active species likely contains only one tpy ligand per cobalt centre, but also of the likely inactive Co dimer formation during bulk electrolysis conditions. To resolve both of these problems, the use of bulky substituents on the terpyridine platform in order to introduce steric strain to disfavour the formation of the unreactive bisterpyridine or dimer can be proposed. This strategy is similar to that which was developed by Kubiak in the study of $Mn(bpy)(CO)_3$ catalysts, where substituting the bpy moiety for a mesbpy (Scheme VI-1, right) led to an increase of catalytic rates for CO_2 reduction through the disfavouring of the formation of the catalytically inactive Mn–Mn dimer.[12]

Finally, as demonstrated in Chapter IV, placing withdrawing groups on the terpyridine ligand should favour CO_2 reduction over proton reduction while at the same time diminishing the required applied overpotential to trigger catalysis.

Moving forward, having the tpy-modified electrodes at hand, several routes are open for future research directions. First, different metals can be incorporated to test their activity towards H^+ or CO_2 in reducing conditions. Other reactions can be evaluated as well, such as the oxidation of nitrites using

the cobalt metallated tpy-modified electrodes. This is of particular interest in the context of replacing the cobalt phtalocyanines that have been shown to be active despite poorly defined electrochemical features in the CVs.[13]

Focusing on understanding the reactivity of **Co-tpy** towards CO_2 and H^+ reduction and identifying the nature of the active catalyst, modified electrodes afford the opportunity of isolating a layer of mostly Co-monotpy on the electrode. This can be taken advantage of and provide a direct comparison of the activity of Co-bistpy and Co-monotpy towards CO_2 or H^+ reduction by immobilising the Co-bistpy catalyst in an analogous controlled fashion. The intensity of the $Co^{II/I}$ redox feature will be useful as a handle on the amount of cobalt atoms accessible on the surface of the electrode.

Overall, the work presented in this dissertation focused on the fundamental understanding of the catalytic behavior towards CO_2 and H^+ electrocatalytic reduction of M-tpy architectures. The ligand platform chosen is ubiquitous and relatively cheap, as are the metal chosen for this study. The resulting cobalt- and nickel-based catalysts are competent CO_2 reduction catalysts, as well as H^+ reduction catalysts in the case of the **Co-tpy**. The catalytic activity of **Co-tpy** is on par with similar polypyridyl systems based on rare precious metals in the case of CO_2 reduction, and with rate constants within the same order of magnitudes as some on the most well studied catalysts for H^+ reduction on cobalt and nickel systems.[14,15]

References

1 C. Arana, M. Keshavarz, K. T. Potts and H. D. Abruña, *Inorg. Chimica Acta*, 1994, **225**, 285.

2 C. Arana, S. Yan, M. Keshavarz-K, K. T. Potts and H. D. Abruña, *Inorg. Chem.*, 1992, **31**, 3680.

3 J. A. Ramos Sende, C. R. Arana, J. L. Hernández, K. T. Potts, M. Keshevarz-K and H. D. Abruña, *Inorg. Chem.*, 1995, **34**, 3339.

4 F. R. Keene, C. Creutz and N. Sutin, *Coord. Chem. Rev.*, 1985, **64**, 247.

5 S. Daniele, P. Ugo, G. Bontempelli and M. Fiorani, *J. Electroanal. Chem.*, 1987, **219**, 259.

6 L. Garnier, Y. Rollin and J. Périchon, *J. Oganomet. Chem.*, 1989, **367**, 347.

7 C. Caix, S. Chardon-Noblat and A. Deronzier, *J. Electroanal. Chem.*, 1997, **434**, 163.

8 C. M. Bolinger, N. Story, B. P. Sullivan and T. J. Meyer, *Inorg. Chem.*, 1988, **27**, 4582.

9 C. Costentin, S. Drouet, M. Robert and J.-M. Savéant, *J. Am. Chem. Soc.*, 2012, **134**, 11235.

10 J. D. Blakemore, A. Gupta, J. J. Warren, B. S. Brunschwig and H. B. Gray, *J. Am. Chem. Soc.*, 2013, **135**, 18288.

11 J. Willkomm, N. M. Muresan and E. Reisner, *Chem. Sci.*, 2015, Advance Article, DOI: 10.1039/C4SC03946G.

12 M. D. Sampson, A. D. Nguyen, K. A. Grice , C. E. Moore, A. L. Rheingold and C. P. Kubiak, *J. Am. Chem. Soc.*, 2014, **136**, 5460.

13 C. A. Caro, F. Bedioui and J. H. Zagal, *Electrochimica Acta*, 2002, **47**, 1489.

14 C. Costentin, M. Robert and J.-M. Saveant, *Chem. Soc. Rev.*, 2013, **42**, 2423.

15 V. Artero and J.-M. Savéant, *Energy Environ. Sci.*, 2014, **7**, 3808.

2. Appendix

Here is presented supplementary data which would have disrupted the flow of the text but is nevertheless necessary for a complete understanding of the results presented in the thesis. For convenience, the data is presented chapter by chapter.

2.1. Chapter III - Evaluation of CO_2 reduction by first row transition metal complexes of the ubiquitous terpyridine ligand

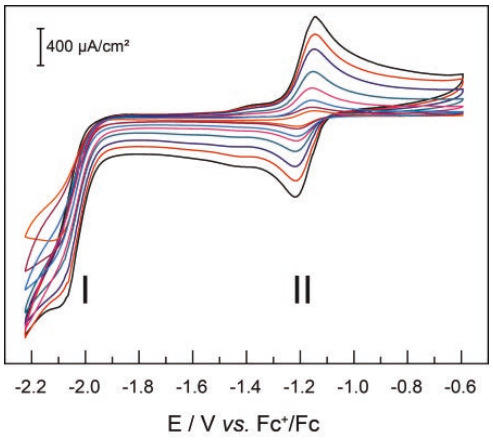

Figure VI-1 Cyclic voltammograms of a 2 mM CO_2-saturated solution of **Co-tpy** at 10 (orange), 20 (purple), 50 (light blue), 100 (pink), 250 (teal), 500 (dark blue), 750 (red) and 1000 (black) mV/s. See Section 2.2 of Chapter III.‡

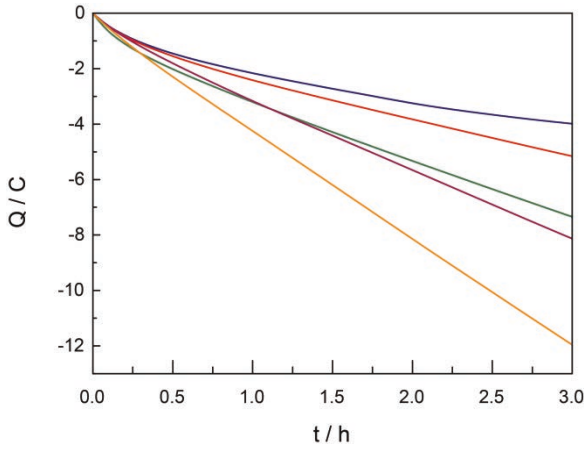

Figure VI-2 Charge measured during controlled-potential electrolyses of 2 mM **Co-tpy** CO_2-saturated solutions at different applied potentials (blue: –1.93 V, red: –2.03 V, green: –2.08 V, purple: –2.13 V and orange: –2.23 V). Bulk electrolyses were performed in 10 mL of DMF/H_2O (95:5, v:v), with 0.1M TBAP, using a 1.5 cm diameter pool of mercury as the working electrode. See Section 3.1.2 of Chapter III.‡

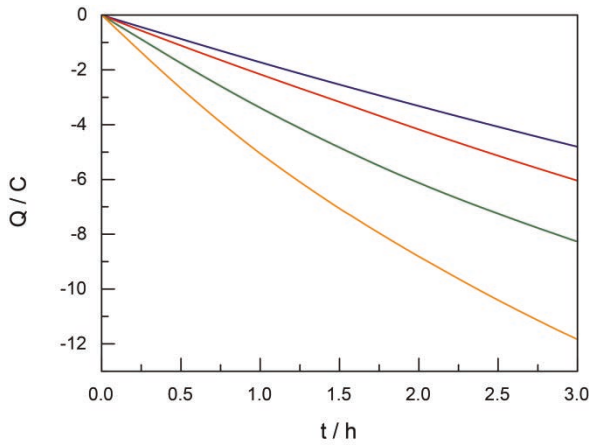

Figure VI-3 Charge measured during controlled-potential electrolyses of 2 mM **Ni-tpy** CO_2-saturated solutions at different applied potentials (blue: –1.72 V, red: –1.76 V, green: –1.89 V and orange: –2.14 V). Bulk electrolyses were performed in 10 mL of DMF/H_2O (95:5, v:v), with 0.1M TBAP, using a 1.5 cm diameter pool of mercury as the working electrode. See Section 3.2 of Chapter III.[‡]

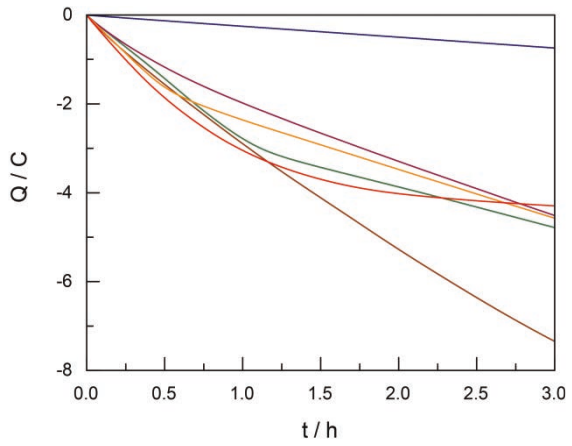

Figure VI-4 Charge measured during controlled-potential electrolyses of CO_2-saturated solutions at –2.03 V of: 2 mM tpy (blue), 2 mM $CoCl_2$ (red), 2 mM tpy and 2 mM $CoCl_2$ (yellow), 4 mM tpy and 2 mM $CoCl_2$ (purple), 1 mM tpy and 2 mM $CoCl_2$ (green) and a mixture of 2 mM $CoCl_2$, 2 mM tpy and 2mM bpy (brown). Bulk electrolyses were performed in 10 mL of DMF/H_2O (95:5, v:v), with 0.1M TBAP, using a 1.5 cm diameter pool of mercury as the working electrode. See Section 5.2 of Chapter III.[‡]

2.2. Chapter IV - CO_2 reduction selectivity over H^+ reduction by Co-tpy

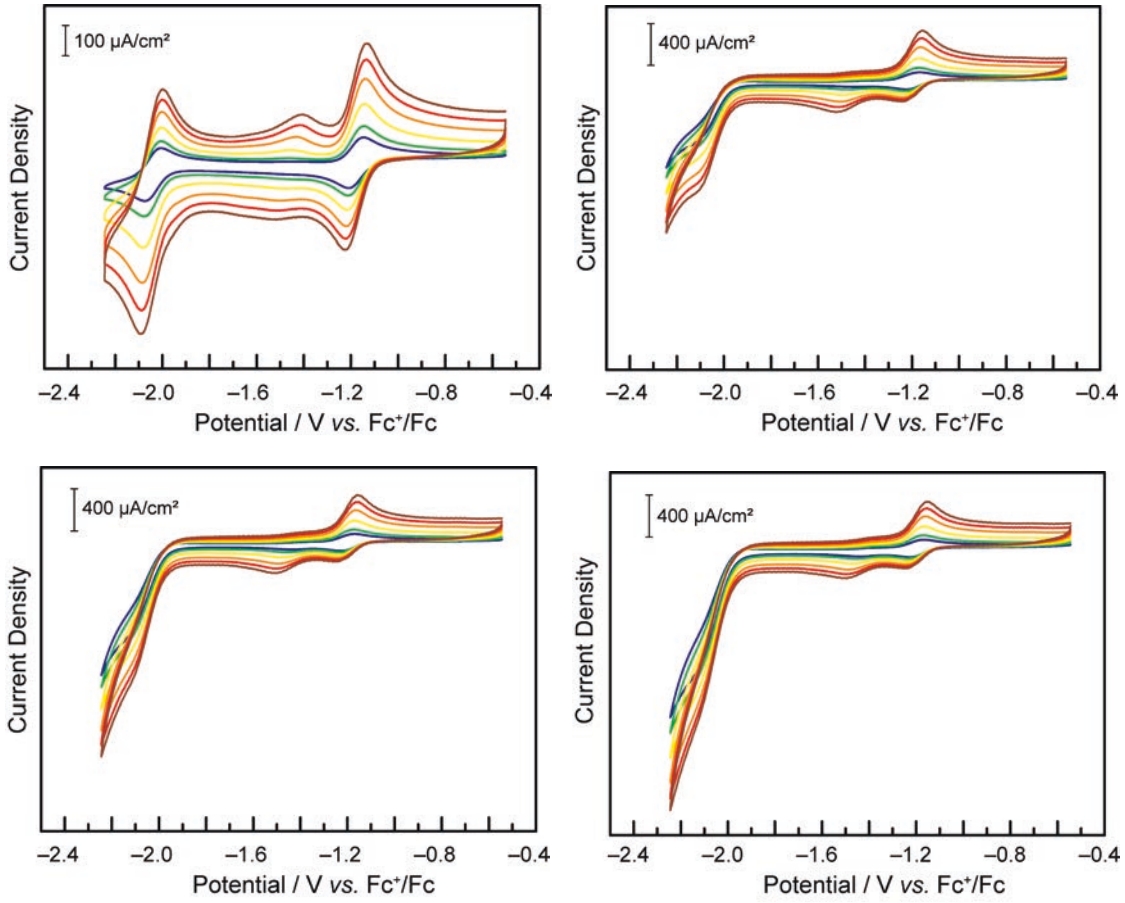

Figure VI-5 Cyclic voltammograms under Ar of a 1 mM solution of compound **3** in DMF, $TBAPF_6$ 0.1M, on a glassy carbon electrode without (top left) and with 20 mM (top right), 40 mM (bottom left) and 60 mM (bottom right) acetic acid at a scan rate of 50 (— blue), 100 (— green), 250 (— yellow), 500 (— orange), 750 (— red) and 1000 (— brown) mV/s. See Section 2.5.2 of Chapter IV.[§]

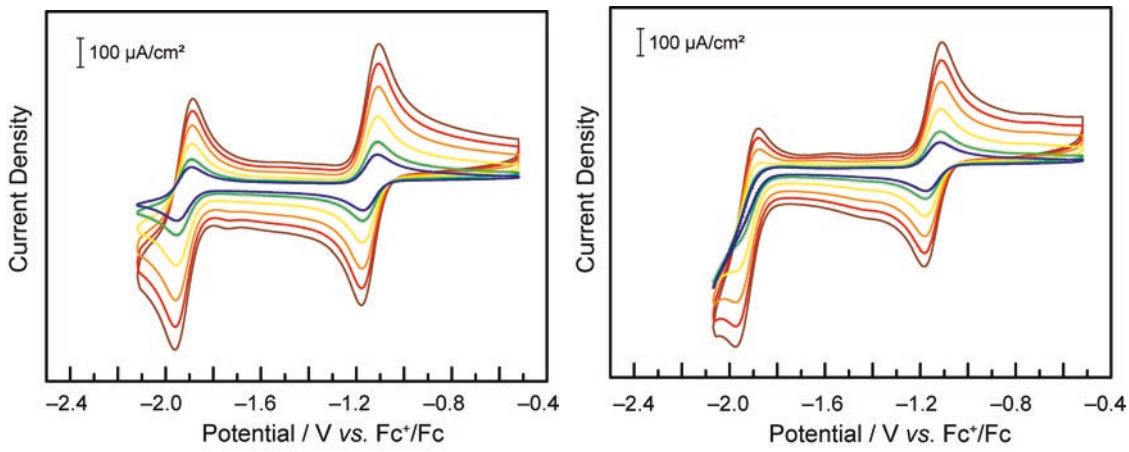

Figure VI-6 Cyclic voltammograms under Ar of 1 mM solutions of **1** in DMF, $TBAPF_6$ 0.1M, on a glassy carbon electrode without (left) and with (right) 60 mM acetic acid at a scan rate of 50(— blue), 100 (— green), 250 (— yellow), 500 (— orange), 750 (— red) and 1000 (— brown) mV/s. See Section 2.5.2 of Chapter IV.[§]

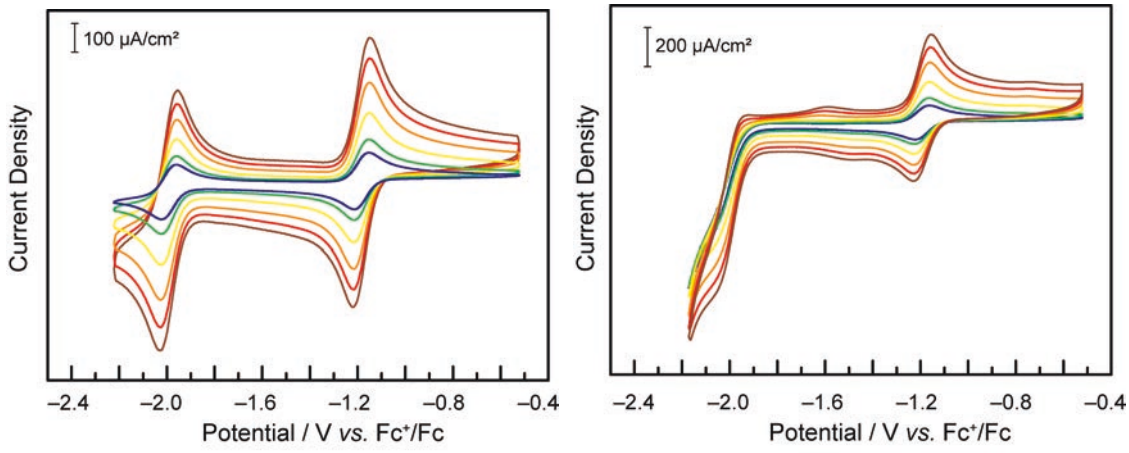

Figure VI-7 Cyclic voltammograms under Ar of 1 mM solutions of **2** in DMF, $TBAPF_6$ 0.1M, on a glassy carbon electrode without (left) and with (right) 60 mM acetic acid at a scan rate of 50 (— blue), 100 (— green), 250 (— yellow), 500 (— orange), 750 (— red) and 1000 (— brown) mV/s. See Section 2.5.2 of Chapter IV.[§]

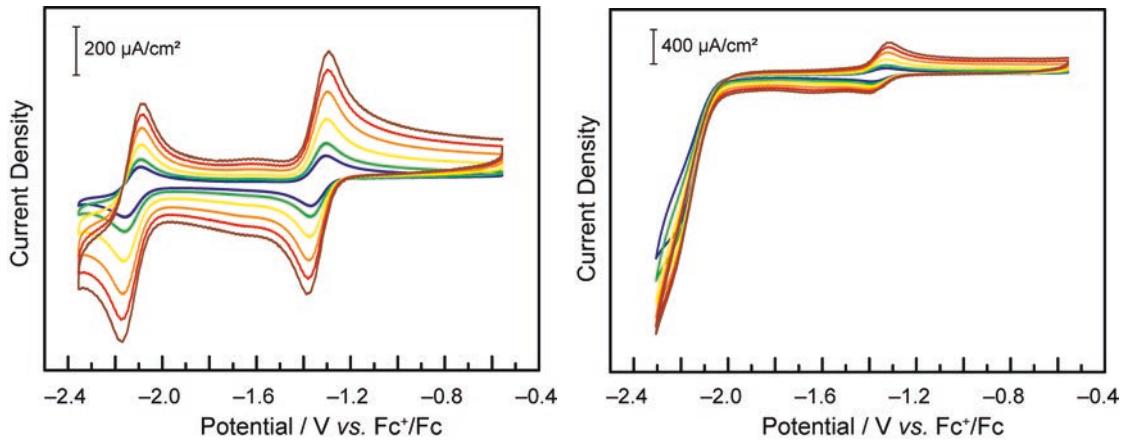

Figure VI-8 Cyclic voltammograms under Ar of 1 mM solutions of **4** in DMF, $TBAPF_6$ 0.1M, on a glassy carbon electrode without (left) and with (right) 60 mM acetic acid at a scan rate of 50 (— blue), 100 (— green), 250 (— yellow), 500 (— orange), 750 (— red) and 1000 (— brown) mV/s. See Section 2.5.2 of Chapter IV.[§]

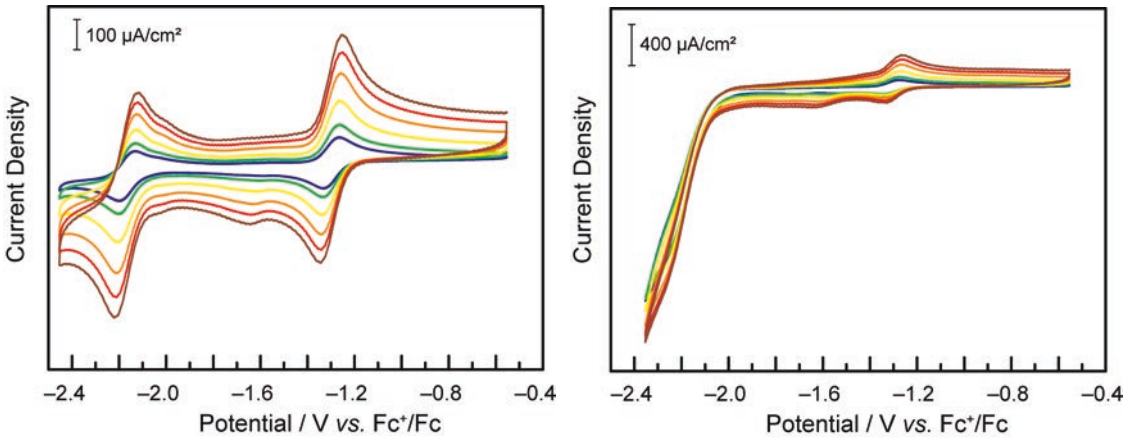

Figure VI-9 Cyclic voltammograms under Ar of 1 mM solutions of **5** in DMF, $TBAPF_6$ 0.1M, on a glassy carbon electrode without (left) and with (right) 60 mM acetic acid at a scan rate of 50 (— blue), 100 (— green), 250 (— yellow), 500 (— orange), 750 (— red) and 1000 (— brown) mV/s. See Section 2.5.2 of Chapter IV.[§]

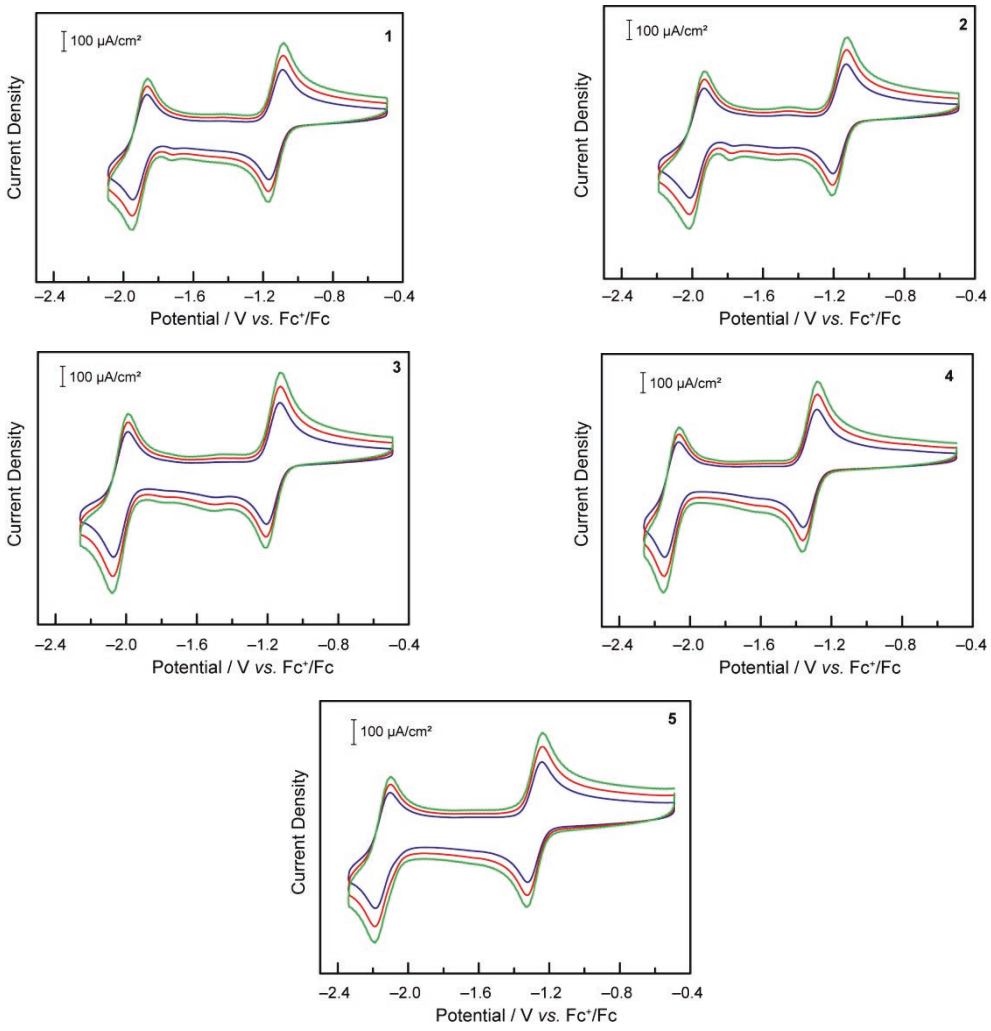

Figure VI-10 Cyclic voltammograms of 1 mM solutions of **1**, **2**, **3**, **4** and **5** in DMF/H_2O (95:5), $TBAPF_6$ 0.1M, on a glassy carbon electrode under Ar at a scan rate of 500 (— blue), 750 (— red) and 1000 (— green) mV/s. See Section 3.1.2 of Chapter IV.[§]

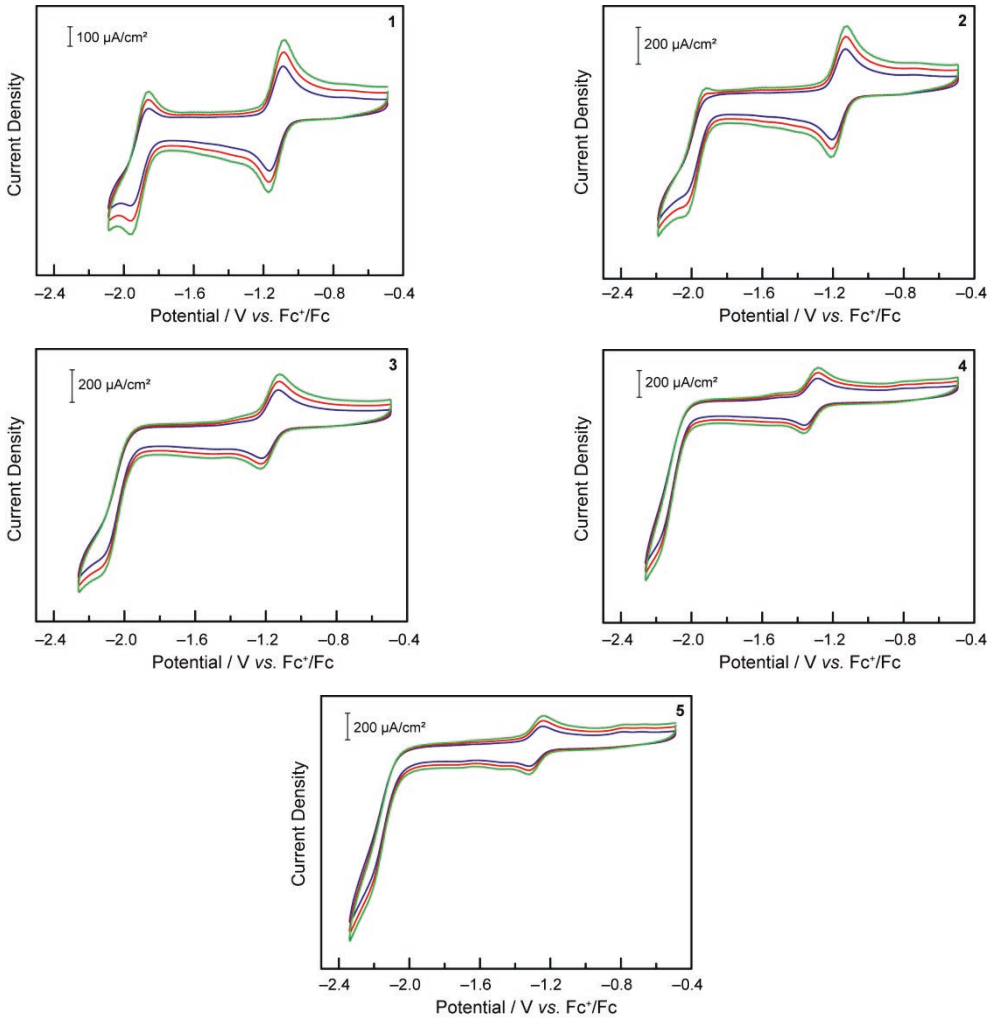

Figure VI-11 Cyclic voltammograms of 1 mM solutions of **1**, **2**, **3**, **4** and **5** in DMF/H_2O (95:5), $TBAPF_6$ 0.1M, on a glassy carbon electrode under CO_2 saturating conditions at a scan rate of 500 (— blue), 750 (— red) and 1000 (— green) mV/s. See Section 3.1.2 of Chapter IV.[§]

2.3. Electrode functionalisation with a terpyridine ligand: preparation, metallation and catalysis

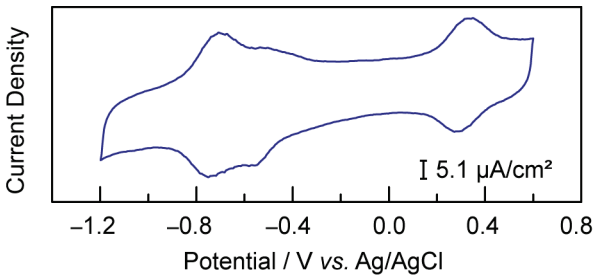

Figure VI-12 Cyclic voltammograms in MeCN solutions containing 0.1 M of $TBAPF_6$ as supporting electrolyte, under Ar, at 100 mV/s of an electropolymerised 1 mm diameter glassy carbon electrode metallated with cobalt (— blue line). See Section 2.2 of Chapter V.

2.4. References

‡ N. Elgrishi, M. B. Chambers, V. Artero and M. Fontecave, *Phys. Chem. Chem. Phys*, 2014, **16**, 13635–13644. Reproduced by permission of the PCCP Owner Societies.

§ N. Elgrishi, M. B. Chambers and M. Fontecave, *Chem. Sci.*, 2015, DOI: 10.1039/C4SC03766A. Reproduced by permission of the Royal Society of Chemistry.

Short summary in English

In an effort to work towards the development of cost-effective catalytic systems capable of storing sunlight energy in the form of chemical bonds using CO_2 and water as substrates, homoleptic terpyridine complexes of first row transition metals were evaluated as catalysts for the electrocatalytic reduction of CO_2. Ni and Co-based catalytic systems were shown to reduce CO_2 to CO under the conditions tested. The Ni complex was found to exhibit selectivity for CO_2 over proton reduction while the Co-system generated mixtures of CO and H_2 with CO:H_2 ratios being tuneable through variations of the applied overpotential.

To investigate the parameters governing the competition for H^+ reduction versus CO_2 reduction, the cobalt *bis*terpyridine class of compounds was then evaluated as H^+ reduction catalysts. Tuning the electronic of the ancillary ligand sphere resulted in a wide range of second-order rate constants for H^+ reduction. When this class of compounds was next submitted to CO_2 reduction conditions the less active catalysts for H^+ reduction were the more selective towards CO_2 reduction to CO. This represented the first report of the selectivity of a molecular system for CO_2 reduction being controlled through turning off one of the competing reactions.

Finally a strategy was proposed for immobilisation of homogeneous catalysts whereby a glassy carbon electrode is functionalised first by electro-grafting of the terpyridine ligand. The modified electrode can easily be metallated with cobalt and showed activity towards catalytic proton and CO_2 reduction. The metal can be removed and the electrode re-metallated at will.

Résumé court en Français

En vue de travailler à l'élaboration de systèmes catalytiques à faibles coût capables de stocker l'énergie solaire sous forme de liaisons chimiques avec du CO_2 et de l'eau comme substrats, des complexes homoleptiques de terpyridine de Mn, Fe, Co, Ni et Cu ont été évaluées en tant que catalyseurs pour la réduction électrocatalytique du CO_2. Les systèmes à base de cobalt et de nickel sont capables de réduire le CO_2 en CO de façon catalytique dans les conditions testées. Le complexe de Ni réduit sélectivement le CO_2 alors que le système de Co génère des mélanges de CO et H_2 ; les ratios CO:H_2 étant contrôlables en faisant varier la surtension appliquée au système.

Pour étudier les paramètres gouvernant la compétition entre la réduction de H^+ et de CO_2, des complexes de cobalt-terpyridine ont ensuite été évalués comme catalyseurs de la réduction de H^+. En modifiant les propriétés électroniques du ligand terpyridine par l'ajout de substituants electro-donneurs ou attracteurs, un large éventail de constantes de vitesse de second ordre pour la réduction de H^+ a été obtenu. Lorsque cette classe de composés a ensuite été soumise à des conditions de réduction de CO_2, les catalyseurs les moins actifs en réduction de H^+ étaient les plus sélectifs en réduction de CO_2.

Enfin, une stratégie a été proposée pour l'immobilisation de catalyseurs homogènes où une électrode de carbone vitreux est d'abord fonctionnalisée par électro-greffage du ligand terpyridine. L'électrode modifiée peut facilement être métallée par la suite avec du cobalt, et a montré une activité catalytique pour la réduction de protons et de CO_2. Le métal peut être retiré et l'électrode de nouveau métallée à volonté.

Résumé

–

Réduction électrochimique du CO_2 en carburants catalysée par des complexes polypyridines moléculaires de métaux abondants

1. Introduction

L'accès à des sources d'énergies propres, abondantes et sécurisées constitue un pivot central de nos sociétés. La sécurité énergétique a conduit à de nombreux conflits mondiaux et crashs boursiers, et son influence prévaut toujours comme en témoigne la sortie de crise économique des États-Unis s'appuyant sur le développement de l'exploitation des gaz de schistes, à mettre en perspective avec la santé économique chancelante des autres pays développés.

Dans le même temps, les signaux concernant le climat sont au rouge, avec un niveau de CO_2 dans l'atmosphère au plus haut (400 ppm) qui contribue non seulement à l'acidification des océans mais aussi à entretenir l'effet de serre, induisant des changements climatiques.[1]

La nature, pourtant, utilise une partie de ce CO_2, qui est à la base du vivant. Tout le carbone dont nous dépendons pour nous nourrir, nous chauffer ou nous habiller provient du vivant, capté dans l'atmosphère et incorporé par les cellules des organismes photosynthétiques lors de la synthèse de sucres durant le cycle de Calvin. Pour alimenter la machinerie cellulaire et produire son carburant, le vivant utilise l'énergie des photons du soleil qu'elle stocke provisoirement sous la forme d'oxygène, de NADPH, et d'ATP comme décrit dans la Figure R-1.

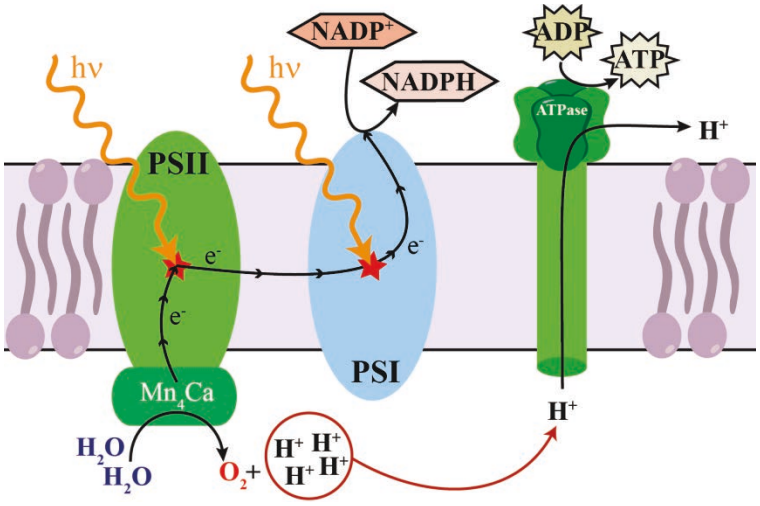

Figure R-1 Représentation schématique des premières étapes de la photosynthèse.[I]

S'inspirant de la nature, les panneaux solaires, qui fleurissent sur les toits des bâtiments un peu partout, permettent de capter l'énergie solaire et de la convertir en électricité, mais le stockage de ce flux d'électrons demeure problématique. Une des stratégies prometteuses consiste à stocker cette énergie dans des liaisons chimiques, denses en énergie, pour créer des « carburants solaires ».

L'utilisation du CO_2 comme substrat pour cette réduction permettrait de créer des carburants carbonés, à haute densité énergétique et volumique, compatibles avec les technologies actuelles, tout en réduisant l'augmentation de la concentration de CO_2 dans l'atmosphère.

En raison de la complexité des transformations à mettre en jeu pour réduire la molécule linéaire de CO_2, le développement de catalyseurs est nécessaire pour faciliter les réactions multiélectroniques impliquées. L'étude de catalyseurs moléculaires constitue le cœur de l'expertise du Laboratoire de Chimie des Processus Biologiques; Nous avons donc choisi comme approche pour cette étude le développement de catalyseurs moléculaires suivi par leur immobilisation sur électrode. A terme, une cellule photo-électrochimique du type de celle décrite dans la Figure R-2 peut être envisagée. Elle serait composée d'une photocathode utilisant l'énergie du soleil pour oxyder l'eau en dioxygène et protons, ces derniers migrants aux travers d'une membrane pour atteindre la cathode (ou photocathode) où ils réagissent avec le CO_2 et des électrons pour produire des carburants.

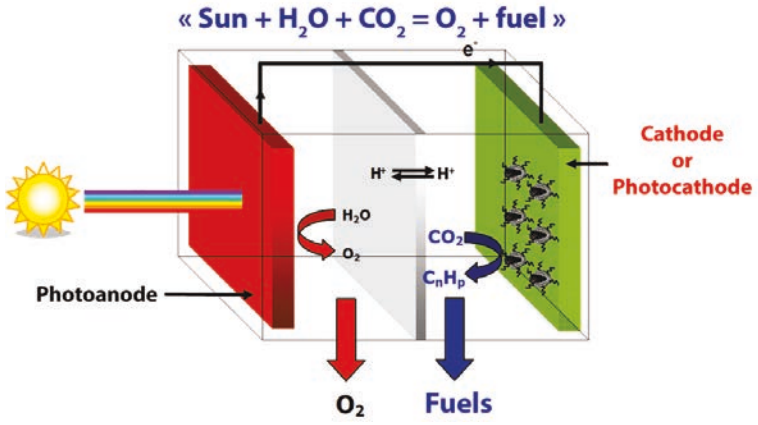

Figure R-2 Représentation schématique de la cellule photo-électrochimique envisagée.

Dans le but de maitriser les coûts, les catalyseurs étudiés dans les travaux présentés dans ce document sont constitués d'une combinaison de métaux abondants et peu onéreux coordinés par des ligands d'une grande simplicité : les polypyridines. Plusieurs classes de catalyseurs de la réduction de CO_2 à base de polypyridines ont déjà été mises en évidence par d'autres groupes, les plus efficaces et emblématiques à base de rhénium, ruthénium, iridium et rhodium. Une exception marquée est l'emploi de catalyseurs au manganèse dérivés de l'architecture $[Mn(bpy)(CO)_3]^+$ (bpy = 2,2'-bipyridine) dont l'activité en réduction de CO_2 a été mise en évidence pour la première fois en 2011 par A. Deronzier et collaborateurs.[2,3,4] Les produits de réduction de CO_2 les plus fréquemment observés sont le monoxyde

de carbone CO et le formiate $HCOO^-$, et sont généralement accompagnés de la formation d'hydrogène (H_2).

Dans les années 90, l'équipe de H. Abruña à Cornell a mis en évidence l'activité catalytique en réduction électrochimique de CO_2 par des catalyseurs à base de ligands terpyridines (tpy) de nickel, cobalt, et fer en solution dans le DMF, dans le cadre d'une comparaison avec ces mêmes catalyseurs polymérisés à la surface d'électrodes de platine.[5,6] Ces études préliminaires semblent indiquer que ces trois composés catalysent la réduction électrochimique du CO_2 en formiate, CO ou formaldéhyde.

Nous avons jugé prometteur le potentiel de ces catalyseurs, et nous les avons donc sélectionnés en vue de réaliser une étude plus poussée de leur activité en électro-réduction catalytique du CO_2. Nous avons visé vérifier et compléter les observations précédentes, puis à les poursuivre en étudiant la sélectivité de ces catalyseurs, ainsi que l'effet de leur immobilisation sur électrodes de carbone.

2. Évaluation de l'activité catalytique de complexes terpyridines de métaux de la première ligne de transition en réduction électrochimique du CO_2

2.1. Étude en voltammétrie cyclique[7]

Pour évaluer l'activité des complexes **M-tpy** en tant que catalyseurs de la réduction électrochimique du CO_2, les différents complexes présentés dans la Figure R-3 ont tout d'abord été étudiés par voltammétrie cyclique dans le DMF.

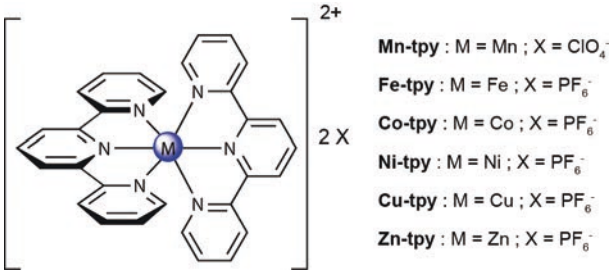

Figure R-3 Représentation schématique de la structure des composés **M-tpy** étudiés.†

Pour comprendre le caractère non innocent du ligand terpyridine, le complexe de zinc a été étudié en premier. Sous une atmosphère inerte, le complexe $[Zn(tpy)_2]^{2+}$ présente deux signaux électrochimiques dans la fenêtre de potentiel étudiée (Figure R-4). L'atome de zinc Zn^{II} n'est pas susceptible d'être réduit dans les conditions de l'expérience, et les signaux électrochimiques observés peuvent donc être attribués au ligand terpyridine.

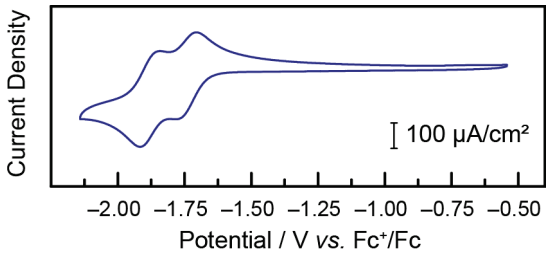

Figure R-4 Voltammogramme représentatif du comportement d'une solution de 1 mM de **Zn-tpy** dans un mélange DMF/H_2O (90:10, v:v) sous argon à 100 mV/s (seul le scan n°3 est représenté).†

Dans le cas du cobalt, trois signaux électrochimiques réversibles sont observés sous argon (courbe bleue Figure R-5, gauche). Ces signaux sont attribués aux couples $Co^{III/II}$ pour le signal III et $Co^{II/I}$ pour le signal II. Le signal noté I dans la Figure R-5 est attribué à une réduction centrée sur le ligand terpyridine. Sous une atmosphère de CO_2, le signal noté I devient irréversible, et une

augmentation du courant cathodique est observée, ce qui indique potentiellement une activité catalytique en réduction (Figure R-5, courbe rouge).

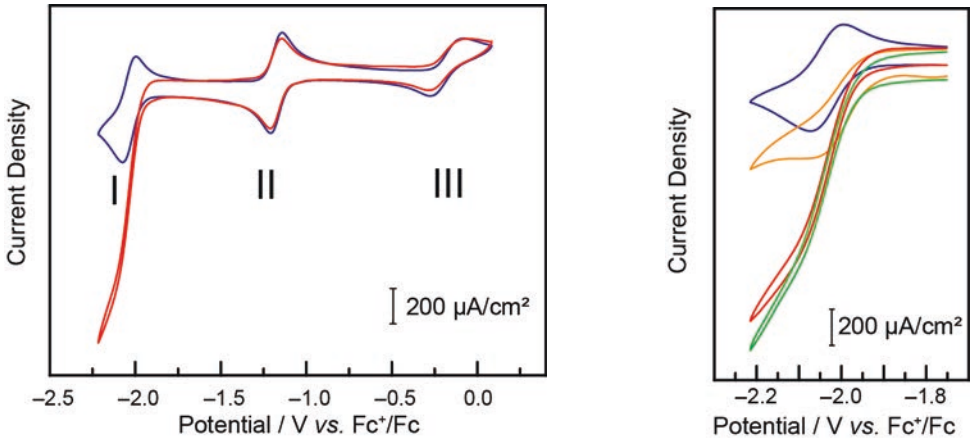

Figure R-5 Gauche : voltammogrammes représentatifs du comportement d'une solution de 2 mM de **Co-tpy** sous une atmosphère d'argon (bleu) et de CO_2 (rouge) à 100 mV/s dans DMF/H_2O (95:5, v:v) en présence de 0,1 M TBAP.[†] Droite : région de la vague notée "I" du voltammogramme précédent à 100 mV/s sous argon (bleu) et sous CO_2 (rouge) dans les conditions précédentes, ainsi que dans le DMF anhydre (orange) et dans un mélange DMF/H_2O (90:10, v:v) (vert).

L'influence de la présence d'une source de protons a été étudiée en comparant les intensités obtenues sous CO_2 dans une solution de **Co-tpy** dans le DMF contenant des pourcentages variables d'eau (0%, 5% et 10% en volume). Il apparaît que la présence d'eau exalte la vague de réduction, mais la différence entre l'ajout de 5% ou 10% est beaucoup moins importante que celle entre le DMF anhydre et le DMF contenant 5% d'eau. Il a donc été décidé dans la suite de cette étude de se limiter à un ajout de 5% d'eau en routine comme source de protons.

Le cas de **Ni-tpy** a également été étudié. Sous une atmosphère d'argon (signal bleu, Figure R-6), deux signaux électrochimiques réversibles sont observables. Par analogie avec les observations faites sur le complexe de zinc, et contrairement à ce qui avait été décrit précédemment,[5] ces deux vagues sont attribuées à des réductions localisées sur les ligands tpy, le centre métallique restant Ni^{II}.

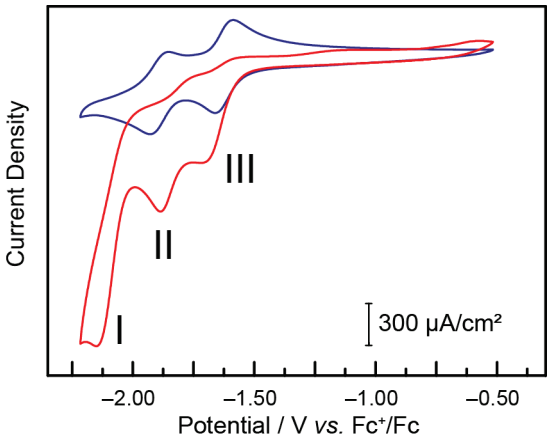

Figure R-6 Voltammogramme représentatif du comportement d'une solution de 2 mM de **Ni-tpy** sous une atmosphère d'argon (bleu) et de CO_2 (rouge) à 100 mV/s.[†]

En présence de CO_2, les deux vagues deviennent irréversibles et là encore une activité potentielle de catalyse de la réduction électrochimique du CO_2 est observée. Le comportement est plus complexe que dans le cas du cobalt cependant, avec le déplacement à des potentiels légèrement plus positifs du pic II et l'apparition du pic I.

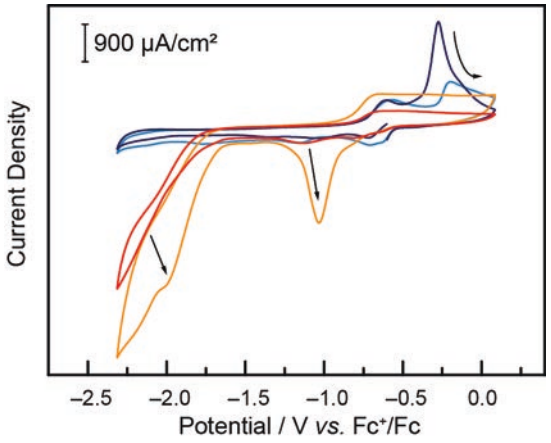

Figure R-7 Voltammogramme représentatif du comportement d'une solution de 2 mM de **Cu-tpy** sous une atmosphère d'argon (bleu clair : 1er scan; bleu foncé : scan n°38) et de CO_2 (rouge : 1er scan; orange : scan n°38) à 100 mV/s.[†]

Les complexes à base de cuivre (Figure R-7), de fer et de manganèse ont également été évalués pour leur activité potentielle comme catalyseurs de la réduction électrochimique du CO_2. Aucune activité n'a été observée par voltammétrie cyclique dans le cas de **Fe-tpy** et de **Mn-tpy** dans les conditions testées. Dans le cas du cuivre, un comportement complexe est observé, avec un dépôt apparent d'une espèce électro-active pour la réduction du CO_2 sur l'électrode en présence de CO_2.

Notre étude se focalisant sur des catalyseurs homogènes de la réduction du CO_2, nous n'avons pas poursuivi cette voie dans le cadre de ces travaux.

2.2. Étude en électrolyse à potentiel contrôlé

Pour confirmer les activités catalytiques observées en voltammétrie cyclique de **Co-tpy** et **Ni-tpy** sous CO_2, des électrolyses à potentiel contrôlé ont été réalisées pour observer la stabilité des systèmes au court du temps, grâce à l'évolution du courant, et pour détecter et mesurer les produits de la réaction.

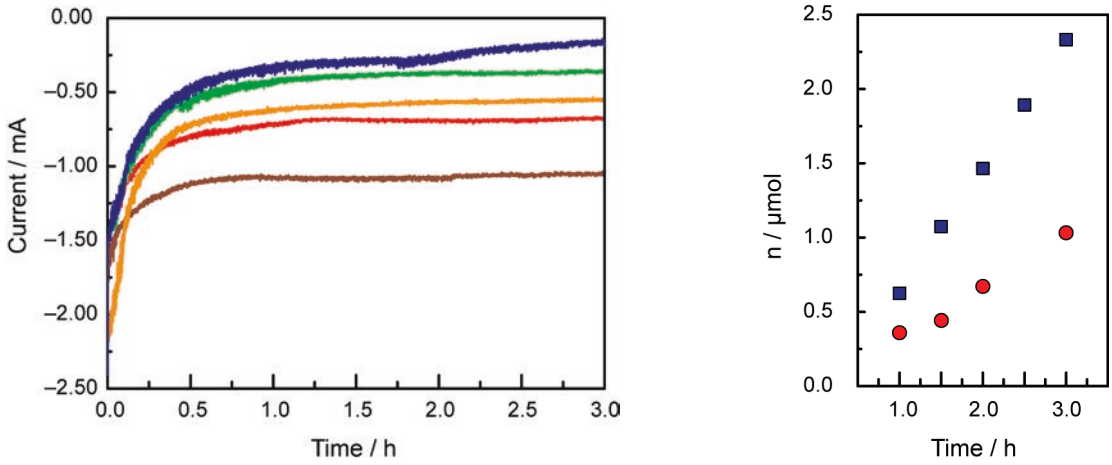

Figure R-8 Gauche : courant mesuré lors de l'électrolyse à potentiel contrôlé d'une solution de 2 mM de **Co-tpy** sous une atmosphère de CO_2 à des potentiels variables (bleu : –1,93 V, vert : –2,03 V, orange : –2,08 V, rouge : –2,13 V et marron : –2,23 V *vs.* Fc^+/Fc). Les électrolyses ont été réalisées dans 10 mL de DMF/H_2O (95:5, v:v) en présence de 0,1 M TBAP. Droite : nombre de moles total de H_2 (cercles rouges) et de CO (carrés bleus) mesurés dans la phase gazeuse lors de l'électrolyse à –2,03 V *vs.* Fc^+/Fc sous CO_2.[†]

Dans le cas de **Co-tpy**, un courant stable est observé en électrolyse, après une phase initiale où les centres Co^{II} sont réduits en Co^{I} (Figure R-8, gauche). Une fois le courant stabilisé, la production de CO est constante au cours du temps et est accompagnée d'une production continue d'hydrogène (Figure R-8, droite). La sélectivité entre la production de CO et de H_2 est contrôlable en ajustant le potentiel appliqué pendant l'électrolyse, ce qui permet d'obtenir des ratios de CO et H_2 aux proportions définies (Figure R-9). Ce résultat est prometteur dans le contexte du procédé Fischer-Tropsch qui est aujourd'hui utilisé industriellement pour la synthèse d'hydrocarbures comme le méthanol en combinant des ratios CO:H_2 déterminés.

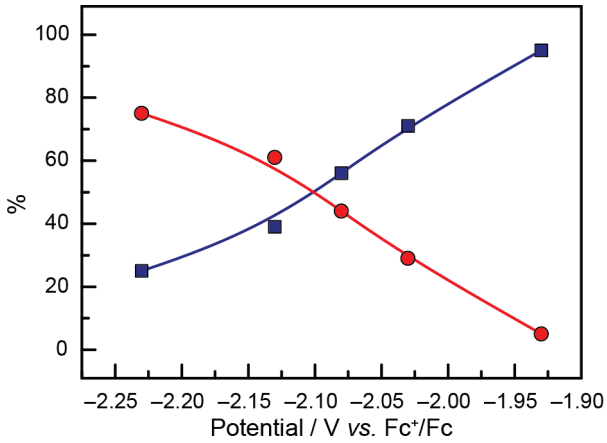

Figure R-9 Évolution des proportions de CO (carrés bleus) et de H_2 (cercles rouges) parmi les produits de réduction du CO_2 observés lors d'électrolyses à potentiel contrôlé de **Co-tpy** sous CO_2 en fonction du potentiel appliqué.[†]

Une étude similaire réalisée sur les complexes à base de nickel a confirmé l'activité de **Ni-tpy** comme catalyseur de la réduction électrochimique du CO_2, produisant sélectivement du monoxyde de carbone. En sélectionnant le potentiel appliqué, la vitesse de la réaction est modifiée mais CO reste l'unique produit observé. Il est à noter que le courant observé en électrolyse diminue (en valeur absolue) au cours du temps, contrairement à ce qui était observé dans le cas de **Co-tpy**, ce qui indique que le système à base de nickel est moins stable que le complexe de cobalt dans les conditions catalytiques testées (Figure R-10).

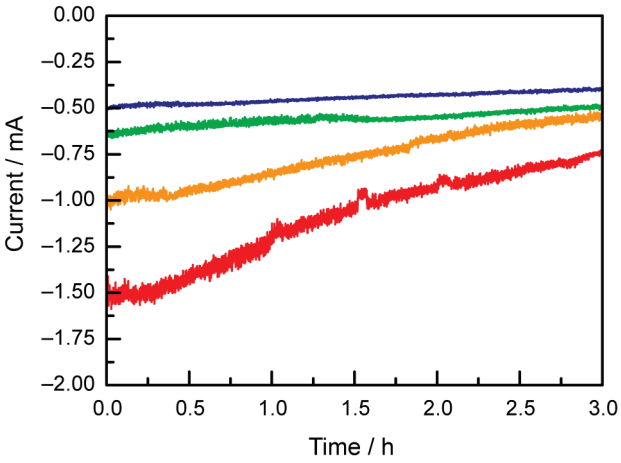

Figure R-10 Courant mesuré lors de l'électrolyse à potentiel contrôlé d'une solution de 2 mM de **Ni-tpy** sous une atmosphère de CO_2, à différents potentiels (bleu : –1,72 V, vert : –1,76 V, orange : –1,89 V et rouge : –2,14 V). Les électrolyses ont été réalisées dans 10 mL de DMF/H_2O (95:5, v:v) en présence de 0,1 M TBAP.[†]

Comparer l'activité catalytique de deux complexes opérants à des potentiels différents n'est pas aisé. Néanmoins, si l'on compare les quantités de CO produites par **Ni-tpy** à –1,72 V à celles produites par **Co-tpy** à –1,93 V, soit 210 mV plus négatif, il apparait que, même dans ces conditions,

le catalyseur à base de nickel produit plus de CO que celui à base de cobalt (Figure R-11). Cependant comme mentionné précédemment, le système à base de cobalt est beaucoup plus stable que le système à base de nickel. D'autre part, pour les deux complexes étudiés, les rendements faradiques, correspondant au ratio entre le nombre d'électrons utilisés de façon productive pour la formation de produit divisé par le nombre total d'électrons injectés dans le système demeurent loin des 100%.

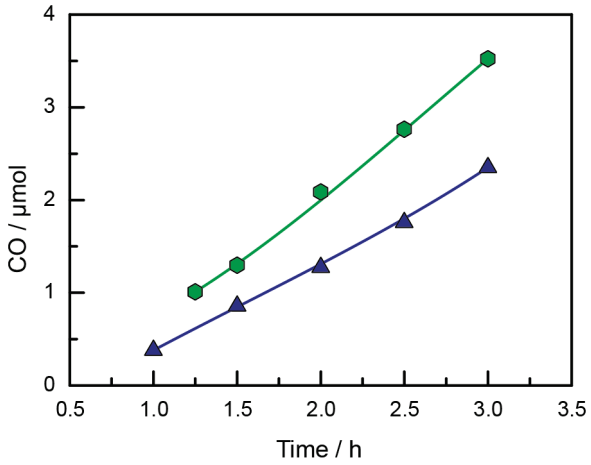

Figure R-11 Comparaison du nombre de moles de CO produit par **Ni-tpy** (hexagones verts) et par **Co-tpy** (triangles bleus) pendant une électrolyse à potentiel contrôlé de 3 h au potentiel de –1,72 V pour **Ni-tpy** et –1,93V pour **Co-tpy**.[†]

2.3. Étude de Co-tpy et proposition de mécanisme

Compte tenu de la plus grande stabilité du système à base de cobalt, ce système a été choisi dans les études suivantes pour déterminer le mécanisme de la réaction ainsi que pour l'exploration des raisons de la faiblesse des rendements faradiques.

Plusieurs voies ont été explorées pour tenter de comprendre l'origine des faibles rendements faradiques observés. Après avoir vérifié que ni la nature du solvant ni celle de l'électrolyte n'étaient en cause, pas plus que d'éventuelles contaminations de l'atmosphère de la cellule d'électrolyse par des traces de dioxygène, la réactivité du ligand a été étudiée. Après une étude photochimique et électrochimique, il est apparu qu'une des sources plausibles des faibles rendements faradiques observés est la possible N-carboxylation de ligands terpyridines libres.[8]

Tirant parti de la simplicité de synthèse des complexes **Co-tpy**, des expériences ont été réalisées en mélangeant différentes proportions de sel de cobalt $CoCl_2$ et de ligand terpyridine. L'électrolyse de ces solutions au potentiel auquel $[Co(tpy)_2]^{2+}$ catalyse la réduction de CO_2 en CO

permet de suivre l'évolution du courant et de la quantité de CO produite par ces mélanges. Il apparait que les rendements faradiques les plus élevés sont obtenus avec les mélanges dont les ratios Co:tpy sont proches ou supérieurs à 1. Ces résultats suggèrent que l'espèce catalytique active est constituée de moins de deux tpy par centre métallique, en accord avec l'hypothèse d'une perte de ligand tpy pour générer le catalyseur.

Sur la base de cette étude, et sachant par ailleurs qu'un ordre apparent de 0,5 par rapport au cobalt est observé lors d'électrolyses à potentiel et concentration de $[Co(tpy)_2]^{2+}$ variables, un mécanisme a été proposé pour la catalyse de la réduction électrochimique de CO_2 en CO par les complexe $[Co(tpy)_2]^{2+}$ (Figure R-12).

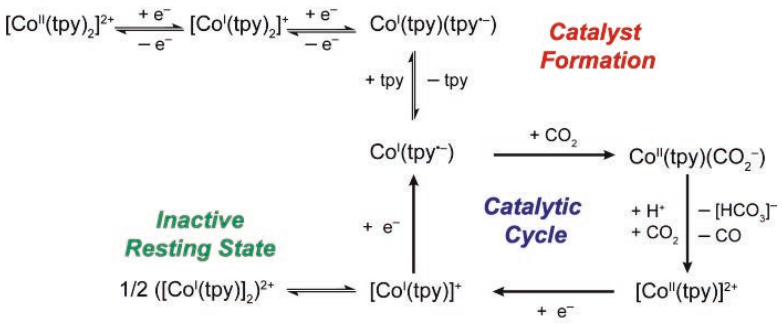

Figure R-12 Proposition de mécanisme pour la catalyse de réduction du CO_2 en CO par **Co-tpy**.[†]

Partant du complexe pré-synthétisé $[Co^{II}(tpy)_2]^{2+}$, deux réductions mono-électroniques génèrent $Co^{I}(tpy)(tpy^{\bullet-})$ qui, après perte d'un ligand tpy neutre, donne le catalyseur $Co^{I}(tpy^{\bullet-})$. Cette espèce réagit avec le CO_2 pour former CO et $[Co^{II}(tpy)]^{2+}$ qui, après deux réductions mono-électroniques, régénère l'espèce $Co^{I}(tpy^{\bullet-})$. D'autre part, la formation d'un dimère inactif est proposée pour expliquer l'ordre apparent en Co en conditions d'électrolyse.

2.4. Conclusions

L'activité catalytique des complexes **Co-tpy** et **Ni-tpy** pour la réduction électrochimique du CO_2 a été confirmée, et CO est l'unique produit carboné formé. **Ni-tpy** est sélectif pour la production de CO, alors que **Co-tpy** produit des mélanges de CO et de H_2. Le système **Co-tpy** présente une stabilité intéressante, et son étude mérite d'être approfondie, notamment en étudiant la catalyse de réduction des protons en H_2 pour comprendre d'avantage les critères influençant la sélectivité.

3. Étude de la sélectivité de dérivés de Co-tpy vis-à-vis de la réduction de CO_2 et de H^+

3.1. Étude de la catalyse de réduction de H^+ par des dérivés de Co-tpy

Pour étudier l'influence des propriétés électroniques du ligand tpy sur les signaux électrochimiques des dérivés **Co-tpy**, cinq composés ont été synthétisés comme représenté Figure R-13. Les différents substituants permettent d'étudier l'influence des propriétés électroniques des substituants placés en para des azotes centraux, mais également les effets stériques grâce au complexe **5** présentant trois groupements ^{t}Bu électro-donneurs en para des azotes du ligand terpyridine. La synthèse des complexes s'effectue selon des procédés de la littérature. [9,10,11]

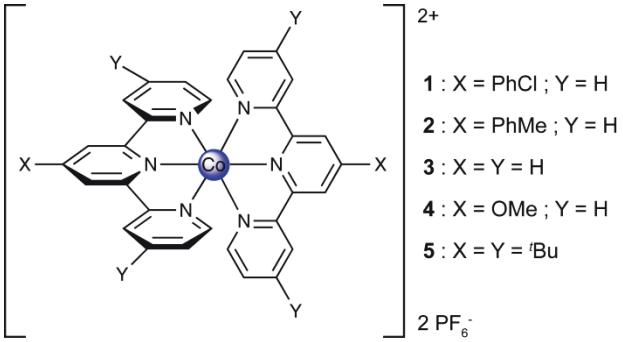

Figure R-13 Structure des cinq catalyseurs à base de cobalt étudiés.‡

Sous atmosphère inerte, les cinq composés présentent les voltammogrames rapportés Figure R-14 dans le DMF anhydre à 50 mV/s. Dans la gamme de potentiels étudiés, deux vagues sont observables, l'une correspondant au couple $Co^{II/I}$ et une autre vague de réduction centrée sur le ligand. Le potentiel de la vague de réduction du ligand varie en fonction des propriétés électroniques des substituants du ligand tpy, sur une gamme de ~250 mV (Figure R-14).

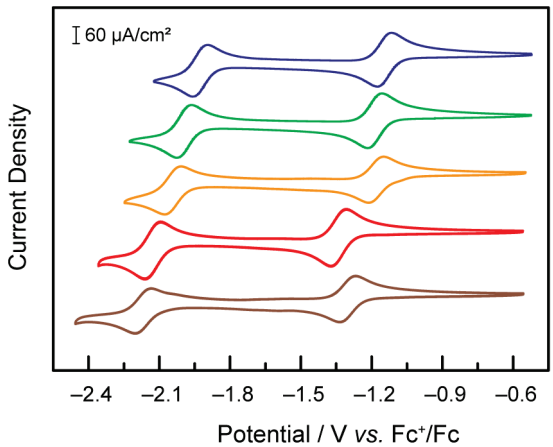

Figure R-14 Voltammogrammes de solutions de 1 mM des composés **1** (— bleu), **2** (— vert), **3** (— orange), **4** (— rouge) et **5** (— marron) sous une atmosphère d'argon à 50 mV/s dans le DMF, $TBAPF_6$ 0,1 M, sur électrode de carbone vitreux.‡

Pour pouvoir étudier la production de H_2 par ces catalyseurs indépendamment de la réduction de CO_2 et des réactions parasites, les complexes **1-5** ont été étudiés par voltammétrie cyclique dans le DMF anhydre, sous atmosphère inerte, en présence de quantités variables d'acide acétique (Figure R-15). Dans les cinq cas, la vague de réduction du ligand devient irréversible et l'intensité du courant cathodique augmente à mesure de l'ajout d'acide acétique. Plus les ligands tpy portent des substituants électroattracteurs, plus l'augmentation de courant cathodique est faible. D'autre part, plus les substituants sont donneurs, plus le potentiel à appliquer est négatif, correspondant à une augmentation de la surtension.

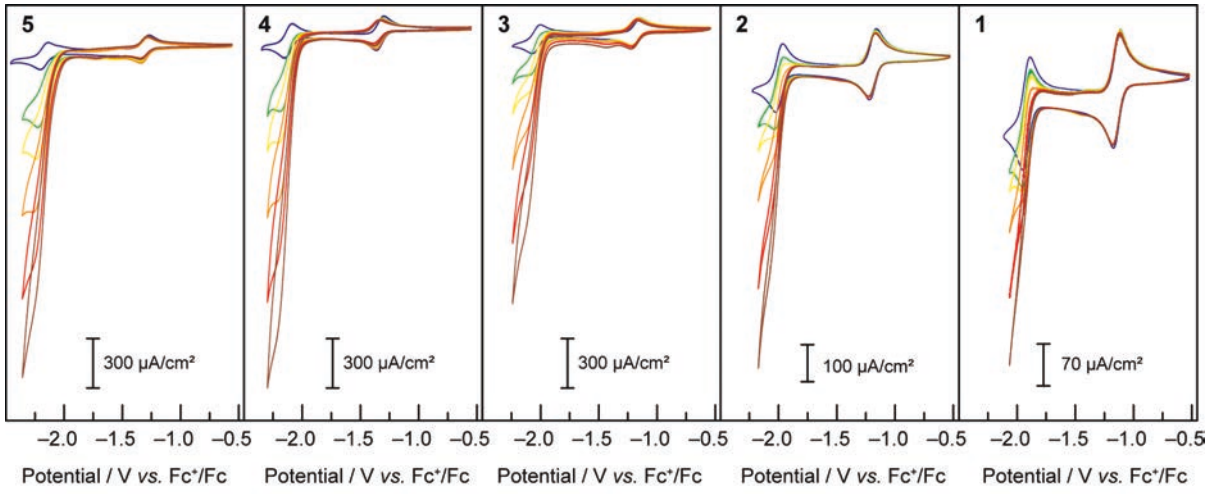

Figure R-15 Voltammogrammes de solutions de 1 mM des composés **1-5** sous une atmosphère d'argon à 50 mV/s dans le DMF, $TBAPF_6$ 0.1 M, sur électrode de carbone vitreux en présence de 0 (— bleu), 5 (— vert), 10 (— jaune), 20 (— orange), 40 (— rouge) et 60 (— marron) mM d'acide acétique.[‡]

Ces augmentations de courant cathodique ont été confirmées comme correspondant à de la réduction catalytique de H^+ en H_2 grâce à l'étude de **3** en électrolyse à potentiel contrôlé en présence d'acide acétique. Cette réaction produit H_2 de façon continue et stable sur au moins 3h avec un rendement faradique de plus de 80%.

3.1.1. Nature de l'espèce active: mono ou bis-terpyridine ?

Les complexes étudiés mis en solution sont de la forme $[M(tpy)_2]^{2+}$. Cependant, une décoordination partielle ou totale du ligand doit être envisagée pour permettre la coordination des substrats, ici H^+. Au vu des précédents dans la littérature de complexes de $[Co(tpy)_2]^{2+}$ capables de libérer un ligand tpy complet, c'est cette hypothèse qui a été retenue.

Pour pouvoir quantifier l'activité catalytique en réduction de protons par les cinq catalyseurs de terpyridine de cobalt, l'analyse du pied de vague en voltammétrie cyclique a été utilisée. Il est nécessaire pour cela de connaître le mécanisme de la réaction. Les deux mécanismes classiques qui ont été envisagés sont présentés dans la Figure R-16. Dans les deux cas l'étape limitant la vitesse est par hypothèse l'étape de formation de l'hydrure par réaction d'un centre noté Co^0 et un proton dont la constante de vitesse est notée k_1. On note que l'écriture Co^0 représente également la possibilité d'une entité $Co^{I}L^{\bullet -}$.

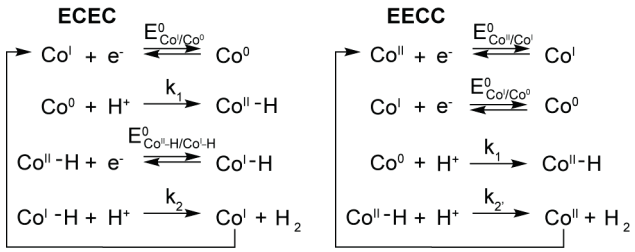

Figure R-16 Mécanismes ECEC et EECC considérés pour la production de H_2 par les complexes **1**-**5**.‡

En appliquant l'analyse du pied de vague développée par Savéant et coll.,[12] on obtient les constantes de vitesse pour les cinq complexes à chaque vitesse de balayage testée. On peut vérifier que les constantes ne varient pas avec la vitesse de scan, ni avec la concentration d'acide ajouté (Figure R-17).

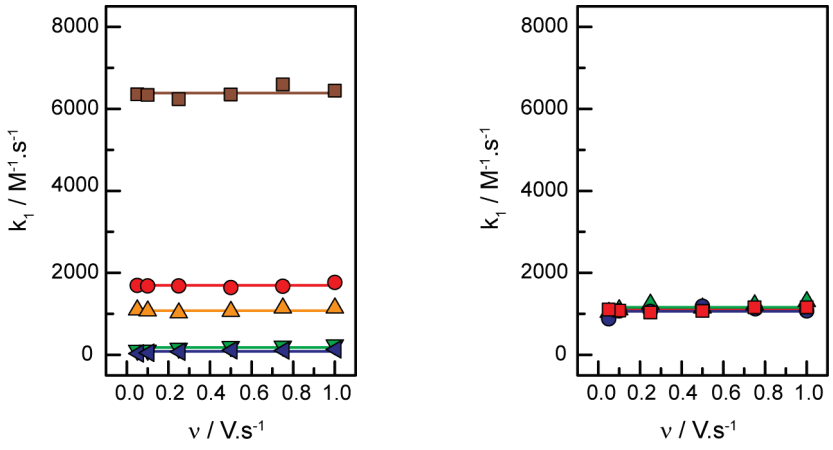

Figure R-17 Gauche : valeurs de k_1 obtenues par la méthode de l'analyse du pieds de vague pour les complexes **1** (— bleu), **2** (— vert), **3** (— orange), **4** (— rouge) et **5** (— marron) à différentes vitesses de balayage. Droite : valeurs de k_1 obtenues par la méthode de l'analyse du pieds de vague pour le complexe **3** en utilisant les données collectées en présence de 20 (— vert), 40 (— bleu) et 60 (— rouge) mM d'acide acétique à plusieurs vitesses de scan.‡

Après avoir vérifié que k_1 est effectivement l'étape déterminant la vitesse de la réaction, il est possible de tracer une « courbe catalytique de Tafel » représentée Figure R-18, qui rend compte de l'évolution de l'activité en fonction de la surtension appliquée.[13]

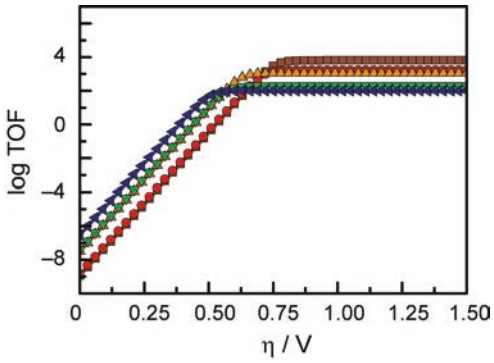

Figure R-18 Courbes catalytiques de Tafel pour une concentration de 1 M d'acide acétique pour les composés **1** (— bleu), **2** (— vert), **3** (— orange), **4** (— rouge) et **5** (— marron).‡

De façon surprenante, les catalyseurs de cobalt à base de terpyridines n'ont reçu que très peu d'attention comme catalyseurs de la réduction des protons au regard des travaux réalisés sur leurs cousins à base de bipyridines. En traçant une courbe catalytique de Tafel, un graphe reliant vitesse de la réaction et surtension nécessaire pour obtenir cette activité, la famille des catalyseurs cobalt-terpyridine apparait comme rivalisant avec les catalyseurs les plus étudiés pour la production de H_2 en termes d'activité maximale intrinsèque. La surtension qu'il est nécessaire de leur appliquer pour générer l'espèce catalytique active constitue néanmoins un frein. On remarque également facilement grâce à cette représentation les compromis qui doivent être faits entre diminution de la surtension et activité catalytique.

3.2. Influence de la structure électronique du ligand sur la compétition entre catalyse de la réduction de CO_2 et de H^+

Après avoir quantifié les activités catalytiques des cinq catalyseurs testés en réduction de H^+, nous avons déterminé que des groupements électroattracteurs permettent de diminuer l'activité catalytique en réduction de H^+. Ces cinq mêmes complexes ont ensuite été étudiés par voltammétrie cyclique comme catalyseurs de la réduction de CO_2. On remarque que les cinq catalyseurs testés présentent une augmentation du courant cathodique sous CO_2 tout comme cela avait été observé dans le cas de **3** (Figure R-19).

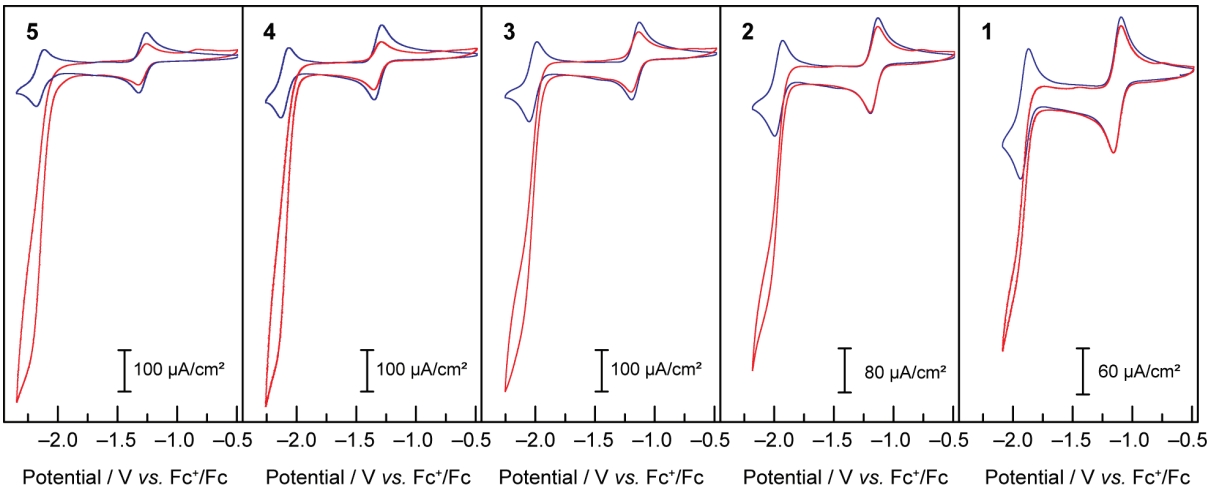

Figure R-19 Voltammogrammes de solutions de 1 mM des composés **1-5** sous une atmosphère d'argon (bleu) et de CO_2 (rouge) à 50 mV/s dans le DMF, $TBAPF_6$ 0.1 M, sur électrode de carbone vitreux.[‡]

Pour comparer l'activité et la sélectivité de la réduction de CO_2 par les complexes **1-5**, des électrolyses à courant imposé ont été réalisées dans un mélange DMF/H_2O (95:5, v :v) en présence de 0,1 M $TBAPF_6$ sur des solutions de 1 mM de catalyseurs, sous atmosphère de CO_2 (Figure R-20). Le fait d'imposer un courant, et donc la fréquence de la réaction, permet de laisser le potentiel évoluer librement et de pouvoir comparer les produits formés par les cinq complexes directement en termes de nombre de moles ou de rendement faradique.

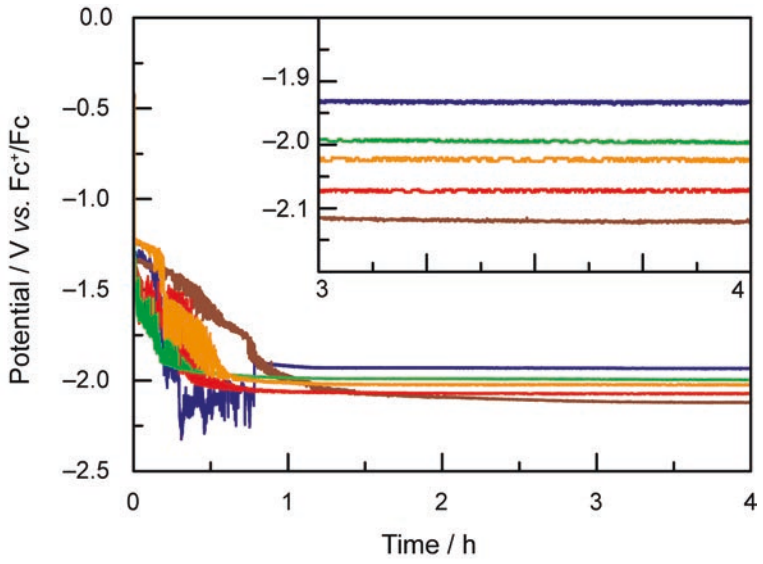

Figure R-20 Évolution du potentiel observées lors d'électrolyses des complexes **1** (— bleu), **2** (— vert), **3** (— orange), **4** (— rouge) et **5** (— marron) sous CO_2 avec un courant imposé de i = –300 µA.[‡]

Les 5 catalyseurs présentent un comportement similaire, avec un potentiel variable pendant la réduction du Co^{II} en Co^{I}, (0,77 C, 43 min) puis une stabilisation du potentiel pendant toute la durée de

l'expérience. Plus le ligand porte de groupements électro-donneurs, plus le potentiel d'équilibre est négatif. Les seuls produits détectés lors de ces expériences sont CO et H_2, produits de façon constante pendant la durée de l'électrolyse. Les rendements faradiques, en %, pour la production de CO et H_2 sont donnés dans la Figure R-21.

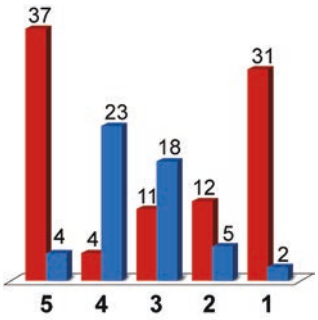

Figure R-21 Rendements faradiques (en %) pour CO (rouge) et H_2 (bleu) mesurés lors des électrolyses de **1**-**5** décrites Figure R-20.[‡]

En étudiant la sélectivité des catalyseurs **1**-**4**, on remarque que les catalyseurs avec les constantes de vitesse pour la production de H_2 les plus faibles sont ceux qui présentent la meilleure sélectivité pour la réduction de CO_2 en CO par rapport à la réduction de protons (Figure R-21). En modifiant les paramètres électroniques du ligand pour défavoriser la réaction de réduction de protons, la réaction de réduction de CO_2 semble favorisée. La réaction de réduction du CO_2 semble moins affectée par la modification des propriétés électroniques du ligand, en accord avec les différences nettement moins marquées d'augmentation du courant cathodique sous CO_2 comparées aux différences observée en présence d'acide acétique.

Ces données permettent d'étoffer le mécanisme proposé de la réaction, en incluant la compétition CO_2/H^+ comme décrit sur la Figure R-22.

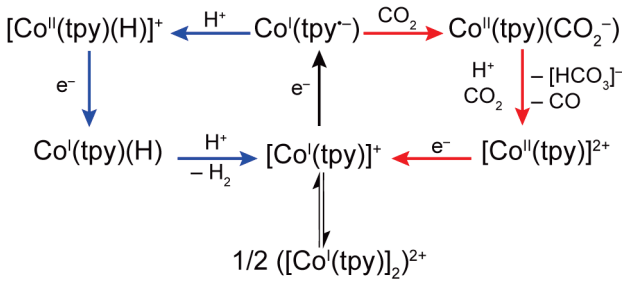

Figure R-22 Mécanisme proposé pour la catalyse de la réduction de CO_2 et de H^+ par **Co-tpy**.[‡]

3.3. Conclusion

L’étude de l’influence des propriétés électroniques du ligand sur la sélectivité observée lors de la de catalyse de la réduction de CO_2 en présence de H^+ a permis d’obtenir un levier simple pour modifier de façon rationnelle les proportions de H_2 et CO obtenues. Dans le but de se rapprocher de la cellule photo-électrochimique décrite Figure R-2, le greffage de cette famille de catalyseurs sur électrode de carbone a ensuite été étudié.

4. Fonctionnalisation d'électrodes de carbone vitreux avec le ligand terpyridine : préparation, métallation et catalyse

4.1. Objectifs

En étudiant les différentes méthodes utilisées dans la littérature pour immobiliser un catalyseur homogène sur une électrode, on s'aperçoit que non seulement des efforts de synthèse doivent être réalisés pour obtenir le catalyseur homogène, mais que d'autres efforts de synthèse doivent être ensuite déployés pour synthétiser et purifier des complexes moléculaires avec des ligands modifiés, ou partiellement modifiés, qui permettent l'immobilisation du catalyseur ainsi synthétisé.

Dans l'optique de continuer à explorer les possibilités offertes par la simplicité et l'ubiquité des ligands terpyridines, et sachant que les complexes que nous étudions peuvent être obtenus en mélangeant simplement des sels de cobalt(II) avec les ligands terpyridines directement en solution, nous avons décidé de suivre une nouvelle voie : obtenir une électrode de carbone fonctionnalisée avec le ligand terpyridine.

Avec cette électrode, il devient alors possible de métaller les ligands par simple immersion dans une solution concentrée de sel métallique. Théoriquement, tous les métaux sont accessibles, et il n'est pas nécessaire de fournir des efforts de synthèse supplémentaires pour passer de l'étude d'un catalyseur **Co-tpy** de production d'hydrogène à un catalyseur de Rh-tpy de réduction de CO_2.

4.2. Fonctionnalisation des électrodes de carbone

La méthode choisie pour obtenir des électrodes fonctionnalisées consiste en une étape de diazotization d'une variante du ligand tpy, suivie par un électro-greffage par voltammétrie cyclique (Figure R-23).

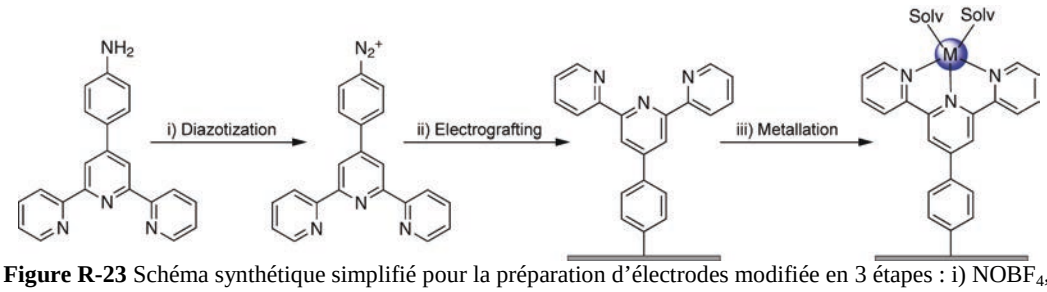

Figure R-23 Schéma synthétique simplifié pour la préparation d'électrodes modifiée en 3 étapes : i) $NOBF_4$, MeCN/Sulfolane (1:1), –40°C, 40 min, Ar, protégé de la lumière. ii) Voltammétrie cyclique, MeCN, $TBAPF_6$ 0,1 M, Ar, protégé de la lumière, 10 cycles de +0,8 à –0,4 V *vs.* Ag/AgCl, 50 mV/s, électrode de carbone vitreux. iii) Trempage dans une solution de 75 mM $CoCl_2$ dans le DMF.[§]

Le sel de diazonium a été obtenu en suivant un protocole publié récemment[14] qui consiste en une réaction entre $NO(BF_4)$ et le dérivé amino de tpy dans un mélange MeCN/sulfolane (1:1) à –40 °C pendant 40 min. La poudre ainsi obtenue est dissoute dans 3 mL de MeCN (2,8 mg pour 3 mL) avec 0,1 M de tetrabutylammonium hexafluorophosphate ($TBAPF_6$) dans une cellule électrochimique avec l'électrode de carbone vitreux polie à greffer, une contre-électrode en platine et une électrode de référence Ag/AgCl. La solution est purgée à l'argon et protégée de la lumière. Le greffage s'effectue par voltammétrie cyclique, en réalisant 10 cycles à 50 mV/s entre +0,8 V et –0,40 V *vs.* Ag/AgCl (Figure R-24, gauche). La vague de réduction du diazonium, visible lors du premier scan, disparait au cours de l'accumulation de scans à mesure que la surface se couvre du ligand tpy, qui est isolant dans la gamme de potentiels testés.

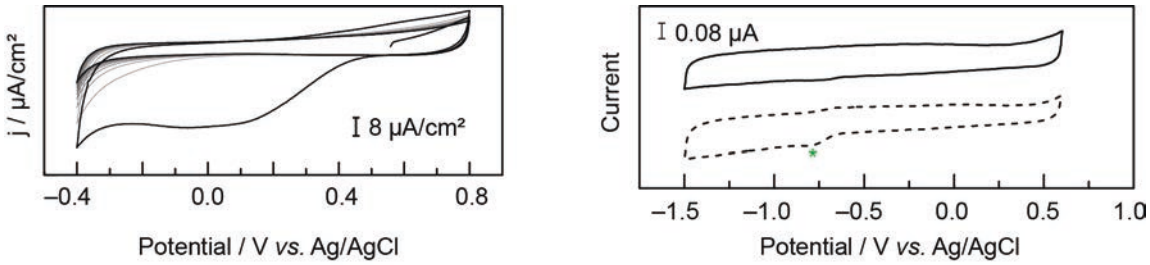

Figure R-24 Gauche : Voltammogramme de la procédure d'électro-greffage : 50 mV/s dans MeCN, 10 scans. Les premiers et derniers scans sont en noir, les autres en gris pour plus de clarté. Droite : Voltammogrammes sous argon, dans le DMF, $TBAPF_6$ 0,1 M, à 100 mV/s d'une électrode nue polie (haute, ▬ ligne noire) et d'une électrode modifiée (bas, --- tirets noirs, l'étoile verte * indique des traces de O_2).[§]

L'électrode ainsi greffée est rincée et plongée dans une solution fraiche de DMF contenant 0,1 M de $TBAPF_6$ puis caractérisée par voltammétrie cyclique. L'électrode présente la même absence de signal que l'électrode nue polie (Figure R-24, droite). Les électrodes ainsi obtenues peuvent ensuite être métallées par simple immersion dans une solution de 75 mM de $CoCl_2$ dans le DMF pendant 3 h à température ambiante. Après un rinçage au DMF et un second rinçage à l'eau, l'électrode ainsi métallée est caractérisée par voltammétrie cyclique dans le DMF (Figure R-25).

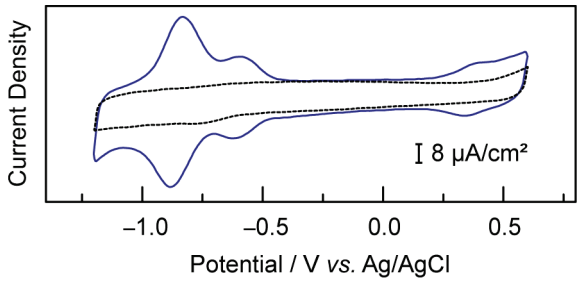

Figure R-25 Voltammogrammes sous argon, dans le DMF, $TBAPF_6$ 0,1 M, à 100 mV/s d'une électrode de carbone vitreux nue polie (---pointillés noirs) et de la même électrode après greffage et métallation au cobalt (— ligne bleue).[§]

Plusieurs signaux électrochimiques sont observables dans la fenêtre étudiée. Les signaux à –0,61 et +0,37 V sont attribués respectivement aux couples $Co(tpy)_2^{II/I}$ et $Co(tpy)_2^{III/II}$ par analogies avec le comportement de **Co-tpy** en solution homogène. Le signal principal, à –0,86 V *vs.* Ag/AgCl, est attribué à un Co-monoterpyridine par analogie là encore avec le système homogène.

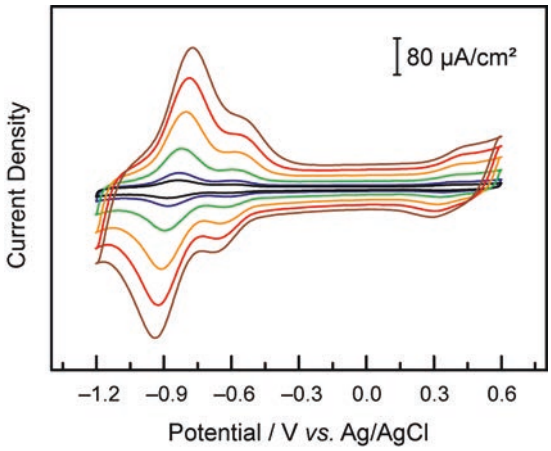

Figure R-26 Voltammogrammes sous argon, dans le DMF, $TBAPF_6$ 0,1 M, d'une électrode de carbone vitreux modifiée avec le ligand tpy et fraichement métallée au cobalt et rincée, à 50 (— noir), 100 (— bleu), 250 (— vert), 500 (— orange), 750 (— rouge) et 1000 (— marron) mV/s.[§]

Ces signaux correspondent bien à une espèce à la surface de l'électrode, comme en attestent l'évolution linéaire de l'intensité du signal avec la vitesse de scan, et également le fait que ces signaux soient observés dans une solution fraichement préparée d'électrolyte (Figure R-26). L'intensité des signaux permet de calculer une estimation de la densité d'atomes de cobalt électrochimiquement accessible à la surface de l'électrode : $5 \cdot 10^{-10}$ mol/cm² soit près d'une monocouche.

Notre étude s'est concentrée sur les propriétés catalytiques de **Co-tpy**, mais les électrodes modifiées avec le ligand tpy peuvent être métallée avec une variété de métaux. Par exemple des électrodes ont été également metallées avec un sel de nickel ($DME{\cdot}NiCl_2$) et présentent alors deux

signaux principaux dans la fenêtre d'étude à des positions similaires à celles observés lors de l'étude du système homogène. En revanche leur intensité varie de façon linéaire avec la vitesse de scan, une caractéristique des systèmes immobilisés (Figure R-27).

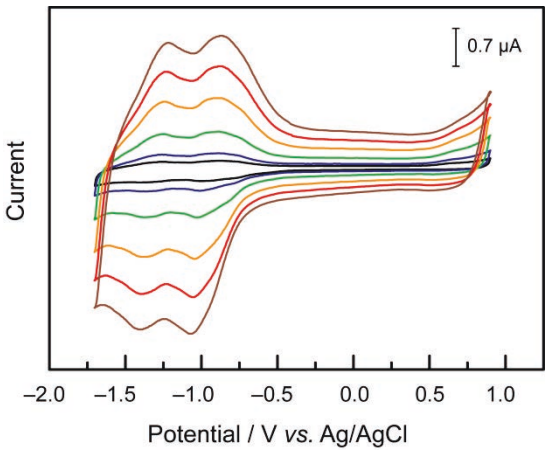

Figure R-27 Voltammogrammes sous argon, dans le DMF, $TBAPF_6$ 0,1 M, d'une électrode de carbone vitreux modifiée avec le ligand tpy et fraichement métallée au nickel et rincée, à 50 (— noir), 100 (— bleu), 250 (— vert), 500 (— orange), 750 (— rouge) et 1000 (— marron) mV/s.[§]

Un autre avantage de la simplicité du système étudié, et du découplage des étapes de greffage du ligand et de métallation, consiste en la possibilité de « recycler » les électrodes greffées par décoordination du métal pour obtenir à nouveau l'électrode modifiée avec le ligand tpy. Pour tester cette possibilité, une électrode modifiée et métallée au cobalt a été plongée 3 h dans une solution d'EDTA à 50 mM dans l'eau à pH 10. La dé-métallation a été confirmée par voltammétrie cyclique, et la même électrode a pu être re-métallée au cobalt (Figure R-28).

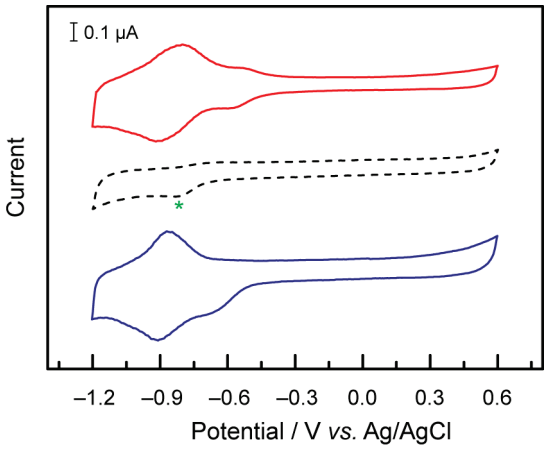

Figure R-28 Voltammogrammes sous argon, dans le DMF, $TBAPF_6$ 0,1 M, à 100 mV/s, d'une électrode de carbone vitreux modifiée avec le ligand tpy et fraichement métallée au cobalt et rincée (— rouge). La même électrode après immersion chélation du cobalt (--- noir, l'étoile verte * indique des traces de O_2) et après re-métallation au cobalt et rinçage (— bleu).[§]

Plus de 95% de l'intensité des pics est retrouvée, ce qui confirme que le processus de chélation du cobalt n'a pas endommagé irrémédiablement la surface de l'électrode modifiée.

4.3. Étude préliminaire des propriétés catalytiques

Les électrodes de carbone modifiées et métallées ont ensuite été testées pour leur activité en catalyse de réduction de protons en H_2, dans le DMF, en présence de 0,1 M du sel de fond $TBAPF_6$ et d'acide acétique. En voltammétrie cyclique, l'augmentation du courant cathodique en présence de 4,3 mM d'acide acétique, multiplié par 11 à −1,40V vs. Ag/AgCl, indique une activité potentielle en réduction de proton. Cette activité a été confirmée par électrolyse à potentiel contrôlé sur une électrode de carbone modifiée de 1,4 cm de diamètre. Une densité de courant constante de 300 µA/cm² a été observée pendant les 3 h d'électrolyse en présence de 0,1 M d'acide acétique, accompagnée par une production continue d'hydrogène, à raison d'environ 6 µmol par heure, soir 2,2 moles de H_2 par mole de catalyseur par secondes. Le rendement faradique pour la production de H_2 tiré de cette expérience est de ~90% (Figure R-29).

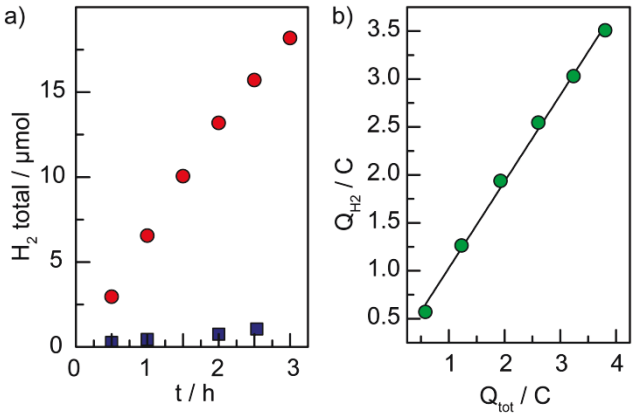

Figure R-29 a) Nombre de moles total de H_2 produit lors d'une électrolyse à –1,50 V d'une électrode de carbone vitreux modifiée et métallée au cobalt (● cercles rouges) et d'une électrode nue (■ carrés bleus) dans une solution de DMF avec 0,1 M de $TBAPF_6$ et 0,1 M d'acide acétique. b) Charge totale utilisée pour la production de H_2 en fonction de la charge totale échangée lors de l'électrolyse de l'électrode modifiée (● cercles verts). Le coefficient de corrélation du fit linéaire est de 0,996, et le rendement faradique pour la production de H_2, donné par le coefficient directeur de la droite, est de 90% ± 5%.[§]

Un des grands avantages des électrodes greffées est la capacité de tester une multitude de conditions qui n'étaient pas forcément accessibles aux catalyseurs homogènes. Par exemple, les électrodes greffées métallées au cobalt ont pu être testées dans l'eau, en tampon phosphate, à pH 7. Les voltammogrammes présentent un mur du solvant, correspondant à la réduction des protons, à des

potentiels moins négatifs que ceux observés sur l'électrode nue, ce qui semble indiquer que la réduction électrochimique de protons en H_2 est catalysée par l'électrode modifiée et métallée.

Les électrodes modifiées et métallées au cobalt ont ensuite été testées pour la catalyse de la réduction de CO_2. En voltammétrie cyclique, une augmentation du courant cathodique sous CO_2 est observée, ce qui semble indiquer une activité potentielle en catalyse de réduction du CO_2 (Figure R-30). Cette observation a été confirmée par électrolyse, et le produit formé est le CO. La différence majeure entre les systèmes homogène et immobilisé est la présence, sur les voltammogrammes des électrodes greffées, d'un nouveau pic en oxydation sous CO_2. Ce pic a été attribué à un adduit CO—Co par analogie avec ce qui est observée lorsque l'électrode modifiée est soumise à 1 atm de CO.

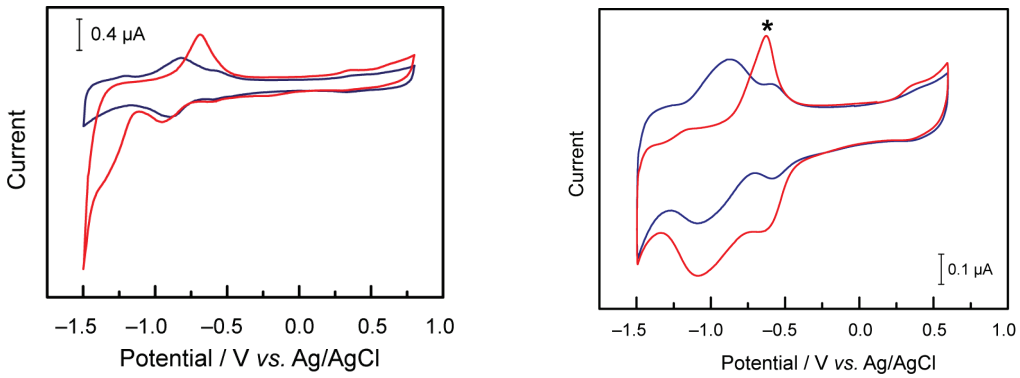

Figure R-30 Voltammogrammes sous argon, dans le DMF, $TBAPF_6$ 0,1 M, à 100 mV/s, d'une électrode de carbone vitreux modifiée et métallée au cobalt sous argon (— bleu) et sous CO_2 (rouge, gauche) ou CO (rouge, droite).[§]

Cette différence majeure est probablement la cause de la faible stabilité de l'activité catalytique en électrolyse, où la production de CO s'arrête après les 30 premières minutes, après la production de 55 nmol of CO ce qui correspond à une moyenne de 70 TON par atome de cobalt présent à la surface de l'électrode.

5. Conclusion et perspectives

Les systèmes cobalt-terpyridine ont montré leur potentiel en tant que catalyseurs de la réduction électrochimique du CO_2 en CO, accompagné d'une réduction contrôlée de H^+ en H_2, générant du gaz de synthèse en proportion contrôlables. Les systèmes nickel-terpyridine permettent de générer sélectivement du monoxyde de carbone. L'immobilisation du système catalytique sur électrode de carbone, en vue d'une preuve de concept de la cathode Figure R-2, a été réalisée.

Ces systèmes sont très avantageux de par la simplicité des ligands utilisés, le faible coût et l'abondance naturelle des centres métalliques, ainsi que les propriétés catalytiques de ces catalyseurs, qui rivalisent avec celles des systèmes à base métaux nobles, comme le ruthénium pour les systèmes homogènes et le rhénium pour les systèmes immobilisés sur électrode.

La voie est ouverte à l'amélioration des performances et de la stabilité du système catalytique, grâce aux paramètres qui ont été mis en évidence dans ce travail, en modifiant les propriétés stériques et électroniques des ligands.

Références

‖ N. Elgrishi, V. Artero and M. Fontecave, *L'Actualité Chimique*, 2013, **371–372**, 95. Reproduced by permission of the French Chemical Society.

† N. Elgrishi, M. B. Chambers, V. Artero and M. Fontecave, *Phys. Chem. Chem. Phys*, 2014, **16**, 13635–13644. Reproduced by permission of the PCCP Owner Societies, with some minor modifications in some cases.

‡ N. Elgrishi, M. B. Chambers and M. Fontecave, *Chem. Sci.*, 2015, DOI: 10.1039/C4SC03766A. Reproduced by permission of the Royal Society of Chemistry, with some minor modifications in some cases.

§ N. Elgrishi, S. Griveau, M. B. Chambers, F. Bedioui and M. Fontecave, *Chemical Communications*, 2015, **51**, 2995–2998. Reproduced by permission of the Royal Society of Chemistry, with some minor modifications in some cases.

1 D. P. Trans, D. R. Keeling, *Trends in Atmospheric Carbon Dioxide*, www.esrl.noaa.gov/gmd/ccgg/trends/. (Accessed 2015).

2 M. Bourrez, F. Molton, S. Chardon-Noblat and A. Deronzier, *Angew. Chem. Int. Ed.*, 2011, **50**, 9903.

3 J. Qiao, Y. Liu, F. Hong and J. Zhang, *Chem. Soc. Rev.*, 2014, **43**, 631.

4 J.-M. Savéant, *Chem. Rev.*, 2008, **108**, 2348.

5 C. Arana, S. Yan, M. Keshavarz-K, K. T. Potts and H. D. Abruña, *Inorg. Chem.*, 1992, **31**, 3680.

6 C. Arana, M. Keshavarz, K. T. Potts and H. D. Abruña, *Inorg. Chimica Acta*, 1994, **225**, 285.

7 Nous notons que le terme « voltammétrie » sera utilisé pour désigner « voltampérométrie » dans la suite de ce document, tout comme « voltammogramme » désignera « voltampérogramme ».

8 P. Fuchs, U. Hess, H. H. Holst and H. Lund, *Acta Chemica Scandinavica B,*1981, **35**, 185.

9 R. S. Gaddie, C. B. Moss and C. M. Elliott, *Langmuir*, 2013, **29**, 825.

10 P. Salvatori, G. Marotta, A. Cinti, E. Mosconi, M. Panigrahi, L. Giribabu, M. K. Nazeeruddin and F. De Angelis, *Inorg. Chim. Acta*, 2013, **406**, 106.

11 J. Chambers, B. Eaves, D. Parker, R. Claxton, P. S. Ray and S. J. Slattery, *Inorg. Chim. Acta*, 2006, **359**, 2400.

12 C. Costentin, S. Drouet, M. Robert and J.-M. Savéant, *J. Am. Chem. Soc.*, 2012, **134**, 11235.

13 V. Artero and J.-M. Savéant, *Energy Environ. Sci.*, 2014, **7**, 3808.

14 Y. Pan, B. Tong, J. Shi, W. Zhao, J. Shen, J. Zhi and Y. Dong, *J. Phys. Chem. C*, 2010, **114**, 8040.